VOLCANIC FORCING: MODELLING IMPACTS ON SOUTHERN HEMISPHERE TEMPERATURES

By

PAMELA HARVEY

480777

A thesis submitted to the Faculty of Science, University of the Witwatersrand, in fulfilment of the requirements for the degree of

DOCTOR OF PHILOSOPHY

April 2021

School of Geography, Archaeology and Environmental Studies

Supervisor: Prof. Stefan Grab

DECLARATION

I declare that this thesis is my own, unaided work. It is being submitted for the Degree of Doctor of Philosophy to the University of the Witwatersrand, Johannesburg. It has not been submitted before for any other degree or examination at this or any other institution.

Pamela Harvey

Signed in Johannesburg, on the 22nd of June 2021

ABSTRACT

Considerable recent research attention has focussed on volcanic forcing effects on global climate, perhaps due to its cooling effects in what is otherwise an era of global warming. In an attempt to contemplate ways to combat the global warming phenomenon, geoengineering options have been considered, such as the idea to manipulate the climate by injecting sulphate aerosols into the stratosphere and thus simulate a volcanic forcing effect. This was of course a very controversial suggestion, and many argue that attempting to resolve global warming in this way could do more harm than good. The fact is, that there are still too many unknown variables and potential outcomes as a consequence of volcanic forcing on climate, such that the impact of manipulating climate to combat global warming cannot be fully appreciated at this stage. Instead, the focus remains on identifying research gaps and addressing these.

While much research attention has focussed on understanding climatic responses to volcanic forcing over the Northern Hemisphere (NH), very little attention has focussed on the Southern Hemisphere (SH) in this regard. This PhD thus aims to address this research gap and establish, in some measure of detail, the temperature responses to major volcanic eruptions over terrestrial regions of the SH. Initially, near-surface temperature responses to eight major eruptions (Krakatau, 1883; Tarawera, 1886; Santa Maria, 1902; Colima, 1913; Quizapu, 1932; Agung, 1963; El Chichón, 1982; Pinatubo 1991) are investigated. Four eruptions (Krakatau, Santa Maria, Agung and Pinatubo) are identified as having caused significant temperature responses over the SH, and thereafter the temperature responses to these eruptions are established at a variety of spatial (hemispheric, continental and sub-regional) and temporal (annual, seasonal and monthly) scales. Model simulations from the Coupled Model Intercomparison Project Phase 5 (CMIP5) are used as the main data source to study these climatic impacts. However, a reanalysis dataset (20th Century Reanalysis V2) provided by the NOAA/OAR/ESRL PSL station data, as well as station data for some sub-regions,

were used to test the reliability of CMIP5 model outputs in its ability to simulate volcanic forcing effects on SH climate.

Results from the CMIP5 ensemble used in this study suggest that significant cooling occurs in the SH following four of the eight eruptions (Krakatau, Santa Maria, Agung and Pinatubo), although the response is weaker than what the models suggest for the NH, as expected. The strongest temperature response follows the Krakatau eruption, which emitted the largest amount of SO_2 into the lower stratosphere. The weakest responses would follow after either Santa Maria or Agung, varying with the region or the season studied. Overall, it is found that stronger responses occur during austral autumn, followed by austral winter, while the weakest responses occur during austral spring. Exploring the responses at a continental scale reveals that Australia experiences strongest cooling anomalies, which peak earlier (av = 5 months) than both southern African (SAF) and southern South American (SSA) anomalies, while SSA experiences weakest anomalies which also have the most delayed peak response (av = 9 months).

Temperature responses in six sub-regions of SAF and eight sub-regions of Australia are then explored to establish responses at a much finer spatial scale. Results show that more northern regions experience stronger cooling than southern regions. Variations of responses appear at the smaller scale, as some regions experience strongest cooling response in one season while other regions experience strongest cooling in another season. Responses can vary depending on the latitude and magnitude of the eruption, the time of year of the eruption, as well as the condition of the atmosphere at the time of the eruption. Investigating variations in the responses to individual eruptions at different spatial and time scales highlights the necessity of studying the impacts of volcanic forcing on an individualistic eruption basis, rather than based on a composite of eruptions.

Comparing CMIP5 results to reanalysis and station data reveals that uncertainties exist in the observed temperature responses. It is possible that at least some results are overestimated, as has been found in other CMIP5 studies investigating volcanic forcing. However, as found in this thesis, at times CMIP5 in fact underestimates the temperature response based on comparisons with reanalysis data (in the Australian sub-regions following the Agung and Pinatubo eruptions). Expecting climate models to perform close to 100% accurately is unrealistic, as large uncertainties also exist when using both reanalysis and station-based instrumental data. Notwithstanding the challenges and limitations when using CMIP5, such model outputs provide a reasonable sense of expected temperature pattern following major volcanic eruptions. Hopefully, such model outputs will continue to improve with the newly established CMIP6.

ACKNOWLEDGEMENTS

This is all for the Glory of God. Without Him, this would not have been possible. Thank you for the journey.

To my supervisor, Prof. Stefan Grab, thank you for years of support, wisdom, and guidance and for your time, patience, and encouragement. Everything that you have provided to me and this project has been invaluable.

I would like to thank the researchers and scientists who have shared their expertise, or helped along the way, especially those at the CSIR, such as Francois Engelbrecht, Johan Malherbe and Jacobus van der Merwe. And also, I thank the anonymous journal reviewers whose advice and knowledge have aided in improving this PhD project immensely.

I would like to acknowledge and thank the National Research Foundation (NRF) for contributing to the funding of this degree.

I acknowledge the World Climate Research Programme's Working Group on Coupled Modelling, responsible for CMIP5. I acknowledge and thank each climate modeling group for contributing to CMIP5, for producing and making their model output available. CMIP5 data were obtained from: https://esgf-data.dkrz.de. I also acknowledge NOAA/OAR/ESRL PSL, Boulder, Colorado, USA which made the 20th Century Reanalysis V2 (20CRv2) data available, and which can be downloaded from https://psl.noaa.gov/data/gridded/data.20thC_ReanV2.html.

To my family and friends, thank you for your support, your prayers and encouragement throughout this journey. I am so grateful for you all.

RESEARCH OUTPUTS AS PART OF THIS PHD

Publications and presentations

1. **Harvey PJ**, Grab SW, Malherbe J. 2020. Major volcanic eruptions and their impacts on Southern Hemisphere temperatures during the late 19th and 20th centuries, as simulated by CMIP5 models. *Geophysical Research Letters*, 47(14). https://doi.org/10.1029/2020GL087792 (published)
2. **Harvey PJ**, Grab SW. 2021. Southern Hemisphere continental temperature responses to major volcanic eruptions since 1883 in CMIP5 models. Submitted to the *Theoretical and Applied Climatology* (under review)
3. **Harvey PJ**, Grab SW. 2021. Southern African temperature responses to major volcanic eruptions since 1883: simulated by CMIP5 models. *International Journal of Climatology* (in press)
4. **Harvey PJ**, Grab SW. 2021. Australian Sub-Regional Temperature Responses to Volcanic Forcing: a critical analysis using CMIP5 Models. Intending to submit to the *International Journal of Climatology* (intending to submit)
5. **Harvey PJ**, Grab SW, Engelbrecht F. 2015. "Volcanic Forcing: new initiatives to establish its impacts on climates of the Southern Hemisphere". Oral paper presented at Our Common Future under Climate Change (CFCC), Paris, France, 7-10 July 2015
6. **Harvey PJ**, Grab SW, Engelbrecht F. 2017. "Volcanic forcing: New initiatives to establish its impacts on climates of the Southern Hemisphere". Poster presentation at the 5th PAGES Open Science Meeting (OSM), Zaragoza, Spain, 9-13 May 2017

TABLE OF CONTENTS

Contents

LIST OF FIGURES

Chapter One

Chapter Two

Chapter Two: Supplementary Material

Chapter Three

Chapter Three: Supplementary Material

Chapter Four

Chapter Five

LIST OF TABLES

Chapter Five

Chapter Six

ABBREVIATIONS

20CRv2:	20th Century Reanalysis V2
av:	average (arithmetic mean)
CEC:	Central Eastern Coast
CMIP5:	Coupled Model Intercomparison Project, Phase 5
CSub:	Central Subcontinent
CWC:	Central Western Coast
DJF:	Austral summer (December, January, February)
DVI:	Dust Veil Index
EAC:	Eastern Coast
EAS:	Eastern Subcontinent
ECC:	Eastern Cape Coast
ENSO:	El Niño Southern Oscillation
ESA:	Eastern South Africa
JJA:	Austral winter (June, July, August)
MAM:	Austral autumn (March, April, May)
NESA:	North-eastern South Africa, southern Zimbabwe and southern Mozambique
NH:	Northern Hemisphere
NWC:	North Western Coast
SAF:	Southern Africa
SAM:	Southern Annular Mode
SH:	Southern Hemisphere
SON:	Austral spring (September, October, November)
SSA:	Southern South America
SWC:	South-Western Cape
SWE:	South Western Coast
Tas:	Tasmania
VEI:	Volcanic Explosivity Index

Vic:	Victoria
WSub:	Western Subcontinent
y0:	Year of the eruption
y1:	First year post eruption
y2:	Second year post eruption
y3:	Third year post eruption

Chapter One: General Introduction

1. Introduction

The concept of 'climate change' has been recognized for many years now (Croll, 1890; Humphreys, 1913; Gilliland, 1982; Imbrie and Imbrie, 1986; León, 2011; Hulme, 2015; Jolley and Rickards, 2019). Recently, much attention has been given to the anthropogenic impacts on climate. However, besides anthropogenic forcing, there are also natural forcers, such as solar and volcanic forcing, which are also known to influence climate [change] (Gilliland, 1982; van Geel *et al.*, 1999; Mann *et al.*, 2005; Sjolte *et al.*, 2018). Climate forcers can work simultaneously and signals from one climate forcing can be tainted or hidden by another (Timmreck, 2012), thus separating and understanding the impact of individual forcing mechanisms can be challenging. Volcanic forcing itself has received much attention, in fact from as early as the 19th century (Mass and Portman, 1989; Cole-Dai, 2010), and particularly so for the Northern Hemisphere (NH). It is now well established that volcanic forcing affects weather, climate, and ultimately the environment and society (Robock, 2000; Cole-Dai, 2010; Timmreck, 2018; Zanchettin *et al.*, 2019; Pausata *et al.*, 2020).

When a major volcanic eruption (usually classified as one with a Volcanic Explosivity Index (VEI) greater than 4) emits at least 5 Tg of sulphur dioxide (SO_2) into the lower stratosphere, it may affect climate (Timmreck, 2018). The SO_2 converts to sulfuric aerosols in the stratosphere (Figure 1), which are rapidly transported latitudinally around the globe (can be as soon as 1-2 weeks after the eruption; Robock, 2000; Bègue *et al.*, 2017). These aerosols then change the planetary albedo and the earth's energy budget, through increased scattering, reflection and absorption of incoming solar radiation and outgoing radiation which in general, result in warming of the stratosphere and cooling of the troposphere (Robock, 2000; Cole-Dai, 2010; Timmreck, 2018). Warming in the equatorial stratosphere results in a stronger temperature gradient between the equator and poles, leading to stronger polar vortices (Timmreck, 2018). In general, eruptions occurring in the tropics can impact weather on a global scale, however, eruptions occurring in high latitudes will only affect the hemisphere in which they erupt (Oman *et al.*, 2005; Schneider *et al.*, 2009; Timmreck, 2018). Changes in climate, such as temperature and precipitation often occur for 1-3 years following a major eruption (Thompson *et al.*, 2009; Kremser *et al.*, 2016). However, numerous major eruptions occurring during short succession (a few years apart, known as a volcanic 'double'-forcing effect), or even a single super-colossal eruption (VEI >7), could lead to longer lasting climate effects and/or even contribute significantly to decades-long temperature depressions, such as was the case following the unknown eruption of 1809 and Tambora (1815) during the Little Ice Age (Crowley *et al.*, 2008; Timmreck, 2012; Toohey *et al.*, 2016; Brönnimann *et al.*, 2019b).

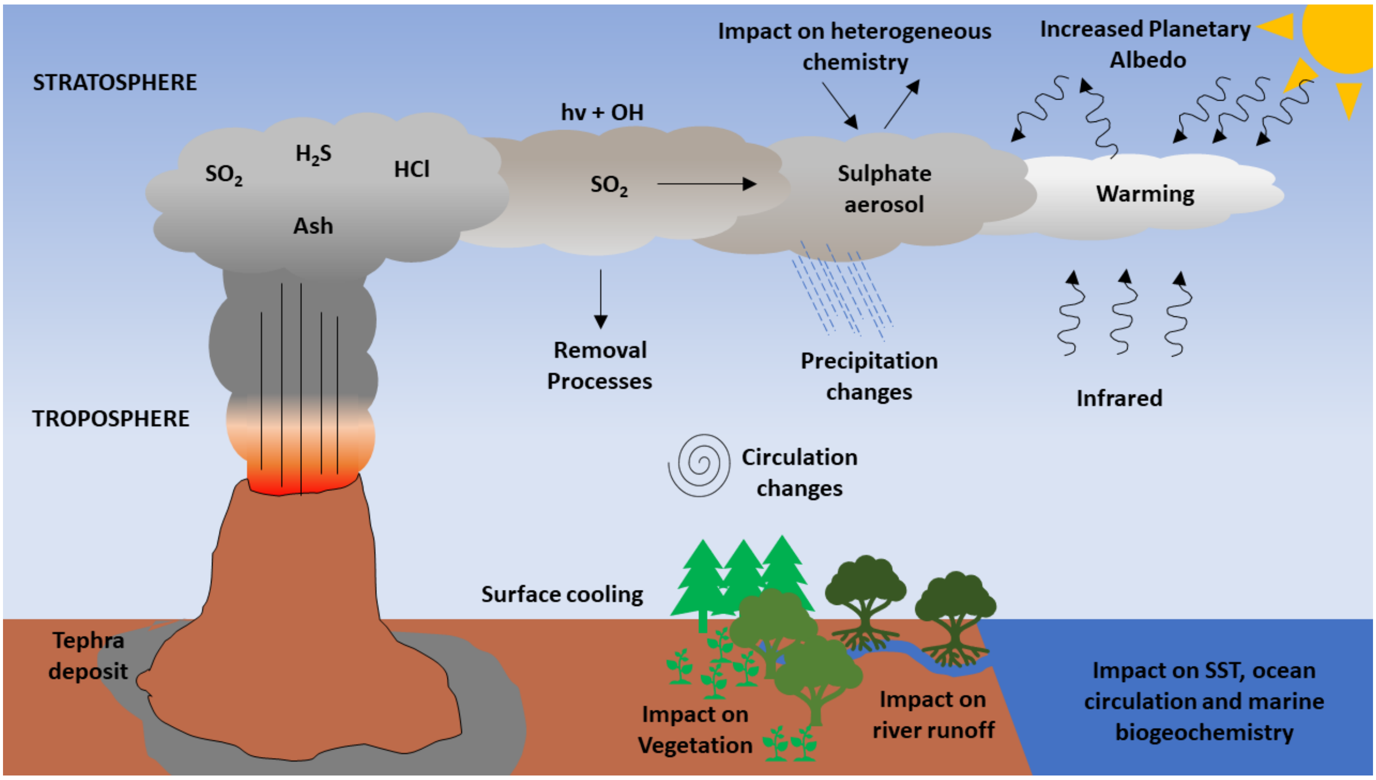

Figure 1. Schematic overview of a major volcanic eruption, and the resulting processes and impacts. Figure adapted from Timmreck (2018), which was originally modified from McCormick *et al.* (1995).

Responses to volcanic eruptions are highly variable both in space and time; for instance these may depend on a) the location of the eruption, b) the time of year (season) during which the eruption occurred, c) the magnitude of the eruption d) the height of the eruption plume and as mentioned above and e) the amount of SO_2 emitted into the lower stratosphere (Oman *et al.*, 2005; Zanchettin *et al.*, 2014; Colose *et al.*, 2015; Stevenson *et al.*, 2017; Zuo *et al.*, 2018; Krishnamohan *et al.*, 2019; Sun *et al.*, 2019). Different climatic responses have also been noted during different seasons; for instance, the NH often experiences winter warming and summer cooling (Robock, 2000; Zambri *et al.*, 2017). While the NH response to volcanic forcing has been widely studied (e.g. Oppenheimer, 2003; Esper *et al.*, 2013; Sigl *et al.*, 2015; Zambri and Robock, 2016; Rao *et al.*, 2017), far less work has focussed on the Southern Hemisphere (SH). One of the reasons being that there have been few climatological records that go back far enough in time, and historical climate reconstructions have been fairly sparse and lacking in sufficient temporal resolution through much of the SH (Yang and Xiao, 2017). There have also been few major eruptions during recent decades for meaningful station based instrumental weather data investigations to ascertain post-eruption responses (Jones *et al.*, 2003). A further possible reason for the general lack of SH attention may be owing to the perception that SH responses are generally weak or insignificant (e.g. Robock *et al.*, 2007; Raible *et al.*, 2016). Studies have indeed found that the SH response to volcanic forcing is weaker than that of the NH (Man *et al.*, 2014; Neukom *et al.*, 2014; Monerie *et al.*, 2017), largely due to the SH being more sensitive to internal variability (such as the polar vortex, Southern Annular Mode (SAM) and El Niño Southern Oscillation (ENSO)) than to external forcers, (Wilmes *et al.*, 2012). The internal variability may mask responses to external forcers making detection of the responses to volcanic forcing more complicated (Barnes *et al.*, 2016). However, SAM and ENSO themselves may be affected by volcanic forcing (Barnes *et al.*, 2016), and thus the real volcanic forcing effect may be difficult to establish and/or may serve as an important indirect factor influencing local weather through its impacts on internal weather producing systems.

Changes in radiation induce stronger zonal winds and increase temperature and density gradients between the poles and equator, thereby altering atmospheric circulation. Due to this, the NH polar vortex is strengthened (Perlwitz and Graf, 1995; Zambri and Robock, 2016). Given the expanse of oceans in mid to high latitudes of the SH, the SH polar vortex is more robust (Robock *et al.*, 2007; Kidston *et al.*, 2015), however it too is susceptible to volcanic forcing (Hudson, 2012; Kidston *et al.*, 2015). The polar vortex can be impacted by changes in the SAM (Shulmeister *et al.*, 2004). While a positive Arctic Oscillation phase occurs in the NH following major eruptions (Stenchikov *et al.*, 2002; Robock *et al.*, 2007), the response of the SAM, which strongly influences SH climate, is still obscure and contradictory (Raible *et al.*, 2016). For instance, although Robock *et al.* (2007) proposed no significant change in the SAM following major eruptions, others have found that such eruptions can force the SAM. Roscoe and Haigh (2007) suggested it is forced into a negative phase, however, modelling studies have argued for the contrary (i.e. positive phase)(e.g. Karpechko *et al.*, 2010; McGraw *et al.*, 2016; Yang and Xiao, 2017). A positive SAM phase results in westerly winds contracting towards the poles and intensifying (Yang and Xiao, 2017). The SAM response can be masked by internal variability, such as the El Niño Southern Oscillation (ENSO) (Yang and Xiao, 2017). Although the ENSO also strongly influences SH climate (Gallego *et al.*, 2005; Raible *et al.*, 2016), here too, there is ongoing debate whether major eruptions influence ENSO events (Ménégoz *et al.*, 2018). Strong El Niño events occurred around the El Chichón (1982) and Pinatubo (1991) eruptions, however these events had already commenced before the eruptions occurred (Self *et al.*, 1997). Some (e.g. Pausata *et al.*, 2016; Zuo *et al.*, 2018) propose that the latitude of the eruption as well as the ENSO state at the time of eruption can determine whether ENSO is affected and how. For instance, it has been suggested that NH and tropical eruptions may result in El Niño-like anomalies which remain for about 1.5 years while SH eruptions have a weaker tendency of causing such anomalies (Zuo *et al.*, 2018). There is an increased possibility of a La Niña phase occurring during the third post eruption year following NH and tropical eruptions (Maher *et al.*, 2015). Regarding the ENSO state in which the eruption occurs, a high latitude eruption occurring during an El Niño state is likely to result in strong La

Niña like anomalies in the second year after the eruption. However, if the eruption occurred during a La Niña state there tend to be no anomalies in the second year, but La Niña anomalies occur in the third year after the eruption. El Niño anomalies also tend to be stronger if the eruption occurs during a La Niña or neutral phase (Pausata *et al.*, 2016).

Volcanic forcing can affect atmospheric circulation even in the stratosphere by affecting stratospheric temperature gradients and wind speeds (Cui *et al.*, 2014; Kidston *et al.*, 2015). While there has been limited research on the impact of volcanic forcing on jet streams, Hudson (2012) argues that jet streams were impacted by both El Chichón and Pinatubo in the NH. From their results (see their Fig 4.), it appears that the NH subtropical jet shifts poleward and that the SH subtropical jet moves poleward initially and then equatorward after both eruptions, while the SH Polar jet seems to move equatorward after the Pinatubo eruption. Jet streams in the SH can shift by about 10˚ with the seasons each year (Tyson *et al.*, 2000; Shulmeister *et al.*, 2004; Gallego *et al.*, 2005; Hudson, 2012). Jet streams can affect the SAM (Xia *et al.*, 2015), as well as planetary waves and storm tracks, and thus influence surface weather (Hudson, 2012; Kidston *et al.*, 2015). Jet streams can also be a direct measure of the westerly circulation (Gallego *et al.*, 2005). NH winter westerly circulation can strengthen after major volcanic eruptions (Karpechko *et al.*, 2010; Cui *et al.*, 2014; Timmreck, 2018). If a positive SAM phase does occur after an eruption, the SH westerlies would also strengthen. Westerly circulation, SAM, ENSO and jet streams can collectively affect cyclogenesis (Malherbe *et al.*, 2014; Xia *et al.*, 2015). Mid-latitude cyclones cause most of the extreme weather in the mid-latitudes (Pepler *et al.*, 2016). There has been little focus on the impact of volcanic eruptions on mid-latitude cyclones, however, Picas and Grab (2020) suggest that an increase in mid-latitude cyclone frequency and strength may be the cause for cooler temperatures over south-western South Africa following major volcanic eruptions. Historical climate reconstruction studies have found that conditions such as unusual (i.e. frequent, severe, early, late) frost and/or snowfalls associated with cooler than usual conditions tend to occur soon after major eruptions over the south-western Cape of South Africa (Dunwiddie and LaMarche, 1980) and Lesotho (Grab and Nash, 2010). Yan *et al.* (2018) studied the impact of eruptions on tropical cyclones and found conditions were unfavourable for cyclogenesis after eruptions in most places besides the North Atlantic. Observations of SH cyclogenesis, both tropical and extratropical, is sparse (Pepler *et al.*, 2016), hindering the understanding of their long-term variability and impact from major eruptions.

Due to the scarcity of temporally long instrumental weather data and general absence of high resolution (annually resolved) climate proxies throughout much of the SH (Brönnimann *et al.*, 2019a), climate models are often used to study the response to volcanic eruptions (Hopcroft *et al.*, 2018; Hua *et al.*, 2019; Toohey *et al.*, 2019). Climate models also help to isolate the various climate forcers as well as explain the resulting climate variations seen. This PhD study makes use of model data from the Coupled Model Intercomparison Project, Phase 5 (CMIP5; Taylor *et al.*, 2012) to identify potential terrestrial temperature responses in the SH, following major volcanic eruptions. CMIP5 was selected for this study due to the various historical experiments that were available, which allowed for temperature responses to different climate forcings (e.g. solar, volcanic, anthropogenic etc.) to be explored individually. There is also the benefit of the number of models that contributed to the CMIP5 project, which has permitted a reasonable sample size of model simulations. It must, however, be acknowledged that climate models are not completely accurate; for instance, it has been established that CMIP5 models generally tend to overestimate the temperature response to volcanic forcing (Driscoll *et al.*, 2012; Zanchettin *et al.*, 2016, Chylek *et al.*, 2020), while Xing *et al.* (2020) suggest that they underestimate the response in the stratosphere. On the other hand, Paik and Min (2018) found that the response of global temperature and precipitation extremes were adequately represented by CMIP5 models. It is proposed that the reason for the overestimation is due to strong internal variability, which can mask the response to volcanic forcing in the observed data (Barnes *et al.*, 2016; McGraw *et al.*, 2016), or alternatively, it is possibly due to incorrect parameterization of the relationship between the aerosols and ice and mixed phase clouds (Chylek *et al.*, 2020). Due to this, climate models can be used in conjunction with reanalysis data, instrumental records, and climate proxies, where available, which may provide a more precise image of what happened to weather and climate in a region (Raible *et al.*, 2016). To this end, the PhD makes use of instrumental station data from sub-regions of Australia and the Western Cape in South Africa. Reanalysis data are also used to compare with the CMIP5 model outputs, and thus establish a measure of reliability or confidence in these outputs. The Twentieth Century Reanalysis (V2) (20CRv2) was decided upon as the best reanalysis dataset for this PhD. The Twentieth Century Reanalysis is one of the only reanalysis outputs to cover the time period required for this PhD (20CRv2 covers 1871-2012), while some datasets start in 1900, most reanalysis datasets only start in the mid-twentieth century (Compo *et al.*, 2011; Slivinski *et al.*, 2021). Apparently, 20CRv2 satisfactorily simulates SH circulation, although this is during the period of 1979-2010 when satellite and radiosonde data were more extensive (Ke and Hui, 2013). Discrepancies were, however, noted in SH circulation between 1897 and 1920 due to the sparseness of available observation data (Ke and Hui, 2013). Despite this, of the reanalysis datasets available, 20CRv2 is recommended as the best reanalysis dataset for studying climate variability over southern Africa (Zhang *et al.*, 2013).

2. Aims and Objectives of Study

Using model data from CMIP5, reanalysis data, as well as available instrumental data and historical documents, this study aims to establish possible SH temperature responses following major volcanic eruptions since 1850, from hemispheric to regional spatial scales, and from annual to monthly temporal scales. A secondary aim is to establish the relative reliability of CMIP5 model data outputs in depicting temperature responses to volcanic eruptions through a comparison with instrumental temperature records and reanalysis data.

The main objectives of this study are thus:

1. To identify which major volcanic eruptions during the period of 1850-2005 have had a notable effect on SH temperatures, as shown by CMIP5 model outputs, and how these might compare to temperatures in the NH.
2. To study and compare SH continental temperature responses (i.e. southern South America, southern Africa and Australia) following the eruptions of Krakatau (1883), Santa Maria (1902), Agung (1963) and Pinatubo (1991).
3. To observe and compare sub-regional southern African temperature responses following the eruptions of Krakatau (1883), Santa Maria (1902), Agung (1963) and Pinatubo (1991).
4. To observe and compare sub-regional Australian temperature responses following the eruptions of Krakatau (1883), Santa Maria (1902), Agung (1963) and Pinatubo (1991).

   And specifically to:

   4.1. Observe if areas of similar climate types record similar temperature responses.
5. To compare CMIP5 model simulation outputs (i.e. temperature response to volcanic eruptions) with instrumental station records, reanalysis data and historical documentary records.

3. Methodology

3.1. CMIP5 data

3.1.1. Data acquisition

This PhD uses data from model simulations from the Coupled Model Intercomparison Project, Phase 5 (CMIP5; Taylor *et al.*, 2012). Data were obtained from the Earth System Grid Federation (ESGF), which can be found through the link: https://esgf.llnl.gov/index.html. Data come in the form of Network Common Data Form (NetCDF) files, which allows for array-orientated data to be stored and provides variables as well as dimensions and attributes for the variables. Not all the models available from CMIP5 were used. Models used were selected based on their ability to accurately simulate a temperature response to volcanic forcing, which had previously been identified by Santer *et al.* (2013) and Barnes *et al.* (2016). Only the first physics version (p1) of each simulation was used, apart from the GISS-E2_R model where both p1 and p3 were used due to the way in which p3 calculated volcanic aerosols within the model. The p1 simulations used prescribed volcanic forcing, by either Sato *et al.* (1993) or Ammann *et al.* (2007). Originally the study had made use of 11 simulations, using only the first realisation of each model. However, upon suggestion by an anonymous reviewer of the first published paper (Chapter 2), the study was adjusted to include the first three realizations of each model (r1-r3), which represent different initial starting conditions of the model simulations, and were thus used where available, bringing the total number of simulations used to 31.

Initially numerous variables (e.g. precipitation; minimum, maximum and average atmospheric and surface temperatures; air pressure; zonal and meridional wind; geopotential height) were obtained from CMIP5. However, it was soon realised that covering all the variables would not fit into the scope of the PhD. It was decided that the climate dynamics of how and why any responses that were seen would not be included in the scope of the PhD. Precipitation and both terrestrial temperatures and sea surface temperature responses were initially analysed, however, it was realised that analysing both at such an in-depth scale, as planned, would again be beyond the scope of a single PhD. Thus, it was finally decided to limit the complete analysis to near-surface (2m) average temperatures (CMIP5 variable: tas). Data were obtained at a monthly timescale and cover the period of 1850 to 2005.

Numerous experiments were obtained from the historical experiment family, which each use different climate forcers. Time was spent understanding the different forcers the CMIP5 models use, in identifying which experiments were required for the PhD, and in selecting these experiments for each model from the

CMIP5 database. These different experiments were used to establish temperature responses to individual forcers, as well as a combination of forcers. The experiments used are as follows:

- Historical experiments, incorporating natural and anthropogenic forcing. Given that this is the most realistic scenario, it is used throughout the study.
- Historical Nat (natural) experiments, incorporating only natural forcing, specifically volcanic and solar forcing.
- Historical Misc (Miscellaneous) experiments, incorporating either a variety of individual forcers, or a combination of forcers. Three different individual forcers are used:
    - solar forcing
    - volcanic forcing
    - anthropogenic forcing

3.1.2. Data Processing

The following languages were used to prepare the data: R, Climate Data Operator (CDO), NCAR Command Language (NCL), and Grid Analysis and Display System (GrADS). For each of the experiments, the individual monthly files were first concatenated into single files. Thereafter, the files were regridded to a 2° by 2° latitude-longitude grid allowing for an ensemble to be made, combining the various models. Using the ensembles, annual temperature means were calculated from the monthly data. Seasonal means were calculated from the monthly data as well, in that the months that make up each season (DJF, MAM, JJA, SON) were extracted and individual files made per season. From the annual and seasonal means, 20-year running climatologies were calculated using CDO using the runmean function. The monthly climatologies were calculated a little differently. Due to it being more complex and requiring more computational power to calculate running climatologies for each month, the monthly climatologies were calculated for each eruption individually instead of for the entire dataset. Climatologies were calculated with respect to a 20-year mean (9 years before, the eruption year, and 10 years after). From the annual seasonal and monthly means and climatologies, annual, seasonal, and monthly temperature anomalies were calculated by subtracting the climatologies from the means. For the purposes of this PhD study, only land temperatures were studied, therefore a land-sea mask was applied to all values, so that only land temperatures were used. Area averages of the anomalies were calculated using the latitudes and longitudes in Table 1. Time was spent learning each new language, and many trials and errors were encountered in correctly processing and analysing the data, and ensuring that the outputs were correct and well represented. Using the aforementioned languages, data were outputted to provide annual, seasonal and monthly anomalies and statistical significance.

Table 1. The latitudes and longitudes of the regions and sub-regions examined in the PhD.

Chapter	Region	Latitude	Longitude
Chapter 2	Southern Hemisphere	-90:0	-180:180
	Northern Hemisphere	0:90	-180:180
Chapter 3	Australia	-50:-5	110:160
	Southern Africa	-40:0	10:40
	Southern South America	-60:0	-85:-30
Chapter 4	South-western Cape	-35:-31	17:20
	Cape South Coast	-35:-33.5	20:27
	Eastern SA	-34:-27	27:33
	Central subcontinent	-33.5:-20	20:27
	North-Eastern SA, South Zim & South Moz	-27:-20	27:36
	Western Subcontinent	-31:-20	12.5:20
Chapter 5	South Western Coast	-35:-29	112:118
	Central Western Coast	-35:-31	118:130
	Central Eastern Coast	-35:-31	132:148
	North Western Coast	-20:-29	112:118
	Eastern Subcontinent	-31:-20	144:148
	Eastern Coast	-35:-20	148:154
	Victoria	-39:-35	136:151
	Tasmania	-43:-39	136:151

3.1.3. Data Analysis

The response to volcanic eruptions is investigated at hemispheric, continental (southern South America, southern Africa and Australia) and sub-regional (southern Africa and Australia) scales. A future detailed investigation on volcanic forcing effects over the Antarctic and sub-Antarctic regions is thus called for. Given relatively similar physical geographic attributes (e.g. latitude, sub-regional climates) between southern Africa and Australia, these continental regions are also investigated at sub-regional levels (Figure 2) at different spatial and temporal scales: 3-year average responses, annual responses, seasonal responses and monthly responses. The Antarctic and sub-Antarctic regions are not included, firstly because there are no direct implications for society living on Antarctica (i.e. on agriculture etc.), and secondly because such high latitude regions deserve attention worthy of the scale of a PhD on its own. Once the eruptions which were significantly impacting the SH were identified, it was decided to focus on these only for the remainder of the study. Patterns and abnormalities are investigated using graphs generated in NCL, and data generated from scripts run in NCL (anomalies, and statistical significance) are examined in Microsoft Excel.

Statistical significance is calculated in NCL, using the Bootstrap method (Efron, 1979), whereby time series are resampled 5000 times, and the 5^{th} and 95^{th} percentiles calculated. If a value falls below or above the 5^{th} and 95^{th} percentile it is considered statistically significant. The ensemble spread (between the 25^{th} and 75^{th} percentiles) is used to test mean ensemble robustness. A Superposed Epoch Analysis is carried out using R, whereby the time series is again resampled 5000 times, and then the 5^{th} and 95^{th} percentiles of the resampled data plotted alongside the average of the actual data around each of the eruptions examined (5 years before and 10 years after the eruptions).

Due to internal climate variability that also modulates climate, the ENSO phase is considered. The ENSO phase simulated by the selection of CMIP5 models is thus calculated in order to see how this would have affected the simulated temperatures. The Nino 3.4 index is used to define the ENSO phases (Trenberth, 1997). A 3-month running mean of sea surface temperature anomalies (calculated in the same way as the near surface temperature anomalies, except that the land-sea mask was used to pull out only ocean temperatures) is calculated for the Pacific region covering 5°N to 5°S and 170°W to 120°W. An event is classified as an El Niño or La Niña if it falls above or below +/-0.4°C respectively.

A superposed epoch analysis (SEA) was calculated in order to determine the likeliness of the temperature responses seen after the volcanic eruptions, occurring randomly (Efron, 1979; Haurwitz and Brier, 1981; Rao *et al.*, 2017). The SEA is calculated for Chapter 2, and incorporates the eight eruptions explored in that chapter (Figure 2; Krakatau, 1883; Tarawera, 1886; Santa Maria, 1902; Colima, 1913; Quizapu, 1932; Agung, 1963; El Chichón, 1982; Pinatubo 1991) as the event years for the SEA. Using annual temperature anomalies, calculated using the method mentioned above, an ensemble of these events was created, and a response matrix generated. The anomalies from the response matrix from five years before the event year and 10 years after the event were plotted. Confidence intervals are then calculated by creating 5000 psuedo event years and pseudo response matrices. The temperature anomalies were selected at random from the original timeseries of temperature anomalies, 5000 times, to create the 5000 pseudo events. Confidence intervals were then calculated from these pseudo events, at the 5^{th} and 95^{th} percentiles. This was plotted with the actual event values. Values that then lie above or below the 95^{th} and 5^{th} percentiles respectively indicated that the chance of such a value/response occurring at random, was unlikely. The results of this are presented in the Supporting Information document of Chapter 2.

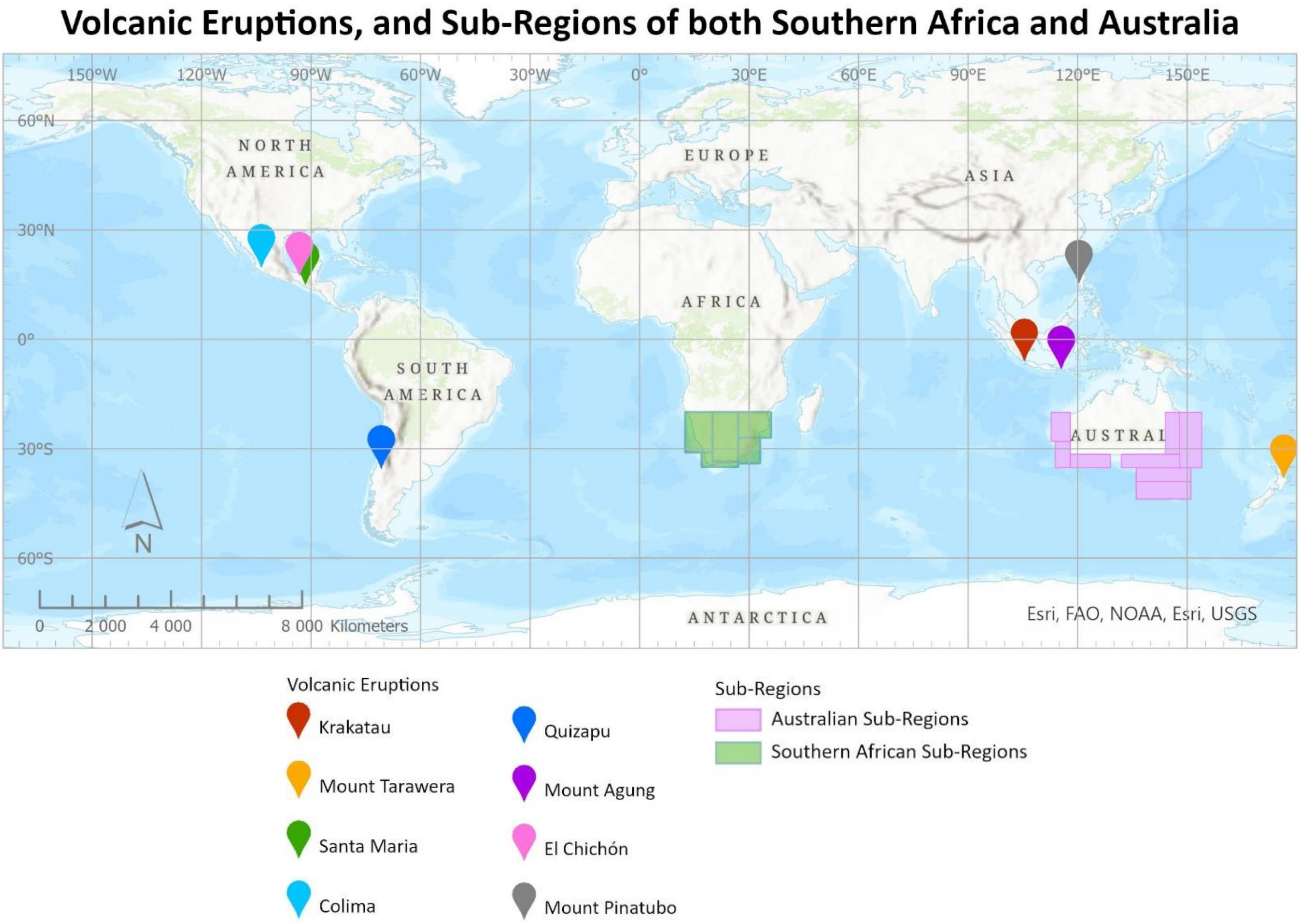

Figure 2. The eight volcanic eruptions analysed in this PhD, as well as the divisions of sub-regions for more detailed investigations over southern Africa and Australia.

3.2. Reanalysis data

The Twentieth Century Reanalysis (V2) (20CRv2) is used in this PhD. The reanalysis data were obtained from the NOAA/OAR/ESRL PSL and is available at: https://psl.noaa.gov/data/gridded/data.20thC_ReanV2.html. Reanalysis, or retrospective analyses, combines data sources in order to estimate weather of the past. Reanalysis data sets use both paleoclimate reconstructions and climate model simulations. The 20CRv2 combines surface observations of synoptic pressure, prescribed sea surface temperatures and sea ice distributions as well as the NCEP Global Forecast System to make their estimations (Compo *et al.*, 2011).

The model incorporates volcanic aerosols which are specified in Saha *et al.* (2010). The purpose of using the reanalysis data in this study is to compare the CMIP5 ensemble simulations to reanalysis ensembles of past climate.

The monthly mean air temperature at 2m was used. Monthly, seasonal and annual means were calculated using the same methodology as the CMIP5 model data, for which the seasonal and annual means were calculated, and monthly, seasonal and annual climatologies calculated with respect to a 20-year running mean. The climatologies were then subtracted from the means to obtain the temperature anomalies. A land-sea mask was applied so that only land temperatures were used. Area averages were also calculated according to the regions mentioned in Table 1, but only for those covered in Chapters 3 and 5. This was due to the decision to add reanalysis data at a later stage of the PhD, when Chapters 2 and 4 had already been published, or accepted as papers by journals. The statistical significance was also calculated in the same way as with the CMIP5 data.

3.3. Instrumental data

Very few instrumental datasets were available for the southern African sub-regions for the time period covered by the PhD. However, temperatures were obtained from Picas and Grab (2020). These were from the Western Cape of South Africa and were used to compare the CMIP5 readings of the Krakatau eruption. The temperatures were station-based temperature readings from the Royal Astronomical Observatory in Cape Town. Results from this comparison are presented in Chapter 4.

Instrumental data for the Australian sub-regions were obtained from National Oceanic and Atmospheric Administration (NOAA)'s National Centers for Environmental Information (NCEI) (https://www.ncdc.noaa.gov/). Monthly average temperature datasets were used for six sub-regions: Hobart (station: Ellerslie Road), Melbourne (station: Regional Office), Perth (station: Regional Office), Adelaide (station: West Terrace), Brisbane (station: Regional Office) and Sydney (station: Observatory Hill). The results are presented in Chapter 5. For both the southern African and Australian regions, annual, seasonal and monthly temperature means were calculated, as was a 20-year running climatology. The climatologies were then subtracted from the means in order to calculate the temperature anomalies.

4. Structure of the Thesis

This thesis comprises six chapters: the current introductory chapter (Chapter 1) and a concluding chapter (Chapter 6), as well as four investigative chapters (Chapters 2-5) which make up the main body of the thesis and are publications which are either published, accepted, under review or ready for submission. Each of the four investigative chapters investigate the response of SH temperatures to volcanic forcing. Chapter 2 studies the average annual, seasonal and monthly terrestrial temperature response of the SH as a whole to volcanic eruptions that occurred between 1850 and 2005 (timeframe covered by the CMIP5 historical experiments). Eruptions were selected based on their location (either tropical or SH eruptions) and their magnitude (VEI ≥ 5). Agung (VEI 4) was also included, due to the amount of SO_2 that reached the lower stratosphere (7.5Tg). Responses to eight eruptions are thus studied in Chapter 2 (Krakatau, 1883; Tarawera, 1886; Santa Maria, 1902; Colima, 1913; Quizapu, 1932; Agung, 1963; El Chichón, 1982; Pinatubo 1991). The eruptions which seem to cause a significant temperature response in the SH are identified. These responses are then also compared to NH responses. Chapter 3 further investigates the eruptions which were shown to cause a significant SH temperature response in Chapter 2, by observing the responses over each continental landmass in the SH (southern South America, southern Africa and Australia), and provides a continental comparison of the strength and seasonality of these responses. Chapter 4 then focuses on more local (sub-regional) temperature responses over the southern African region, and compares the strengths and seasonal responses within various sub-regions over the sub-continent. The final investigative chapter, Chapter 5, similarly examines sub-regional responses over Australia. These responses are additionally compared with instrumental station based and reanalysis climate data, where available, primarily to test the validity of the CMIP5 outputs. Chapter 6 provides a conclusion of the main findings from each investigative chapter and draws these together into some overarching conclusions. Each of these chapters is formatted according to journal specific instructions to authors, hence there is some inconsistency in the formatting and referencing styles, and image and table numbering used throughout this thesis. Each chapter also has its own reference list, and supplementary file where applicable.

5. References

Ammann CM, Joos F, Schimel DS, Otto-Bliesner BL, Tomas RA. 2007. Solar influence on climate during the past millennium: Results from transient simulations with the NCAR Climate System Model. Proceedings of the National Academy of Sciences, 104(10): 3713–3718. https://doi.org/10.1073/pnas.0605064103.

Barnes EA, Solomon S, Polvani LM. 2016. Robust wind and precipitation responses to the Mount Pinatubo eruption, as simulated in the CMIP5 models. Journal of Climate, 29(13): 4763–4778. https://doi.org/10.1175/JCLI-D-15-0658.1.

Bègue N, Vignelles D, Berthet G, Portafaix T, Payen G, Jégou F, Benchérif H, Jumelet J, Vernier J-P, Lurton T, Renard J-B, Clarisse L, Duverger V, Posny F, Metzger J-M, Godin-Beekmann S. 2017. Long-range isentropic transport of stratospheric aerosols over Southern Hemisphere following the Calbuco eruption in April 2015. preprint. Aerosols/Field Measurements/Stratosphere/Physics (physical properties and processes).

Brönnimann S, Allan R, Ashcroft L, Baer S, Barriendos M, Brázdil R, Brugnara Y, Brunet M, Brunetti M, Chimani B, Cornes R, Domínguez-Castro F, Filipiak J, Founda D, Herrera RG, Gergis J, Grab S, Hannak L, Huhtamaa H, Jacobsen KS, Jones P, Jourdain S, Kiss A, Lin KE, Lorrey A, Lundstad E, Luterbacher J, Mauelshagen F, Maugeri M, Maughan N, Moberg A, Neukom R, Nicholson S, Noone S, Nordli Ø, Ólafsdóttir KB, Pearce PR, Pfister L, Pribyl K, Przybylak R, Pudmenzky C, Rasol D, Reichenbach D, Řezníčková L, Rodrigo FS, Rohr C, Skrynyk O, Slonosky V, Thorne P, Valente MA, Vaquero JM, Westcottt NE, Williamson F, Wyszyński P. 2019a. Unlocking Pre-1850 Instrumental Meteorological Records: A Global Inventory. Bulletin of the American Meteorological Society, 100(12): ES389–ES413. https://doi.org/10.1175/BAMS-D-19-0040.1.

Brönnimann S, Franke J, Nussbaumer SU, Zumbühl HJ, Steiner D, Trachsel M, Hegerl GC, Schurer A, Worni M, Malik A, Flückiger J, Raible CC. 2019b. Last phase of the Little Ice Age forced by volcanic eruptions. Nature Geoscience. https://doi.org/10.1038/s41561-019-0402-y.

Chylek P, Folland C, Klett JD, Dubey MK. 2020. CMIP5 climate models overestimate cooling by volcanic aerosols. Geophysical Research Letters, 47(3). https://doi.org/10.1029/2020GL087047.

Cole-Dai J. 2010. Volcanoes and climate. Wiley Interdisciplinary Reviews: Climate Change, 1(6): 824–839. https://doi.org/10.1002/wcc.76.

Colose CM, LeGrande AN, Vuille M. 2015. The influence of tropical volcanic eruptions on the climate of South America during the last millennium. Climate of the Past, 11: 3375–3424. https://doi.org/10.5194/cpd-11-3375-2015.

Compo GP, Whitaker JS, Sardeshmukh PD, Matsui N, Allan RJ, Yin X, Gleason BE, Vose RS, Rutledge G, Bessemoulin P, Brönnimann S, Brunet M, Crouthamel RI, Grant AN, Groisman PY, Jones PD, Kruk MC, Kruger AC, Marshall GJ, Maugeri M, Mok HY, Nordli Ø, Ross TF, Trigo RM, Wang XL, Woodruff SD, Worley SJ. 2011. The Twentieth Century Reanalysis Project. Quarterly Journal of the Royal Meteorological Society. John Wiley & Sons, Ltd, 137(654): 1–28. https://doi.org/10.1002/qj.776.

Croll J. 1890. Climate and Time in Their Geological Relations: A Theory of Secular Changes of the Earth’s Climate. Appleton.

Crowley T, Zielinsk G, Vinther BM, Udisti R, Kreutz K, Cole-Dai J, Castellano E. 2008. Volcanism and the Little Ice Age. PAGES News, 16(2): 22–23.

Cui X, Gao Y, Sun J. 2014. The response of the East Asian summer monsoon to strong tropical volcanic eruptions. Advances in Atmospheric Sciences, 31(6): 1245–1255. https://doi.org/10.1007/s00376-014-3239-8.

Driscoll S, Bozzo A, Gray LJ, Robock A, Stenchikov G. 2012. Coupled Model Intercomparison Project 5 (CMIP5) simulations of climate following volcanic eruptions. Journal of Geophysical Research: Atmospheres, 117(D17): D17105. https://doi.org/10.1029/2012JD017607.

Dunwiddie PW, LaMarche VC. 1980. A climatically responsive tree-ring record from Widdringtonia cedarbergensis, Cape Province, South Africa. Nature, 286(5775): 796–797. https://doi.org/10.1038/286796a0.

Efron B. 1979. Bootstrap Methods: another look at the Jackknife. The Annals of Statistics, 7(1): 1–26. https://doi.org/10.1214/aos/1176344552.

Esper J, Schneider L, Krusic PJ, Luterbacher J, Büntgen U, Timonen M, Sirocko F, Zorita E. 2013. European summer temperature response to annually dated volcanic eruptions over the past nine centuries. Bulletin of Volcanology, 75(7): 736. https://doi.org/10.1007/s00445-013-0736-z.

Gallego D, Ribera P, Garcia-Herrera R, Hernandez E, Gimeno L. 2005. A new look for the Southern Hemisphere jet stream. Climate Dynamics, 24(6): 607–621. https://doi.org/10.1007/s00382-005-0006-7.

Gilliland RL. 1982. Solar, volcanic, and CO2 forcing of recent climatic changes. Climatic Change, 4(2): 111–131. https://doi.org/10.1007/BF02423387.

Grab SW, Nash DJ. 2010. Documentary evidence of climate variability during cold seasons in Lesotho, southern Africa, 1833-1900. Climate Dynamics, 34(4): 473–499.

Haurwitz MW, Brier GW. 1981. A critique of the Superposed Epoch Analysis Method: Its application to solar–weather relations. Monthly Weather Review, 109(10): 2074–2079. https://doi.org/10.1175/1520-0493(1981)109<2074:ACOTSE>2.0.CO;2.

Hopcroft PO, Kandlbauer J, Valdes PJ, Sparks RSJ. 2018. Reduced cooling following future volcanic eruptions. Climate Dynamics, 51(4): 1449–1463. https://doi.org/10.1007/s00382-017-3964-7.

Hua W, Dai A, Zhou L, Qin M, Chen H. 2019. An Externally Forced Decadal Rainfall Seesaw Pattern Over the Sahel and Southeast Amazon. Geophysical Research Letters, 46(2): 923–932. https://doi.org/10.1029/2018GL081406.

Hudson RD. 2012. Measurements of the movement of the jet streams at mid-latitudes, in the Northern and Southern Hemispheres, 1979 to 2010.

Atmospheric Chemistry and Physics, 12(16): 7797–7808. https://doi.org/10.5194/acp-12-7797-2012.

Hulme M. 2015. (STILL) DISAGREEING ABOUT CLIMATE CHANGE: WHICH WAY FORWARD?: with Mike Hulme, "(Still) Disagreeing about Climate Change: Which Way Forward?"; Annick de Witt, "Climate Change and the Clash of Worldviews: An Explo. Zygon®, 50(4): 893–905. https://doi.org/10.1111/zygo.12212.

Humphreys WJ. 1913. Volcanic dust and other factors in the production of climatic changes, and their possible relation to ice ages. Journal of the Franklin Institute, 176(2): 131–160. https://doi.org/10.1016/S0016-0032(13)91294-1.

Imbrie J, Imbrie KP. 1986. Ice Ages: Solving the Mystery. Harvard University Press.

Jolley C, Rickards L. 2019. Contesting coal and climate change using scale: emergent topologies in the Adani mine controversy. Geographical Research, 19.

Jones PD, Moberg A, Osborn TJ, Briffa KR. 2003. Surface climate responses to explosive volcanic eruptions seen in long European temperature records and mid-to-high latitude tree-ring density around the Northern Hemisphere. Washington DC American Geophysical Union Geophysical Monograph Series, 139: 239–254. https://doi.org/10.1029/139GM15.

Karpechko AY, Gillett NP, Dall'Amico M, Gray LJ. 2010. Southern Hemisphere atmospheric circulation response to the El Chichón and Pinatubo eruptions in coupled climate models. Quarterly Journal of the Royal Meteorological Society, 136(652): 1813–1822. https://doi.org/10.1002/qj.683.

Ke F, Hui L. 2013. Evaluation of Atmospheric Circulation in the Southern Hemisphere in 20CRv2. Atmospheric and Oceanic Science Letters, 6(5): 337–342. https://doi.org/10.1080/16742834.2013.11447104.

Kidston J, Scaife AA, Hardiman SC, Mitchell DM, Butchart N, Baldwin MP, Gray LJ. 2015. Stratospheric influence on tropospheric jet streams, storm tracks and surface weather. Nature Geoscience, 8(6): 433–440. https://doi.org/10.1038/ngeo2424.

Kremser S, Thomason LW, von Hobe M, Hermann M, Deshler T, Timmreck C, Toohey M, Stenke A, Schwarz JP, Weigel R, Fueglistaler S, Prata FJ, Vernier J-P, Schlager H, Barnes JE, Antuña-Marrero J-C, Fairlie D, Palm M, Mahieu E, Notholt J, Rex M, Bingen C, Vanhellemont F, Bourassa A, Plane JMC, Klocke D, Carn SA, Clarisse L, Trickl T, Neely R, James AD, Rieger L, Wilson JC, Meland B. 2016. Stratospheric aerosol-Observations, processes, and impact on climate: Stratospheric Aerosol. Reviews of Geophysics, 54(2): 278–335. https://doi.org/10.1002/2015RG000511.

Krishnamohan K-PS-P, Bala G, Cao L, Duan L, Caldeira K. 2019. Climate system response to stratospheric sulfate aerosols: sensitivity to altitude of aerosol layer. Earth System Dynamics, 10(4): 885–900. https://doi.org/10.5194/esd-10-885-2019.

León B. 2011. Portrayal of scientific controversy on climate change. A study of the coverage of the Copenhagen summit in the Spanish press. , 19.

Maher N, McGregor S, England MH, Gupta AS. 2015. Effects of volcanism on tropical variability: EFFECTS OF VOLCANISM. Geophysical Research Letters, 42(14): 6024–6033. https://doi.org/10.1002/2015GL064751.

Malherbe J, Landman WA, Engelbrecht FA. 2014. The bi-decadal rainfall cycle, Southern Annular Mode and tropical cyclones over the Limpopo River Basin, southern Africa. Climate Dynamics, 42(11–12): 3121–3138. https://doi.org/10.1007/s00382-013-2027-y.

Man W, Zhou T, Jungclaus JH. 2014. Effects of large volcanic eruptions on global summer climate and East Asian Monsoon changes during the Last Millennium: analysis of MPI-ESM simulations. Journal of Climate, 27(19): 7394–7409. https://doi.org/10.1175/JCLI-D-13-00739.1.

Mann ME, Cane MA, Zebiak SE, Clement A. 2005. Volcanic and Solar Forcing of the Tropical Pacific over the Past 1000 Years. Journal of Climate, 18(3): 447–456. https://doi.org/10.1175/JCLI-3276.1.

Mass CF, Portman DA. 1989. Major volcanic eruptions and climate: a critical evaluation. Journal of Climate, 2(6): 566–593. https://doi.org/10.1175/1520-0442(1989)002<0566:MVEACA>2.0.CO;2.

McCormick MP, Thomason LW, Trepte CR. 1995. Atmospheric effects of the Mt Pinatubo eruption. Nature, 373: 399–404. https://doi.org/10.1038/373399a0.

McGraw MC, Barnes EA, Deser C. 2016. Reconciling the observed and modeled Southern Hemisphere circulation response to volcanic eruptions: Reconciling SH Response to Volcanoes. Geophysical Research Letters, 43(13): 7259–7266. https://doi.org/10.1002/2016GL069835.

Ménégoz M, Bilbao R, Bellprat O, Guemas V, Doblas-Reyes FJ. 2018. Forecasting the climate response to volcanic eruptions: prediction skill related to stratospheric aerosol forcing. Environmental Research Letters, 13(6): 064022. https://doi.org/10.1088/1748-9326/aac4db.

Monerie P-A, Moine M-P, Terray L, Valcke S. 2017. Quantifying the impact of early 21st century volcanic eruptions on global-mean surface temperature. Environmental Research Letters, 12(5): 054010. https://doi.org/10.1088/1748-9326/aa6cb5.

Neukom R, Gergis J, Karoly DJ, Wanner H, Curran M, Elbert J, González-Rouco F, Linsley BK, Moy AD, Mundo I, Raible CC, Steig EJ, van Ommen T, Vance T, Villalba R, Zinke J, Frank D. 2014. Inter-hemispheric temperature variability over the past millennium. Nature Climate Change, 4(5): 362–367. https://doi.org/10.1038/nclimate2174.

Oman L, Robock A, Stenchikov G, Schmidt GA, Ruedy R. 2005. Climatic response to high-latitude volcanic eruptions. Journal of Geophysical Research: Atmospheres, 110(D13): D13103. https://doi.org/10.1029/2004JD005487.

Oppenheimer C. 2003. Climatic, environmental and human consequences of the largest known historic eruption: Tambora volcano (Indonesia) 1815. Progress in Physical Geography, 27(2): 230–259. https://doi.org/10.1191/0309133303pp379ra.

Paik S, Min S-K. 2018. Assessing the Impact of Volcanic Eruptions on Climate Extremes Using CMIP5 Models. Journal of Climate, 31(14): 5333–5349. https://doi.org/10.1175/JCLI-D-17-0651.1.

Pausata FSR, Karamperidou C, Caballero R, Battisti DS. 2016. ENSO response to high-latitude volcanic eruptions in the Northern Hemisphere: The role of the initial conditions: ENSO Response to High-Latitude Volcanic Eruptions. Geophysical Research Letters, 43(16): 8694–8702. https://doi.org/10.1002/2016GL069575.

Pausata FSR, Zanchettin D, Karamperidou C, Caballero R, Battisti DS. 2020. ITCZ shift and extratropical teleconnections drive ENSO response to volcanic eruptions. Science Advances, 6.

Pepler AS, Fong J, Alexander LV. 2016. Australian east coast mid-latitude cyclones in the 20th Century Reanalysis ensemble. International Journal of Climatology, 37(4): 2187–2192. https://doi.org/10.1002/joc.4812.

Perlwitz J, Graf H-F. 1995. The statistical connection between tropospheric and stratospheric circulation of the northern hemisphere in winter. Journal of Climate, 8: 2281–2295.

Picas J, Grab S. 2020. Potential impacts of major nineteenth century volcanic eruptions on temperature over Cape Town, South Africa: 1834–1899. Climatic Change. https://doi.org/10.1007/s10584-020-02678-6.

Raible CC, Brönnimann S, Auchmann R, Brohan P, Frölicher TL, Graf H-F, Jones P, Luterbacher J, Muthers S, Neukom R, Robock A, Self S, Sudrajat A, Timmreck C, Wegmann M. 2016. Tambora 1815 as a test case for high impact volcanic eruptions: Earth system effects. Wiley Interdisciplinary Reviews: Climate Change, 7(4): 569–589. https://doi.org/10.1002/wcc.407.

Rao MP, Cook BI, Cook ER, D’Arrigo RD, Krusic PJ, Anchukaitis KJ, LeGrande AN, Buckley BM, Davi NK, Leland C, Griffin KL. 2017. European and Mediterranean hydroclimate responses to tropical volcanic forcing over the last millennium. Geophysical Research Letters, 44(10): 5104–5112. https://doi.org/10.1002/2017GL073057.

Robock A. 2000. Volcanic eruptions and climate. Reviews of Geophysics, 38(2): 191–219. https://doi.org/10.1029/1998RG000054.

Robock A, Adams T, Moore M, Oman L, Stenchikov G. 2007. Southern Hemisphere atmospheric circulation effects of the 1991 Mount Pinatubo eruption. Geophysical Research Letters, 34(23): L23710. https://doi.org/10.1029/2007GL031403.

Roscoe HK, Haigh JD. 2007. Influences of ozone depletion, the solar cycle and the QBO on the Southern Annular Mode. Quarterly Journal of the Royal Meteorological Society, 133(628): 1855–1864. https://doi.org/10.1002/qj.153.

Santer BD, Painter JF, Bonfils C, Mears CA, Solomon S, Wigley TML, Gleckler PJ, Schmidt GA, Doutriaux C, Gillett NP, Taylor KE, Thorne PW, Wentz FJ. 2013. Human and natural influences on the changing thermal structure of the atmosphere. Proceedings of the National Academy of Sciences, 110(43): 17235–17240. https://doi.org/10.1073/pnas.1305332110.

Saha S, Moorthi S, Pan H-L, Wu X, Wang J, Nadiga S, Tripp P, Kistler R, Woollen J, Behringer D, Liu H, Stokes D, Grumbine R, Gayno G, Wang J, Hou Y-T, Chuang H, Juang H-MH, Sela J, Iredell M, Treadon R, Kleist D, Delst PV, Keyser D, Derber J, Ek M, Meng J, Wei H, Yang R, Lord S, Dool H van den, Kumar A, Wang W, Long C, Chelliah M, Xue Y, Huang B, Schemm J-K, Ebisuzaki W, Lin R, Xie P, Chen M, Zhou S, Higgins W, Zou C-Z, Liu Q, Chen Y, Han Y, Cucurull L, Reynolds RW, Rutledge G, Goldberg M. 2010. The NCEP Climate Forecast System Reanalysis. Bulletin of the American Meteorological Society. American Meteorological Society, 91(8): 1015–1058. https://doi.org/10.1175/2010BAMS3001.1.

Sato M, Hansen JE, McCormick MP, Pollack JB. 1993. Stratospheric aerosol optical depths, 1850–1990. Journal of Geophysical Research, 98(D12): 22987. https://doi.org/10.1029/93JD02553.

Schneider DP, Ammann CM, Otto-Bliesner BL, Kaufman DS. 2009. Climate response to large, high-latitude and low-latitude volcanic eruptions in the Community Climate System Model. Journal of Geophysical Research: Atmospheres, 114(D15): D15101. https://doi.org/10.1029/2008JD011222.

Self S, Rampino MR, Zhao J, Katz MG. 1997. Volcanic aerosol perturbations and strong El Niño events: No general correlation. Geophysical Research Letters, 24(10): 1247–1250. https://doi.org/10.1029/97GL01127.

Shulmeister J, Goodwin I, Renwick J, Harle K, Armand L, McGlone MS, Cook E, Dodson J, Hesse PP, Mayewski P, Curran M. 2004. The Southern Hemisphere westerlies in the Australasian sector over the last glacial cycle: a synthesis. Quaternary International, 118–119: 23–53. https://doi.org/10.1016/S1040-6182(03)00129-0.

Sigl M, Winstrup M, McConnell JR, Welten KC, Plunkett G, Ludlow F, Büntgen U, Caffee M, Chellman N, Dahl-Jensen D, Fischer H, Kipfstuhl S, Kostick C, Maselli OJ, Mekhaldi F, Mulvaney R, Muscheler R, Pasteris DR, Pilcher JR, Salzer M, Schüpbach S, Steffensen JP, Vinther BM, Woodruff TE. 2015. Timing and climate forcing of volcanic eruptions for the past 2,500 years. Nature, 523(7562): 543–549. https://doi.org/10.1038/nature14565.

Sjolte J, Sturm C, Adolphi F, Vinther BM, Werner M, Lohmann G, Muscheler R. 2018. Solar and volcanic forcing of North Atlantic climate inferred from a process-based reconstruction. Climate of the Past, 14(8): 1179–1194. https://doi.org/10.5194/cp-14-1179-2018.

Slivinski LC, Compo GP, Sardeshmukh PD, Whitaker JS, McColl C, Allan RJ, Brohan P, Yin X, Smith CA, Spencer LJ, Vose RS, Rohrer M, Conroy RP, Schuster DC, Kennedy JJ, Ashcroft L, Brönnimann S, Brunet M, Camuffo D, Cornes R, Cram TA, Domínguez-Castro F, Freeman JE, Gergis J, Hawkins E, Jones PD, Kubota H, Lee TC, Lorrey AM, Luterbacher J, Mock CJ, Przybylak RK, Pudmenzky C, Slonosky VC, Tinz B, Trewin B, Wang XL, Wilkinson C, Wood K, Wyszyński P. 2021. An Evaluation of the Performance of the Twentieth

Century Reanalysis Version 3. Journal of Climate. American Meteorological Society, 34(4): 1417–1438. https://doi.org/10.1175/JCLI-D-20-0505.1.

Stenchikov G, Robock A, Ramaswamy V, Schwarzkopf MD, Hamilton K, Ramachandran S. 2002. Arctic Oscillation response to the 1991 Mount Pinatubo eruption: Effects of volcanic aerosols and ozone depletion. Journal of Geophysical Research: Atmospheres.

Stevenson S, Fasullo JT, Otto-Bliesner BL, Tomas RA, Gao C. 2017. Role of eruption season in reconciling model and proxy responses to tropical volcanism. Proceedings of the National Academy of Sciences, 114(8): 1822–1826. https://doi.org/10.1073/pnas.1612505114.

Sun W, Wang B, Liu J, Chen D, Gao C, Ning L, Chen L. 2019. How northern high-latitude volcanic eruptions in different seasons affect ENSO. Journal of Climate, 32(11): 3245–3262. https://doi.org/10.1175/JCLI-D-18-0290.1.

Taylor KE, Stouffer RJ, Meehl GA. 2012. An overview of CMIP5 and the experiment design. Bulletin of the American Meteorological Society, 93(4): 485–498. https://doi.org/10.1175/BAMS-D-11-00094.1.

Thompson DWJ, Wallace JM, Jones PD, Kennedy JJ. 2009. Identifying signatures of natural climate variability in time series of global-mean surface temperature: methodology and insights. Journal of Climate, 22(22): 6120–6141. https://doi.org/10.1175/2009JCLI3089.1.

Timmreck C. 2012. Modeling the climatic effects of large explosive volcanic eruptions. WIREs: Climate Change, 3(6): 545–564. https://doi.org/10.1002/wcc.192.

Timmreck C. 2018. Climatic effects of large volcanic eruptions. Habilitation Thesis, Hamburg, Universität Hamburg.

Toohey M, Krüger K, Schmidt H, Timmreck C, Sigl M, Stoffel M, Wilson R. 2019. Disproportionately strong climate forcing from extratropical explosive volcanic eruptions. Nature Geoscience, 12(2): 100–107. https://doi.org/10.1038/s41561-018-0286-2.

Toohey M, Krüger K, Sigl M, Stordal F, Svensen H. 2016. Climatic and societal impacts of a volcanic double event at the dawn of the Middle Ages. Climatic Change, 136(3–4): 401–412. https://doi.org/10.1007/s10584-016-1648-7.

Trenberth KE. 1997. The Definition of El Niño. Bulletin of the American Meteorological Society. American Meteorological Society, 78(12): 2771–2778. https://doi.org/10.1175/1520-0477(1997)078<2771:TDOENO>2.0.CO;2.

Tyson PD, Tyson PD, Preston-Whyte RA. 2000. The Weather and Climate of Southern Africa. Oxford University Press.

van Geel B, Raspopov OM, Renssen H, van der Plicht J, Dergachev VA, Meijer HAJ. 1999. The role of solar forcing upon climate change. Quaternary Science Reviews, 18(3): 331–338. https://doi.org/10.1016/S0277-3791(98)00088-2.

Wilmes SB, Raible CC, Stocker TF. 2012. Climate variability of the mid- and high-latitudes of the Southern Hemisphere in ensemble simulations from 1500 to 2000 AD. Climate of the Past, 8(1): 373–390. https://doi.org/10.5194/cp-8-373-2012.

Xia L, von Storch H, Feser F, Wu J. 2015. A study of quasi-millennial extratropical winter cyclone activity over the Southern Hemisphere. Climate Dynamics, 47(7–8): 2121–2138. https://doi.org/10.1007/s00382-015-2954-x.

Xing C, Liu F, Wang B, Chen D, Liu J, Liu B. 2020. Boreal Winter Surface Air Temperature Responses to Large Tropical Volcanic Eruptions in CMIP5 Models. Journal of Climate. American Meteorological Society, 33(6): 2407–2426. https://doi.org/10.1175/JCLI-D-19-0186.1.

Yan Q, Zhang Z, Wang H. 2018. Divergent responses of tropical cyclone genesis factors to strong volcanic eruptions at different latitudes. Climate Dynamics, 50(5–6): 2121–2136. https://doi.org/10.1007/s00382-017-3739-1.

Yang J, Xiao C. 2017. The evolution and volcanic forcing of the southern annular mode during the past 300 years. International Journal of Climatology, 38(4): 1706–1717. https://doi.org/10.1002/joc.5290.

Zambri B, LeGrande AN, Robock A, Slawinska J. 2017. Northern Hemisphere winter warming and summer monsoon reduction after volcanic eruptions over the last millennium. Journal of Geophysical Research: Atmospheres, 122(15): 7971–7989. https://doi.org/10.1002/2017JD026728.

Zambri B, Robock A. 2016. Winter warming and summer monsoon reduction after volcanic eruptions in Coupled Model Intercomparison Project 5 (CMIP5) simulations. Geophysical Research Letters, 43(20): 10,920-10,928. https://doi.org/10.1002/2016GL070460.

Zanchettin D, Bothe O, Timmreck C, Bader J, Beitsch A, Graf H-F, Notz D, Jungclaus JH. 2014. Inter-hemispheric asymmetry in the sea-ice response to volcanic forcing simulated by MPI-ESM (COSMOS-Mill). Earth System Dynamics, 5(1): 223–242. https://doi.org/10.5194/esd-5-223-2014.

Zanchettin D, Khodri M, Timmreck C, Toohey M, Schmidt A, Gerber EP, Hegerl G, Robock A, Pausata FSR, Ball WT, Bauer SE, Bekki S, Dhomse SS, LeGrande AN, Mann GW, Marshall L, Mills M, Marchand M, Niemeier U, Poulain V, Rozanov E, Rubino A, Stenke A, Tsigaridis K, Tummon F. 2016. The Model Intercomparison Project on the climatic response to Volcanic forcing (VolMIP): experimental design and forcing input data for CMIP6. Geosci. Model Dev., 19.

Zanchettin D, Timmreck C, Toohey M, Jungclaus JH, Bittner M, Lorenz SJ, Rubino A. 2019. Clarifying the relative role of forcing uncertainties and initial-condition unknowns in spreading the climate response to volcanic eruptions. Geophysical Research Letters, 46(3): 1602–1611. https://doi.org/10.1029/2018GL081018.

Zhang Q, Körnich H, Holmgren K. 2013. How well do reanalyses represent the southern African precipitation? Climate Dynamics, 40(3–4): 951–962. https://doi.org/10.1007/s00382-012-1423-z.

Zuo M, Man W, Zhou T, Guo Z. 2018. Different impacts of Northern, Tropical, and Southern Volcanic Eruptions on the Tropical Pacific SST in the Last Millennium. Journal of Climate, 31(17): 6729–6744. https://doi.org/10.1175/JCLI-D-17-0571.1.

Chapter Two: Major Volcanic Eruptions and their Impacts on Southern Hemisphere Temperatures during the late-19th and 20th Centuries, as Simulated by CMIP5 Models
(Published in Geophysical Research Letters)

Harvey PJ, Grab SW, Malherbe J. 2020. Major volcanic eruptions and their impacts on Southern Hemisphere temperatures during the late 19th and 20th centuries, as simulated by CMIP5 models. *Geophysical Research Letters*, 47(14). https://doi.org/10.1029/2020GL087792

Published paper in Appendix A

Abstract

While much is known about the impacts of volcanic forcing on Northern Hemisphere (NH) climates, knowledge about Southern Hemisphere (SH) responses is still in its infancy. Volcanic impacts on SH temperatures following eight major late-19th and 20th century eruptions (Krakatau, 1883; Tarawera, 1886; Santa Maria, 1902; Colima, 1913; Quizapu, 1932; Agung, 1963; El Chichón, 1982; Pinatubo, 1991) is examined. CMIP5 historical simulations are used to analyse near-surface land temperatures. This chapter demonstrates that four of the eight major eruptions (Krakatau, Santa Maria, Agung and Pinatubo) significantly lowered mean SH temperatures; these tropical eruptions emitted at least 3.8 Tg of SO_2 into the stratosphere. SH responses typically lagged NH temperature cooling responses by one-two months, excluding Pinatubo. Responses differ spatially and temporally with each eruption, highlighting the importance of investigating events individually. Overall, relatively strong (between -0.19°C and -0.36°C) austral autumn/winter SH cooling is simulated.

Plain Language Summary

Climate is affected by major volcanic eruptions if the eruption emits large amounts of SO_2 into the stratosphere. Volcanic forcing generally causes temperatures to cool, but in some instances, temperatures rise. Many studies have identified Northern Hemisphere (NH) climatic responses to volcanic forcing, but the Southern Hemisphere (SH) has received less attention in this regard. Hence this investigation on SH climatic responses to volcanic forcing. Temperature responses to eight eruptions that occurred during the late-19th and 20th centuries are established. SH and NH responses to these eruptions are compared. Using climate models from CMIP5 experiments, it is found that four of the eight major eruptions significantly cooled SH temperatures. These four eruptions emitted 3.8 Tg or more of SO_2 into the stratosphere and occurred in the tropics. It is found that responses were not uniform, but differed according to location and time. A generally strong austral autumn/winter cooling response occurs over SH continental regions. Following the four major eruptions of Krakatau, Santa Maria, Agung and Pinatubo,

SH temperatures typically responded later than temperatures in the NH. Understanding the impact that major volcanic eruptions have on regional climates is important for establishing early warning systems, particularly where climate-sensitive bio-systems and agriculture are influenced by such events.

1. Introduction

Major volcanic eruptions can significantly influence climate (Man *et al*., 2014; Neukom *et al*., 2014; Sigl *et al*., 2015) if a substantial quantity of SO_2 (sulphur dioxide) is emitted into the lower stratosphere. The SO_2 converts to sulfuric acid or sulphate aerosols which can be globally dispersed within a few weeks (Cole-Dai, 2010; Robock, 2000) altering radiation budgets through increasing the scattering and absorption of incoming solar radiation (Kremser *et al*., 2016; Liu *et al*., 2018; Textor *et al*., 2004). Major tropical eruptions can impact climates globally (e.g. Tambora, 1815; Krakatau, 1883; Pinatubo, 1991) through the effective upwelling of the Brewer-Dobson circulation which facilitates poleward transportation of stratospheric aerosols in both hemispheres more efficiently than eruptions occurring at high latitudes (e.g. Laki, 1783; Katmai, 1912) (Young *et al*., 2011). Mid-high latitude eruptions have less-severe, shorter-term impacts that are restricted to the hemisphere in which the eruption occurred (Oman *et al*., 2005; Schneider *et al*., 2009; Timmreck, 2012, 2018).

Findings typically indicate that mean annual global temperatures may decrease for two-three years after a major eruption, from as little as a fraction of a degree (Kremser *et al*., 2016) to as much as 0.4°C after the Pinatubo eruption (Kremser *et al*., 2016; Thompson *et al*., 2009). Northern Hemisphere (NH) temperature responses to volcanic forcing has received substantial research attention (e.g. Esper *et al*., 2013; Oman *et al*., 2005; Toohey *et al*., 2019; Zambri, *et al*., 2017). Establishing temperature responses across various sub-regions of the NH has received much focus, such as over North America (Lough & Fritts, 1987), Europe (e.g. Esper *et al*., 2013; Rao *et al*., 2017) and Asia (e.g. Zhang *et al*., 2013). Although general trends indicate cooling throughout the NH, mid-high latitudes often experience winter warming (Robock, 2000; Timmreck, 2012; Zambri *et al*., 2017). However, winter warming is not coincident after every major eruption (Schneider *et al*., 2009), and in some cases summer warming occurs (Stothers, 1999), suggesting that temperature responses are spatially diverse and disparate following such eruptions (Zanchettin *et al*., 2019).

In contrast, knowledge on volcanic forcing impacts on Southern Hemisphere (SH) climates is in its infancy. Nonetheless, it is understood that asymmetric results are expected between hemispheres (Zanchettin *et al*., 2014); for instance, studies show that volcanic forcing impacts have a generally weaker impact on SH than NH climate (especially temperature) (Man *et al*., 2014; Monerie *et al*., 2017; Neukom *et al*., 2014). SH climate is potentially influenced more by internal than external variability (Neukom *et al*., 2014; Wilmes *et al*., 2012). Mean SH temperature departures are only 0.10-0.37°C below normal for one-two years after major eruptions (Mass & Portman, 1989; Neukom *et al*., 2014; Robock & Mao, 1995). However, temperatures at individual locations in the SH can reduce by as much as 2-3°C (Wilmes *et al*., 2012). At regional scales, widespread cooling is identified for South America (Colose *et al*., 2015; Graf *et al*. 1993), significant cooling occurs over southern Africa (Man *et al*., 2014), and rapid negative temperature departures (-0.3°C to -0.4°C) prevail over New Zealand (Salinger, 1998). However, climatic responses over the SH (as is the case for the NH) are strongly dependent on the volcanic event itself (e.g. season, location, magnitude, aerosol altitude) (e.g. Colose *et al*., 2015; Krishnamohan *et al*., 2019; Oman *et al*., 2005; Stevenson *et al*., 2017; Sun *et al*., 2019; Zanchettin *et al*., 2014; Zuo *et al*., 2018).

Climate models are now widely used to provide expansive good resolution depictions of climatic responses to major volcanic eruptions, and can adequately simulate associated SH circulation (Hopcroft *et al*., 2018; Hua *et al*., 2019; McGraw *et al*., 2016; Raible *et al*., 2016; Toohey *et al*., 2019). Therefore, given the largely NH focus thus far, the aim is to use the Coupled Model Intercomparison Project, phase 5 (CMIP5) (Taylor *et al*., 2012), to better quantify temperature responses across the SH following the major eruptions of Krakatau (1883), Tarawera (1886), Santa Maria (1902), Colima (1913), Quizapu (1932), Agung (1963), El Chichón (1982) and Pinatubo (1991). More specifically, SH temperature response times are investigated and the magnitude of temperature departures are compared to those for the NH. While latitudinal variability of such responses is considered, longitudinal (i.e. inter-continental) differences will be discussed in a subsequent paper.

2. Models and Data

Historical experiments from CMIP5 (Taylor *et al*., 2012) are used in this study and selected based on how well they simulated a lower stratosphere temperature response to volcanic forcing (after Barnes *et al*., 2016). The first three realizations (r1, r2 and r3; which represent different initial conditions) are used for each model; apart from the MIROC-ESM-CHEM model, for which only r1 is available. The first physics version is used for each model. Given differences in the ways in which aerosols are calculated in the GISS-E2_R model, both physics-version 1 (p1) and 3 (p3) are used. While aerosols in p1 are prescribed, those in p3 are calculated in the model simulation. An ensemble of 31 simulations are analysed (Table S1). Different variations of the historical experiments (covering the period 1850-2005) are explored to establish any 'unusual' anomalies (see Text S1).

Given that volcanic forcing was not uniquely prescribed for CMIP5, the schemes used are according to either Ammann *et al*. (2007) or Sato *et al*. (1993), except for the MRI_CGCM3 model which computed stratospheric aerosols interactively (comparison in Text S2). While all models used had performed the historical experiments, not all had contributed to the Historical Nat or Historical Misc experiments. Table S1 indicates: a) which models had executed these experiments and b) the volcanic forcing dataset incorporated for each model.

Near-surface (2m) land temperatures are considered for this study. Models are linearly regridded to a 2˚ by 2˚ latitude-longitude grid. Multi-model means are used for all analyses, and anomalies are calculated with respect to a 20-year running mean. Only land temperatures are considered to avoid oceanic masking effects on land temperature responses, given that ocean temperatures have a delayed response to radiative forcing (Joseph and Zeng, 2011).

The quantity of SO_2 emitted into the lower stratosphere greatly influences potential climatic responses (Oman *et al.*, 2005), with 5 Tg or more required to impact climate (Timmreck, 2012). In this study, climate responses following eight major tropical and SH eruptions with a VEI > 3.3 (Volcanic Explosivity Index; measuring the explosiveness of an eruption (Newhall & Self, 1982) are tested. These include Krakatau (1883), Tarawera (1886), Santa Maria (1902), Colima (1913), Quizapu (1932), El Chichón (1982) and Pinatubo (1991). The 1963 Agung eruption which had a VEI value of 4, but a lower stratosphere SO_2 mass of 7.5 Tg is also considered (see Table 1).

To test multi-model mean robustness, the 25th and 75th percentiles of individual model responses to historical forcing experiments are considered. Statistical significance was calculated by resampling 5000 time series using the bootstrap approach (Efron, 1979) whereby the 5th and 95th percentiles were used to distinguish between likely random occurrences and significant climatic responses (Haurwitz & Brier, 1981; Rao *et al.*, 2017).

Table 1. Volcanic eruptions analysed in this study. Labels given to these eruptions are used in all figures (Driscoll *et al.*, 2012).

Label	Eruption	Date	Latitude	VEI[i]	DVI[ii]	Lower Stratosphere SO_2, mass (Tg)[iii]
a	Krakatau	27 August 1883	6S	6	1000	22
b	Tarawera	10 June 1886	38S	5	800	3.3
c	Santa Maria	24 October 1902	15N	6	600	3.8
d	Colima	1913	19N	5	?	?
e	Quizapu	10 April 1932	36S	5	70	?
f	Agung	17 March 1963	8S	4	800	7.5
g	El Chichón	4 April 1982	17N	5	800	5.6
h	Mt Pinatubo	15 June 1991	15N	6	1000	18

[i] VEI: Volcanic Explosivity Index (Newhall & Self, 1982).
[ii] DVI: Dust Veil Index (Lamb, 1970): a measure of the impact (e.g. on climate) of dust and aerosols released from an eruption.
[iii] SO_2 values from Neely III and Schmidt (2016).

3. Results and Discussion

3.1 SH near-surface land (terrestrial) temperatures following major eruptions

CMIP5 historical experiment outputs indicate reductions in mean annual near-surface temperatures after each of the eight eruptions (Table 1) for the NH, and seven of the eight for the SH (Figure 1). However, only four of the temperature reductions are statistically significant for the SH; namely after the Krakatau (1883), Santa Maria (1902), Agung (1963) and Pinatubo (1991) eruptions. For the purpose of this paper, these four eruptions are referred to as the 'primary eruptions'. The NH-averaged annual temperatures are significantly cooler after only three of the primary eruptions, as cooling after the Agung eruption is not significant (-0.21°C). Of these primary eruptions, three had a VEI of 6, and Agung a VEI of 4. However, all four of these eruptions had emitted between 3.8 and 22 Tg of SO_2 and originated between 8°S and 15°N latitude. This would have facilitated effective distribution of SO_2 around both hemispheres by the Brewer-Dobson circulation (Butchart, 2014; Robock, 2000; Trepte *et al.*, 1993; Young *et al.*, 2011). The remaining four eruptions (Tarawera, 1886; Colima, 1913; Quizapu, 1932; El Chichón, 1982) occurred either in SH mid-latitude or NH tropical regions, but had emitted between a negligible amount and 5.6 Tg of SO_2 into the lower stratosphere. Coincidently, apart from Tarawera, none of these are associated with a significant surface temperature response in the SH. Following Tarawera, significant anomalies occur in SH summer and autumn and NH winter, however, this response is a likely enhancement (extension) of the Krakatau response. NH temperatures are significantly reduced following the El Chichón eruption. The above suggests that for a significant response to occur in the SH, an eruption would ideally be in the tropics, and emit at least 3.8 Tg of SO_2 into the lower stratosphere.

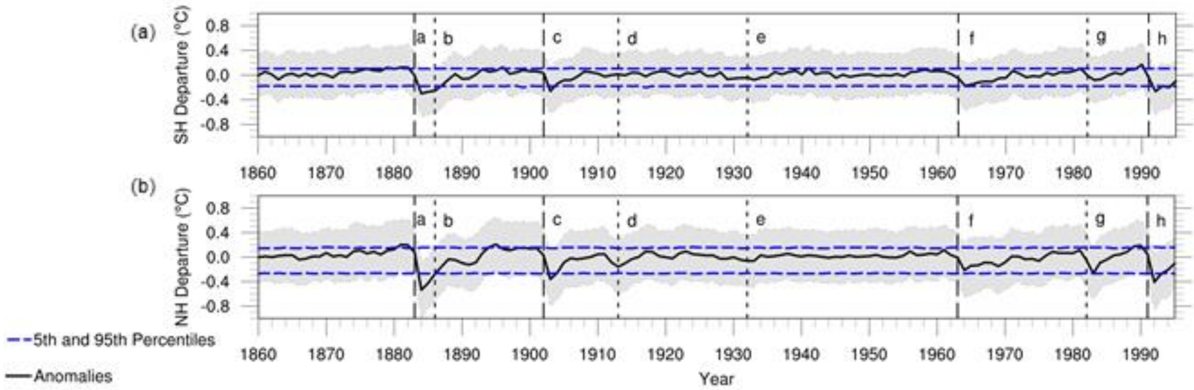

Figure 1. CMIP5-simulated annual SH (a) and NH (b) land-only near-surface temperatures anomalies. Vertical lines represent eruptions. Long dashed lines signify the primary eruptions and short dashed lines the remaining eruptions. The ensemble spread (25th to 75th percentiles) of the 12-month moving average is depicted by grey shading, and statistical significance at the 90% confidence interval by the blue lines. See Table 1 for eruption names.

Both magnitude and duration of significant temperature responses vary between major eruptions (Table 2). The longest response follows Krakatau, lasting four years. Negative temperature departures were significant for only one year following Santa Maria, for both SH and NH annual anomalies. Response following Agung was weakest of the primary eruptions, with negative anomalies only significant in austral winter (JJA). Anomalies after Pinatubo were significant for two consecutive years in both hemispheres. Temperature responses to these eruptions do not correspond directly with the quantity of SO_2 emitted by each eruption (Figure S2). For instance, Agung placed 7.5 Tg of SO_2 into the stratosphere but produced weaker temperature responses than Santa Maria, which emitted only 3.8 Tg. Hence, while large amounts of SO_2 are required to cause a temperature response, other factors can affect post-eruption responses. Such factors include season and location of eruption, aerosol layer height, and state of the atmosphere and ocean at the time of eruption; all of which likely contribute to observed differences in responses (Krishnamohan *et al*., 2019; Stevenson *et al*., 2017; Sun *et al*., 2019; Zuo *et al*., 2018). For instance, Pinatubo erupted during the SH winter but Santa Maria during spring. Atmospheric circulation is most favourable to distributing aerosols during SH winter when coupling between the troposphere and stratosphere is strongest and the Brewer-Dobson circulation most pronounced (Birner & Bönisch, 2010; Perlwitz & Graf, 1995; Young *et al.*, 2011), which might explain the stronger response after Pinatubo.

Table 2. CMIP5-simulated annual SH and NH near-surface temperature anomalies following the four primary eruptions. Blue shading indicates significant anomalies and grey shading the year of the eruption.

		SH Anomaly					NH Anomaly				
Eruption	Year	ANN	DJF	MAM	JJA	SON	ANN	DJF	MAM	JJA	SON
Krakatau	1883	0.00	0.17	0.05	0.07	-0.15	0.08	0.13	0.16	0.11	0.00
	1884	-0.30	-0.21	-0.36	-0.36	-0.24	-0.54	-0.23	-0.40	-0.65	-0.68
	1885	-0.27	-0.31	-0.24	-0.27	-0.26	-0.42	-0.47	-0.41	-0.44	-0.43
Tarawera	1886	-0.26	-0.31	-0.25	-0.26	-0.23	-0.28	-0.35	-0.34	-0.23	-0.27
	1887	-0.17	-0.21	-0.26	-0.15	-0.07	-0.15	-0.27	-0.16	-0.12	-0.11
Santa Maria	1902	0.03	0.10	0.07	0.04	-0.04	0.03	0.03	0.03	0.09	0.02
	1903	-0.26	-0.15	-0.31	-0.32	-0.24	-0.36	-0.22	-0.29	-0.43	-0.44
	1904	-0.14	-0.16	-0.15	-0.10	-0.17	-0.26	-0.28	-0.23	-0.26	-0.25
	1905	-0.08	-0.15	-0.13	-0.12	0.02	-0.09	-0.19	-0.06	-0.11	-0.10
Agung	1963	-0.05	0.03	0.00	-0.07	-0.13	-0.01	-0.01	0.00	-0.02	-0.05
	1964	-0.17	-0.19	-0.19	-0.20	-0.15	-0.21	-0.12	-0.19	-0.22	-0.16
	1965	-0.15	-0.13	-0.16	-0.12	-0.16	-0.14	-0.23	-0.14	-0.16	-0.17
	1966	-0.12	-0.12	-0.10	-0.15	-0.10	-0.13	-0.13	-0.09	-0.16	-0.10
Pinatubo	1991	-0.04	0.20	0.12	0.00	-0.30	0.05	0.20	0.14	0.07	-0.10
	1992	-0.26	-0.28	-0.30	-0.27	-0.23	-0.41	-0.26	-0.34	-0.51	-0.47
	1993	-0.18	-0.22	-0.21	-0.14	-0.21	-0.27	-0.20	-0.29	-0.30	-0.30
	1994	-0.20	-0.15	-0.18	-0.18	-0.24	-0.21	-0.29	-0.21	-0.17	-0.19

Internal variability is considered as past ensemble simulations have shown that these obscure volcanic forcing impacts (e.g. Frölicher *et al.*, 2013; Lehner *et al.*, 2016). In addition, eruptions themselves can affect internal variability, indirectly influencing temperatures. Studies using CMIP5 models suggest a positive Southern Annular Mode (SAM) after major eruptions (Barnes *et al.*, 2016; McGraw *et al.*, 2016). This implies that westerlies intensify and contract poleward resulting in significantly cooler temperatures over Antarctica and most of Australia, but warming over regions between 40-60°S (Gillett *et al.*, 2006). Volcanic eruptions can strengthen the polar vortex, resulting in cooling over the poles (Barnes *et al.*, 2016; Karpechko *et al.*, 2010; Perlwitz & Graf, 1995; Zambri & Robock, 2016) and influence El Niño Southern Oscillation (ENSO) (Pausata *et al.*, 2015). Varied ENSO responses are likely associated with different volcanic forcing stages (Wang *et al.*, 2018). To this end, model-generated SSTs indicate a tendency to be depressed in the Nino3.4 area, implying La Niña-like conditions following the four major eruptions, as found by Maher *et al*. (2015). La Niña-like conditions usually imply overall cooler SH temperatures (Kuleshov *et al*., 2008), which may have contributed to the observed cooling after eruptions.

Tarawera (1886) erupted three years after Krakatau and marks the strongest known mid-latitude SH (38°S) eruption during the last couple of centuries. Although it emitted only 3.3 Tg of SO_2 into the lower stratosphere, this occurred during an already volcanically-induced cool period, and thus offers a unique opportunity to consider the so called 'volcanic-double' forcing effect as discussed by Toohey *et al*. (2016). Both NH and SH mean temperatures remain below normal for an extended period (significant anomalies remained until 1887, four years after Krakatau). This temporally extended negative temperature anomaly is in strong contrast to all other major eruptions, particularly so when compared with Pinatubo (see Figure 2); thus demonstrating the likely combined influence of Krakatau and Tarawera, supporting the case for a 'volcanic-double' forcing effect. Although Toohey *et al*. (2016) provide an example of a strong 'volcanic-double' forced cooling effect for the Middle Ages, the example above is the first (and possibly only) such example of a 'volcanic-double' climate forcing effect since the late modern period. Notably, mean negative temperature departures were marginally stronger in the SH than NH in 1887 (SH: -0.17°C; NH: -0.15°C) following Tarawera, thus indicating a slightly stronger initial (and volcanic cumulative) impact on the SH than NH. The three remaining major eruptions (Colima, 1913; Quizapu, 1932; El Chichón, 1982; Table 1) investigated here do not indicate statistically significant temperature responses in the SH, however, weak responses are noticeable. Weak responses are most likely due to insufficient SO_2 emitted into the stratosphere. It is suggested that > 5 Tg of SO_2 needs to reach the stratosphere for any notable temperature effect (Timmreck, 2018), although Santa Maria emitted only 3.3 Tg and shows a significant response. In the NH, the strength of temperature responses after these smaller eruptions coincides with the amount of SO_2 that each eruption emitted into the stratosphere, but not so in the SH. The strongest of these eruptions (El Chichón) emitted 5.6 Tg of SO_2 into the lower stratosphere and coincides with a statistically insignificant negative annual NH temperature anomaly in 1983 (-0.27°C). In contrast, the SH response is negligible (1983: -0.08°C). The stronger NH response is to be expected given weaker SH Brewer-Dobson circulation than that in the NH (Rosenlof, 1995; Young *et al.*, 2011).

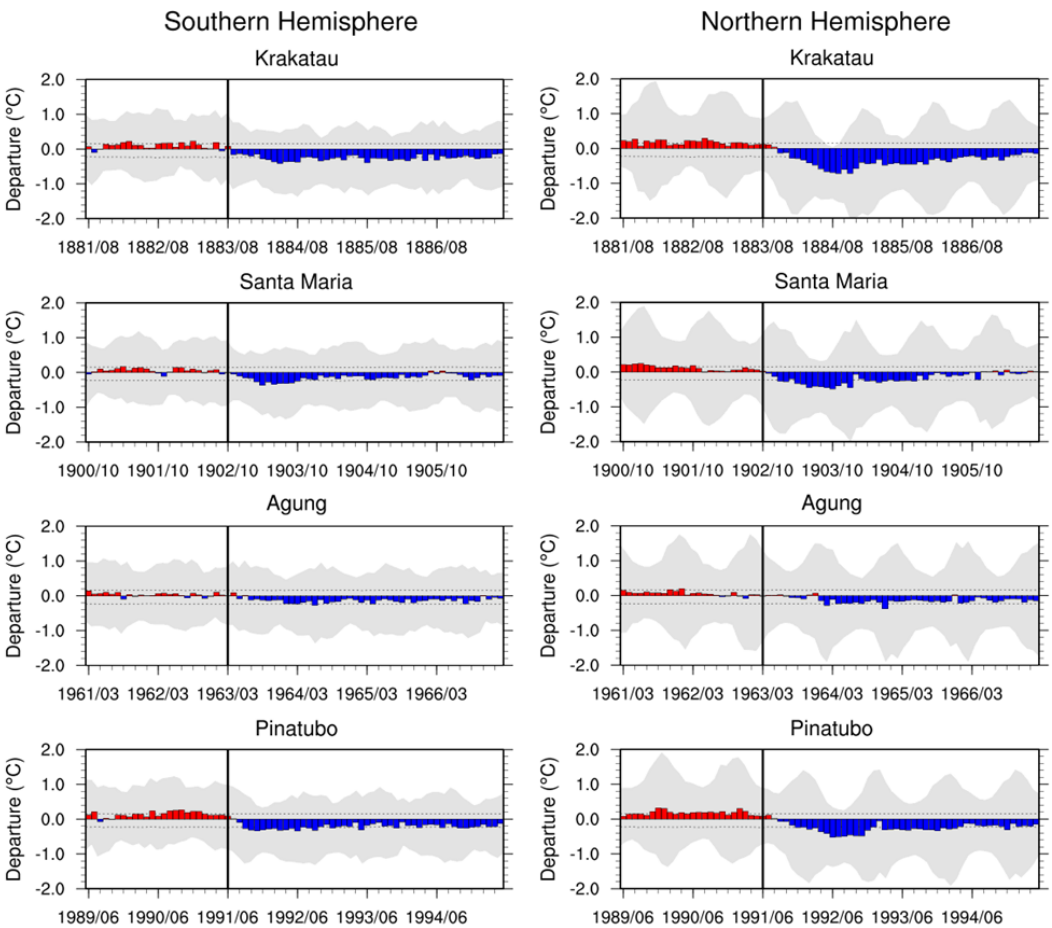

Figure 2. CMIP5-simulated monthly near-surface temperature responses for the four primary eruptions for the SH and NH. Vertical lines indicate the eruption month. Grey shading depicts the ensemble spread between the 25th and 75th percentiles of the monthly moving averages. Statistical significance at the 90th% confidence interval is represented by the horizontal dotted lines.

Monthly surface temperature response times for both hemispheres are now considered, following the four primary eruptions (Figure 2). With the exception of anomalies following Pinatubo, SH anomalies develop before (1-2 months), peak earlier (4-6 months) and terminate before NH anomalies. However, given that SH anomalies are weaker (peak anomalies in SH: -0.27°C to -0.42°C; NH: -0.38°C to -0.72°C for all eruptions), they only become significant 1-2 months after those in the NH. In addition, the NH had a higher percentage of significantly cooler than normal months during the first 36 months following each primary eruption (NH: 55-83%; SH: 22-72%), apart from Agung when both hemispheres had only three months of significantly depressed temperatures. These outcomes are in agreement with previous work which has emphasized stronger NH than SH temperature responses (e.g. Man *et al*., 2014; Monerie *et al*., 2017; Neukom *et al*., 2014). The delayed significant response in the SH is likely associated with the vast expanse of oceans which help regulate surface temperatures (Joseph and Zeng, 2011) and the weaker SH Brewer-Dobson circulation (Young *et al*., 2011). The first significant responses in the NH are typically observed between December and February, and in the SH between February and September (i.e. cooler seasons of each hemisphere), but maximum anomalies generally occur during SH winter and coincide with maximum cooling during NH summer/autumn (Zanchettin *et al*., 2019).

As alluded to earlier, temperature departures in response to volcanic forcing may be spatially highly variable at the hemispheric scale. While strong negative temperature anomalies may be detected across most NH latitudes after the four primary eruptions, the same is not observed in the SH (Figure 3). Following each eruption, stronger cooling occurs in the NH than SH in the first (y1) and second (y2) years after eruptions, and in the third year (y3) after Krakatau and Pinatubo. Negative temperature departures after Agung are strongest between 20 and 40°S (-0.20°C) in y1 but uniform over all latitudes in y2 and y3 (-0.11 and -0.18°C respectively). Following Santa Maria, negative departures in y3 are strongest over the tropics of both hemispheres (-0.18°C). For all eruptions, strongest negative SH anomalies occur between 10 and 30°S for y1 to y3 (y1: -0.34°C; y2:-0.23°C; y3: -0.21°C). Weakest anomalies are observed at high latitudes (y1: -0.11°C, y2: -0.13°C, y3: -0.08°C).

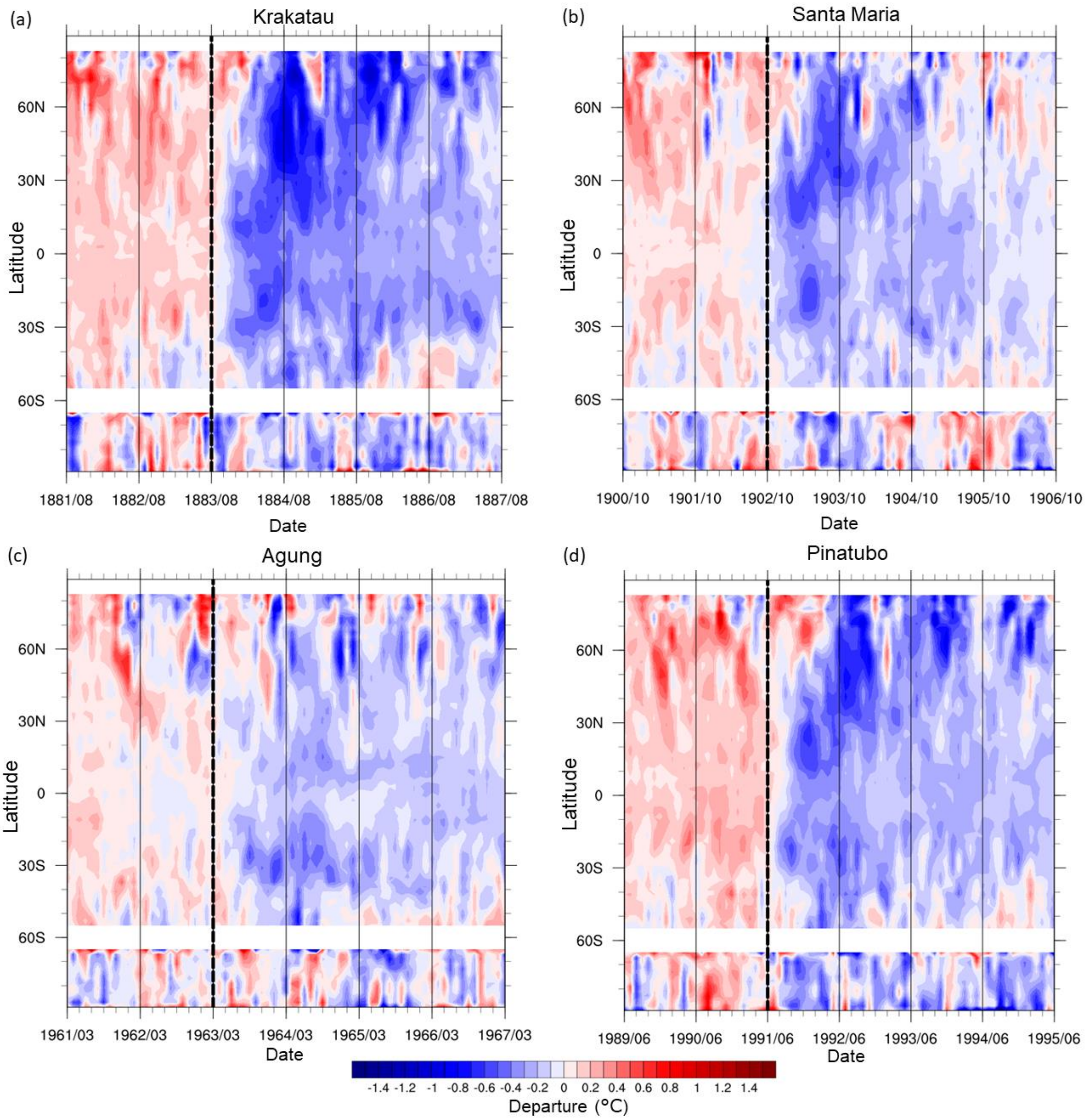

Figure 3. CMIP5-simulated zonal averages of the land-only near-surface temperature anomalies over time for the (a) Krakatau, (b) Santa Maria, (c) Agung, and (d) Pinatubo eruptions. Thick dashed vertical lines represent eruptions. The gaps around 90°N and 60°S are a result of the absence of land at those latitudes.

3.2 Statistics

The 25th and 75th percentiles of the models indicate that temperature responses are similar to mean values obtained from the four primary eruptions, suggesting that responses shown by the multi-model mean are robust. A Superposed Epoch Analysis (Figure S3) suggests that significantly cooler mean NH and SH land temperatures may occur after major eruptions, with 3.8 Tg or greater SO_2 loading in the lower stratosphere, for up to 3-4 years. The SEA and bootstrap methods (Efron, 1979; Haurwitz & Brier, 1981; Rao *et al*., 2017) further indicate that responses are statistically significant, as these occur below the 5th percentile. Although studies have used composites of multiple eruptions to study the spatial effects of volcanic forcing (e.g. Alfaro-Sánchez *et al*., 2018; Zambri *et al*., 2017), it must be acknowledged that the timing, location, strength and chemistry of the eruption, in combination with other forcing mechanisms, will result in different temperature-response outcomes. It should also be cautioned that if larger magnitude eruptions are composited with weaker ones, it might mask out the full response exhibited by larger eruptions (Figures S3c and S3d).

4. Conclusion

Past work comparing Northern and Southern hemispheric temperature responses to volcanic forcing has generally focused on mean annual or seasonal trends during post-eruption years and has broadly shown weaker responses in the SH. While this study's findings are largely in agreement with this, they also indicate some exceptions to this 'rule', and particularly so when examining responses at a finer temporal scale (i.e. months rather than years). For instance, significant SH temperature responses lag by 1-2 months compared to those in the NH following major eruptions. However, initial cooling (although insignificant) starts earlier (by 1 to 2 months) in the SH. The findings suggest that common factors resulting in an eruption causing a significant SH temperature response include the eruption occurring in the tropics and emitting 3.8 Tg or more of SO_2 into the lower stratosphere. Eruptions occurring during SH autumn or winter induce a greater temperature response due to more favorable circulation conditions in winter. The

SH response is strongest during autumn/winter, which coincides with strongest NH cooling in summer/autumn. While subtropical and mid-latitude SH eruptions do not force a significant temperature response, in the case of Tarawera, it prolonged negative temperature anomalies (initially in response to Krakatau) in both hemispheres, demonstrating a relatively recent so-called 'volcanic double' forcing effect. Analyses considering only mean annual temperature responses is cautioned. Immediate and relatively strong monthly negative temperature anomalies in the SH, following major eruptions, have important implications for climate sensitive bio-systems and the agricultural sector in particular.

5. References

Alfaro-Sánchez, R., Nguyen, H., Klesse, S., Hudson, A., Belmecheri, S., Köse, N., Diaz, H. F., Monson, R. K., Villalba, R., & Trouet, V. (2018). Climatic and volcanic forcing of tropical belt northern boundary over the past 800 years. Nature Geoscience, 11(12), 933–938. https://doi.org/10.1038/s41561-018-0242-1

Ammann, C. M., Joos, F., Schimel, D. S., Otto-Bliesner, B. L., & Tomas, R. A. (2007). Solar influence on climate during the past millennium: Results from transient simulations with the NCAR Climate System Model. Proceedings of the National Academy of Sciences, 104(10), 3713–3718. https://doi.org/10.1073/pnas.0605064103

Barnes, E. A., Solomon, S., & Polvani, L. M. (2016). Robust Wind and Precipitation Responses to the Mount Pinatubo Eruption, as Simulated in the CMIP5 Models. Journal of Climate, 29(13), 4763–4778. https://doi.org/10.1175/JCLI-D-15-0658.1

Birner, T., & Bönisch, H. (2010). Residual circulation trajectories and transit times into the extratropical lowermost stratosphere. Atmospheric Chemistry and Physics Discussions, 10(7), 16837–16860. https://doi.org/10.5194/acpd-10-16837-2010

Butchart, N. (2014). The Brewer-Dobson circulation. Reviews of Geophysics, 52(2), 157–184. https://doi.org/10.1002/2013RG000448

Cole-Dai, J. (2010). Volcanoes and climate. Wiley Interdisciplinary Reviews: Climate Change, 1(6), 824–839. https://doi.org/10.1002/wcc.76

Colose, C. M., LeGrande, A. N., & Vuille, M. (2015). The influence of tropical volcanic eruptions on the climate of South America during the last millennium. Climate of the Past, 11, 3375–3424. https://doi.org/10.5194/cpd-11-3375-2015

Driscoll, S., Bozzo, A., Gray, L. J., Robock, A., & Stenchikov, G. (2012). Coupled Model Intercomparison Project 5 (CMIP5) simulations of climate following volcanic eruptions. Journal of Geophysical Research: Atmospheres, 117(D17), D17105. https://doi.org/10.1029/2012JD017607

Efron, B. (1979). Bootstrap Methods: Another Look at the Jackknife. The Annals of Statistics, 7(1), 1–26. https://doi.org/10.1214/aos/1176344552

Esper, J., Schneider, L., Krusic, P. J., Luterbacher, J., Büntgen, U., Timonen, M., Sirocko, F., & Zorita, E. (2013). European summer temperature response to annually dated volcanic eruptions over the past nine centuries. Bulletin of Volcanology, 75(7), 736. https://doi.org/10.1007/s00445-013-0736-z

Frölicher, T. L., Joos, F., Raible, C. C., & Sarmiento, J. L. (2013). Atmospheric CO2 response to volcanic eruptions: The role of ENSO, season, and variability. Global Biogeochemical Cycles, 27(1), 239–251. https://doi.org/10.1002/gbc.20028

Gillett, N. P., Kell, T. D., & Jones, P. D. (2006). Regional climate impacts of the Southern Annular Mode. Geophysical Research Letters, 33(23), L23704. https://doi.org/10.1029/2006GL027721

Graf, H.-F., Kirchner, I., Robock, A., & Schult, I. (1993). Pinatubo eruption winter climate effects: Model versus observations. Climate Dynamics, 9(2), 81–93. https://doi.org/10.1007/BF00210011

Haurwitz, M. W., & Brier, G. W. (1981). A Critique of the Superposed Epoch Analysis Method: Its Application to Solar–Weather Relations. Monthly Weather Review, 109(10), 2074–2079. https://doi.org/10.1175/1520-0493(1981)109<2074:ACOTSE>2.0.CO;2

Hopcroft, P. O., Kandlbauer, J., Valdes, P. J., & Sparks, R. S. J. (2018). Reduced cooling following future volcanic eruptions. Climate Dynamics, 51(4), 1449–1463. https://doi.org/10.1007/s00382-017-3964-7

Hua, W., Dai, A., Zhou, L., Qin, M., & Chen, H. (2019). An Externally Forced Decadal Rainfall Seesaw Pattern Over the Sahel and Southeast Amazon. Geophysical Research Letters, 46(2), 923–932. https://doi.org/10.1029/2018GL081406

Joseph, R., & Zeng, N. (2011). Seasonally Modulated Tropical Drought Induced by Volcanic Aerosol. Journal of Climate, 24(8), 2045–2060. https://doi.org/DOI: 10.1175/2009JCLI3170.1

Karpechko, A. Y., Gillett, N. P., Dall'Amico, M., & Gray, L. J. (2010). Southern Hemisphere atmospheric circulation response to the El Chichón and Pinatubo eruptions in coupled climate models. Quarterly Journal of the Royal Meteorological Society, 136(652), 1813–1822. https://doi.org/10.1002/qj.683

Kremser, S., Thomason, L. W., von Hobe, M., Hermann, M., Deshler, T., Timmreck, C., Toohey, M., Stenke, A., Schwarz, J. P., Weigel, R., Fueglistaler, S., Prata, F. J., Vernier, J.-P., Schlager, H., Barnes, J. E., Antuña-Marrero, J.-C., Fairlie, D., Palm, M., Mahieu, E., … Meland, B. (2016). Stratospheric aerosol-Observations, processes, and impact on climate: Stratospheric Aerosol. Reviews of Geophysics, 54(2), 278–335. https://doi.org/10.1002/2015RG000511

Krishnamohan, K.-P. S.-P., Bala, G., Cao, L., Duan, L., & Caldeira, K. (2019). Climate system response to stratospheric sulfate aerosols: Sensitivity to altitude of aerosol layer. Earth System Dynamics, 10(4), 885–900. https://doi.org/10.5194/esd-10-885-2019

Kuleshov, Y., Qi, L., Fawcett, R., & Jones, D. (2008). On tropical cyclone activity in the Southern Hemisphere: Trends and the ENSO connection. Geophysical Research Letters, 35(14), L14S08. https://doi.org/10.1029/2007GL032983

Lamb, H. H. (1970). Volcanic Dust in the Atmosphere; with a Chronology and Assessment of Its Meteorological Significance. Philosophical Transactions of the Royal Society A: Mathematical, Physical and Engineering Sciences, 266(1178), 425–533. https://doi.org/10.1098/rsta.1970.0010

Lehner, F., Schurer, A. P., Hegerl, G. C., Deser, C., & Frölicher, T. L. (2016). The importance of ENSO phase during volcanic eruptions for detection and attribution. Geophysical Research Letters, 43(6), 2851–2858. https://doi.org/10.1002/2016GL067935

Liu, F., Zhao, T., Wang, B., Liu, J., & Luo, W. (2018). Different Global Precipitation Responses to Solar, Volcanic, and Greenhouse Gas Forcings. Journal of Geophysical Research: Atmospheres, 123(8), 4060–4072. https://doi.org/10.1029/2017JD027391

Lough, J. M., & Fritts, H. C. (1987). An assessment of the possible effects of volcanic eruptions on North American climate using tree-ring data, 1602 to 1900 A.D. Climatic Change, 10(3), 219–239. https://doi.org/10.1007/BF00143903

Maher, N., McGregor, S., England, M. H., & Gupta, A. S. (2015). Effects of volcanism on tropical variability: EFFECTS OF VOLCANISM. Geophysical Research Letters, 42(14), 6024–6033. https://doi.org/10.1002/2015GL064751

Man, W., Zhou, T., & Jungclaus, J. H. (2014). Effects of Large Volcanic Eruptions on Global Summer Climate and East Asian Monsoon Changes during the Last Millennium: Analysis of MPI-ESM Simulations. Journal of Climate, 27(19), 7394–7409. https://doi.org/10.1175/JCLI-D-13-00739.1

Mass, C. F., & Portman, D. A. (1989). Major Volcanic Eruptions and Climate: A Critical Evaluation. Journal of Climate, 2(6), 566–593. https://doi.org/10.1175/1520-0442(1989)002<0566:MVEACA>2.0.CO;2

McGraw, M. C., Barnes, E. A., & Deser, C. (2016). Reconciling the observed and modeled Southern Hemisphere circulation response to volcanic eruptions: RECONCILING SH RESPONSE TO VOLCANOES. Geophysical Research Letters, 43(13), 7259–7266. https://doi.org/10.1002/2016GL069835

Monerie, P.-A., Moine, M.-P., Terray, L., & Valcke, S. (2017). Quantifying the impact of early 21st century volcanic eruptions on global-mean surface temperature. Environmental Research Letters, 12(5), 054010. https://doi.org/10.1088/1748-9326/aa6cb5

Neely III RR, Schmidt A. 2016. VolcanEESM: Global volcanic sulphur dioxide (SO_2) emissions database from 1850 to present. Centre for Environmental Data Analysis.

Neukom, R., Gergis, J., Karoly, D. J., Wanner, H., Curran, M., Elbert, J., González-Rouco, F., Linsley, B. K., Moy, A. D., Mundo, I., Raible, C. C., Steig, E. J., van Ommen, T., Vance, T., Villalba, R., Zinke, J., & Frank, D. (2014). Inter-hemispheric temperature variability over the past millennium. Nature Climate Change, 4(5), 362–367. https://doi.org/10.1038/nclimate2174

Newhall, C. G., & Self, S. (1982). The volcanic explosivity index (VEI) an estimate of explosive magnitude for historical volcanism. Journal of Geophysical Research: Oceans, 87(C2), 1231–1238. https://doi.org/10.1029/JC087iC02p01231

Oman, L., Robock, A., Stenchikov, G., Schmidt, G. A., & Ruedy, R. (2005). Climatic response to high-latitude volcanic eruptions. Journal of Geophysical Research: Atmospheres, 110(D13), D13103. https://doi.org/10.1029/2004JD005487

Pausata, F. S. R., Chafik, L., Caballero, R., & Battisti, D. S. (2015). Impacts of high-latitude volcanic eruptions on ENSO and AMOC. Proceedings of the National Academy of Sciences, 112(45), 13784–13788. https://doi.org/10.1073/pnas.1509153112

Perlwitz, J., & Graf, H.-F. (1995). The Statistical Connection between Tropospheric and Stratospheric Circulation of the Northern Hemisphere in Winter. Journal of Climate, 8, 2281–2295.

Raible, C. C., Brönnimann, S., Auchmann, R., Brohan, P., Frölicher, T. L., Graf, H.-F., Jones, P., Luterbacher, J., Muthers, S., Neukom, R., Robock, A., Self, S., Sudrajat, A., Timmreck, C., & Wegmann, M. (2016). Tambora 1815 as a test case for high impact volcanic eruptions: Earth system effects. Wiley Interdisciplinary Reviews: Climate Change, 7(4), 569–589. https://doi.org/10.1002/wcc.407

Rao, M. P., Cook, B. I., Cook, E. R., D’Arrigo, R. D., Krusic, P. J., Anchukaitis, K. J., LeGrande, A. N., Buckley, B. M., Davi, N. K., Leland, C., & Griffin, K. L. (2017). European and Mediterranean hydroclimate responses to tropical volcanic forcing over the last millennium. Geophysical Research Letters, 44(10), 5104–5112. https://doi.org/10.1002/2017GL073057

Robock, A. (2000). Volcanic eruptions and climate. Reviews of Geophysics, 38(2), 191–219. https://doi.org/10.1029/1998RG000054

Robock, A., & Mao, J. (1995). The Volcanic Signal in Surface Temperature Observations. Journal of Climate, 8(5), 1086–1103. https://doi.org/10.1175/1520-0442(1995)008<1086:TVSIST>2.0.CO;2

Rosenlof, K. H. (1995). Seasonal cycle of the residual mean meridional circulation in the stratosphere. Journal of Geophysical Research, 100(D3), 5173. https://doi.org/10.1029/94JD03122

Salinger, M. J. (1998). New Zealand Climate: The Impact of Major Volcanic Eruptions. Weather and Climate, 18(1), 11–19.

Sato, M., Hansen, J. E., McCormick, M. P., & Pollack, J. B. (1993). Stratospheric aerosol optical depths, 1850–1990. Journal of Geophysical Research, 98(D12), 22987. https://doi.org/10.1029/93JD02553

Schneider, D. P., Ammann, C. M., Otto-Bliesner, B. L., & Kaufman, D. S. (2009). Climate response to large, high-latitude and low-latitude volcanic eruptions in the Community Climate System Model. Journal of Geophysical Research: Atmospheres, 114(D15), D15101. https://doi.org/10.1029/2008JD011222

Sigl, M., Winstrup, M., McConnell, J. R., Welten, K. C., Plunkett, G., Ludlow, F., Büntgen, U., Caffee, M., Chellman, N., Dahl-Jensen, D., Fischer, H., Kipfstuhl, S., Kostick, C., Maselli, O. J., Mekhaldi, F., Mulvaney, R., Muscheler, R., Pasteris, D. R., Pilcher, J. R., … Woodruff, T. E. (2015). Timing and climate forcing of volcanic eruptions for the past 2,500 years. Nature, 523(7562), 543–549. https://doi.org/10.1038/nature14565

Stevenson, S., Fasullo, J. T., Otto-Bliesner, B. L., Tomas, R. A., & Gao, C. (2017). Role of eruption season in reconciling model and proxy responses to tropical volcanism. Proceedings of the National Academy of Sciences, 114(8), 1822–1826. https://doi.org/10.1073/pnas.1612505114

Stothers, R. B. (1999). Volcanic Dry Fogs, Climate Cooling, and Plague Pandemics in Europe and the Middle East. 713–723.

Sun, W., Wang, B., Liu, J., Chen, D., Gao, C., Ning, L., & Chen, L. (2019). How Northern High-Latitude Volcanic Eruptions in Different Seasons Affect ENSO. Journal of Climate, 32(11), 3245–3262. https://doi.org/10.1175/JCLI-D-18-0290.1

Taylor, K. E., Stouffer, R. J., & Meehl, G. A. (2012). An Overview of CMIP5 and the Experiment Design. Bulletin of the American Meteorological Society, 93(4), 485–498. https://doi.org/10.1175/BAMS-D-11-00094.1

Textor, C., Graf, H.-F., Timmreck, C., & Robock, A. (2004). Emissions from volcanoes. In C. Granier, P. Artaxo, & C. E. Reeves (Eds.), Emissions of Atmospheric Trace Compounds (Vol. 18, pp. 269–303). Springer Netherlands. https://doi.org/10.1007/978-1-4020-2167-1_7

Thompson, D. W. J., Wallace, J. M., Jones, P. D., & Kennedy, J. J. (2009). Identifying Signatures of Natural Climate Variability in Time Series of Global-Mean Surface Temperature: Methodology and Insights. Journal of Climate, 22(22), 6120–6141. https://doi.org/10.1175/2009JCLI3089.1

Timmreck, C. (2012). Modeling the climatic effects of large explosive volcanic eruptions. WIREs: Climate Change, 3(6), 545–564. https://doi.org/10.1002/wcc.192

Timmreck, C. (2018). Climatic effects of large volcanic eruptions [Habilitation Thesis, Universität Hamburg]. https://pure.mpg.de/rest/items/item_2566000/component/file_2565999/content

Toohey, M., Krüger, K., Schmidt, H., Timmreck, C., Sigl, M., Stoffel, M., & Wilson, R. (2019). Disproportionately strong climate forcing from extratropical explosive volcanic eruptions. Nature Geoscience, 12(2), 100–107. https://doi.org/10.1038/s41561-018-0286-2

Toohey, M., Krüger, K., Sigl, M., Stordal, F., & Svensen, H. (2016). Climatic and societal impacts of a volcanic double event at the dawn of the Middle Ages.

Climatic Change, 136(3–4), 401–412. https://doi.org/10.1007/s10584-016-1648-7

Trepte, C. R., Veiga, R. E., & McCormick, M. P. (1993). The poleward dispersal of Mount Pinatubo volcanic aerosol. Journal of Geophysical Research: Atmospheres, 98(D10), 18563–18573. https://doi.org/10.1029/93JD01362

Wang, T., Guo, D., Gao, Y., Wang, H., Zheng, F., Zhu, Y., Miao, J., & Hu, Y. (2018). Modulation of ENSO evolution by strong tropical volcanic eruptions. Climate Dynamics, 51(7–8), 2433–2453. https://doi.org/10.1007/s00382-017-4021-2

Wilmes, S. B., Raible, C. C., & Stocker, T. F. (2012). Climate variability of the mid- and high-latitudes of the Southern Hemisphere in ensemble simulations from 1500 to 2000 AD. Climate of the Past, 8(1), 373–390. https://doi.org/10.5194/cp-8-373-2012

Young, P. J., Thompson, D. W. J., Rosenlof, K. H., Solomon, S., & Lamarque, J.-F. (2011). The Seasonal Cycle and Interannual Variability in Stratospheric Temperatures and Links to the Brewer–Dobson Circulation: An Analysis of MSU and SSU Data. Journal of Climate, 24(23), 6243–6258. https://doi.org/10.1175/JCLI-D-10-05028.1

Zambri, B., LeGrande, A. N., Robock, A., & Slawinska, J. (2017). Northern Hemisphere winter warming and summer monsoon reduction after volcanic eruptions over the last millennium. Journal of Geophysical Research: Atmospheres, 122(15), 7971–7989. https://doi.org/10.1002/2017JD026728

Zambri, B., & Robock, A. (2016). Winter warming and summer monsoon reduction after volcanic eruptions in Coupled Model Intercomparison Project 5 (CMIP5) simulations. Geophysical Research Letters, 43(20), 10,920-10,928. https://doi.org/10.1002/2016GL070460

Zanchettin, D., Bothe, O., Timmreck, C., Bader, J., Beitsch, A., Graf, H.-F., Notz, D., & Jungclaus, J. H. (2014). Inter-hemispheric asymmetry in the sea-ice response to volcanic forcing simulated by MPI-ESM (COSMOS-Mill). Earth System Dynamics, 5(1), 223–242. https://doi.org/10.5194/esd-5-223-2014

Zanchettin, Davide, Timmreck, C., Toohey, M., Jungclaus, J. H., Bittner, M., Lorenz, S. J., & Rubino, A. (2019). Clarifying the Relative Role of Forcing Uncertainties and Initial-Condition Unknowns in Spreading the Climate Response to Volcanic Eruptions. Geophysical Research Letters, 46(3), 1602–1611. https://doi.org/10.1029/2018GL081018

Zhang, D., Blender, R., & Fraedrich, K. (2013). Volcanoes and ENSO in millennium simulations: Global impacts and regional reconstructions in East Asia. Theoretical and Applied Climatology, 111(3–4), 437–454. https://doi.org/10.1007/s00704-012-0670-6

Zuo, M., Man, W., Zhou, T., & Guo, Z. (2018). Different Impacts of Northern, Tropical, and Southern Volcanic Eruptions on the Tropical Pacific SST in the Last Millennium. Journal of Climate, 31(17), 6729–6744. https://doi.org/10.1175/JCLI-D-17-0571.1

Supplementary Material: Chapter Two

Geophysical Research Letters

Supporting Information for

Major Volcanic Eruptions and their impacts on Southern Hemisphere temperatures during the late-19th and 20th centuries, as simulated by CMIP5 models

P. J. Harvey[1], S. W. Grab[1], J. Malherbe[2,3]

[1]School of Geography, Archaeology and Environmental Studies, University of the Witwatersrand, Johannesburg, South Africa

[2]CSIR Natural Resources and the Environment: Climate Studies, Modelling and Environmental Health, Pretoria, South Africa

[3]Agriculture Research Council – Institute for Soil, Climate and Water, Pretoria, South Africa

Contents of this file

Text S1 to S2

Figures S1 to S3

Table S1

Introduction

This supporting information provides a comparison of various historical experiments (natural, solar, volcanic, anthropogenic and historical) and a comparison of the different volcanic forcing datasets used in the CMIP5 models in this paper. Three figures are supplied, the first showing temperature responses to various forcing experiments, the second showing a scatter plot of temperature response vs SO_2 (Sulphur Dioxide) for each eruption, and the third a variety of Superposed Epoch Analysis (SEA) diagrams. Finally, a table is supplied to show the CMIP5 models that were used in this study, as well as which forcing experiments they provided.

Text S1.

To identify likely reasons for temperature anomalies, SH temperature responses are compared to the various forcing experiments (Figure S1). The various forcing experiments include:

- Historical experiments which incorporate both natural and anthropogenic forcing. Given that this is the most realistic scenario, it is used it for all analyses.
- Historical Nat experiments, which incorporate only volcanic and solar forcing, are used to establish temperature responses to natural forcing.
- Historical Misc experiments use a variety of individual forcers, or a combination of forcers. Three of these experiments are examined to establish temperature response to individual forcers. The first experiment uses only solar forcing as a variant, the second only volcanic forcing, and the third only anthropogenic forcing.

Significant cooling is observed where volcanic forcing is included in the experiments (i.e. historical and natural experiments and the volcanic-only forced experiment, for which temperature reductions are strongest). Significant temperature reductions are absent in the solar-only and anthropogenically forced experiments; it is thus inferred that these negative temperature anomalies are associated with volcanic forcing.

Text S2.

Both the Sato (1993) and Ammann (2007) datasets provide monthly stratospheric optical depth values. However, particle radius varies in Sato, but is fixed in Ammann. The MRI-CGCM3 model simulates the conversion of SO_2 within the model itself.

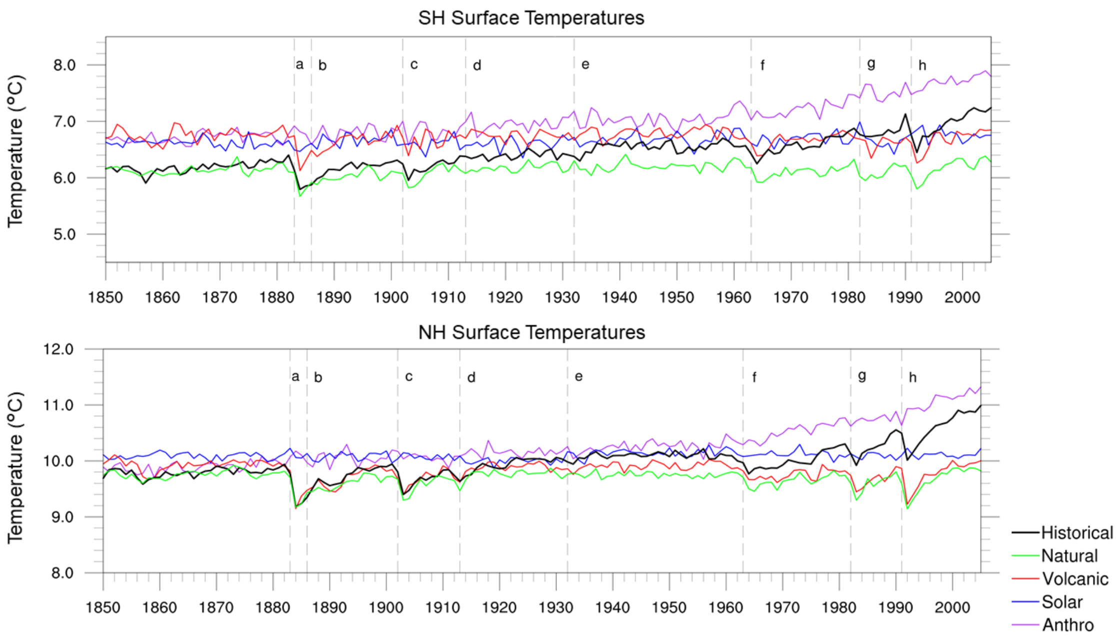

Figure S1. CMIP5-simulated annual near-surface temperature responses to the various forcing experiments for SH and NH averages. The historical experiment is represented by the black line, the natural-only forcing (volcanic + solar) by the green line, the volcanic-only forcing shown by the red line, the solar-only forcing by the blue line and the anthropogenic by the purple. See Table 2 for eruption names.

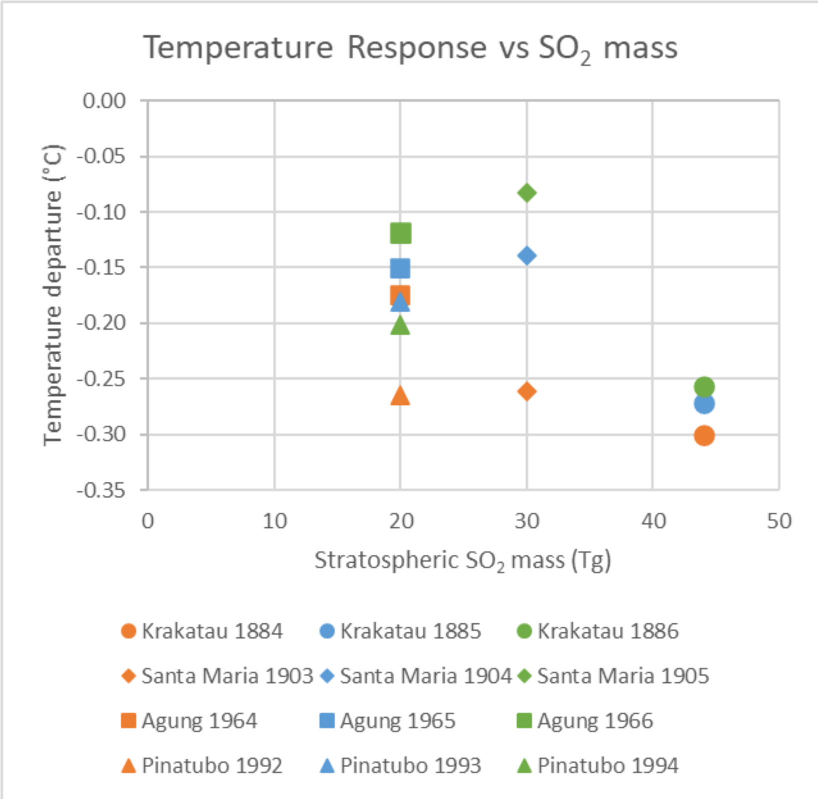

Figure S2. CMIP5-simulated annual SH temperature response vs the stratospheric SO_2 mass for the first, second and third year after each major eruption.

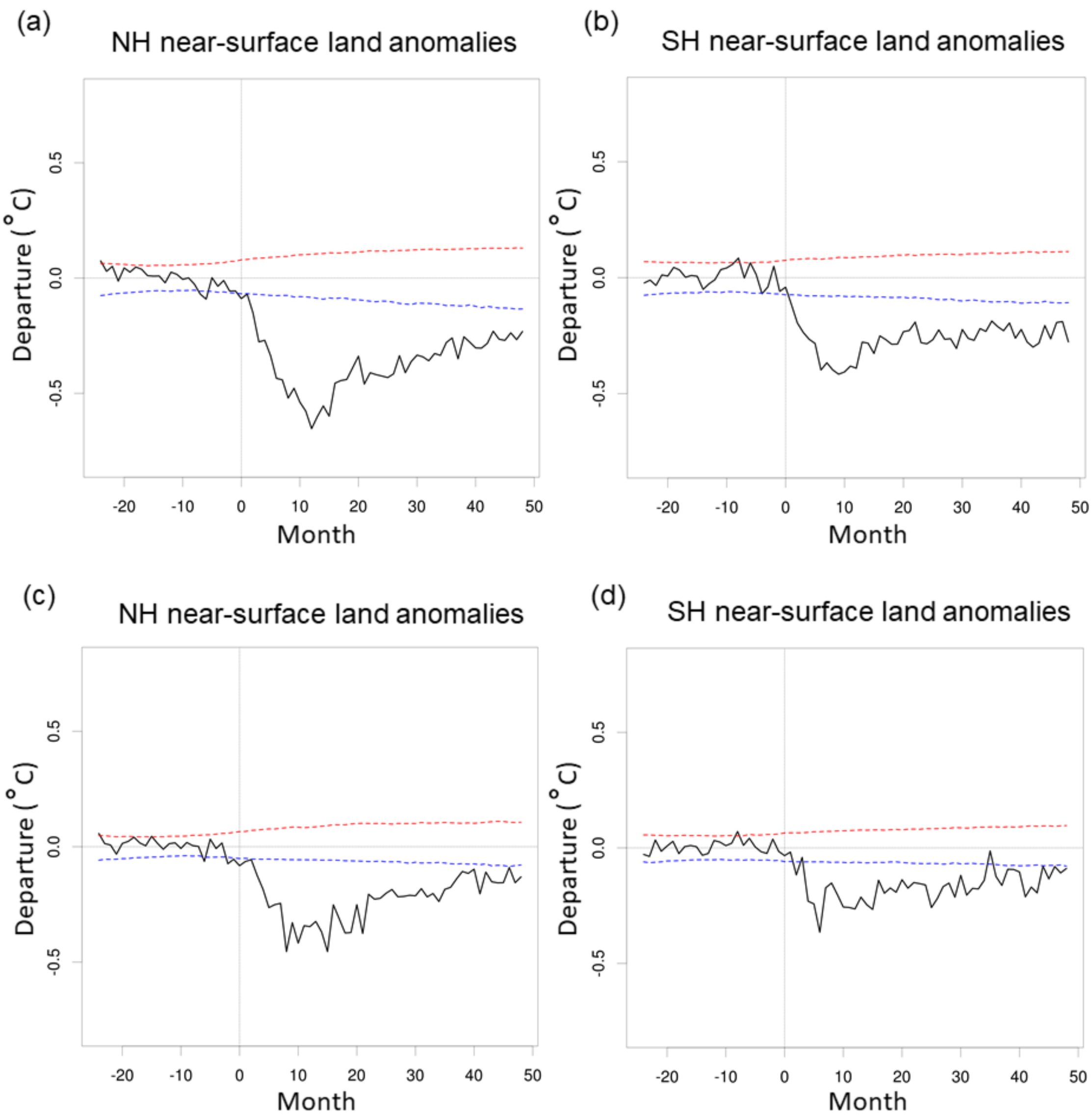

Figure S3. Superposed Epoch Analysis of: CMIP5-simulated (a) monthly NH and (b) SH near-surface land temperature anomalies following major eruptions (SO_2 > 20 Tg); and of (c) monthly NH and (d) SH near-surface land temperature anomalies following all eight eruptions analysed in this paper. The 5th and 95th percentiles are represented by blue and red lines respectively.

Table S1. The CMIP5 models used, volcanic forcing data set, and experiments each model group had contributed to (Driscoll *et al.*, 2012; Taylor *et al.*, 2012).

Model Name	Institution	Volcanic Forcing	Hist[a]	Nat[b]	Vol[c]	Sol[d]	Anthro[e]
CanESM2	Canadian Centre for Climate Modelling and Analysis	Sato *et al.* (1993)	Y	Y		Y	
CCSM4	National Center for Atmospheric Research	Ammann *et al.* (2007)	Y	Y	Y	Y	Y
CNRM-CM5	Centre National de Recherches Météorologiques & Centre Européen de Recherche et de Formation Avancée en Calcul Scientifique	Ammann *et al.* (2007)	Y	Y			
CSIRO-Mk3-6-0	Commonwealth Scientific and Industrial Research Organisation	Sato *et al.* (1993)	Y	Y	Y		
GISS-E2-H	NASA Goddard Institute for Space Studies	Sato *et al.* (1993)	Y	Y	Y	Y	
GISS-E2-R (P1)	NASA Goddard Institute for Space Studies	Sato *et al.* (1993)	Y	Y	Y	Y	Y
GISS-E2-R (P3)	NASA Goddard Institute for Space Studies	Sato *et al.* (1993)	Y	Y	Y	Y	Y
MIROC-ESM	Japan Agency for Marine-Earth Science and Technology, Atmosphere and Ocean Research Institute (The University of Tokyo), and National Institute for Environmental Studies	Sato *et al.* (1993)	Y	Y			
MIROC-ESM-CHEM		Sato *et al.* (1993)	Y	Y			
MRI-CGCM3	Meteorological Research Institute	Interactive	Y	Y			
NorESM1-M	Norwegian Climate Centre	Ammann *et al.* (2007)	Y	Y			

[a] Hist - historical experiments where all forcings are incorporated

[b] Nat - historicaNat experiments where only natural forcing (volcanic and solar) was incorporated

[c] Vol - historicalMisc experiments where only volcanic forcing varies

[d] Sol - historicalMisc experiments where only Solar forcing varies

[e] Anthro - historicalMisc experiments where only anthropogenic forcing varies

Chapter Three: Southern Hemisphere Continental Temperature Responses to Major Volcanic Eruptions since 1883 in CMIP5 Models
(Submitted to Theoretical and Applied Climatology)

Abstract

Although global and Northern Hemisphere (NH) temperature responses to volcanic forcing have been extensively investigated, knowledge of such responses over Southern Hemisphere (SH) continental regions is still limited. Here an ensemble of CMIP5 models is used to explore SH temperature responses to four major volcanic eruptions: Krakatau (1883), Santa Maria (1902), Agung (1963) and Pinatubo (1991). Focus is on near-surface temperature responses over southern continental landmasses including southern South America (SSA), southern Africa (SAF) and Australia and their seasonal differences. Findings indicate that for all continents, temperature responses were strongest and lasted longest following the Krakatau eruption. Responses in Australia had the shortest lag time, strongest maximum seasonal response, as well as the most significant monthly anomalies. In contrast, SSA records the longest lag time, weakest maximum seasonal temperature response, and lowest number of monthly negative anomalies following these eruptions. In most cases, the strongest single-season response occurred in austral autumn or winter, and the weakest in summer or spring. It is tentatively proposed that cooler temperature responses are likely caused, at least in part, by the intensification of the westerlies and associated mid-latitude cyclones and anti-cyclones.

1. Introduction

The relationship between volcanoes and climate has long been a scientific fascination (Humphreys 1913; Gilliland 1982; Robock 2000; Allen *et al*. 2018), and so much so, that Past Global Changes (PAGES) now has a working group examining volcanic impacts on climate and society (VICS). It is well-recognized that volcanic events emitting c. 5 Tg or more of sulphur-containing gases into the lower stratosphere, where chemical reactions form sulphate aerosols, can affect climate (Timmreck 2018). These aerosols not only change the earth's energy balance by reducing incoming solar radiation through reflection and scattering, but also cause absorption of near infrared and long-wave radiation, with consequential warming of the lower stratosphere (Stenchikov *et al*. 1998; Langmann 2014). It is understood that changes in radiation induce stronger zonal winds and increase temperature and density gradients between the poles and equator, thereby strengthening the Northern Hemisphere (NH) polar vortex (Perlwitz and Graf 1995; Zambri and Robock 2016). However, given the expanse of oceans in mid- to high latitudes of the Southern Hemisphere (SH), the SH polar vortex and jet streams are more robust. This weakens the expected impact in southerly latitudes (Robock *et al*. 2007), nonetheless, it too is susceptible to volcanic forcing (Hudson 2012; Kidston *et al*. 2015).

Major eruptions may cause global annual temperatures to decrease by at least 0.1°C for two to three years following the eruption (Robock 2000; Brönnimann *et al*. 2019). Findings generally show cooling over much of the NH, particularly in summer, and widespread mid to high latitude winter warming (Stoffel *et al*. 2015; Zambri and Robock 2016; Zambri *et al*. 2017). SH temperature responses are somewhat weaker than those in the NH (Man *et al*. 2014; Raible *et al*. 2016), with cooling of c. 0.1-0.2°C for 1-2 years after major eruptions (Mass & Portman 1989; Robock & Mao 1995). CMIP5 models have simulated a SH autumn/winter cooling between -0.19°C and -0.36°C (Harvey *et al*. 2020). Somewhat stronger cooling responses (< -0.25°C) have been modelled over SH mid-latitudes, but with warming over eastern Antarctica following the Agung (1963), El Chichón (1982) and Pinatubo (1991) eruptions (Ménégoz *et al*. 2018). Although tropospheric responses to major eruptions still require further detailed investigation, Barnes *et al*. (2016) have identified stratospheric warming in the tropics and cooling over both poles, following the 1991 Pinatubo eruption. While temperatures cooled over most of South America, strongest negative departures were modelled at higher latitudes following the Pinatubo eruption (Colose *et al*. 2016). Despite such recent work on volcanic forcing effects on SH climate, a large knowledge gap still remains, with many questions still unanswered. For instance, comparisons of seasonal climatic responses to such eruptions between inter-continental SH landmasses has yet to be investigated.

Given that many factors (e.g. eruption season, location and strength; pre-condition of the atmosphere, aerosol altitude) influence climatic response to volcanic forcing (Oman *et al*. 2005; Colose *et al*. 2015; Predybaylo *et al*. 2017; Stevenson *et al*. 2017; Zuo *et al*. 2018; Sun *et al*. 2019, Krishnamohan *et al*. 2019), responses (spatially and temporally) are likely to differ between eruptions. To this end, the aim is to establish how individual major volcanic eruptions since 1883 may have affected SH continental temperatures, and specifically how these responses varied spatially (within and between continents) and temporally (during specific seasons) following these eruptions. Using historical simulations from the Coupled Model Intercomparison Project, phase 5 (CMIP5) (Taylor *et al*. 2012), temperature responses following the eruptions of Krakatau (1883), Santa Maria (1902), Agung (1963) and Pinatubo (1991) are investigated.

2. Models and Data

Climate model simulations from the Coupled Model Intercomparison Project, phase 5 (CMIP5) (Taylor *et al*. 2012), are utilized for the purpose of this study (see Table 1). A subset of 11 different models (Table 1) are used, selected based on their ability to simulate a satisfactory temperature response (in Santer *et al*. 2013; Supplementary Fig. S1) to volcanic forcing in the lower stratosphere (see Barnes *et al*. 2016 for more details). The first three realizations of each model were used, with the exception of the MIROC-ESM-CHEM model, for which only one realization was available, and the GISS-E2_R model for which two different physics-versions were used. Both physics-version one (p1) and three (p3) were incorporated due to the different ways in which aerosols are calculated (prescribed for p1 and calculated internally in p3). This enabled the analysis of 31 simulations.

For this study, an ensemble of the historical experiments is used, which include both natural (volcanic and solar) and anthropogenic climate forcing and cover the period 1850-2005. Volcanic forcing was not prescribed for CMIP5, so models implemented the forcing from either Sato *et al*. (1993) or Ammann *et al*. (2007), except for the MRI-CGCM3 model, which calculated it interactively. Notably, climate models do not perfectly simulate responses to volcanic forcing, and may either over- or under-estimate the response (Neukom *et al*. 2019). CMIP5 models generally overestimate the response to volcanic forcing (Driscoll *et al*. 2012; Lehner *et al*. 2016; Raible *et al*. 2016). Results thus reflect what the selection of CMIP5 models show, and may not necessarily accurately represent actual near-surface temperature conditions. Results do nevertheless provide valuable indications of relative temperature responses to volcanic forcing and offer an opportunity for future comparison with ground-based instrumental records where these exist. However, the CMIP5 results are compared with reanalysis data from NOAA/OAR/ESRL, the 20th Century Reanalysis V2 (20CRv2).

Table 1. Models used in this study, and the volcanic forcing dataset that each incorporated (Driscoll et al., 2012; Taylor et al., 2012).

Model Name	Institution	Volcanic Forcing
CanESM2	Canadian Centre for Climate Modelling and Analysis	Sato et al. (1993)
CCSM4	National Center for Atmospheric Research	Ammann et al. (2007)
CNRM-CM5	Centre National de Recherches Météorologiques & Centre Européen de Recherche et de Formation Avancée en Calcul Scientifique	Ammann et al. (2007)
CSIRO-Mk3-6-0	Commonwealth Scientific and Industrial Research Organisation	Sato et al. (1993)
GISS-E2-H	NASA Goddard Institute for Space Studies	Sato et al. (1993)
GISS-E2-R (P1)	NASA Goddard Institute for Space Studies	Sato et al. (1993)
GISS-E2-R (P3)	NASA Goddard Institute for Space Studies	Sato et al. (1993)
MIROC-ESM	Japan Agency for Marine-Earth Science and Technology, Atmosphere and Ocean Research Institute (The University of Tokyo), and National Institute for Environmental Studies	Sato et al. (1993)
MIROC-ESM-CHEM		Sato et al. (1993)
MRI-CGCM3	Meteorological Research Institute	Interactive
NorESM1-M	Norwegian Climate Centre	Ammann et al. (2007)

Each of the model simulations were linearly regridded to a 2° by 2° lat-long grid before having been combined into a multi-model mean. Near-surface (2m) temperatures are analysed, and all temperatures mentioned in this paper are a SH mean of each continent (calculated from 0° latitude and southwards). For both the CMIP5 and 20CRv2 datasets, annual, seasonal and monthly mean anomalies are presented with respect to a 20-year running mean. So as to calculate statistical significance, a bootstrap approach (Efron 1979) was used to resample the time series of departures 5000 times. To distinguish between random occurrences and significant climatic responses, the 5th and 95th percentiles of the bootstrapped dataset were incorporated to test for significant temperature responses (Haurwitz and Brier 1981; Rao *et al*. 2017).

Four eruptions from the period 1850-2005 are considered including Krakatau (August 1883), Santa Maria (October 1902), Agung (March 1963) and Pinatubo (June 1991) (Table 2). Apart from Agung (VEI = 4), the selected eruptions had a VEI ≥ 6 and all these are known to have impacted global temperatures, apart from Agung which largely impacted the SH (Mass and Portman 1989; Gleckler *et al*. 2006; Zanchettin *et al*. 2012; Khodri *et al*. 2017; Ménégoz *et al*. 2018, Harvey *et al*. 2020). Temperatures are examined for southern South America (SSA) at latitudes 0° to 60°S, southern Africa from 0° to 35°S and Australia which lies between 10°S and 45°S.

Table 2. The four eruptions analysed in this paper.

Eruption	Date	Latitude	VEI[i]	DVI[ii]	Total Emission (Tg of SO2)[iii]
Krakatau	1883	6S	6	1000	22
Santa Maria	1902	15N	6	600	3.8
Agung	1963	8S	4	800	7.5
Mt Pinatubo	1991	15N	6	1000	18

[i] VEI: Volcanic Explosivity Index (Newhall & Self, 1982).

[ii] DVI: Dust Veil Index (Lamb, 1970): a measure of the impact (e.g. on climate) of dust and aerosols released from an eruption.

[iii] from Neely III and Schmidt (2016).

3. Results

3.1 Temperature response to volcanic eruptions: Southern South America (SSA)

3.1.1 SSA: Krakatau

Krakatau erupted on 27th August 1883, placing 22 Tg of SO_2 into the lower stratosphere (Neely III and Schmidt 2016). In SSA, near-surface temperatures responded significantly (Fig. 1) during all seasons of the first (y1), second (y2) and third (y3) years after the eruption, with austral summer and autumn seasons cooling significantly below normal during the fourth year as well (DJF y1: -0.26°C, y2: -0.26°C, y3 -0.28°C; MAM y1: -0.34°C, y2: -0.26°C, y3: -0.27°C; JJA y1: -0.38°C, y2: -0.42°C, y3: -0.28°C; SON y1: -0.29°C, y2: -0.35°C, y3: -0.28°C) (Fig. 2). The strongest response is measured for the second winter (-0.42°C) and based on a 3-year mean seasonal temperature departure, the strongest responding season was winter (-0.36°C), while the weakest was summer (-0.27°C). The first month in which a significant below-normal anomaly is simulated in SSA is May 1884 (-0.24°C), nine months after the eruption (Fig. 3a). While 78% of monthly anomalies from the time of the event until the end of y3 were below normal, 32% were significantly below normal.

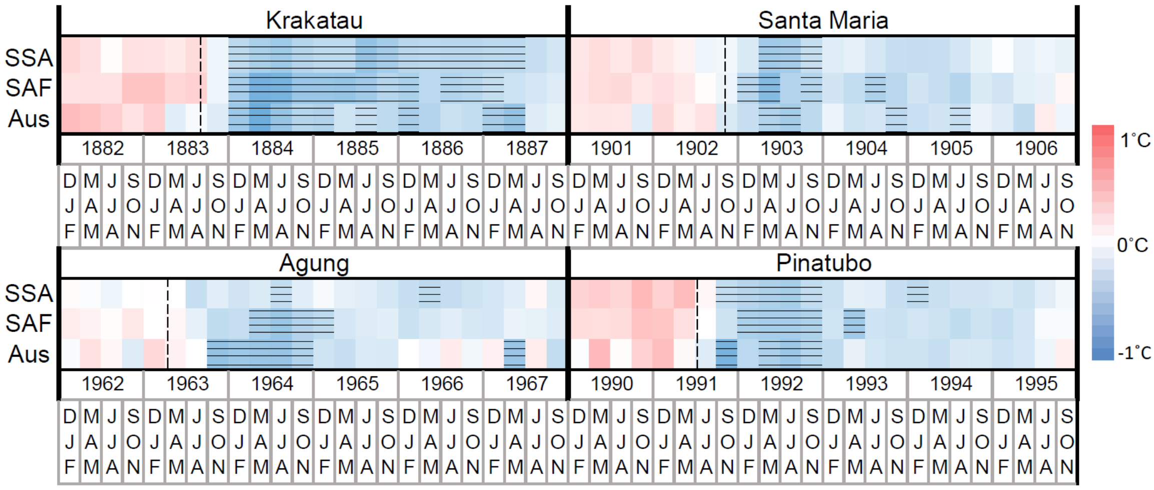

Fig. 1. CMIP5-simulated seasonal temperature anomalies for each continent in the SH (southern South America (SSA); southern Africa (SAF) and Australia (Aus)), over the period for each of the four eruptions (Krakatau, Santa Maria, Agung, Pinatubo), starting two years before the eruption and ending three years after the event. The vertical dashed lines represent the eruption event. Blocks with hashed lines represent significant anomalies.

Cooling occurred during all seasons over all of SSA in y1 and y2 (Fig. 4 and Fig. S1, Fig. S2, Fig. S3 in Online Resource 1). Temperatures had recovered over southernmost South America in y3, but remained below normal over the northern regions of SSA during all seasons (apart from autumn when temperatures remained below normal throughout SSA). Winter, which records the most prominent temperature response, had strongest cooling over northern parts of SSA (35-0°S) in y1. In winter of y2, strongest cooling occurred over Chile and western Argentina (between -0.40°C and -0.80°C) over latitudes 40-20°S. However, in y3, temperatures in the southern parts of SSA (60-30°S) had recovered to near normal, while those further north (25°S-0°) remained below normal (between -0.20 and -0.60°C).

3.1.2 SSA: Santa Maria

Santa Maria erupted on 24th October 1902, emitting 3.8 Tg of SO_2 into the lower stratosphere (Neely III and Schmidt 2016). Although seasonal temperatures cooled below normal in SSA during the first three years (Fig. 1), responses were only significant in austral autumn, winter and spring of y1 (1903), with the strongest response occurring in autumn (MAM y1: -0.37°C; JJA y1: -0.35°C; SON y1: -0.23°C) (Fig. 2). The strongest 3-year mean seasonal temperature departure was for austral autumn (-0.23°C) and the weakest for austral summer (-0.17°C), and overall, considerably weaker than that for Krakatau. From the time of the eruption until the end of y3, none of the negative monthly anomalies were statistically significant, although 87% of monthly temperature anomalies were below normal (Fig. 3a).

Temperatures cooled throughout SSA in both autumn and winter, with northern parts of SSA (30-0°S) experiencing strongest cooling (between -0.20°C and -0.80°C) (Fig. 4, Fig. S2) in y1 (1903). In y2, temperatures in autumn and winter warmed to above normal (between 0.00°C and 0.60°C) over the central regions of SSA (35-20°S), while those in northern and southern regions were below normal (between -0.10°C and -0.60°C). During autumn and winter of y3, temperatures in northern parts of SSA remained below normal (between -0.10°C and -0.60°C), while those in the south returned to near normal (between -0.20°C and +0.20°C). During summer and spring seasons, the response is much weaker (between -0.10°C and -0.40°C), with partial cooling over SSA.

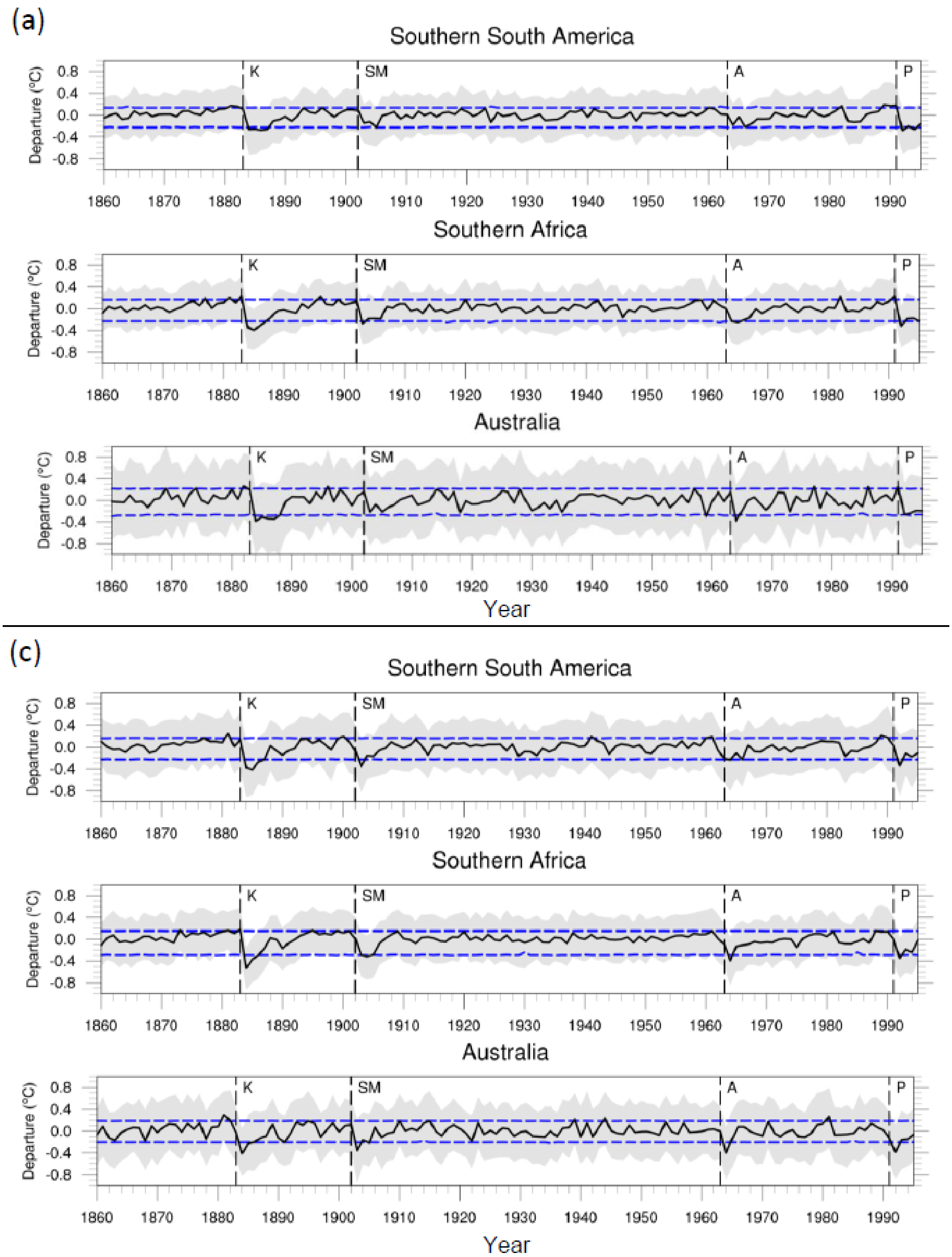

Fig. 2 CMIP5-simulated seasonal near-surface temperature anomalies for the continents of southern South America, southern Africa and Australia for the seasons of (a) austral summer (DJF), (b) autumn (MAM), (c) winter (JJA) and (d) spring (SON). Gray shading = 25th and 75th percentile ensemble spread, blue dashed lines= statistical significance (90% confidence interval), dashed vertical lines = eruption events of (K) Krakatau, (SM) Santa Maria, (A) Agung, and (P) Pinatubo.

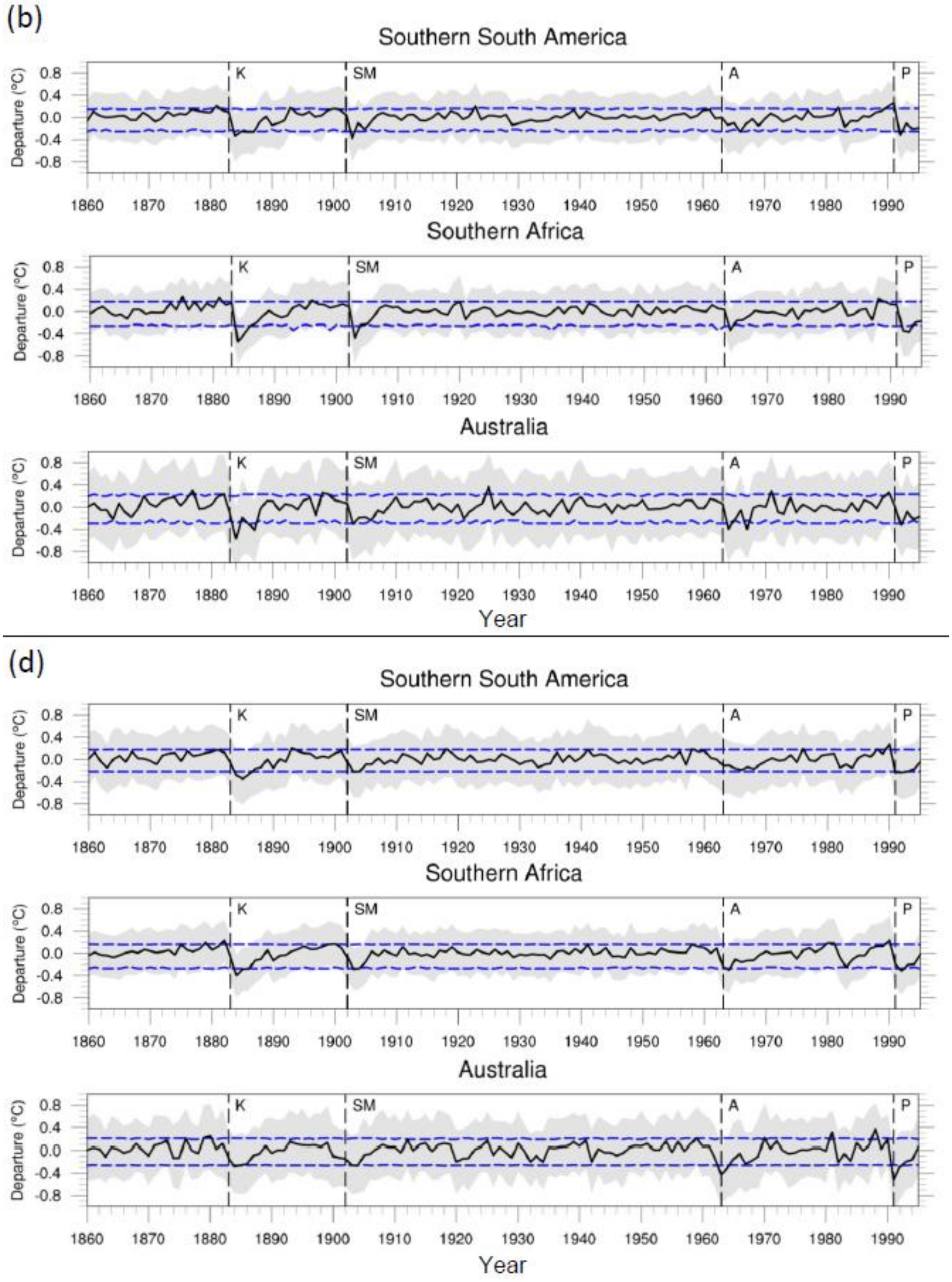

Fig. 2 continued.

3.1.3 SSA: Agung

Mt Agung erupted on 17th March 1963 and emitted 7.5 Tg of SO_2 into the lower stratosphere (Neely III and Schmidt 2016). Only austral winter of 1964 and autumn of 1966 had significant negative temperature departures in SSA (JJA y1: -0.24°C; MAM y3: -0.26°C)(Fig. 2). The greatest single-season response occurred in autumn of y3, and despite this, the strongest 3-year mean seasonal temperature departure was for austral winter (JJA) (-0.19°C), while the weakest was for austral summer (-0.15°C). The first significant monthly temperature departure is noted for January 1964 (-0.27°C), 10 months after the eruption (Fig. 3a). While 91% of monthly temperature anomalies were below normal from the time of the eruption until the end of y3, only 7% were significantly below normal.

Temperatures cooled over portions of SSA during all seasons in y1 (1964) and y2 (Fig. 4 and Fig. S1, Fig. S2, Fig. S3 in Online Resource 1), but it was not until y3 when the entire SSA experienced negative temperature anomalies. Contrary to the response simulated after the Krakatau and Santa Maria eruptions, temperatures in y2 after the Agung eruption were warmer than normal in northern parts of SSA (between 0.00 and 0.60°C) but remained cooler than normal in southern regions (between -0.10°C and -0.60°C).

3.1.4 SSA: Pinatubo

Mt Pinatubo erupted on 15th June 1991, emitting 18 Tg of SO_2 into the stratosphere (Neely III and Schmidt 2016). Each season exhibited significant mean seasonal responses after the Pinatubo eruption in SSA during y1 (Fig. 1). Austral autumn and winter temperatures responded significantly for one season respectively (y1: -0.32°C, -0.34°C respectively) (Fig. 2). Austral spring and summer experienced significant negative temperature departures for two seasons in y0 and y1 for spring (y0: -0.23°C, y1: -0.24°C), and y1 and y3 for summer (y1: -0.28°C, y3: -0.26°C). While the strongest single-season response occurred in winter, the strongest 3-year mean seasonal temperature departure occurred in austral summer (-0.25°C), and the mean 3-season response for all remaining seasons was -0.21°C. The first month for which a significant anomaly occurred was March 1992 (-0.24°C) (nine months after the eruption) (Fig. 3a). During the period from the eruption date until the end of y3, 81% of monthly anomalies were below normal while 23% were significantly below normal.

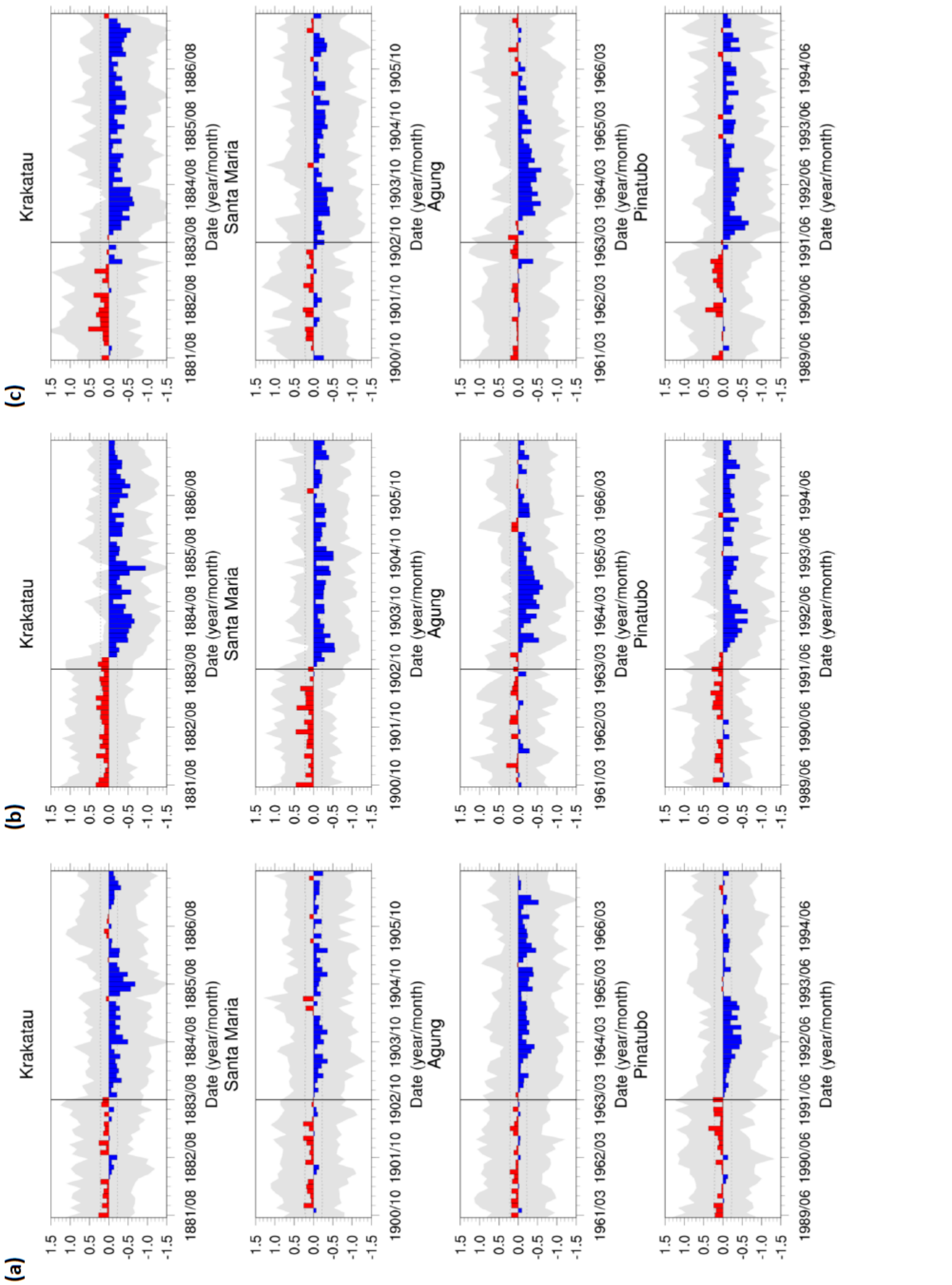

Fig. 3 CMIP5-simulated monthly near-surface temperature anomalies for the continents of (a) southern South America, (b) southern Africa and (c) Australia for each of the four major eruptions. Gray shading = ensemble spread between 25th and 75th percentiles.

Temperatures cooled over all of SSA in y1 during all seasons (Fig. 4 and Fig. S1, Fig. S2, Fig. S3 in Online Resource 1). In y2, temperatures were close to normal for autumn and winter, but summer maintained temperatures below normal (between -0.20°C to -0.80°C) in the central and southernmost regions of SSA, as also found by Colose *et al*. (2016). Northernmost temperatures remained below normal (between -0.10°C and -0.40°C) during spring of y2. Although temperatures during autumn and winter seemed to recover in y2, they were cooler again in y3 over most of SSA (between -0.10°C and -0.60°C).

3.1.5 SSA Summary

In SSA, significant negative annual temperature anomalies are detected after all major eruptions since 1883. The longest and strongest annual response is measured after Krakatau, which had significant annual anomalies for three years (average of -0.30°C), whereas the annual anomalies following the other three eruptions were only significant for y1 (-0.17°C and -0.22°C respectively). The strongest seasonal response occurred during winter for Krakatau and Pinatubo, and autumn for Santa Maria and Agung, while the weakest response generally occurred during summer. Significant monthly responses typically first occur 9-10 months after an eruption. Spatially, cooling occurred over most of SSA in y1 (except Agung, following which temperatures in the tropics did not fall below normal until y3). Strongest cooling often occurs between 25°S and northwards except after Pinatubo. Temperatures typically first recovered in southern parts of SSA following the investigated eruptions.

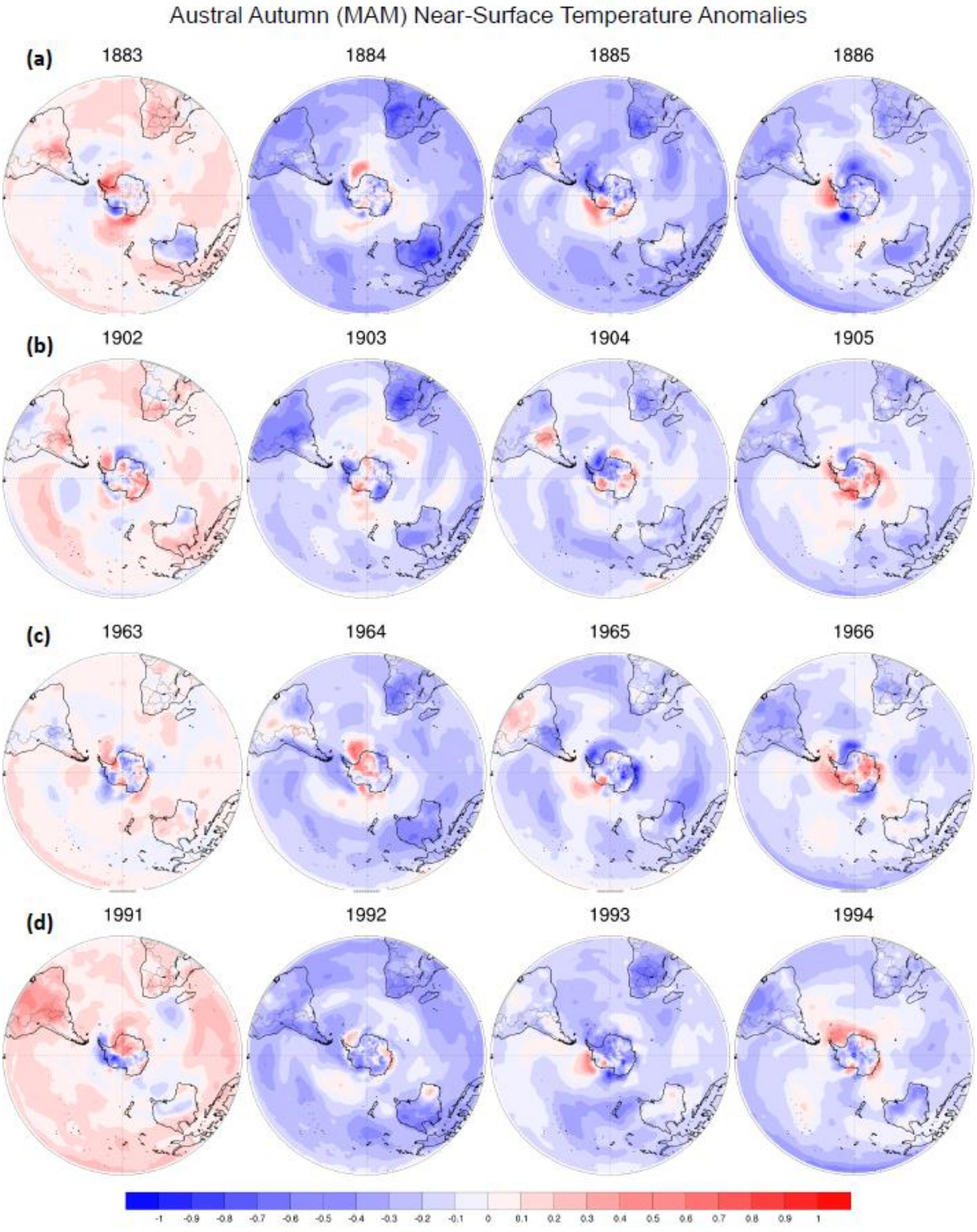

Fig. 4 CMIP5-simulated spatial maps of austral autumn temperature anomalies over the SH for the eruptions of (a) Krakatau, (b) Santa Maria, (c) Agung and (d) Pinatubo. The same figures for summer, winter and spring can be found in the Online Resource 1 (Fig. S1, Fig. S2, Fig. S3).

3.2 Temperature response to volcanic eruptions: Southern Africa (SAF)

3.2.1 SAF: Krakatau

Following the Krakatau eruption, SAF temperatures were significantly cooler than normal during all seasons in y1 and y2, and in all except autumn in y3 (Fig. 1). The strongest responses appeared in austral autumn and winter during y1 (-0.54°C and -0.53°C respectively). Spring and summer of y1 had anomalies of -0.40°C and -0.35°C respectively. Autumn and winter also displayed the strongest 3-year mean seasonal negative temperature departures of -0.41°C and -0.40°C respectively (Fig. 2), with the weakest 3-season mean occurring in spring (-0.32°C). During the second and third years, mean temperature anomalies ranged between -0.26°C and -0.41°C for all seasons. The first significant monthly temperature response is recorded in February 1884 (-0.34°C), six months after the eruption (Fig. 3b). Between the eruption event and the end of y3, 93% of monthly temperature anomalies were negative, and 39% were significantly below normal.

All of SAF cooled during y1-y3 after the Krakatau eruption. During autumn (Fig. 4), winter (Fig. S2) and spring (Fig. S3) of y1, strong cooling (between -0.40°C and -1.00°C) occurred throughout the sub-continent. The same strong anomalies continued into y2 over southernmost SAF (Namibia, Botswana and South Africa) during summer and autumn, shifting over central SAF during winter but decreasing in spring of y2. In y3, strong cooling (between -0.40°C and -0.80°C) continued over Namibia, Botswana and surrounding regions during summer, and over Namibia and western South Africa during winter and spring (between -0.40°C and -0.60°C).

3.2.2 SAF: Santa Maria

Temperature anomalies following the Santa Maria eruption, although negative for all seasons, were only significant for the summer of y0, autumn and spring of y1, and winter of y2 (-0.28°C, -0.48°C, -0.29°C, -0.32°C respectively)(Fig. 1). Mean winter temperature departures in y1, though not significant, cooled by -0.30°C. The strongest seasonal response occurred in autumn of y1 (-0.48°C), while the most pronounced 3-year mean seasonal temperature departure also occurred in autumn (-0.31°C) and was weakest (-0.21°) during summer (Fig. 2). The first month demonstrating a significant temperature departure is February 1903 (-0.23°C), four months after the eruption (Fig. 3b). While 95% of monthly anomalies from the time of the event until the end of y3 were below normal, only 18% were significantly below normal.

Spatially, all of SAF had below normal temperatures for y1 to y3 during all seasons except spring (Fig. S3) in y3 when temperatures over South Africa and the western coast of SAF remained above normal (between 0.20°C and 0.40°C). Strongest cooling occurred over most of SAF during autumn (Fig. 4) of y1 (-0.40°C to -1.00°C). Notable strong cooling (-0.40°C to -0.60°C) occurred between 20 and 30°S in summer of y1, between 10 and 20°S in winter and spring of y1, and between 15 and 25°S during autumn and winter of y2, which extended to southernmost SAF during spring of y2.

3.2.3 SAF: Agung

Following the Agung eruption, temperature departures were significant for one year (y1); and for autumn (-0.34°C), winter (-0.39°C) and spring (-0.30°C) of y1 and summer of y2 (-0.25°C) (Fig. 1). Although the strongest seasonal response in y1 occurred during winter, the strongest 3-year mean seasonal temperature departure is measured for summer (-0.23°C), while the weakest 3-season mean departure occurred during spring (-0.19°C) (Fig. 2). Negative temperature anomalies are first significant in September 1963 (-0.22°C), six months after the eruption (Fig. 3b). From the time of the eruption until the end of y3, 82% of monthly temperature anomalies were below normal, however, only 23% were significantly below normal.

All of SAF had negative temperature departures during all seasons in y1 (Fig. 4 and Fig. S1, Fig. S2, Fig. S3 in Online Resource 1). Strong autumn and winter cooling occurred over most of SAF, and over southernmost SAF during spring (between -0.40°C and -0.80°C). All seasonal temperatures, apart from summer, returned to near normal in y2 and y3 (between -0.20°C and 0.20°C), with summer temperatures remaining below normal (between -0.20°C and -0.04°C).

3.2.4 SAF: Pinatubo

SAF temperature anomalies were significantly below normal after the Pinatubo eruption during all seasons of y1, and autumn of y2 (DJF: -0.33°C; MAM y1: -0.35°C; y2: -0.37°C; JJA: -0.35°C; SON: -0.31°C) (Fig. 1). Autumn had the strongest response in y1, and also the strongest 3-year mean seasonal temperature departure (-0.30°C), while the weakest 3-year response occurred in summer (-0.23°C) (Fig. 2). The first month in which a significant temperature departure occurred was February 1992 (-0.28°C), 8 months after the eruption (Fig. 3b). During the period from the eruption date until the end of y3, 91% of monthly anomalies were below normal, of which 28% were significantly below normal.

Throughout y1-y3, all seasonal temperatures cooled to below normal over most of SAF (Fig. 4 and Fig. S1, Fig. S2, Fig. S3 in Online Resource 1). Strong cooling (-0.40°C to -0.60°C) occurred in southernmost regions during summer, autumn and winter of y1, and over the central regions during spring. Strong cooling (-0.40°C to -0.80°C) in y2 only occurred during autumn over the central regions (10 to 25°S).

3.2.5 SAF Summary

Mean annual temperatures over southern Africa decreased significantly after all four eruptions in y1, and also in y2 and y3 after Krakatau. The strongest response is detected after Krakatau, and the weakest followed Santa Maria. Seasonal temperature responses are strongest during autumn for most eruptions, apart from Agung, after which winter had the strongest response. The weakest responses occurred in either spring (following Krakatau and Agung) or summer (after Santa Maria and Pinatubo). Significant responses typically occurred 4-8 months after an eruption. Spatially, strongest cooling trends occurred over the central or southern regions of SAF (10°S and southwards).

3.3 Temperature response to volcanic eruptions: Australia

3.3.1 Australia: Krakatau

Following the eruption of Krakatau, temperatures in Australia were significantly cooler than normal during all seasons in y1 (1884) (DJF: -0.38°C; MAM: -0.57°C;

JJA: -0.41°C, SON: -0.28°C) (Fig. 1). Significant anomalies continued into summer of y2 and y3 (y2: -0.31°C; y2: -0.34°C), and winter of y2 (-0.23°C) (Fig. 2). The strongest 3-year mean seasonal departures occurred in autumn (-0.35°C) and weakest in spring (-0.26°C). The first month recording a significant response (-0.31°C) was January 1884 (five months after the eruption) (Fig. 3c). While 95% of monthly anomalies from the time of the event until the end of y3 were below normal, 49% were significantly below normal.

With the exception of spring, cool anomalies occurred over the entire continent during all other seasons in 1884 (Fig. 4 and Fig. S1, Fig. S2, Fig. S3 in Online Resource 1). Strong cooling (-0.40°C to -0.80°C) commences in southern parts of Australia during summer of y1, which expands to the whole continent and intensifies (-0.40°C to -1.20°C) during autumn, but then starts to weaken and spatially retract during winter. However, the cooling effect is still notable in northern regions during winter and spring of y1. Temperature anomalies are weaker in y2, with some being above normal during autumn (0.20°C). Strong cooling (-0.40°C to -0.60°C) occurs again in summer and autumn of y3 over central and eastern Australia.

3.3.2 Australia: Santa Maria

After the Santa Maria eruption, Australian temperature anomalies were below normal during austral autumn and winter of y1 (MAM: -0.31°C; JJA: -0.35°C), spring of y2 (-0.27°C) and winter of y3 (-0.22°C) (Fig. 1). Summer anomalies were not significant, but still cooled by -0.22°C in y1 (Fig. 2). Winter had the strongest modelled response in y1 as well as the strongest 3-year mean seasonal temperature departure (-0.25°C), with summer recording the weakest 3-year mean departure (-0.17°C). Although negative temperature anomalies are modelled for the same month in which Santa Maria erupted, significant cooling (-0.25°C) over Australia is only apparent from the sixth month (April 1903) after the eruption (Fig. 3c). From the time of the eruption until the end of y3, 97% of monthly temperature anomalies were below normal, but only 20% were significantly below normal.

After Santa Maria, cooling occurred over all of Australia during all seasons of y1 (Fig. 4 and Fig. S1, Fig. S2, Fig. S3 in Online Resource 1). Strong cooling (between -0.40°C and -0.60°C) is measured over eastern parts of Australia in autumn and spring, and over western regions in summer and winter of y1. In y2, most of the continent still experienced below normal anomalies, except during summer when temperatures returned to normal over parts of Australia (max 0.20°C). Strong cooling (-0.20 to -0.80°C) only occurred over south-western regions during spring. Notable negative temperature departures (-0.40°C to -0.80°C) occurred in eastern regions of Australia, while above normal anomalies (up to 0.40°C) occurred in the western regions during summer of y3.

3.3.3 Australia: Agung

Australian spring temperatures were significantly lower than normal during the same year that Agung erupted (y0: -0.42°C) (Fig. 2). Temperatures then remained significantly below normal during all seasons in y1 (DJF: -0.38°C; MAM: -0.40°C; JJA: -0.40°C; SON: -0.31°C) (Fig. 2). Although the strongest single season response is spring of y0, the strongest 3-year mean seasonal temperature departure occurs in autumn (-0.22°C), and the weakest is modelled for winter (-0.14°C). The first month recording a significantly below normal temperature was October 1963 (-0.23°C), seven months after the eruption (Fig. 3c). While 80% of monthly temperature anomalies were below normal from the time of the eruption until the end of y3, 34% were significantly below normal.

All of Australia cooled during all seasons in 1964 (Fig. 4 and Fig. S1, Fig. S2, Fig. S3 in Online Resource 1). There were strong negative temperature departures (-0.40°C to -0.80°C) in south-eastern regions throughout all seasons. This strong cooling also occurred throughout the south of Australia in summer, throughout the east of Australia during autumn and most of Australia in winter. Below normal anomalies remained throughout Australia in y2, except in summer when some regions were above normal (max 0.20°C). Temperature anomalies returned to near normal (±0.20°C departures) during all seasons of y3.

3.3.4 Australia: Pinatubo

Significant cooling is measured over Australia after the Pinatubo eruption during spring of y0 (-0.52°C), and autumn (-0.33°C), winter (-0.39°C) and spring (-0.29°C) of y1 (Fig. 1). Although spring of y1 experiences the strongest negative anomaly, the strongest 3-year mean seasonal response occurred in both summer and winter (-0.23°C), and the weakest in both autumn and spring (-0.21°C) (Fig. 2). The first significant negative anomaly is recorded in September 1991 (-0.29°C), three months after the eruption (Fig. 3c). From the time of the eruption until the end of y3, 95% of monthly anomalies were negative, and 40% significantly below normal.

Below normal anomalies occurred throughout Australia during y1-y3 for all seasons except autumn during which temperatures in the west were above normal (between 0.20°C and 0.40°C) in y1 and y2 (Fig. 4 and Fig. S1, Fig. S2, Fig. S3 in Online Resource 1). However, autumn also experienced strong cooling (-0.40°C to -0.80°C) over north-eastern regions in y1. Similar anomalies are modelled for eastern areas of Australia during the summers of y1 and y3, over central and northern areas in winter of y1, and northern areas during spring of y1.

3.3.5 Australia Summary

Mean annual temperatures decreased significantly for one year across Australia following each of the major eruptions investigated, and three years following Krakatau. The strongest (negative) mean annual temperature departures occurred after Krakatau (-0.40°C) and weakest after Santa Maria (-0.28°C). Strongest 3-year negative temperature anomalies were for autumn (after Krakatau and Agung) and winter (after Santa Maria and Pinatubo). The entire continent cooled during all seasons of y1. Near normal or above normal temperatures seem to occur more frequently over Australia than SSA or SAF, but no uniform pattern is apparent.

3.4 CMIP5 comparison to reanalysis data

The CMIP5 data were compared to the 20CRv2 reanalysis data (Fig. 5 and Fig. S4, Fig. S5, Fig. S6 in Online Resource 1). It is found that most CMIP5 values, both annual and seasonal, are stronger (cooler) than the 20CRv2 values by an average

0.30°C. Following the Krakatau eruption, all CMIP5 values are cooler (on average by 0.37°C) than the 20CRv2 values, except during JJA of y1 in SAF and SON of y3 in Australia when the reanalysis temperatures are cooler (by an average of 0.12°C). After the Santa Maria eruption, the CMIP5 annual anomalies are only warmer than the reanalysis data in y2 and y3 in Australia (by -0.03°C and -0.17°C respectively). Seasonal values show that this occurs during DJF, MAM, JJA of y2 and JJA and SON of y3 in Australia but also in SON of y1, and DJF and MAM of y2 in SAF. Modelled CMIP5 anomalies are more often cooler than the 20CRv2 anomalies following the Agung eruption, particularly in SAF in y1 and y2 (annual anomalies by 0.07°C and 0.24°C respectively), and in Australia in y3 (by 0.29°C). This also applies to SSA during JJA and SON of y1 (by 0.29°C and 0.20°C respectively) and MAM of y2 (by 0.17°C). Following Pinatubo, CMIP5 annual anomalies are stronger than the 20CRv2 values in Australia during y1 and y2, in DJF (by 0.09°C and 0.49°C respectively) and SON (by 1.20°C and 0.44°C respectively), but also during JJA in SAF (by 0.01°C and JJA and SON in SAF (by 0.03°C and 0.04°C respectively). There are very few 20CRv2 temperature departures that are significantly below normal following the investigated eruptions. Although no annual anomalies are significantly cooler, SON of y1 following the Pinatubo eruption is significantly cooler over Australia (-1.49°C). In SAF, the only significant temperature anomalies based on the 20CRv2 data occur after the Agung eruption, during MAM of y0 (-0.71°C), and JJA (-0.72°C) and SON (-1.12°C) of y1, while no significantly cool anomalies are recorded over SSA.

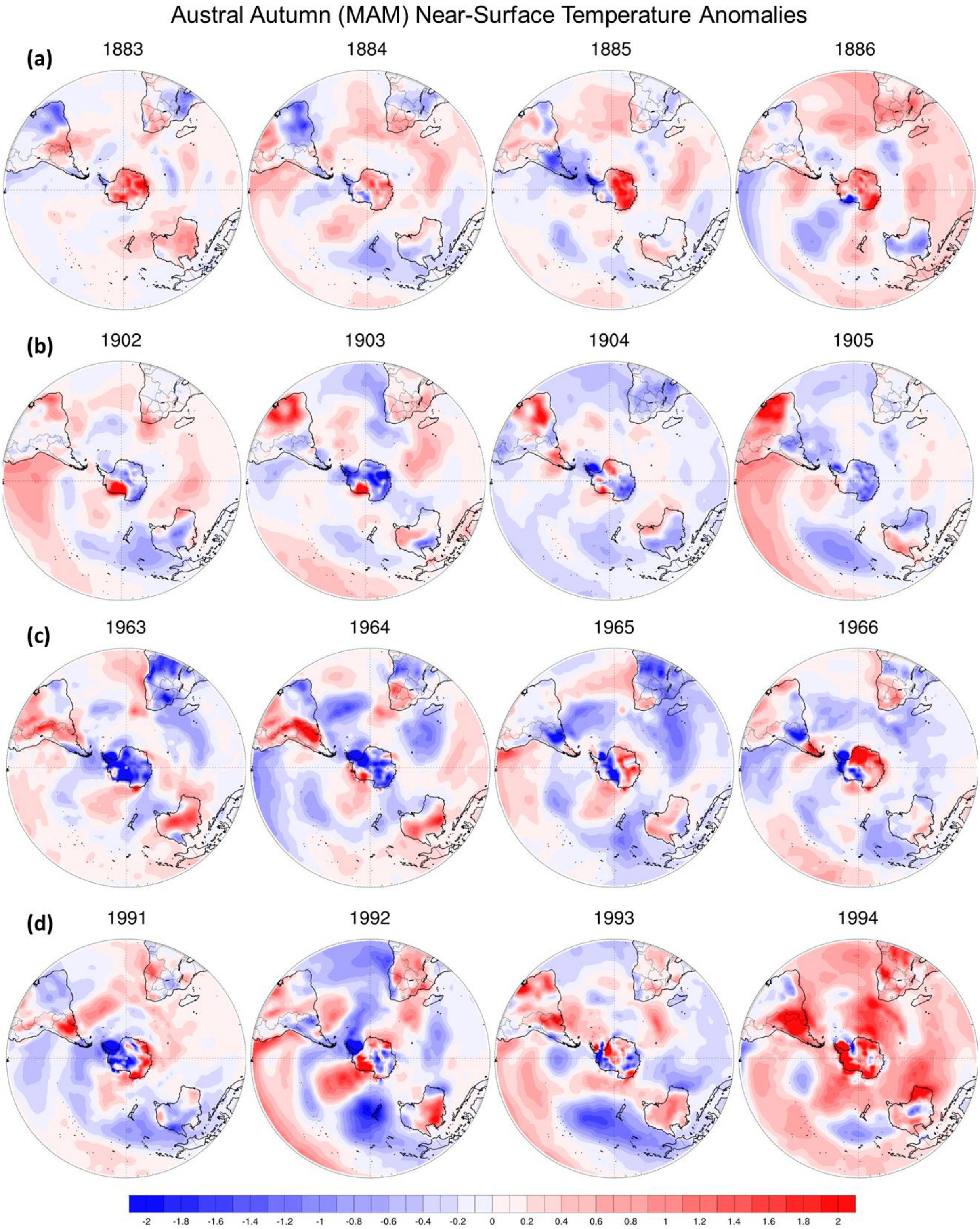

Fig. 5 20CRv2-simulated spatial maps of austral autumn temperature anomalies over the SH for the eruptions of (a) Krakatau, (b) Santa Maria, (c) Agung and (d) Pinatubo. The same figures for summer, winter and spring can be found in the Online Resource 1 (Fig. S4, Fig. S5, Fig. S6).

4. Discussion

Mean modelled temperature anomalies generally demonstrate that all three continents investigated here experienced strongest departures following the Krakatau eruption. For SAF and Australia, responses were second strongest following the Pinatubo eruption and weakest following Santa Maria. Conversely, in SSA the mean response following Pinatubo was weakest, while the response after Agung was second strongest. Despite the Agung eruption having a strong response in SSA, NH responses following the eruption were minimal (Ménégoz *et al*. 2018). Conversely, for Santa Maria, NH responses were stronger than those over SSA (Mass and Portman 1989). Following Krakatau, the first three years were significantly cooler for each continent, whereas only y1 was significantly cooler after the eruptions of Santa Maria, Agung and Pinatubo. The shorter-lived response after the later eruptions (Agung and Pinatubo) might, at least in part, be a consequence of increased ocean temperatures associated with enhanced anthropogenic forcing which help regulate surface temperatures (Gleckler *et al*. 2006).

For all three continents investigated, the number of significant monthly negative temperature anomalies was highest post the Krakatau eruption, second highest following the Pinatubo eruption, and lowest following the Santa Maria eruption. Modelled temperature responses were for the most part weakest for Santa Maria (except in SSA, where the response after Pinatubo was weakest). Such outcomes might be a product of the eruption time (Stevenson *et al*. 2017; Sun *et al*. 2019). For example, circulation in the SH is more favourable to aerosol distribution during winter due to strengthening of the Brewer Dobson circulation in both the deep and shallow branches in winter (Perlwitz and Graf 1995; Birner and Bönisch 2010; Young *et al*. 2011). Agung erupted before austral winter, and Pinatubo during austral winter, allowing for better aerosol distribution soon after the eruptions than Santa Maria, which erupted after the austral winter season when aerosol distribution may have been weaker. Differences in the extent of climatic response between Pinatubo and Santa Maria might also be due to the height at which aerosols reached the stratosphere. Aerosols from the Pinatubo eruption were likely dispersed at a higher altitude given that the plume reached a considerably higher (c. 40km) altitude than that for Santa Maria (c. 23.7-27km) (Bonadonna and Costa 2013). Recent work by Krishnamohan *et al*. (2019) advocates that the higher the altitude of aerosol injection, the greater the potential cooling effect, which would support greater cooling associated with Pinatubo than Santa Maria. However, the space-time spread of aerosols may not have as much of an influence in the CMIP5 model outputs.

Notably, strongest and most widespread SH continental negative temperature anomalies following the four major eruptions occur in autumn and to a lesser extent in winter, with exceptions following the Agung and Pinatubo eruptions when Australia experienced strongest responses in spring. In contrast, NH temperatures warm in some regions during boreal winter (Zambri and Robock 2016; Zambri *et al*. 2017). NH winter warming occurs over mid-high latitudes, and while SH land temperatures do not show warming, there is very little land mass at those SH latitudes. However, Fig. 4 and Fig. S1-S3 show a warming in surface temperatures over the oceans in the mid-high latitudes during all seasons.

Over continental regions of the SH (excluding Antarctica), initial significant negative temperature departures following major volcanic eruptions occur most rapidly (within 5 months on average) over Australia, followed closely by SAF (6-month average), but are somewhat more delayed over SSA (9 months on average). Typically, the first significant response is seen between January and May for SSA, in February in SAF, and between October and April over Australia. Temperature responses following all eruptions except Santa Maria (for which the response was strongest over SAF) are strongest over Australia and weakest over SSA. However, the mean response of all eruptions is equally strong for both SAF and Australia. The overall percentage of months recording significant negative temperature anomalies over the initial three years following major eruptions was highest over Australia (20-49%) and lowest over SSA (0-32%).

Volcanic forcing influences atmospheric circulation even into the stratosphere by affecting stratospheric temperature gradients and wind speed – i.e. the jet streams (Cui *et al*. 2014; Kidston *et al*. 2015). Jet streams can affect the Southern Annular Mode (SAM) (Karpechko *et al*. 2010; Xia *et al*. 2015), planetary waves, westerly circulation, and storm tracks, and hence influence surface weather (Gallego *et al*. 2005; Hudson 2012; Kidston *et al*. 2015). The SH jet stream may seasonally shift by c. 10° (Tyson *et al*. 2000; Shulmeister *et al*. 2004; Gallego *et al*. 2005; Hudson 2012). Although knowledge on how volcanic forcing impacts the jet streams is still limited, it is understood that jet streams were impacted by both the 1982 El Chichón and 1991 Pinatubo eruptions in the NH (Hudson 2012). Hudsons' results indicate that the subtropical jets in both hemispheres initially shifted poleward, and subsequently equatorward, after both eruptions. The study additionally found that the SH Polar jet moved equatorward after the Pinatubo eruption. With mid-latitude circulation being affected by volcanic forcing through major SH circulation variability modes (such as SAM, ENSO, jet streams etc.), it seems that major volcanic eruptions affect mid-latitude cyclones (Picas and Grab 2020). An increased intensity and frequency of cold fronts (associated with mid-latitude cyclones) would unquestionably provide for enhanced cooling over SH continental regions affected by such frontogenesis (see Grab and Simpson 2000). Topographic differences between the SH continental land masses (i.e. high Andes mountain range along western SSA versus relatively flat relief across western, southern and central Australia) would influence the northerly/easterly spread of such cold air wave disturbances. This may, at least in part, explain why cooling is most enhanced over Australia and least so over much of central SSA, following major eruptions.

Spatially, strongest cooling occurs between 0 and 25°S in SSA (see also Colose *et al*. 2016), between 20°S and 30°S over SAF, and is highly variable over Australia which is located mostly between 15-35°S. The likely enhanced frequency and/or intensity of mid-latitude cyclones, as discussed above, could consequently enhance cooling over southern to mid-latitude continental regions, particularly during austral autumn-winter-spring. Southwestern Western Australia, south-eastern Australia (Smith *et al*. 1982; Buckley and Leslie 2004) and southern SAF (Tyson *et al*. 2000) are affected by cyclones/cold fronts under normal conditions, which coincidently are areas of strongest volcanically induced cooling anomalies during austral autumn-winter-spring. Such cold surges in SSA are known to bring frost and freezing temperatures to Brazil, oftentimes damaging crops (Vera and Vigliarolo 2000; Espinoza *et al*. 2013). The cold surges are also responsible for transporting dryer air northwards, which at times has led to drought, as was the case with the severe 1817 drought over Brazil, soon after the 1815 Tambora eruption (Garreaud 2001).

The comparison between the CMIP5 data outputs and the 20CRv2 reanalysis data suggests that the CMIP5 models have overestimated the cooling response to volcanic eruptions over SH continental regions of SSA, SAF and Australia. The fact that CMIP5 overestimates the response to volcanic forcing has also been noted by Driscoll *et al*. (2012), Marotzke and Forster (2015) and Chylek *et al*. (2020). However, the 20CRv2 outputs are themselves not an absolutely accurate. While the reanalysis data has successfully captured most SH atmospheric circulation during the period of 1979 to 2010, data pre 1979 has greater discrepancies due to the lack of available observational data (Ke and Hui 2013; Zhang *et al*. 2013b). This means that the data covering the period of the Pinatubo eruption is more accurate, but that inaccuracies likely exist for temperatures following the eruptions of Krakatau, Santa Maria and Agung. While the CMIP5 models have been said to inaccurately represent SH circulation responses to volcanic forcing, McGraw *et al*. (2016) argues that the observations do fall within the distributions of modelled SH circulation, in particular the Southern Annular Mode, and Barnes *et al*. (2016) suggests that the internal climate variability may cause the response to volcanic eruptions seen in the CMIP5 models, to be disguised in the observed response. This leaves a lot of opportunity for CMIP6 to improve the modelled response to volcanic forcing.

5. Conclusion

Until recently, little attention has been given to volcanic forcing impacts on climates of the SH, with a general perception that such forcing has had relatively minimal impact on the SH in relation to its northern counterpart. Attention is here given to the SH with a case of examining such forcing at finer spatial and temporal resolutions than earlier approaches (i.e. at continental rather than hemispheric scale and seasonal rather than annual scale). Investigations at such a finer scale are able to demonstrate, for the first time, that (significant) negative temperature departures over SH land masses typically occur first over parts of Australia and lag most strongly over SSA. In addition, strongest cooling is noticed over parts of Australia and weakest responses measured over SSA. Strongest responses generally occur during austral autumn, and are usually weakest during spring. It is postulated that cooling anomalies during austral autumn and winter in particular, are associated with an increased intensity and/or frequency of mid-latitude cyclones passing over southern continental land masses. Such increased intensity of mid-latitude cyclones is likely caused by the intensification of the westerly winds associated with a positive SAM phase simulated in CMIP5 models. However, other SH circulation variability modes such as ENSO are also likely contributing factors that would require further investigation and verification. Given the many climate sensitive socio-economic systems in southerly regions of SH land masses, it would be beneficial to model such volcano-climate forcing at finer spatial and temporal scales, in order to have a better predictive sense of likely future climate responses to any future major eruptions in order to allow for appropriate preparation for such scenarios.

6. References

Allen KJ, Cook ER, Evans R, *et al* (2018) Lack of cool, not warm, extremes distinguishes late 20th Century climate in 979-year Tasmanian summer temperature reconstruction. Environ Res Lett 13:034041. https://doi.org/10.1088/1748-9326/aaafd7

Ammann CM, Joos F, Schimel DS, *et al* (2007) Solar influence on climate during the past millennium: Results from transient simulations with the NCAR Climate System Model. Proc Natl Acad Sci 104:3713–3718. https://doi.org/10.1073/pnas.0605064103

Barnes EA, Solomon S, Polvani LM (2016) Robust wind and precipitation responses to the Mount Pinatubo eruption, as simulated in the CMIP5 models. J Clim 29:4763–4778. https://doi.org/10.1175/JCLI-D-15-0658.1

Birner T, Bönisch H (2010) Residual circulation trajectories and transit times into the extratropical lowermost stratosphere. Atmospheric Chem Phys Discuss 10:16837–16860. https://doi.org/10.5194/acpd-10-16837-2010

Bonadonna C, Costa A (2013) Plume height, volume, and classification of explosive volcanic eruptions based on the Weibull function. Bull Volcanol 75:742. https://doi.org/10.1007/s00445-013-0742-1

Brönnimann S, Franke J, Nussbaumer SU, *et al* (2019) Last phase of the Little Ice Age forced by volcanic eruptions. Nat Geosci. https://doi.org/10.1038/s41561-019-0402-y

Buckley BW, Leslie LM (2004) Preliminary climatology and improved modelling of south Indian Ocean and Southern Ocean mid-latitude cyclones. Int J Climatol 24:1211–1230. https://doi.org/10.1002/joc.1050

Chylek P, Folland C, Klett JD, Dubey MK (2020) CMIP5 climate models overestimate cooling by volcanic aerosols. Geophys Res Lett 47:. https://doi.org/10.1029/2020GL087047

Colose CM, LeGrande AN, Vuille M (2015) The influence of tropical volcanic eruptions on the climate of South America during the last millennium. Clim Past 11:3375–3424. https://doi.org/10.5194/cpd-11-3375-2015

Colose CM, LeGrande AN, Vuille M (2016) The influence of volcanic eruptions on the climate of tropical South America during the last millennium in an isotope-enabled general circulation model. Clim Past 12:961–979. https://doi.org/10.5194/cp-12-961-2016

Cui X, Gao Y, Sun J (2014) The response of the East Asian summer monsoon to strong tropical volcanic eruptions. Adv Atmospheric Sci 31:1245–1255. https://doi.org/10.1007/s00376-014-3239-8

Dogar MM, Stenchikov G, Osipov S, *et al* (2017) Sensitivity of the regional climate in the Middle East and North Africa to volcanic perturbations: sensitivity of MENA region to volcanism. J Geophys Res Atmospheres 122:7922–7948. https://doi.org/10.1002/2017JD026783

Driscoll S, Bozzo A, Gray LJ, *et al* (2012) Coupled Model Intercomparison Project 5 (CMIP5) simulations of climate following volcanic eruptions. J Geophys Res Atmospheres 117:D17105. https://doi.org/10.1029/2012JD017607

Efron B (1979) Bootstrap Methods: another look at the Jackknife. Ann Stat 7:1–26. https://doi.org/10.1214/aos/1176344552

Esper J, Schneider L, Krusic PJ, *et al* (2013) European summer temperature response to annually dated volcanic eruptions over the past nine centuries. Bull Volcanol 75:736. https://doi.org/10.1007/s00445-013-0736-z

Espinoza JC, Ronchail J, Lengaigne M, *et al* (2013) Revisiting wintertime cold air intrusions at the east of the Andes: propagating features from subtropical Argentina to Peruvian Amazon and relationship with large-scale circulation patterns. Clim Dyn 41:1983–2002. https://doi.org/10.1007/s00382-012-1639-y

Gallego D, Ribera P, Garcia-Herrera R, *et al* (2005) A new look for the Southern Hemisphere jet stream. Clim Dyn 24:607–621. https://doi.org/10.1007/s00382-005-0006-7

Garreaud RD (2001) Subtropical cold surges: regional aspects and global distribution. Int J Climatol 21:1181–1197. https://doi.org/10.1002/joc.687

Gilliland RL (1982) Solar, volcanic, and CO2 forcing of recent climatic changes. Clim Change 4:111–131. https://doi.org/10.1007/BF02423387

Gleckler PJ, Wigley TML, Santer BD, *et al* (2006) Volcanoes and climate: Krakatoa's signature persists in the ocean. Nature 439:675. https://doi.org/10.1038/439675a

Grab SW, Simpson AJ (2000) Climatic and environmental impacts of cold fronts over KwaZulu-Natal and the adjacent interior of southern Africa. South Afr J Sci 96:602–608

Harvey PJ, Grab SW, Malherbe J (2020) Major volcanic eruptions and their impacts on southern hemisphere temperatures during the late 19th and 20th centuries, as simulated by CMIP5 models. Geophys Res Lett 47:. https://doi.org/10.1029/2020GL087792

Haurwitz MW, Brier GW (1981) A critique of the Superposed Epoch Analysis Method: Its application to solar–weather relations. Mon Weather Rev 109:2074–2079. https://doi.org/10.1175/1520-0493(1981)109<2074:ACOTSE>2.0.CO;2

Hudson RD (2012) Measurements of the movement of the jet streams at mid-latitudes, in the Northern and Southern Hemispheres, 1979 to 2010. Atmospheric Chem Phys 12:7797–7808. https://doi.org/10.5194/acp-12-7797-2012

Humphreys WJ (1913) Volcanic dust and other factors in the production of climatic changes, and their possible relation to ice ages. J Frankl Inst 176:131–160. https://doi.org/10.1016/S0016-0032(13)91294-1

Karpechko AY, Gillett NP, Dall'Amico M, Gray LJ (2010) Southern Hemisphere atmospheric circulation response to the El Chichón and Pinatubo eruptions in coupled climate models. Q J R Meteorol Soc 136:1813–1822. https://doi.org/10.1002/qj.683

Ke F, Hui L (2013) Evaluation of Atmospheric Circulation in the Southern Hemisphere in 20CRv2. Atmospheric Ocean Sci Lett 6:337–342. https://doi.org/10.1080/16742834.2013.11447104

Khodri M, Izumo T, Vialard J, *et al* (2017) Tropical explosive volcanic eruptions can trigger El Niño by cooling tropical Africa. Nat Commun 8:. https://doi.org/10.1038/s41467-017-00755-6

Kidston J, Scaife AA, Hardiman SC, *et al* (2015) Stratospheric influence on tropospheric jet streams, storm tracks and surface weather. Nat Geosci 8:433–440. https://doi.org/10.1038/ngeo2424

Krishnamohan K-PS-P, Bala G, Cao L, *et al* (2019) Climate system response to stratospheric sulfate aerosols: sensitivity to altitude of aerosol layer. Earth Syst Dyn 10:885–900. https://doi.org/10.5194/esd-10-885-2019

Langmann B (2014) On the Role of Climate Forcing by Volcanic Sulphate and Volcanic Ash. Adv Meteorol 2014:17

Lehner F, Schurer AP, Hegerl GC, *et al* (2016) The importance of ENSO phase during volcanic eruptions for detection and attribution. Geophys Res Lett 2851–2858. https://doi.org/10.1002/2016GL067935

Lough JM, Fritts HC (1987) An assessment of the possible effects of volcanic eruptions on North American climate using tree-ring data, 1602 to 1900 A.D. Clim Change 10:219–239. https://doi.org/10.1007/BF00143903

Man W, Zhou T, Jungclaus JH (2014) Effects of large volcanic eruptions on global summer climate and East Asian Monsoon changes during the Last Millennium: analysis of MPI-ESM simulations. J Clim 27:7394–7409. https://doi.org/10.1175/JCLI-D-13-00739.1

Marotzke J, Forster PM (2015) Forcing, feedback and internal variability in global temperature trends. Nature 517:565–570. https://doi.org/10.1038/nature14117

Mass CF, Portman DA (1989) Major volcanic eruptions and climate: a critical evaluation. J Clim 2:566–593. https://doi.org/10.1175/1520-0442(1989)002<0566:MVEACA>2.0.CO;2

McGraw MC, Barnes EA, Deser C (2016) Reconciling the observed and modeled Southern Hemisphere circulation response to volcanic eruptions:

Reconciling SH Response to Volcanoes. Geophys Res Lett 43:7259–7266. https://doi.org/10.1002/2016GL069835

Ménégoz M, Bilbao R, Bellprat O, *et al* (2018) Forecasting the climate response to volcanic eruptions: prediction skill related to stratospheric aerosol forcing. Environ Res Lett 13:064022. https://doi.org/10.1088/1748-9326/aac4db

Neely III RR, Schmidt A (2016) VolcanEESM: Global volcanic sulphur dioxide (SO_2) emissions database from 1850 to present

Neukom R, Barboza LA, Erb MP, *et al* (2019) Consistent multidecadal variability in global temperature reconstructions and simulations over the Common Era. Nat Geosci. https://doi.org/10.1038/s41561-019-0400-0

Oman L, Robock A, Stenchikov G, *et al* (2005) Climatic response to high-latitude volcanic eruptions. J Geophys Res Atmospheres 110:D13103. https://doi.org/10.1029/2004JD005487

Perlwitz J, Graf H-F (1995) The statistical connection between tropospheric and stratospheric circulation of the northern hemisphere in winter. J Clim 8:2281–2295

Picas J, Grab S (2020) Potential impacts of major nineteenth century volcanic eruptions on temperature over Cape Town, South Africa: 1834–1899. Clim Change. https://doi.org/10.1007/s10584-020-02678-6

Predybaylo E, Stenchikov GL, Wittenberg AT, Zeng F (2017) Impacts of a Pinatubo-size volcanic eruption on ENSO. J Geophys Res Atmospheres 122:925–947. https://doi.org/10.1002/2016JD025796

Raible CC, Brönnimann S, Auchmann R, *et al* (2016) Tambora 1815 as a test case for high impact volcanic eruptions: Earth system effects. Wiley Interdiscip Rev Clim Change 7:569–589. https://doi.org/10.1002/wcc.407

Rao MP, Cook BI, Cook ER, *et al* (2017) European and Mediterranean hydroclimate responses to tropical volcanic forcing over the last millennium. Geophys Res Lett 44:5104–5112. https://doi.org/10.1002/2017GL073057

Robock A (2000) Volcanic eruptions and climate. Rev Geophys 38:191–219. https://doi.org/10.1029/1998RG000054

Robock A, Adams T, Moore M, *et al* (2007) Southern Hemisphere atmospheric circulation effects of the 1991 Mount Pinatubo eruption. Geophys Res Lett 34:L23710. https://doi.org/10.1029/2007GL031403

Robock A, Mao J (1995) The volcanic signal in surface temperature observations. J Clim 8:1086–1103. https://doi.org/10.1175/1520-0442(1995)008<1086:TVSIST>2.0.CO;2

Santer BD, Painter JF, Bonfils C, *et al* (2013) Human and natural influences on the changing thermal structure of the atmosphere. Proc Natl Acad Sci 110:17235–17240. https://doi.org/10.1073/pnas.1305332110

Sato M, Hansen JE, McCormick MP, Pollack JB (1993) Stratospheric aerosol optical depths, 1850–1990. J Geophys Res 98:22987. https://doi.org/10.1029/93JD02553

Shulmeister J, Goodwin I, Renwick J, *et al* (2004) The Southern Hemisphere westerlies in the Australasian sector over the last glacial cycle: a synthesis. Quat Int 118–119:23–53. https://doi.org/10.1016/S1040-6182(03)00129-0

Smith RK, Ryan BF, Troup AJ, Wilson KJ (1982) Cold Fronts Research: The Australian Summertime "Cool Change." Bull Am Meteorol Soc 63:1028–1028. https://doi.org/10.1175/1520-0477(1982)063<1028:CFRTAS>2.0.CO;2

Stenchikov G, Kirchner I, Robock A, *et al* (1998) Radiative forcing from the 1991 Mount Pinatubo volcanic eruption. J Geophys Res 103:13837–13857

Stevenson S, Fasullo JT, Otto-Bliesner BL, *et al* (2017) Role of eruption season in reconciling model and proxy responses to tropical volcanism. Proc Natl Acad Sci 114:1822–1826. https://doi.org/10.1073/pnas.1612505114

Stoffel M, Khodri M, Corona C, *et al* (2015) Estimates of volcanic-induced cooling in the Northern Hemisphere over the past 1,500 years. Nat Geosci 8:784–788. https://doi.org/10.1038/ngeo2526

Sun W, Wang B, Liu J, *et al* (2019) How northern high-latitude volcanic eruptions in different seasons affect ENSO. J Clim 32:3245–3262. https://doi.org/10.1175/JCLI-D-18-0290.1

Taylor KE, Stouffer RJ, Meehl GA (2012) An overview of CMIP5 and the experiment design. Bull Am Meteorol Soc 93:485–498. https://doi.org/10.1175/BAMS-D-11-00094.1

Timmreck C (2018) Climatic effects of large volcanic eruptions. Habilitation Thesis, Universität Hamburg

Tyson PD, Tyson PD, Preston-Whyte RA (2000) The Weather and Climate of Southern Africa. Oxford University Press

Vera CS, Vigliarolo PK (2000) A Diagnostic Study of Cold-Air Outbreaks over South America. Mon Weather Rev 128:3–24. https://doi.org/10.1175/1520-0493(2000)128<0003:ADSOCA>2.0.CO;2

Xia L, von Storch H, Feser F, Wu J (2015) A study of quasi-millennial extratropical winter cyclone activity over the Southern Hemisphere. Clim Dyn 47:2121–2138. https://doi.org/10.1007/s00382-015-2954-x

Young PJ, Thompson DWJ, Rosenlof KH, *et al* (2011) The Seasonal Cycle and Interannual Variability in Stratospheric Temperatures and Links to the Brewer–Dobson Circulation: An Analysis of MSU and SSU Data. J Clim 24:6243–6258. https://doi.org/10.1175/JCLI-D-10-05028.1

Zambri B, LeGrande AN, Robock A, Slawinska J (2017) Northern Hemisphere winter warming and summer monsoon reduction after volcanic eruptions over the last millennium. J Geophys Res Atmospheres 122:7971–7989. https://doi.org/10.1002/2017JD026728

Zambri B, Robock A (2016) Winter warming and summer monsoon reduction after volcanic eruptions in Coupled Model Intercomparison Project 5 (CMIP5) simulations. Geophys Res Lett 43:10,920-10,928. https://doi.org/10.1002/2016GL070460

Zanchettin D, Timmreck C, Graf H-F, *et al* (2012) Bi-decadal variability excited in the coupled ocean–atmosphere system by strong tropical volcanic eruptions. Clim Dyn 39:419–444. https://doi.org/10.1007/s00382-011-1167-1

Zhang D, Blender R, Fraedrich K (2013a) Volcanoes and ENSO in millennium simulations: global impacts and regional reconstructions in East Asia. Theor Appl Climatol 111:437–454. https://doi.org/10.1007/s00704-012-0670-6

Zhang Q, Körnich H, Holmgren K (2013b) How well do reanalyses represent the southern African precipitation? Clim Dyn 40:951–962. https://doi.org/10.1007/s00382-012-1423-z

Zuo M, Man W, Zhou T, Guo Z (2018) Different impacts of Northern, Tropical, and Southern Volcanic Eruptions on the Tropical Pacific SST in the Last Millennium. J Clim 31:6729–6744. https://doi.org/10.1175/JCLI-D-17-0571.1

Supplementary Material: Chapter Three

Theoretical and Applied Climatology

Online Resource 1 for

Southern Hemisphere Continental Temperature Responses to Major Volcanic Eruptions since 1883 in CMIP5 Models

P. J. Harvey[1], S. W. Grab[1]

[1]School of Geography, Archaeology and Environmental Studies, University of the Witwatersrand, Johannesburg, South Africa

Corresponding author: Pamela Harvey (pamjharvey14@gmail.com)

Contents of this document

Figures S1 to S6

Introduction

This supplemental material provides three figures, each showing the Southern Hemisphere (SH) temperature response after the eruptions of Krakatau, Santa Maria, Agung and Pinatubo for the seasons DJF (Fig. S1), JJA (Fig. S2) and SON (Fig. S3).

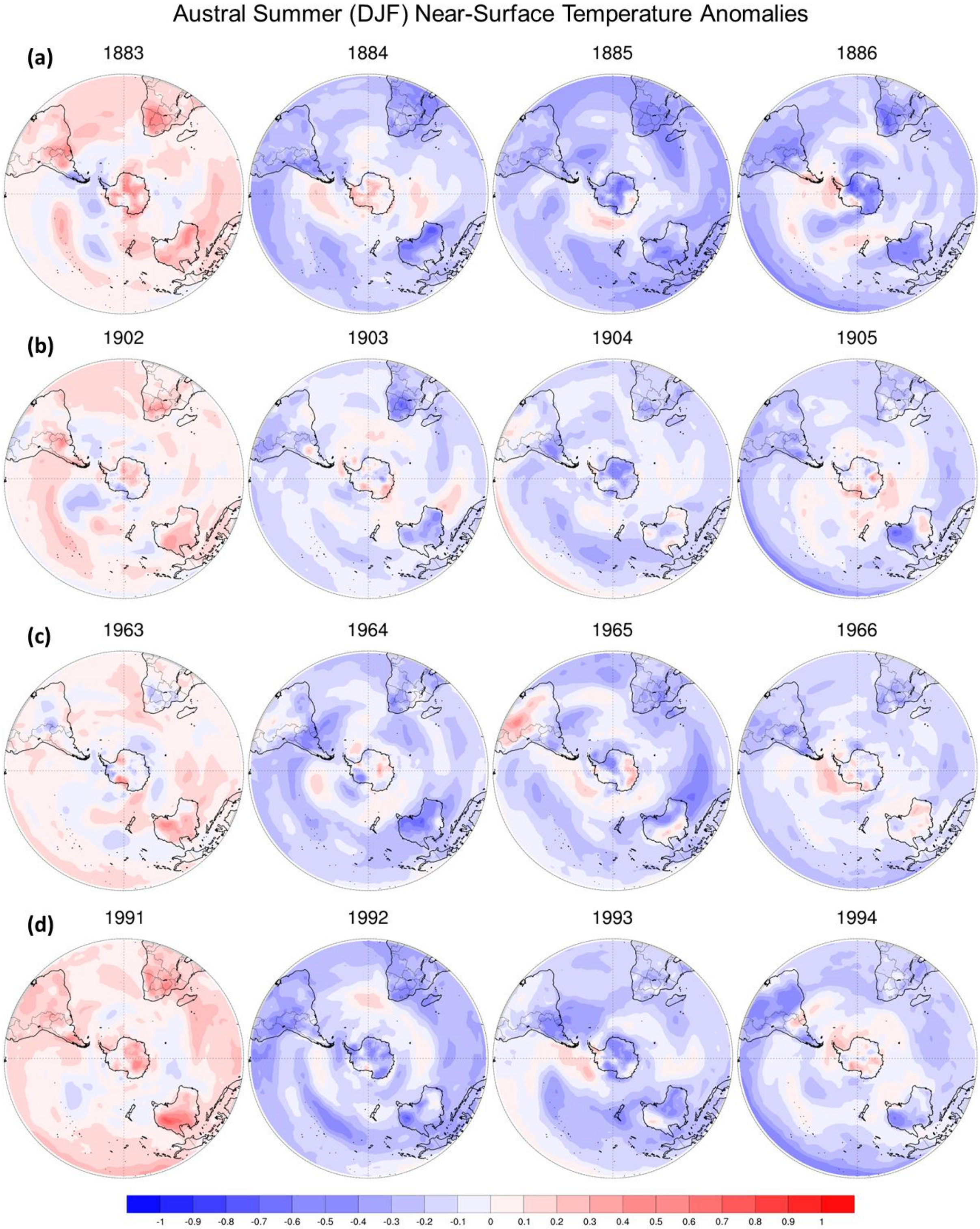

Fig. S1 CMIP5-simulated spatial maps of austral summer temperature anomalies over the Southern Hemisphere (SH) for the eruptions of (a) Krakatau, (b) Santa Maria, (c) Agung and (d) Pinatubo.

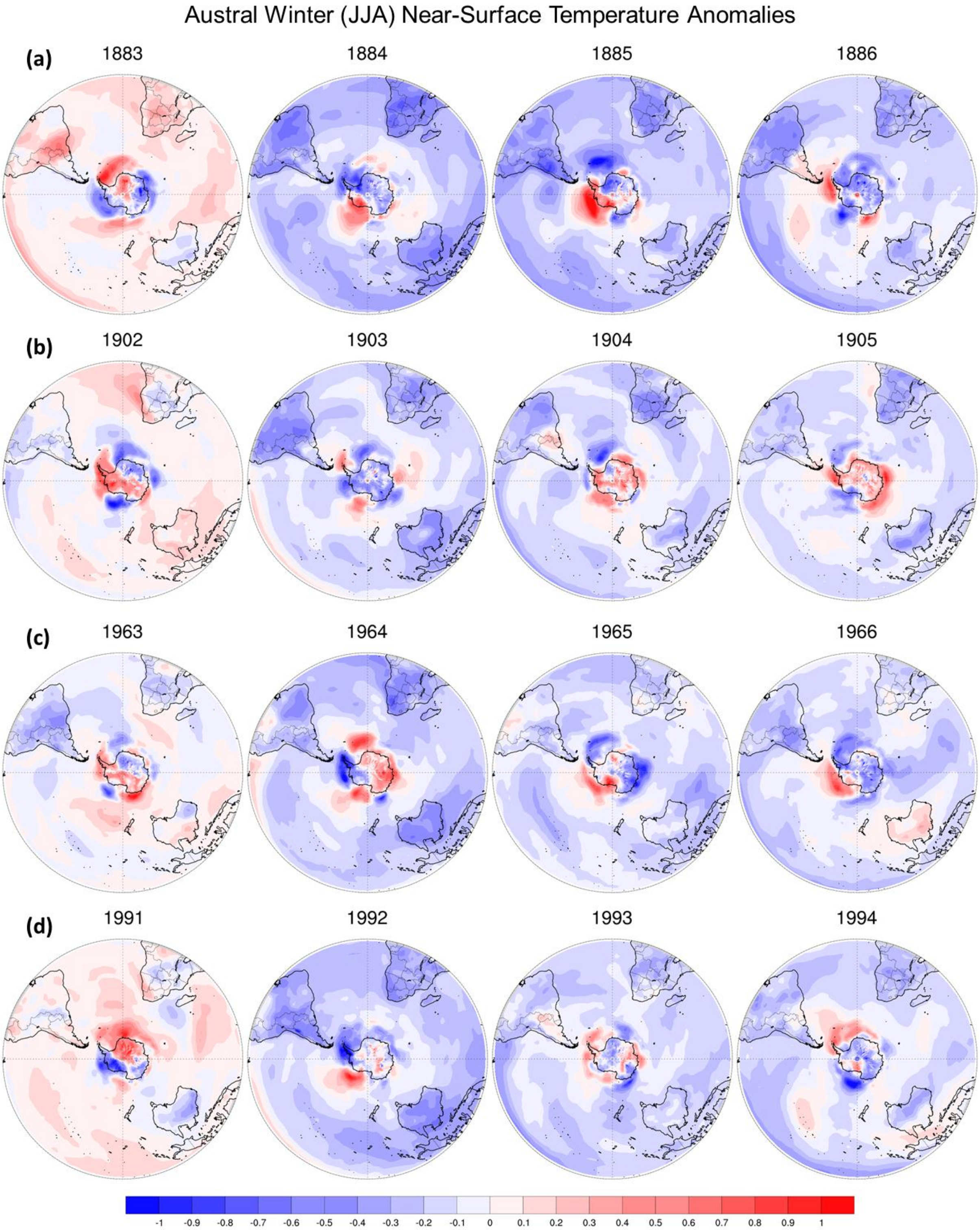

Fig. S2 CMIP5-simulated spatial maps of austral winter temperature anomalies over the SH for the eruptions of (a) Krakatau, (b) Santa Maria, (c) Agung and (d) Pinatubo.

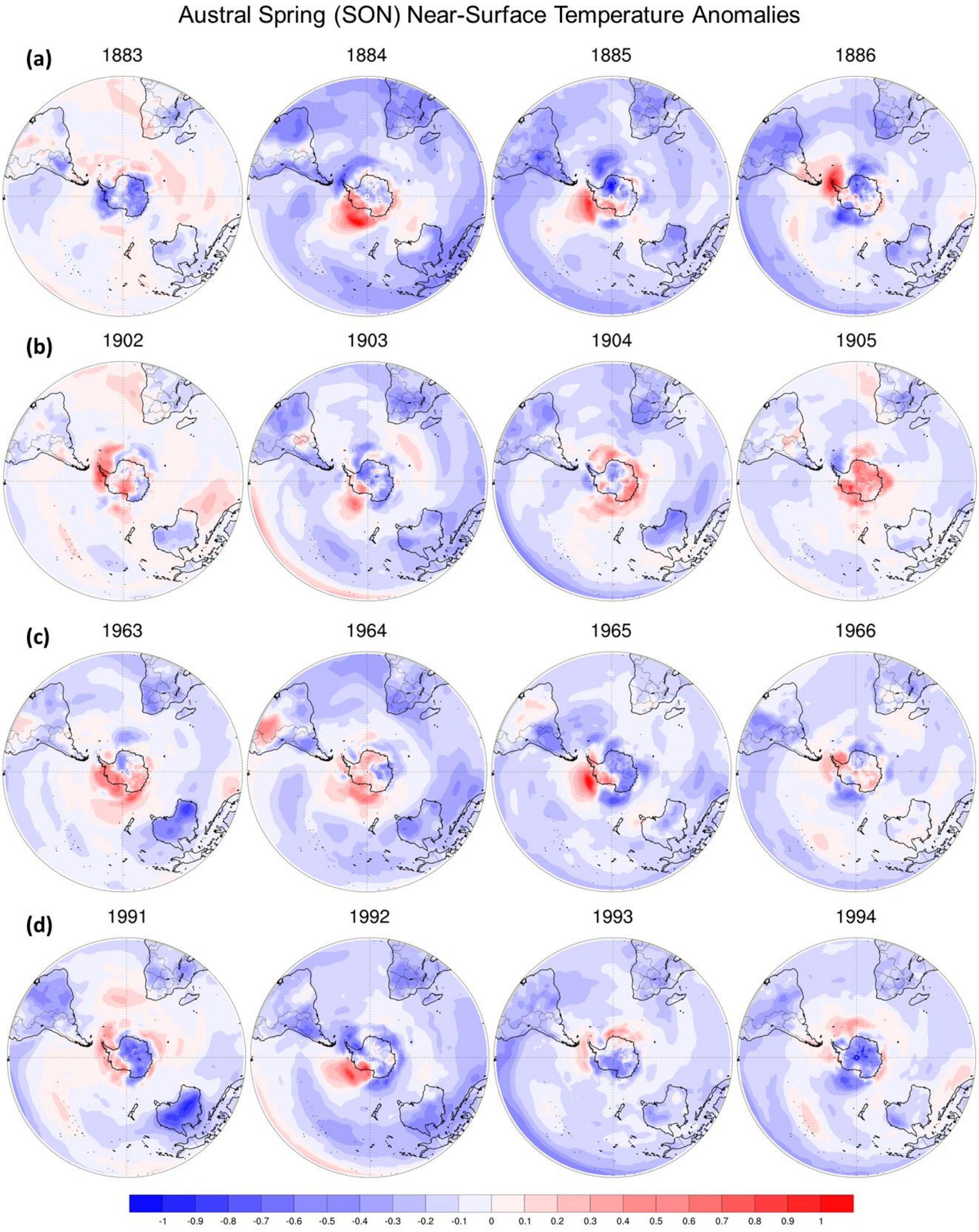

Fig. S3 CMIP5-simulated spatial maps of austral spring temperature anomalies over the SH for the eruptions of (a) Krakatau, (b) Santa Maria, (c) Agung and (d) Pinatubo.

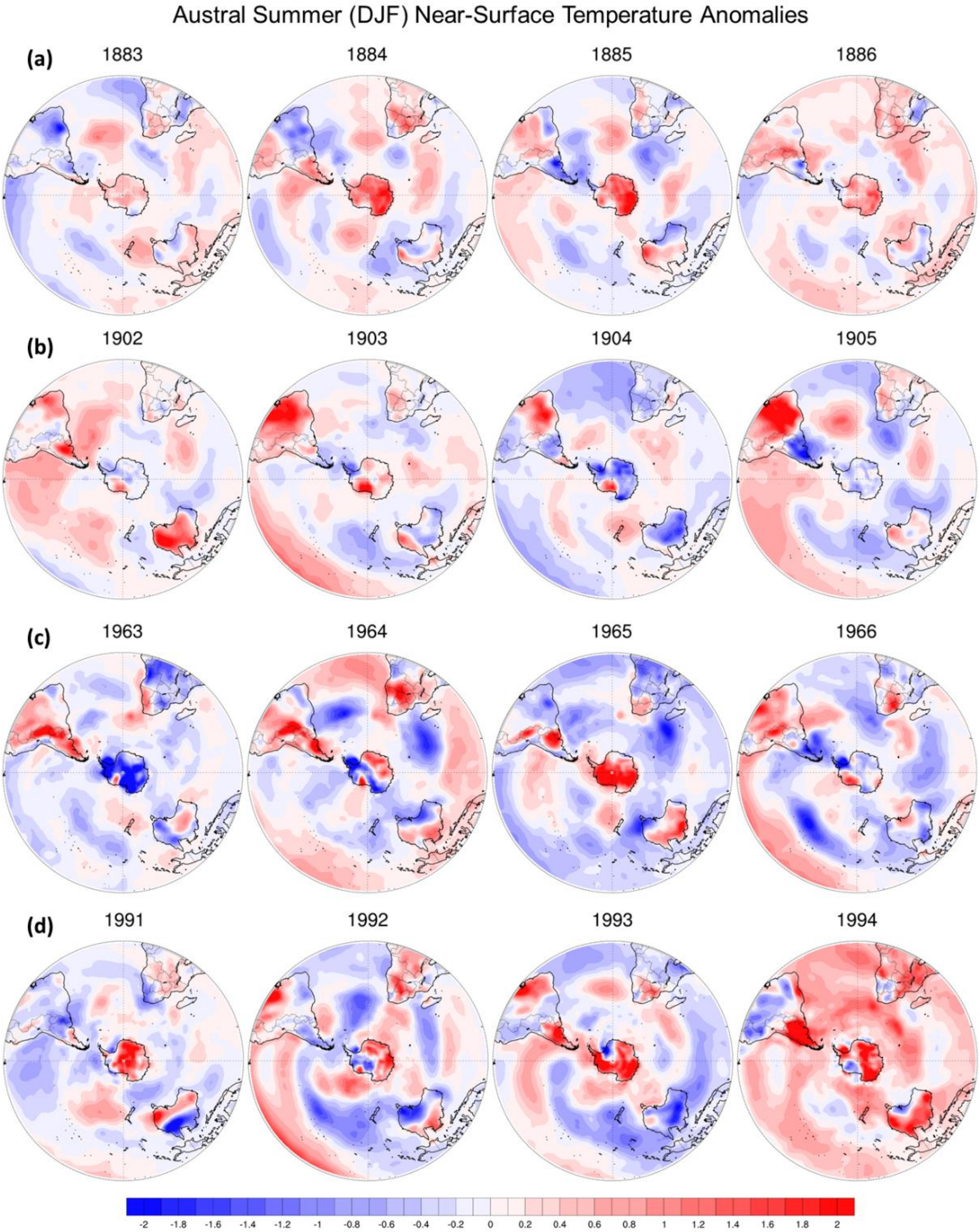

Fig. S4 20CRv2-simulated spatial maps of austral summer temperature anomalies over the SH for the eruptions of (a) Krakatau, (b) Santa Maria, (c) Agung and (d) Pinatubo.

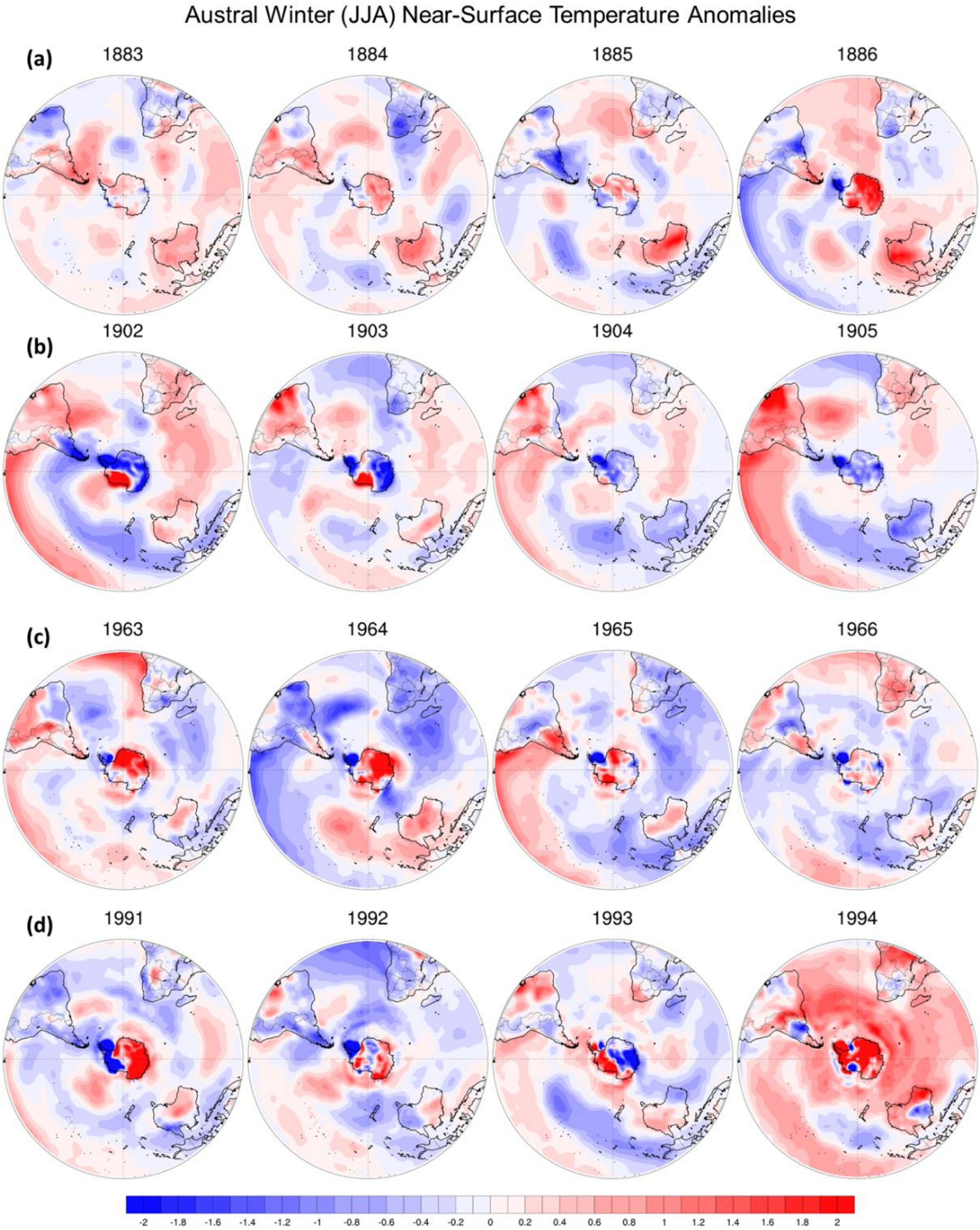

Fig. S5 20CRv2-simulated spatial maps of austral winter temperature anomalies over the SH for the eruptions of (a) Krakatau, (b) Santa Maria, (c) Agung and (d) Pinatubo.

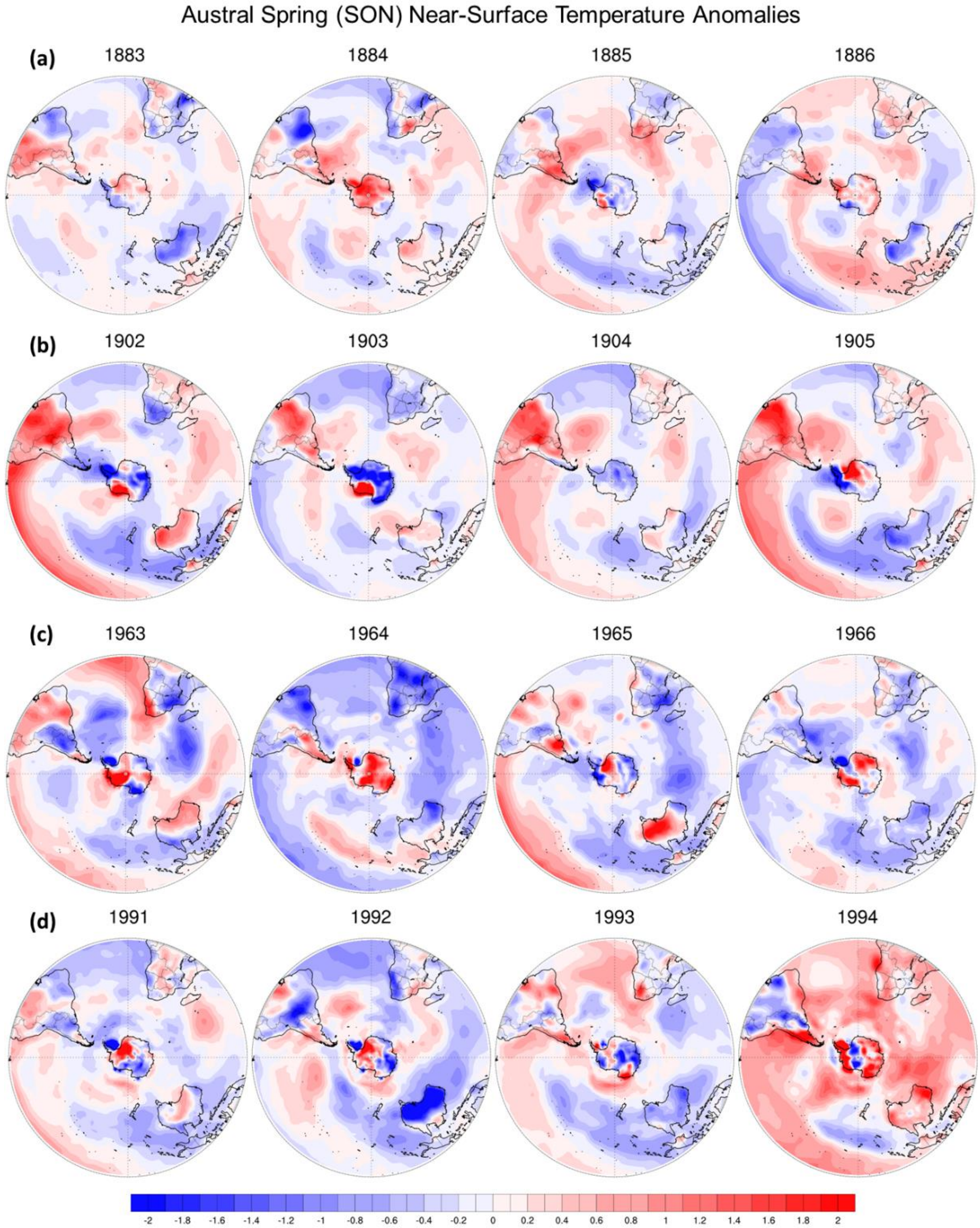

Fig. S6 20CRv2-simulated spatial maps of austral spring temperature anomalies over the SH for the eruptions of (a) Krakatau, (b) Santa Maria, (c) Agung and (d) Pinatubo.

Chapter Four: Southern African Temperature Responses to Major Volcanic Eruptions since 1883: Simulated by CMIP5 Models

(In press; International Journal of Climatology)

Abstract

Although volcanic forcing impacts on climate have gained much international attention during recent years, focus has largely been at hemispheric scale, and most particularly on the Northern Hemisphere (NH). Here the impact of major volcanic eruptions since 1883 on southern African climate is investigated, with a view to establishing potential sub-regional differences across a variety of temporal scales. To this end, historical simulations from the Coupled Model Intercomparison Project, phase 5 (CMIP5) are used to study near-surface temperature responses to four major eruptions (Krakatau, 1883; Santa Maria, 1902; Agung, 1963; Pinatubo, 1991) over six sub-regions of southern Africa. Results show significant cooling across all sub-regions after each eruption. However, considerable sub-regional differences in the amplitude, timing and duration of responses are detected. For instance, stronger temperature departures occur in northern rather than southern sub-regions where diurnal and annual temperature ranges are normally greater. While significant responses occur within the first year after each eruption, there is a more delayed response in three of the sub-regions (southwestern coast and central southern Africa) following the Santa Maria eruption. Strongest responses follow the Krakatau eruption in all sub-regions, while the weakest response follows the Santa Maria eruption in western sub-regions and the Agung eruption in eastern sub-regions. Most regions experience strongest temperature departures during austral autumn and winter (MAM and JJA), and weakest during spring (SON).

1. Introduction

Global to regional climates are affected by both internal variability (e.g. El Niño–Southern Oscillation, Southern Annular Mode etc.) and external forcing mechanisms (e.g. solar, volcanic, anthropogenic CO_2 etc.) (Lyu *et al.*, 2015; Dieng *et al.*, 2017). Although the role of volcanic forcing on earth's climate has captured scientific interest for over a century (e.g. Humphreys, 1913; Gentilli, 1948; Wexler, 1951; Lamb, 1970; Gilliland, 1982), such inquiry has grown substantially over the last ~30 years (Robock, 2000; Timmreck, 2012). Major volcanic eruptions releasing more than 5 Teragrams (Tg) of emitted sulphur dioxide (SO_2) into the lower stratosphere can affect global, hemispheric and regional climates (Timmreck, 2018). SO_2 from extratropical volcanic eruptions are predominantly transported within the hemisphere in which the eruption occurred, while those from tropical eruptions are typically transported throughout both hemispheres (Oman *et al.*, 2005), depending on the quasi-biennial oscillation phase (a westerly phase will cause aerosols to be transported towards the winter hemisphere faster than during the easterly phase, during which the aerosols would then be transferred to both hemispheres; Dhomse *et al.*, 2020). The aerosol lifetime is also longer if the eruption occurs during a westerly phase (Visioni *et al.*, 2018). Volcanic aerosols increase scattering and absorption of incoming solar radiation, thereby altering the earth's energy budget (Textor *et al.*, 2004; Kremser *et al.*, 2016; Liu *et al.*, 2018). A further consequence of this is the strengthening of zonal winds and increase in temperature and density differences between the equator and poles, thus also affecting atmospheric circulation (Perlwitz and Graf, 1995; Zambri and Robock, 2016).

Volcanic impact on hemispheric- to regional-scale climates is complex and seems highly variable given multiple influencing factors. These include eruption size, duration, location and timing, and contemporaneous internal climate variability (e.g. ENSO and Northern or Southern Annular Modes) (Zanchettin *et al.*, 2014; Colose *et al.*, 2015; Stevenson *et al.*, 2017; Sun *et al.*, 2019). Negative global temperature departures of as much as 1.00°C have been proposed following the

Tambora (1815) eruption (Kandlbauer et al., 2013); but even for somewhat lower magnitude eruptions such as Pinatubo (1991), global temperatures may be reduced by as much as 0.40°C (Thompson *et al.*, 2009; Kremser *et al.*, 2016). Summer cooling and winter warming is a common climatic response to major eruptions over North America, large parts of Europe and northern Eurasia (Robock, 2000; Timmreck, 2012; Zambri *et al.*, 2017). However, the response is not uniform throughout the Northern Hemisphere (NH) and is not the same after each eruption; for instance, the strength and timing of the response can vary by location as well as by eruption. For example, a study using models, observations and reanalysis data (Dogar *et al.*, 2017) found that the Middle East and northern Africa experienced both summer and winter cooling after the El Chichón (1982) and Pinatubo eruptions, with winter cooling being stronger than that in summer (between -0.50°C and -2.00°C). In Asia, a modelling study which uses a composite of 21 eruptions (AD 800 to 2005) occurring during neutral ENSO phases, found particularly strong cooling over western China (-2.00°C) in the first year after eruptions (Zhang et al., 2013), while instrumental data show that Japanese summer temperatures dropped by ~1.3°C following major eruptions between 1835 and 1955 (Kondo, 1988). Temperature responses over Europe, identified from both tree ring and instrumental data, are also somewhat variable. Central Europe typically records cooling of ~-0.18°C one year after major eruptions (i.e. those with a Volcanic Explosivity Index [VEI] value of ≥4), while northern Europe usually records stronger (-0.52°C) cooling responses, but with a two-year lag between the eruption and maximum cooling (Esper *et al.*, 2013). North American responses are typified by cooling over northernmost regions but may include warming scenarios over parts of the USA, depending on eruption location (Lough and Fritts, 1987 – tree ring data; Shindell, 2004 – climate modelling).

Temperature responses to major eruptions tend to be weaker in the SH than NH due to the stronger influence of internal variability on SH climate than that of external forcing (Wilmes *et al.*, 2012; Neukom *et al.*, 2014; Monerie *et al.*, 2017). Several authors (e.g. Mass and Portman, 1989; Robock and Mao, 1995; Harvey *et* *al.*, 2020) have established mean negative SH temperature departures of between 0.10°C and 0.36°C following major eruptions. Cooling is possible over South America, southern Africa and Australasia from as early as 1 month after a major eruption (Salinger, 1998; Man *et al.*, 2014; Colose *et al.*, 2016). Recently, Harvey *et al.* (2020) used historical simulations from the Coupled Model Intercomparison Project, phase 5 (CMIP5), to establish finer temporal-scale (monthly/seasonal) SH continental temperature departures following the eruptions of Krakatau (1883), Santa Maria (1902), Agung (1963) and Pinatubo (1991). Their findings indicate significant cooling over continents in response to these eruptions, and that anomalies are generally strongest during austral autumn and winter seasons.

Given the relative scarcity of long and reliable instrumental weather records for much of the SH, a variety of other climate proxies have been used to reconstruct climates of the SH. Several tree ring based climate reconstructions for the Australasia and Patagonia regions have revealed strong negative temperature anomalies occurring around the time of major volcanic eruptions, such as after the Tambora, Krakatau and Santa Maria events (Cook *et al.*, 2002; Palmer and Xiong, 2004; Vincent *et al.*, 2007; Roig and Villalba, 2008). In the southwestern Cape region of South Africa, a *Widdringtonia cedarbergensis* tree ring record confirms unusual frost rings in 1787 and 1816 following the Laki (1783/4) and Tambora (1815) eruptions (Dunwiddie and LaMarche, 1980; LaMarche and Hirschboeck, 1984). In addition, evidence for unusual dry fog occurrences in Rio de Janeiro (Brazil, South America) between 1784 and 1786 coincidently occurred after the Laki eruption (Trigo *et al.,* 2010). In central southern Africa, 19th century documentary accounts (e.g. diaries, newspapers, missionary reports) of severe cold and snow are regularly recorded in years after major eruptions (Grab and Nash, 2010). Most recently, Picas and Grab (2020) use a long station-based temperature series from the Royal Astronomical Observatory in Cape Town to demonstrate significant negative temperature departures following 19th century eruptions. Collectively, these studies indicate considerable climatic responses to volcanic forcing in the SH. Notwithstanding the value of these and previous modelling studies, a major knowledge gap remains with identifying finer spatio-temporal scale volcanic-forcing impacts across selected SH continental regions. Such an investigation is particularly important given that the impact of volcanic forcing on temperature is not necessarily spatially consistent across continents (Schneider *et al.*, 2009). In fact, adjoining regions may sometimes experience contrasting temperature responses to volcanic forcing, which cannot be captured in globally or hemispherically averaged outputs (Lyu *et al.*, 2015). To this end, the aim is to establish the characteristics of near-surface temperature responses to four major volcanic eruptions (Krakatau, 1883; Santa Maria, 1902; Agung, 1963; Pinatubo, 1991) across sub-regions of southern Africa using simulations from CMIP5 (Taylor *et al*., 2012). This is achieved through a multi-temporal investigative approach (annual to monthly).

2 Methodology

2.1 Study region and climatic setting

The southern African region represented in this paper is located between 20°S and 35°S latitude and 12.5°E and 36°E longitude (Figure 1). This covers the southern parts of Namibia, Botswana, Zimbabwe and Mozambique, as well as the countries of South Africa, Eswatini and Lesotho. The region is flanked by the Indian Ocean along the east coast where the sub-continent is impacted by the warm southerly flowing Mozambique and Agulhas currents; while the Atlantic Ocean along the west coast experiences upwelling due to the cool northerly flowing Benguela current. Coupling between atmosphere and oceans greatly influences the climate of southern Africa (Tyson *et al.*, 2000). In particular, ocean currents regulate temperatures along coastal sub-regions, with the Benguela current contributing to an arid climate, and the Mozambique and Agulhas currents resulting in warm and humid climates (Landman *et al.*, 2017; Roffe *et al.*, 2020).

Southern Africa's climate is strongly influenced by atmospheric circulation in tropical and temperate latitudes. High pressure systems resulting from anticyclonic circulation are dominant climatic influencers in the region, in particular the Subtropical South Atlantic and Subtropical South Indian Anticyclones, and the continental high (Tyson *et al.*, 2000; Landman *et al.*, 2017). However, the region is also affected by westerly waves and troughs, often resulting in cold fronts reaching into the southern sub-regions and interior of southern Africa. Although high pressure systems dominate year round, both anticyclonic systems and westerlies strengthen and move equatorward during austral winter, which at times permits the passage of cold fronts over southern and central parts of the sub-continent (Grab and Simpson, 2000).

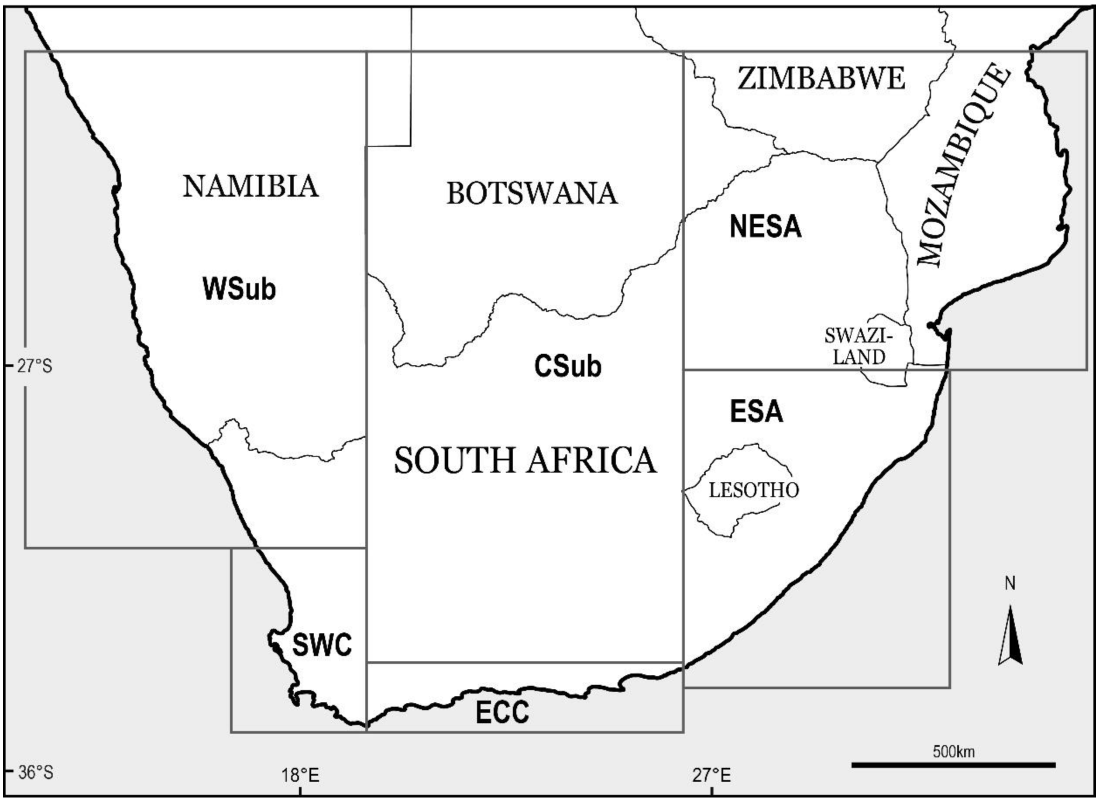

Figure 1. Various sub-regions of southern Africa used in this study (after Engelbrecht *et al*., 2008): SWC = South Western Cape; ECC = Eastern Cape Coast; ESA = Eastern South Africa; WSub = Western Subcontinent; CSub = Central Subcontinent; NESA = North-eastern South Africa, southern Zimbabwe and southern Mozambique.

For the purpose of this study, the southern African region is divided into six climatically defined sub-regions according to Engelbrecht *et al*. (2008) (Figure 1). These include the South Western Cape (SWC), the Eastern Cape Coast (ECC), Eastern South Africa (ESA), the Western Subcontinent (WSub), the Central

Subcontinent (CSub) and North-Eastern South Africa, southern Zimbabwe and southern Mozambique (NESA) (see Table 1 for exact latitude and longitude positions). Climates of these sub-regions are classified according to the Köppen-Geiger (Köppen, 1936) classification. The three southernmost sub-regions (SWC, ECC and ESA) have temperate climate types with warm humid summers and mild winters. The SWC has a Mediterranean climate with cool/wet winters and warm/dry summers, while the ECC has both Mediterranean and subtropical climate characteristics, with year-round rainfall. Both the SWC and ECC regions are affected by frontal weather associated with mid latitude cyclones, particularly during late autumn, winter and early spring. The occurrence and passage of cold fronts are primary factors influencing winter severity over ESA and southern parts of WSub, CSub and NESA (Grab and Simpson, 2000), but their influence dissipates northwards, where they have increasingly rare/minimal impacts. ESA has a large annual temperature range but relatively small diurnal range (Pidwirny, 2006; Kruger and Sekele, 2013; Engelbrecht and Engelbrecht, 2016). The CSub and NESA regions are mostly semi-arid (steppe) and the WSub region is mostly dry arid (desert). The WSub and NESA regions have high annual and monthly mean temperatures with high diurnal temperature ranges (Pidwirny, 2006). In particular, the diurnal range for the WSub region is considerably higher than that for the other six regions (Kruger and Sekele, 2013). Continentality of the CSub region accounts for moderate-high annual and monthly mean temperatures and relatively cool winters (Pidwirny, 2006; Kruger and Sekele, 2013; Engelbrecht and Engelbrecht, 2016).

Table 1. Southern African sub-regions used in this study (adapted from Engelbrecht *et al*., 2008).

Region	**Abbreviation**	**Latitude**	**Longitude**
South-Western Cape	SWC	-35° to -31°	17° to 20°
Eastern Cape Coast	ECC	-35° to -33.5°	20° to 27°
Eastern South Africa	ESA	-34° to -27°	27° to 33°
Western Subcontinent	WSub	-31° to -20°	12.5° to 20°
Central Subcontinent	CSub	-33.5° to -20°	20° to 27°
North-eastern South Africa, southern Zimbabwe and southern Mozambique	NESA	-27° to -20°	27° to 36°

2.2 Models and data

An assortment of CMIP5 (Taylor *et al.*, 2012) models were used, of which eleven were selected (Table 2) based on their ability to simulate a reasonable lower stratospheric temperature response to volcanic forcing (see Santer *et al.* 2013; Supplementary Fig. S1). Historical experiments, incorporating both natural and anthropogenic forcing, were applied. Three ensemble members were used from each model (realizations 1-3), except for the MIROC-ESM-CHEM model, for which only one realization was available. Two different physics versions were used for the GISS-E2_R model: p1, which uses prescribed aerosols, and p3, in which aerosols are calculated within the model. This equates to 33 simulations for this study. All models used are either after Sato *et al*. (1993) or Ammann *et al*. (2007) for volcanic forcing, given that it was not prescribed for CMIP5, apart from MRI_CGCM3 which computed aerosols within the model itself.

Table 2. Models used in this study, and the volcanic forcing dataset used by each (after Driscoll *et al*., 2012; Taylor *et al*., 2012; Harvey and Grab, submitted).

Model Name	Institution	Volcanic Forcing
CanESM2	Canadian Centre for Climate Modelling and Analysis	Sato *et al*. (1993)
CCSM4	National Center for Atmospheric Research	Ammann *et al*. (2007)
CNRM-CM5	Centre National de Recherches Météorologiques & Centre Européen de Recherche et de Formation Avancée en Calcul Scientifique	Ammann *et al*. (2007)
CSIRO-Mk3-6-0	Commonwealth Scientific and Industrial Research Organisation	Sato *et al*. (1993)
GISS-E2-H	NASA Goddard Institute for Space Studies	Sato *et al*. (1993)
GISS-E2-R (P1)	NASA Goddard Institute for Space Studies	Sato *et al*. (1993)
GISS-E2-R (P3)	NASA Goddard Institute for Space Studies	Sato *et al*. (1993)
MIROC-ESM	Japan Agency for Marine-Earth Science and Technology, Atmosphere and Ocean Research Institute (The University of Tokyo), and National Institute for Environmental Studies	Sato *et al*. (1993)
MIROC-ESM-CHEM		Sato *et al*. (1993)
MRI-CGCM3	Meteorological Research Institute	Interactive
NorESM1-M	Norwegian Climate Centre	Ammann *et al*. (2007)

Data were regridded linearly to a 2˚ by 2˚ latitude-longitude grid before having established a multi-model ensemble. Annual, seasonal and monthly near-surface

(2m) temperature anomalies (departures from mean) were calculated with respect to 20-year running means. Statistical significance of the anomalies is calculated through resampling the original time series of anomalies 5000 times using the bootstrap approach (Efron, 1979). Thereafter, the 5th and 95th percentiles of this resampled time series were used to compare against the original time series in order to establish the likelihood of post-eruption responses occurring randomly, and from this, significant anomalies may be identified (Haurwitz and Brier, 1981; Rao *et al.*, 2017). The ensemble mean robustness is tested by comparing the 25th and 75th percentiles of individual simulations to the ensemble mean. In order to test for the reliability of the CMIP5 models in generating responses for southern African regions, monthly temperature responses for the SWC region for the Krakatau eruption were compared to the findings of Picas and Grab (2020), who used instrumental data to identify temperature response to eruptions between 1834 and 1899 in Cape Town, South Africa. Given that Picas and Grab (2020) use a climatological reference period of 1834-1899 to calculate temperature departures, it must be acknowledged that the differences in reference periods for anomaly calculations in the respective studies will account for some differences in the comparison.

Four major volcanic eruptions are investigated: Krakatau (1883), Santa Maria (1902), Agung (1963) and Pinatubo (1991). Each of these eruptions significantly impacted mean SH and southern African temperatures (Harvey *et al.*, 2020). This paper presents considerably finer spatial-scale area-averaged temperature responses to these eruptions, than those of previous investigations for the SH. To this end, the timing, duration, seasonality and magnitude of temperature responses for each of the six sub-regions (i.e. climate types) of southern Africa, are established.

3 Results

3.1 Krakatau

The SH (6°S - Indonesia) Krakatau eruption occurred in August 1883, with a VEI of 6 and emission of 22 Tg of SO_2 into the stratosphere (Neely III and Schmidt, 2016). Negative mean annual temperature anomalies are simulated for all regions in southern Africa in the first three years after the eruption (Table 3). However, negative anomalies were only significant for all three years in the ESA, WSub and CSub regions; significant in the first (y1) and second (y2) post eruption years in the NESA region; and in y1 and year y3 in the SWC and ECC regions. For each year, the weakest mean annual anomaly (-0.13°C to -0.19°C) was observed in the ECC region, followed closely by the SWC region (-0.18°C to -0.33°C). The strongest negative anomaly was depicted in the WSub region in y1 (-0.49°C), in NESA in y2 (-0.44°C) and in CSub in y3 (-0.40°C).

Seasonal responses are now compared for each region following the Krakatau eruption (Figure 2). Anomalies are negative for each season in each region for y1 to y3, albeit not always significant. Seasonal anomalies are most frequently significant in the ESA, WSub, CSub and NESA regions, and less so over the SWC and ECC regions. In the SWC, negative anomalies are significant in all seasons during y1 (Figure 3), in austral autumn (MAM) of y2 and in austral winter (JJA) and spring (SON) of y3 (Table 4). Although anomalies are not significant during austral summer (DJF) in the ECC, they are so for JJA in y1-y3, MAM in y2 and SON in y1 and y3 (Table 4). ESA has significant negative temperature anomalies in DJF for y1-3, and in MAM and JJA for y1-2, but only in SON for y3. The WSub has significant negative anomalies in each season in y1, in DJF and MAM of y2, and in DJF, JJA and SON of y3 (Table 4). The CSub is the only other region during which the DJF anomaly of y1 is not significant, however, anomalies for MAM and JJA are significant. In y2, the DJF anomaly becomes significant, and the MAM and JJA anomalies remain significant. In y3, significant anomalies occur during DJF, JJA and SON. Over NESA, significant negative anomalies occur in DJF for y1-y3, in MAM for y1-y2, in JJA for y1-y2, and SON for y2-y3 (Table 4). Notably, while anomalies in

SON are not always significant in y1 or y2 for each region, they are always significant in y3.

Table 3. CMIP5-simulated mean annual temperatures for each sub-region following the four eruptions. Grey shading = year of eruption; blue shading = significant anomalies.

		SWC	ECC	ESA	WSub	CSub	NESA
Krakatau	1883	0.07	0.05	0.10	0.14	0.18	0.09
	1884	-0.33	-0.19	-0.44	-0.49	-0.47	-0.38
	1885	-0.18	-0.13	-0.41	-0.35	-0.39	-0.44
	1886	-0.21	-0.16	-0.33	-0.34	-0.40	-0.30
Santa Maria	1902	0.12	0.05	0.07	0.11	0.09	0.07
	1903	-0.11	-0.03	-0.31	-0.30	-0.34	-0.37
	1904	-0.22	-0.13	-0.28	-0.27	-0.36	-0.32
	1905	-0.12	-0.10	-0.13	-0.16	-0.20	-0.21
Agung	1963	-0.05	0.01	-0.08	-0.10	-0.11	-0.08
	1964	-0.35	-0.17	-0.37	-0.50	-0.50	-0.31
	1965	-0.19	-0.14	-0.14	-0.10	-0.12	-0.15
	1966	-0.14	-0.08	-0.05	-0.17	-0.09	-0.11
Pinatubo	1991	0.06	0.04	0.01	0.06	0.06	0.04
	1992	-0.29	-0.18	-0.34	-0.36	-0.37	-0.35
	1993	-0.17	-0.13	-0.22	-0.22	-0.23	-0.13
	1994	-0.20	-0.16	-0.18	-0.25	-0.24	-0.25

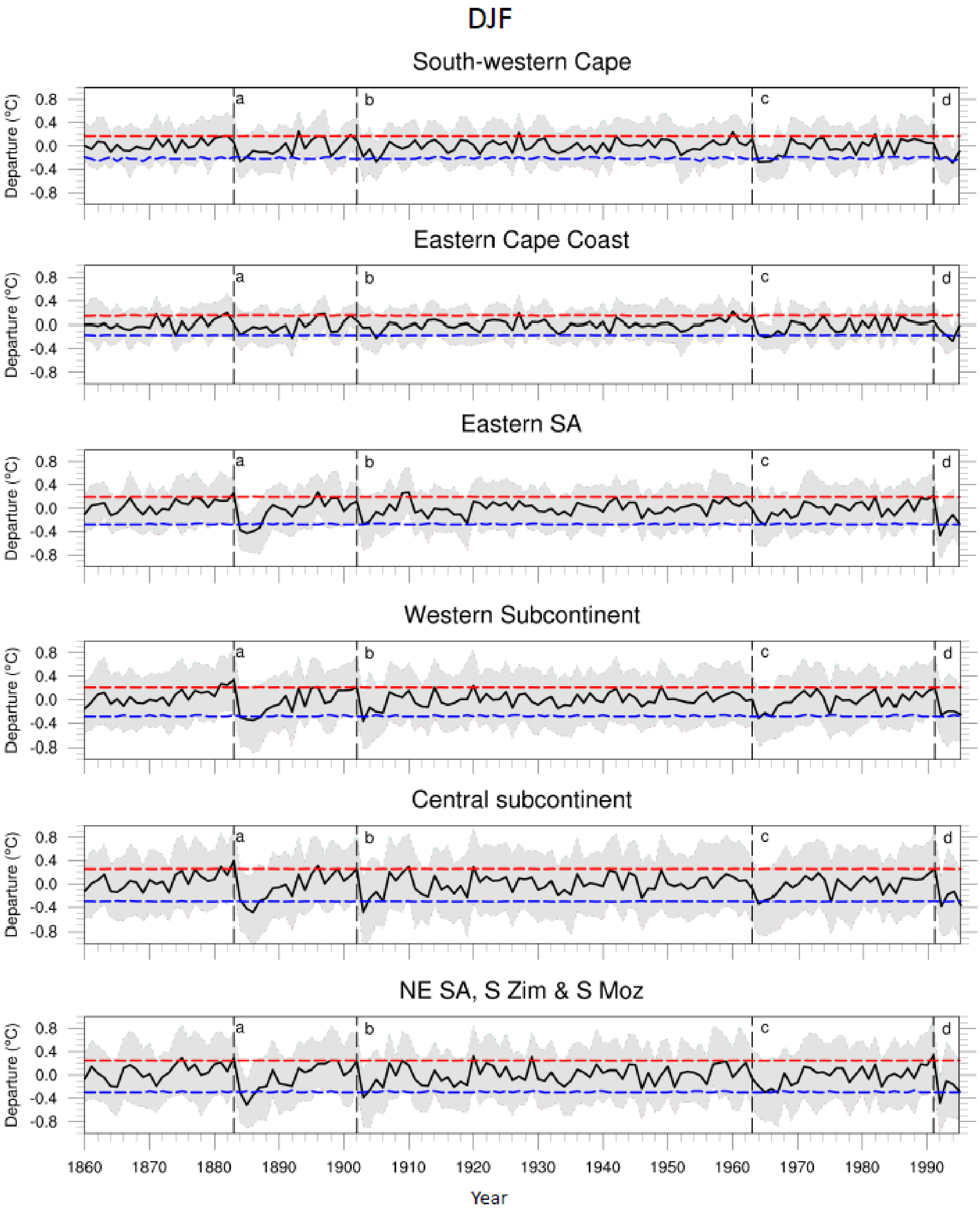

Figure 2. CMIP5-simulated seasonal temperature anomalies for each southern African sub-region (1860-1996). Vertical lines represent the eruptions: a = Krakatau, b = Santa Maria, c = Agung, d = Pinatubo. Grey shading represents the ensemble mean, and the blue and red lines the 5th and 95th percentile.

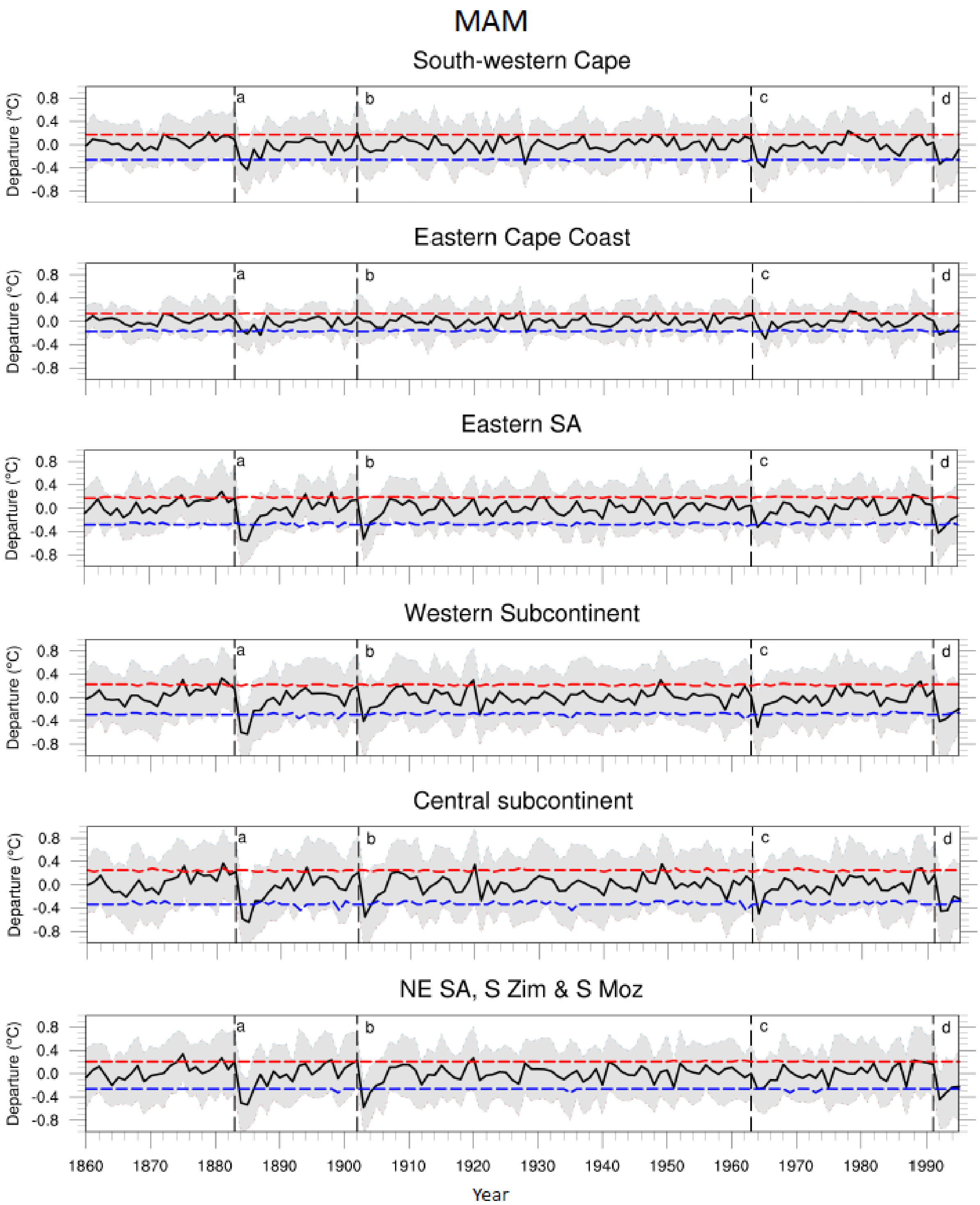

Figure 2 continued.

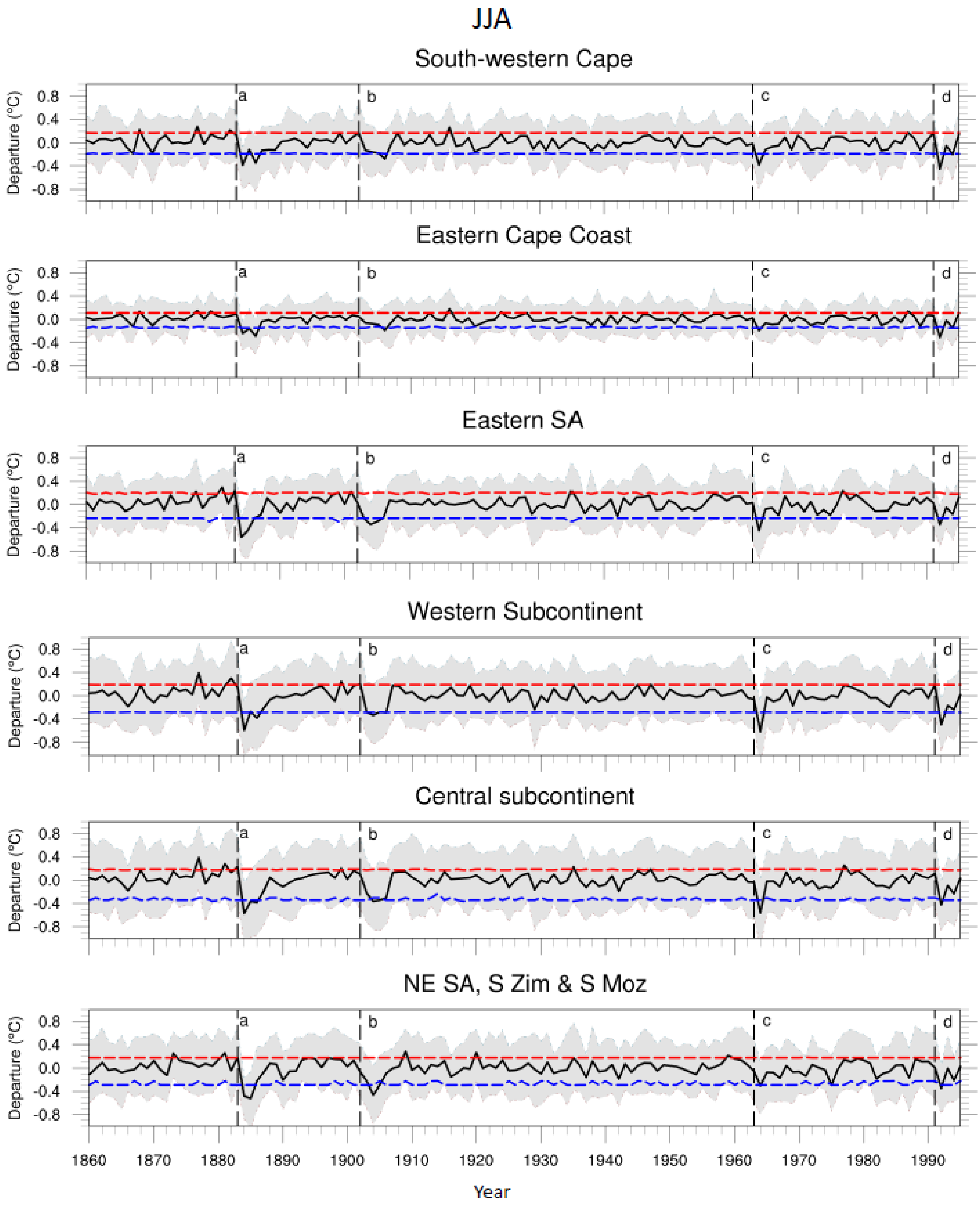

Figure 2 continued.

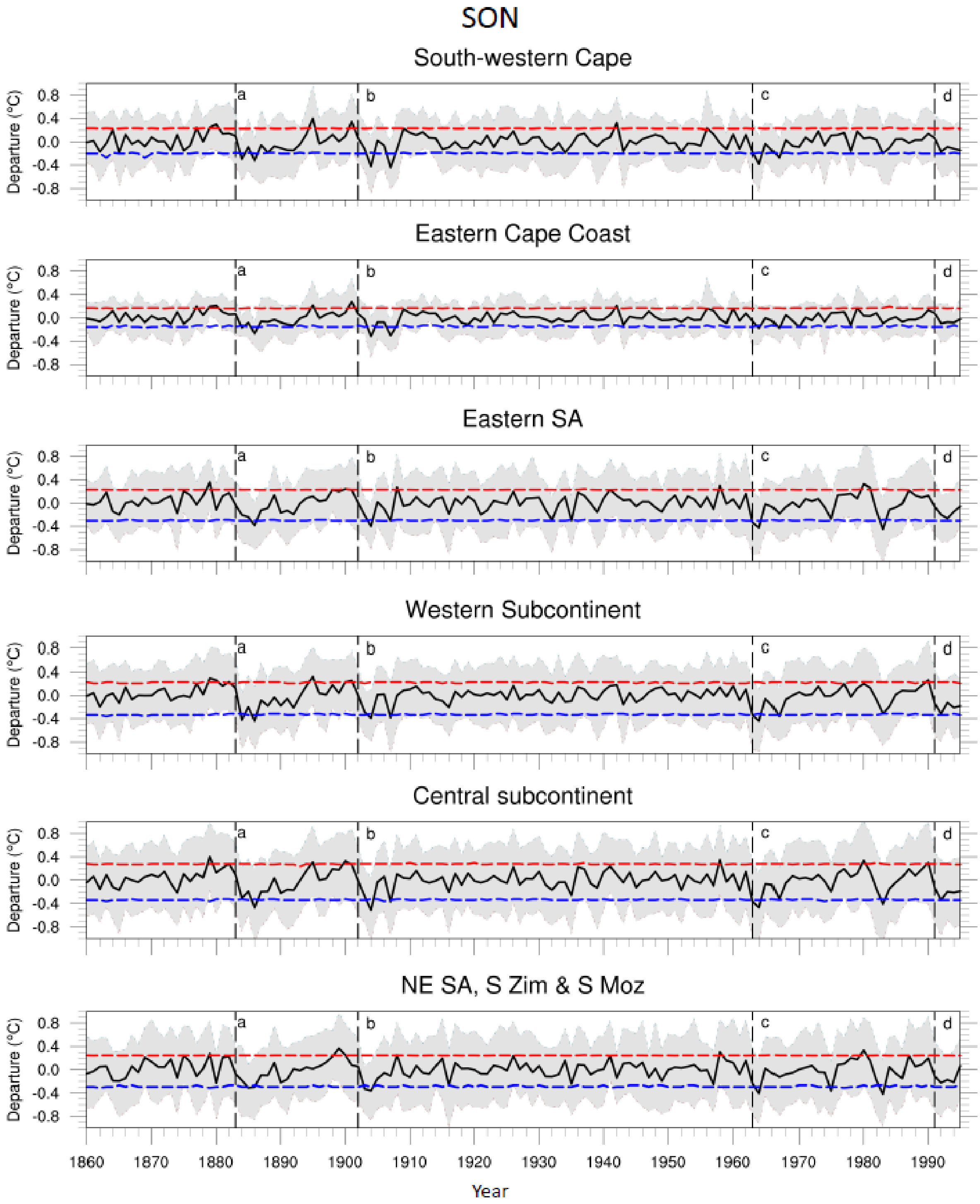

Figure 2 continued.

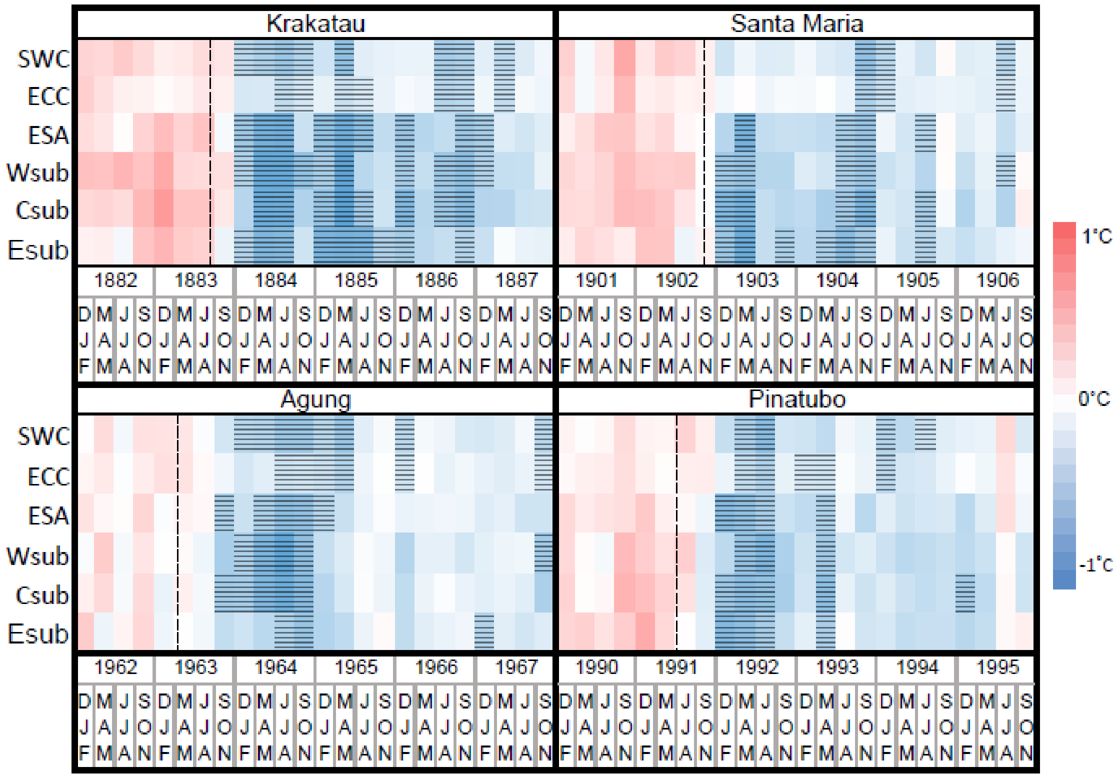

Figure 3. CMIP5-simulated seasonal temperature anomalies for each southern African sub-region for the eruptions of Krakatau, Santa Maria, Agung & Pinatubo. Eruption events are depicted by dashed vertical lines and significant anomalies are depicted by horizontal hashed lines.

Table 4. CMIP5-simulated seasonal temperatures for each sub-region following the four eruptions. Grey shading = year of eruption; bold values = significant anomalies. The values have been ranked from weakest to strongest seasonal response for each year in each region: dark blue = strongest, pale blue = second strongest, pale red = third strongest, red = weakest.

	SWC				ECC				ESA			
Season	**DJF**	**MAM**	**JJA**	**SON**	**DJF**	**MAM**	**JJA**	**SON**	**DJF**	**MAM**	**JJA**	**SON**
1883	0.07	0.09	0.14	0.10	0.02	0.04	0.10	0.06	0.26	0.17	0.24	-0.03
1884	**-0.27**	**-0.32**	**-0.39**	**-0.30**	**-0.16**	**-0.15**	**-0.24**	**-0.17**	**-0.38**	**-0.54**	**-0.56**	**-0.21**
1885	**-0.19**	**-0.43**	**-0.12**	**-0.09**	**-0.10**	**-0.21**	**-0.16**	**-0.08**	**-0.43**	**-0.56**	**-0.44**	**-0.24**
1886	**-0.08**	**-0.08**	**-0.35**	**-0.33**	**-0.03**	**-0.06**	**-0.29**	**-0.27**	**-0.40**	**-0.29**	**-0.24**	**-0.39**
1902	0.10	0.21	0.17	0.07	0.06	0.08	0.05	0.06	0.12	0.15	0.03	0.01
1903	**-0.19**	**-0.06**	**-0.13**	**-0.12**	**-0.05**	**0.01**	**-0.06**	**-0.03**	**-0.28**	**-0.53**	**-0.23**	**-0.21**
1904	**-0.05**	**-0.13**	**-0.16**	**-0.43**	**-0.04**	**-0.01**	**-0.08**	**-0.32**	**-0.22**	**-0.25**	**-0.34**	**-0.40**
1905	**-0.27**	**-0.09**	**-0.18**	**0.02**	**-0.22**	**-0.11**	**-0.09**	**-0.07**	**-0.06**	**-0.17**	**-0.29**	**0.02**
1963	0.12	0.10	-0.01	-0.17	0.13	0.11	0.02	-0.06	-0.01	0.05	0.03	**-0.33**
1964	**-0.28**	**-0.29**	**-0.39**	**-0.39**	**-0.16**	**-0.11**	**-0.19**	**-0.18**	**-0.21**	**-0.33**	**-0.45**	**-0.43**
1965	**-0.27**	**-0.39**	**-0.12**	**-0.03**	**-0.20**	**-0.30**	**-0.07**	**0.00**	**-0.29**	**-0.21**	**-0.08**	**-0.02**
1966	**-0.26**	**-0.04**	**-0.07**	**-0.14**	**-0.19**	**0.00**	**-0.09**	**-0.05**	**-0.08**	**-0.07**	**-0.06**	**-0.06**
1991	0.05	0.04	0.17	0.07	0.06	0.01	0.07	0.08	0.21	0.06	0.03	-0.06
1992	**-0.22**	**-0.34**	**-0.45**	**-0.17**	**-0.08**	**-0.23**	**-0.31**	**-0.10**	**-0.47**	**-0.43**	**-0.35**	**-0.20**
1993	**-0.19**	**-0.25**	**-0.05**	**-0.09**	**-0.17**	**-0.18**	**-0.02**	**-0.07**	**-0.25**	**-0.32**	**-0.05**	**-0.27**
1994	**-0.29**	**-0.26**	**-0.20**	**-0.12**	**-0.27**	**-0.17**	**-0.15**	**-0.08**	**-0.11**	**-0.19**	**-0.17**	**-0.15**

	WSub				CSub				NESA			
Season	**DJF**	**MAM**	**JJA**	**SON**	**DJF**	**MAM**	**JJA**	**SON**	**DJF**	**MAM**	**JJA**	**SON**
1883	0.34	0.15	0.14	0.12	0.40	0.23	0.23	0.09	0.29	0.21	0.18	-0.07
1884	**-0.30**	**-0.60**	**-0.59**	**-0.42**	**-0.28**	**-0.58**	**-0.57**	**-0.31**	**-0.30**	**-0.50**	**-0.48**	**-0.19**
1885	**-0.34**	**-0.63**	**-0.27**	**-0.20**	**-0.43**	**-0.64**	**-0.37**	**-0.19**	**-0.52**	**-0.53**	**-0.52**	**-0.31**
1886	**-0.36**	**-0.23**	**-0.39**	**-0.44**	**-0.49**	**-0.28**	**-0.39**	**-0.47**	**-0.35**	**-0.27**	**-0.23**	**-0.30**
1902	0.21	0.19	0.20	0.00	0.26	0.22	0.10	-0.01	0.23	0.23	-0.06	0.05
1903	**-0.37**	**-0.41**	**-0.29**	**-0.29**	**-0.49**	**-0.55**	**-0.23**	**-0.27**	**-0.39**	**-0.58**	**-0.23**	**-0.33**
1904	**-0.13**	**-0.18**	**-0.34**	**-0.39**	**-0.25**	**-0.34**	**-0.36**	**-0.52**	**-0.27**	**-0.33**	**-0.46**	**-0.36**
1905	**-0.21**	**-0.16**	**-0.28**	**0.01**	**-0.14**	**-0.18**	**-0.35**	**-0.03**	**-0.08**	**-0.21**	**-0.30**	**-0.15**
1963	0.00	0.02	-0.06	-0.34	-0.08	0.07	-0.04	**-0.36**	-0.06	0.00	-0.05	-0.24
1964	**-0.32**	**-0.51**	**-0.62**	**-0.44**	**-0.35**	**-0.50**	**-0.57**	**-0.47**	**-0.19**	**-0.27**	**-0.31**	**-0.40**
1965	**-0.23**	**-0.13**	**-0.02**	**-0.06**	**-0.28**	**-0.16**	**-0.02**	**-0.07**	**-0.30**	**-0.25**	**-0.07**	**0.02**
1966	**-0.29**	**-0.10**	**-0.10**	**-0.17**	**-0.24**	**-0.07**	**-0.02**	**-0.08**	**-0.24**	**-0.11**	**-0.08**	**-0.06**
1991	0.20	0.12	0.19	-0.13	0.25	0.18	0.12	-0.12	0.33	0.15	0.01	-0.11
1992	**-0.26**	**-0.42**	**-0.50**	**-0.32**	**-0.39**	**-0.46**	**-0.43**	**-0.34**	**-0.48**	**-0.44**	**-0.35**	**-0.23**
1993	**-0.19**	**-0.37**	**-0.17**	**-0.12**	**-0.18**	**-0.44**	**-0.10**	**-0.20**	**-0.10**	**-0.33**	**-0.01**	**-0.17**
1994	**-0.20**	**-0.27**	**-0.24**	**-0.21**	**-0.13**	**-0.20**	**-0.24**	**-0.21**	**-0.16**	**-0.24**	**-0.22**	**-0.22**

Strongest y1 anomalies occur during austral autumn (MAM) in the WSub (-0.60°C), CSub (-0.58°C) and over NESA (-0.50°C), and during austral winter (JJA) over the ECC (-0.24°C), SWC (-0.39°C) and ESA (-0.56°C) regions. Weakest response occurs in DJF in the SWC (-0.27°C), CSub (-0.28°C) and WSub (-0.30°C) regions, in SON over NESA (-0.19°C) and ESA (-0.21°C) and in MAM over the ECC (-0.15°C) region.

The strongest temperature response during the initial three years following Krakatau (Table 4) occurs during MAM of y2 for all regions (mean = -0.56°C) except the ECC, where the strongest response (-0.29°C) occurs during JJA of y3.

The strongest post-Krakatau monthly temperature departure occurs almost two years after the eruption (21 months), namely in May 1885 for all regions (mean = -0.76°C) except over NESA where the maximum monthly response occurs four months earlier (January 1885; -0.62°C; Figure 4). The strongest maximum monthly departure is recorded for the CSub region (-0.98°C – May 1885), followed by the WSub region (-0.85°C – May 1885), while the weakest peak response occurs in the ECC region (-0.53°C – May 1885). For the first three years post Krakatau, most mean monthly temperatures are below normal for all regions, ranging from 95% (NESA) to 83% (SWC) of months, however, significantly below normal mean values range from only 17% (ECC) to 68% (CSub) of months (Table 5).

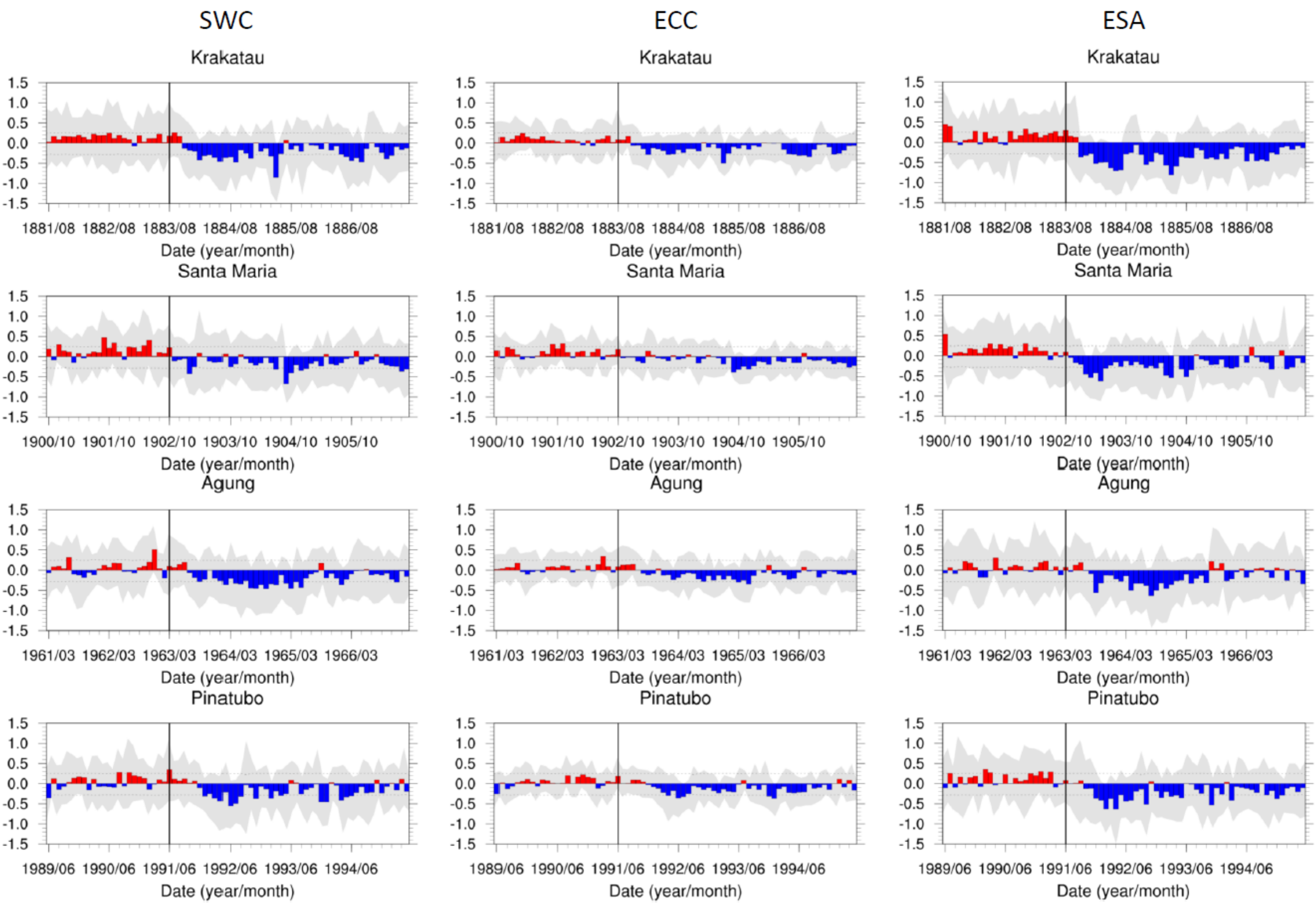

Figure 4. CMIP5-simulated sub-regional monthly temperature anomalies after the eruptions of Krakatau, Santa Maria, Agung & Pinatubo. Grey shading represents the ensemble mean.

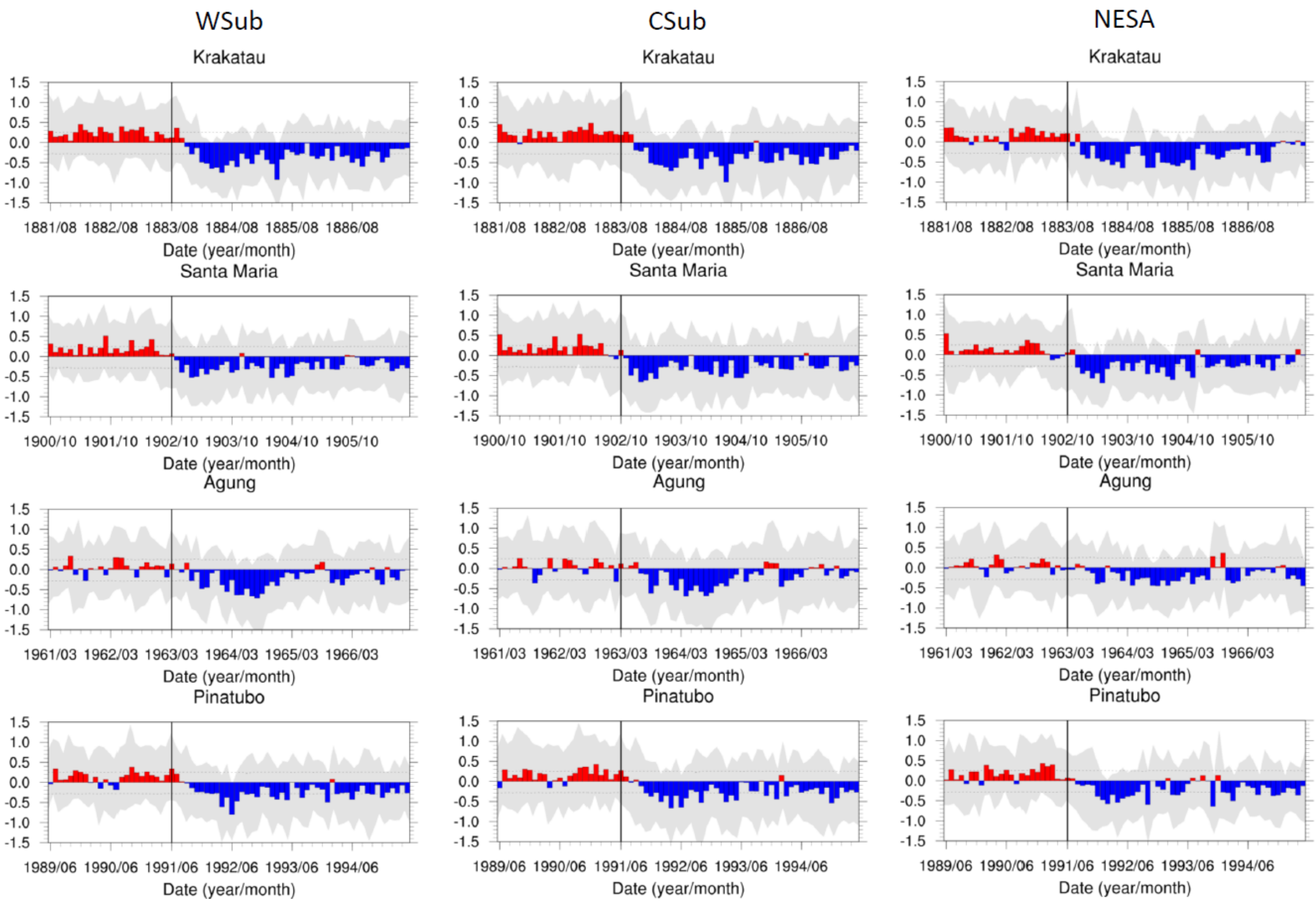

Figure 4 continued.

Table 5. CMIP5-simulated peak monthly temperature anomalies and the percentage of monthly anomalies below normal and significantly below normal (from the time of each eruption [y0] until the end of post eruption year 3 [y3]).

Eruption	Region	SWC	ECC	ESA	Wsub	Csub	NESA	Mean
Krakatau	Peak Monthly Value (°C)	-0.77	-0.53	-0.69	-0.85	-0.98	-0.62	-0.74
	Percentage of negative monthly anomalies	83	88	93	93	90	95	90
	Percentage of significant negative monthly anomalies	32	17	54	54	68	61	48
Santa Maria	Peak Monthly Value (°C)	-0.62	-0.40	-0.48	-0.47	-0.66	-0.62	-0.54
	Percentage of negative monthly anomalies	82	77	92	90	90	92	87
	Percentage of significant negative monthly anomalies	13	5	23	23	54	38	26
Agung	Peak Monthly Value (°C)	-0.43	-0.35	-0.54	-0.62	-0.70	-0.42	-0.51
	Percentage of negative monthly anomalies	85	78	70	85	74	83	79
	Percentage of significant negative monthly anomalies	28	4	17	33	37	26	24
Pinatubo	Peak Monthly Value (°C)	-0.52	-0.35	-0.56	-0.72	-0.66	-0.58	-0.57
	Percentage of negative monthly anomalies	77	88	86	88	88	86	86
	Percentage of significant negative monthly anomalies	28	12	30	28	42	35	29
Mean	Peak Monthly Value (°C)	-0.58	-0.41	-0.57	-0.66	-0.75	-0.56	-0.59
	Percentage of negative monthly anomalies	82	83	85	89	86	89	86
	Percentage of significant negative monthly anomalies	25	10	31	34	50	40	32

To test the reliability of CMIP5 model results used in this study, temperature responses following the Krakatau eruption for the SWC region are compared to instrumental data provided by Picas and Grab (2020). Picas and Grab (2020) identify cooling within the first 24 months after the eruption, but then some recovery between months 25-32, only to be followed by another cooling phase between months 33-43. The CMIP5 model outputs demonstrate a similar pattern, which provides for at least a reasonable measure of confidence in the results. Instrumental records indicate that of the first 24 months following Krakatau, 15 of these had negative temperature departures, of which 12 were significantly below 'normal' (Picas and Grab, 2020). In comparison, although it is found that 20 of these months are below 'normal', only 9 are significantly below 'normal'. For seasonal averages, negative instrumental temperature departures are stronger than those of model departures during MAM of y2 and SON of both y1 and y3. In addition, maximum monthly cooling occurs in different months of y1, but during the same months of y2 and y3, when comparing model and instrumental data (Table 6). For months 1-13 following the Krakatau eruption, the mean instrumental temperature departure is -0.30°C, while that for CMIP5 model outputs is -0.22°C. According to Picas and Grab (2020), strongest negative temperature departures are recorded during May 1885 (-1.75°C), which is also the case for the model outputs despite a considerably lower magnitude of departure (i.e. May 1885: -0.77°C). In summary, while values of temperature departure are not the same for the two data sets (Table 6), their temporal patterns of departure are very similar. Notably, while most modelling studies suggest that CMIP5 models overestimate cooling following volcanic eruptions (Chylek *et al.*, 2020), the opposite is found to be true in the case of the comparative analysis for the SWC. Nonetheless, CMIP6 models are now required to use a common volcanic forcing dataset (Space-based Stratospheric Aerosol Climatology) to improve reliability. This dataset uses an improved and adjusted stratospheric aerosol optical depth, which should be more reliable than the forcing files available in CMIP5 models

(Dhomse *et al.*, 2020). CMIP6 should thus help to resolve some of the over/under-estimation issues encountered in CMIP5.

Table 6. Comparison of instrumental (after Picas and Grab, 2020) and CMIP5 (current study) temperature departures for the SWC, following the Krakatau eruption.

		This Study			Picas and Grab (2020)		
		1884	**1885**	**1886**	**1884**	**1885**	**1886**
3-year departure (1884-1886)		-0.24			-0.06		
Annual departures		-0.33	-0.18	-0.21	-0.22	0.10	-0.06
Seasonal averages	**DJF**	-0.27	-0.19	-0.08	-0.16	0.56	0.07
	MAM	-0.32	-0.43	-0.08	-0.13	-0.73	0.35
	JJA	-0.39	-0.12	-0.35	-0.32	0.13	0.05
	SON	-0.30	-0.09	-0.33	-0.84	0.81	-0.56
Month of maximum monthly departure		June/ September	May	October	November	May	October
Percentage of negative monthly anomalies from time of eruption to end y3		83%			56%		

3.2 Santa Maria

The eruption of Santa Maria (VEI 6) occurred in the NH tropics (15°N - Guatemala) during October 1902, emitting 3.8 Tg of SO_2 into the lower stratosphere (Neely III and Schmidt, 2016). Mean annual temperatures following the eruption were below normal during y1-y3 for all regions (Table 3). However, they were only significantly below normal for two years in NESA (y1 = -0.37°C and y2 = -0.32°C), and for one year (y1) in ESA (0.31°C) and the WSub (-0.30°C). While temperature anomalies were not significantly below normal during y1 in the SWC, ECC and CSub regions, significant negative temperature departures are recorded for y2 (-0.22°C, -0.13°C and -0.36°C respectively). However, by y3, anomalies were weaker and not significant in any region. The strongest responses occurred in NESA during y1 (-0.37°C) and y3 (-0.21°C), and in the CSub (-0.36°C) during y2, while the weakest negative anomalies again occurred in the ECC each year (-0.03°C to -0.13°C).

Significant seasonal anomalies following the Santa Maria eruption are less pronounced than after the Krakatau eruption. In fact, in the SWC and ECC regions, significant responses do not occur at all during y1 (Figure 3). However, they occur during SON (y2) and DJF (y3) for both these regions (Table 4). In ESA, a negative anomaly occurs in MAM of y1, in JJA and SON of y2 and JJA of y3. Significant negative anomalies occur in DJF and MAM of y1 as well as JJA and SON of y2 in both the WSub and CSub, as well as JJA of y3 in the CSub (Table 4). In NESA, significant negative anomalies occur in DJF, MAM and SON of y1, MAM, JJA and SON of y2 and JJA of y3.

Strongest seasonal responses in y1 occur during MAM over the WSub (-0.41°C), ESA (-0.53°C), CSub (-0.55°C) and NESA (-0.58°C), and during JJA over the ECC (-0.06°C; not significant) (Figure 2). The SWC anomaly is strongest during DJF (-0.19; not significant), which contrasts with the Krakatau response which recorded weakest anomalies during these months (Table 4). Weakest negative temperature departures occurred during MAM in the ECC (0.01°C) and SWC (-0.06°C), during SON in ESA (-0.21°C), during both SON and JJA over the WSub (both -0.29°C), and in JJA for both the CSub (-0.23°C) and NESA (-0.23°C). In most regions, strongest overall negative temperature departures occur in y1, except for the SWC and ECC regions where strongest responses are recorded during SON of y2 (-0.43°C, -0.32°C respectively).

As was the case for Krakatau, strongest negative monthly temperature departures occurred over the CSub region (-0.66°C in February 1903), followed by the SWC and NESA regions (both -0.62°C in September 1904 and May 1903 respectively), but was weakest over the ECC region in September 1904 (-0.40°C). Maximum response occurred 23-24 months (i.e. September and October 1904) after the Santa Maria eruption in the SWC, ECC, ESA and WSub regions, but as early as four (February 1903) to seven (May 1903) months post eruption in the CSub and NESA regions respectively. For the first three years post Santa Maria, most mean monthly temperatures are below normal, ranging from 92% (NESA) to 77% (ECC) of months, however, significantly below normal mean values range from only 5% (ECC) to 54% (CSub) of months (Table 5).

3.3 Agung

Mount Agung (8°S - Indonesia) erupted during March 1963 and emitted 7.5 Tg of SO_2 into the stratosphere (Neely III and Schmidt, 2016). Unlike the other eruptions discussed in this paper, it had a VEI of only 4. During y1, all regions record a significant negative mean annual temperature anomaly, varying from as much as -0.50°C (WSub and CSub) to as little as -0.17°C (ECC)(Table 3). During y2, however, only the SWC (-0.19°C) and ECC (-0.13°C) regions record significant mean annual temperature departures. The weakest responses occurred over the ECC during y1 (0.17°C), over the WSub during y2 (-0.10°C) and over ESA during y3 (-0.05°C). In strong contrast to the Krakatau and Santa Maria eruptions, the SWC records the strongest response of all sub-regions in y2 (-0.19°C) and second strongest response in y3 (-0.14°C).

Seasonal temperature anomalies in response to the Agung eruption are below normal during y1-y3 (Figure 2), but overall less significant than following the Krakatau eruption. Again, in contrast with Krakatau, negative anomalies after the Agung eruption are most significant over the SWC and ECC regions. Negative anomalies in the SWC are significant during DJF for y1-y3, during MAM for y1 and y2, and during JJA and SON for y1 (Table 4). In the ECC region, negative temperature departures are significant during JJA and SON of y1 only. Anomalies are significant during DJF and MAM of y2, and during DJF of y3. In the ESA region, anomalies are significantly below normal in SON of y0, about five months after the eruption (Table 4). They are then not significant during DJF but are again significant during MAM, JJA and SON of y1. Both the WSub and CSub regions have significant negative temperature anomalies for each season in y1 only, except that the anomaly during SON y0 in the CSub region is significantly below normal as well. Over NESA, negative temperature departures are only significant during JJA and SON of y1 (Table 4).

The strongest seasonal response of y1 occurred during JJA over all regions (mean: -0.44°C; Table 4) except NESA, where the strongest response occurred during SON (-0.40°C) (Figure 3). Weakest anomalies occur in DJF over all regions (mean: -

0.27°C) except the ECC, where the weakest response is again recorded for MAM (-0.11°C). As was the case with Santa Maria, negative mean seasonal temperature anomalies are most pronounced in y1 over most sub-regions, apart from the SWC and ECC regions where strongest response was in MAM of y2 (-0.39°C; -0.30°C respectively).

The strongest monthly temperature response is again recorded in the CSub region (-0.70°C in February 1903), as was also the case for Krakatau and Santa Maria (Figure 4). In the ECC region, the strongest response is in May 1965 (-0.35°C), but this is the weakest maximum response for any of the regions following all four eruptions. Strongest monthly anomalies lack temporal uniformity between sub-regions, occurring earlier (13-17 months post eruption) in the CSub, WSub and ESA regions, and later (20-26 months post eruption) in the NESA, SWC and ECC regions. For the first three years post Agung, most mean monthly temperatures are below normal, ranging from 85% (SWC and WSub) to 70% (ESA) of months, however, significantly below normal mean values range from only 4% (ECC) to 37% (CSub) of months (Table 5). Although the SWC region had a comparably low percentage of significantly cooler than normal months after the Krakatau and Santa Maria eruptions, compared to most other sub-regions, the situation is somewhat different after the Agung eruption. In the latest case, the SWC region records 28% of months as significantly cooler than normal for y1-3, while that for ESA and NESA is considerably less (17% and 16% respectively).

3.4 Pinatubo

Mount Pinatubo (15°N – Philippines) erupted in June 1991, emitting 18 Tg of SO_2 into the stratosphere (Neely III and Schmidt, 2016) with a VEI = 6. Although mean annual temperature departures are again negative for y1-y3 (Table 3), significant departures for all regions are only recorded in y1 (mean: -0.32°C). No southern African region records a significant temperature anomaly in y2, however, in y3, significant departures are observed for the SWC and ECC regions (-0.20°C and -0.16°C respectively). The weakest mean annual temperature response is once again recorded over the ECC region for y1-y3 (mean: -0.16°C). The strongest annual response occurs over the CSub region during y1 (-0.37°C) and y2 (-0.23°C), and in the WSub region in y3 (-0.25°C). Notably, the SWC and ECC regions record significant cooling during both y1 and y3 but not y2, as was the case for Krakatau.

Although not always significant, seasonal temperature anomalies are below normal during all seasons for y1 to y3 (Figure 3). Over the SWC, significant negative anomalies are recorded during MAM and JJA in y1, and DJF and JJA in y3 (Table 4). Significant negative temperature departures over the ECC are observed during MAM and JJA in y1, DJF and MAM in y2, and DJF in y3. The SWC and ECC regions are the only sub-regions recording significant departures in y3. Over ESA, the CSub and NESA regions, significant negative temperature departures occur during DJF, MAM and JJA in y1, and MAM in y2. The WSub region follows the same pattern, apart from DJF of y1 not being significant (Table 4).

The strongest seasonal response during y1 is in JJA over the SWC, ECC and WSub regions (mean= -0.42°C, Table 4), in DJF over ESA and NESA (mean = -0.48°C), and in MAM over the CSub region (-0.44°C). Weakest responses occur in SON over the SWC, ESA, CSub and NESA regions (mean= -0.23°C), and in DJF in the ECC and WSub regions (mean = -0.17°C). Unlike the three earlier eruptions, the strongest overall seasonal responses after Pinatubo occur during y1.

Strongest monthly temperature responses following the Pinatubo eruption occur much earlier (within 10-12 months) across most southern African regions than was the case for the other eruptions, apart from NESA where strongest response seems very delayed (29^{th} month)(Figure 4). The strongest negative temperature departure occurs in the WSub region (-0.72°C in June 1992). Again, the strongest negative monthly anomaly in the ECC region (-0.35°C in June 1992) is weakest of all regional maximum responses. For the first three years post Pinatubo, most mean monthly temperatures are below normal, ranging from 88% (ECC, WSub, and CSub) to 77% (SWC) of months, however, significantly below normal mean values range from only 12% (ECC) to 42% (CSub) of months (Table 5).

4 Discussion

Although countless studies have examined the impacts of major volcanic eruptions on global-, continental- and regional-scale temperatures, investigations at the sub-regional scale are limited for the NH (Kondo, 1988; Shindell, 2004; Esper *et al.*, 2013; Zhang *et al.*, 2013; Dogar *et al.*, 2017) and have been absent until now for the SH. To this end, the CMIP5 model outputs demonstrate significant temperature responses to major volcanic eruptions across the southern African region, yet also portray strong sub-regional contrasts in such responses over relatively small spatial scales. In particular, findings indicate that the magnitude and timing of the response, and also the season of maximum response varies considerably by region and by eruption location/timing/magnitude. In addition, underlying climatic conditions will vary with each eruption event and thus also impact on such forcing outcomes (Zanchettin *et al.*, 2014; Stevenson *et al.*, 2017; Krishnamohan *et al.*, 2019; Sun *et al.*, 2019).

Model outputs show mean annual negative temperature departures are strongest over the northern, arid regions (WSub, CSub and NESA) after all major eruptions investigated in this paper (mean of all eruptions= y1: -0.40°C; -y2: -0.26°C; y3: -0.23°C). In particular, the CSub region has the strongest anomalies following the Krakatau and Pinatubo eruptions, the NESA region following the Santa Maria eruption, and in WSub following the Agung eruption. Weakest responses are consistently modelled for the ECC after each of the four eruptions investigated (mean of all eruptions= y1: -0.14°C; y2: -0.13°C; y3: -0.12°C). The SWC region with its Mediterranean climate, records second weakest responses after all eruptions (mean of all eruptions= y1: -0.27°C; y2: -0.19°C; y3: -0.17°C).

Post eruption temperature responses vary in strength according to season. Overall, weakest seasonal anomalies occur particularly during SON in the SWC, ESA, and NESA regions and in DJF in the WSub and CSub regions. The exception to this being for the ECC region where the weakest negative temperature departures occur more often during MAM, while the strongest departures occur in JJA, and hence is in strong contrast to other sub-regions. Strongest cooling occurs most notably in MAM over the WSub, CSub, ESA and NESA regions and in JJA in the SWC and ECC regions, coinciding with strongest cooling in summer/autumn over the NH (Zanchettin *et al.*, 2019). However, the ESA and SWC regions also record strong cooling during austral summer (DJF). Strong autumn and winter cooling over the SWC region is most likely associated with more intense and frequent cold front overpasses during such seasons (Picas and Grab , 2020), and the result of more favourable circulation during winter when the Brewer-Dobson circulation is intensified (Harvey *et al*., 2020). This response is seen most prominently following Krakatau and Pinatubo which erupted during August and June respectively (austral winter), thus transporting aerosols most effectively and contributing to the stronger observed responses (Perlwitz and Graf, 1995; Birner and Bönisch, 2010; Harvey *et al.*, 2020).

The CSub region usually experiences maximum monthly temperature departures at an earlier date (mean = 12 months after eruption date) than all other regions (mean = 17 months after eruption date), while that for the ECC is most delayed (mean = 21 months after eruption date). Maximum departures generally occur during the cooler austral months (March – August) after each eruption, except for the NESA (January following Krakatau, November following Pinatubo) and CSub (November following Agung) regions. The CSub region also records more significant negative monthly temperature departures (mean = 50%) than any other region (mean = 30%), while those for the ECC are lowest (mean = 10%). The findings thus demonstrate strongly contrasting temperature responses to volcanic forcing between the more continental climatic/summer rainfall regions (CSub, NESA), and the Mediterranean/subtropical climates of the winter/all year rainfall regions (i.e. SWC/ECC respectively). Strong El Niño Southern Oscillation (ENSO) phases tend to have more significant temperature effects over the interior than coastal regions of southern Africa, with the CSub and NESA regions most strongly impacted by the El Niño anomaly, and result in positive temperature departures (Lakhraj-Govender and Grab, 2018). The somewhat weaker responses along coastal regions (ECC and SWC) may also be due to oceanic temperature-regulating effects, particularly the cool Benguela current that borders the SWC (Philippon *et al*., 2012). Although SSTs are also affected by volcanic eruptions (Gleckler *et al.*, 2006; McGregor *et al.*, 2015; Klein and Goosse, 2018), these are not as extreme in amplitude (Gupta and Marshall, 2018) as those for terrestrial air temperatures. In addition, SSTs continue to dampen the impacts of climate change/variability along coastal regions (Dittus *et al.*, 2018). In contrast, the more continental southern African regions (i.e. CSub, WSub and NESA) typically experience stronger temperature extremes than coastal regions (Kruger and Sekele, 2013). Collectively, these are likely important factors regulating temperature responses, and account for sub-regional differences following major volcanic eruptions over the African sub-continent.

The southern African climate is strongly controlled by ENSO (Pezza *et al*., 2007; Philippon *et al*., 2012), which is known to have variable sub-regional climatic impacts across the sub-continent (Nicholson and Kim, 1997; Mason, 2001; Lakhraj-Govender and Grab, 2019). The central interior (coinciding with the CSub region) experiences the strongest ENSO-related temperature response, followed by the northern interior (coinciding with the NESA region); in contrast, the north-eastern interior (coinciding with the ESA region) records strongest temperature responses during La Niña events (Lakhraj-Govender and Grab, 2018). It has also been identified that responses to ENSO events are usually most pronounced during austral summer (Nicholson and Kim, 1997; Mason, 2001; Lakhraj-Govender and Grab, 2018). The SSTs generated in the study suggest a likeness to La Niña conditions following each of the four eruptions, which could contribute to the cooler temperatures over southern Africa. However, volcanic eruptions can themselves affect ENSO, with NH and tropical eruptions leading to a tendency towards El Niño-like anomalies (Pausata *et al*., 2016; Ménégoz *et al.*, 2018; Zuo *et al*., 2018). While La Niña conditions arise in the model simulations, in reality, El Niño events occurred during years after all the eruptions investigated in this paper (for ENSO anomalies see Gergis and Fowler, 2009). Volcanic forcing possibly has a dual temperature impact over regions of the SH, not only through its cooling effects associated with an altered global energy budget, but indirectly through its influence on ENSO phases and strengths, which then either moderates (limits) or further enhances the extent of such cooling. Given El Niño generally has a warming effect over much of southern Africa, it is possible that this is the reason for somewhat weaker negative observed temperature departures following major eruptions, compared to the modelled response (Barnes *et al.*, 2016).

CMIP5 models tend to show a positive Southern Annular Mode (SAM) following major volcanic eruptions (Barnes *et al*., 2016; McGraw *et al*., 2016), as was also the case after the Agung and Pinatubo eruptions. A positive SAM generally means strengthened westerlies, which contract towards the poles and result in intensified cyclogenesis (Yang and Xiao, 2017). Mid-latitude cyclones cause most of the extreme weather encountered over mid-latitudes of the SH, or southernmost terrestrial regions of South America, southern Africa and Australasia (Pepler *et al*., 2016). Picas and Grab (2020) suggested that an increase in strength or frequency of mid-latitude cyclones following volcanic eruptions could contribute to cooling observed over the SWC. Given that volcanic forcing has an impact on the Southern Annular Mode and Polar Vortex, it thus also (indirectly) influences the position and strength of mid-latitude cyclones. Given that the SWC and ECC sub-regions are regularly affected by cold fronts during the cooler seasons, any increased (equatorward extension) of frontal activity might only have a marginal impact on temperature reductions here. In contrast, the CSub, WSub and NESA regions, being further north, are less affected by frontal systems than the SWC and ECC. However, strong and further northward penetrating frontal systems, as is advocated during post-volcanic years, would have considerable cooling effects over the interior and northern regions of the sub-continent, hence accounting for stronger cooling than in southernmost regions.

Finally, the changing nature of temperature responses are considered for the earlier two eruptions (Krakatau and Santa Maria) with that for the latter two (Agung and Pinatubo). Significant seasonal cooling over the more northern and interior regions (WSub, CSub, NESA and ESA) seems reduced when comparing the earlier two eruptions (mean:-0.34°C) with the more recent two (mean: -0.24°C). Mean anomalies for the four regions combined show that the greatest difference between the earlier and more recent eruptions occurs in JJA (mean for earlier two: -0.36°C; latter two: -0.22°C), while the smallest difference occurs during SON (mean for earlier two: -0.27°C; latter two: -0.20°C). The weakened volcanic signature may, in part, be due to the variable strengths of these eruptions, but might also be influenced by an increased moderating effect of anthropogenic (CO_2) forcing during more recent times, as has similarly been suggested by Tett (2002) and Gleckler *et al.* (2006). However, in contrast to these southern African sub-regions, the same is not found for the more southerly SWC and ECC regions, where mean seasonal forcing after the earlier two eruptions is only marginally stronger than the more recent eruptions in JJA (mean for earlier two = -0.19°C; latter two = -0.18°C), while in DJF and MAM the seasonal response has actually strengthened over more recent times (DJF mean for earlier two = -0.14°C; latter two = -0.22°C. MAM mean for earlier two = -0.14°C; latter two = -0.21°C).

5 Conclusion

Despite considerable recent advances in knowledge pertaining to volcanic forcing impacts on global to hemispheric scale climates, the understanding of such impacts at finer spatial scales, and particularly so in the Southern Hemisphere, has remained in its infancy. To this end, this paper demonstrates considerable variability (timing, duration and amplitude) of CMIP5 modelled temperature responses between climatic sub-regions of southernmost Africa. Importantly, this suggests that global- or hemispheric-scale modelled forcing-responses need to be considered with utmost caution for regional to sub-regional scale climate modelling, or when ascertaining likely volcanic impacts at such finer spatial scales. This is particularly critical to climate-sensitive agricultural regions such as southern Africa where down-scaled climatic responses need to be well understood for appropriate preparedness initiatives.

Strongest negative temperature departures following major volcanic eruptions are recorded for the northern semi-arid sub-regions of southern Africa, which coincides with regions that are climatically most responsive to ENSO. This reinforces the already established volcanic forcing impact on generating El Niño-like conditions. In this context, one would expect that regions most strongly impacted by El Niño, would thus also (indirectly) be strongly affected by such eruptions. However, CMIP5 models also simulate a positive phase of the Southern Annular Mode after such eruptions, which strengthens the westerlies, and hence cyclogenesis. This likely accounts for strongest negative temperature departures during austral autumn (MAM) and winter (JJA) over most of the African sub-continent. It is possible, however, that the influence of El Niño conditions dampens the extent of seasonal/annual cooling, despite strengthened cyclogenesis. It is acknowledged that such an inference requires further verification and detailed investigation, but might imply that volcanically induced climatic trigger events may not always reinforce a common climatic outcome (such as cooling) and thus possibly account for varied amplitudes of cooling (or in some cases possible seasonal warming) responses between sub-regions, regions and even hemispheres.

6 References

Ammann CM, Joos F, Schimel DS, Otto-Bliesner BL, Tomas RA. 2007. Solar influence on climate during the past millennium: Results from transient simulations with the NCAR Climate System Model. Proceedings of the National Academy of Sciences, 104(10): 3713–3718. https://doi.org/10.1073/pnas.0605064103.

Barnes EA, Solomon S, Polvani LM. 2016. Robust wind and precipitation responses to the Mount Pinatubo eruption, as simulated in the CMIP5 models. Journal of Climate, 29(13): 4763–4778. https://doi.org/10.1175/JCLI-D-15-0658.1.

Birner T, Bönisch H. 2010. Residual circulation trajectories and transit times into the extratropical lowermost stratosphere. Atmospheric Chemistry and Physics Discussions, 10(7): 16837–16860. https://doi.org/10.5194/acpd-10-16837-2010.

Chylek P, Folland C, Klett JD, Dubey MK. 2020. CMIP5 climate models overestimate cooling by volcanic aerosols. Geophysical Research Letters, 47(3). https://doi.org/10.1029/2020GL087047.

Colose CM, LeGrande AN, Vuille M. 2015. The influence of tropical volcanic eruptions on the climate of South America during the last millennium. Climate of the Past, 11: 3375–3424. https://doi.org/10.5194/cpd-11-3375-2015.

Colose CM, LeGrande AN, Vuille M. 2016. The influence of volcanic eruptions on the climate of tropical South America during the last millennium in an isotope-enabled general circulation model. Climate of the Past, 12(4): 961–979. https://doi.org/10.5194/cp-12-961-2016.

Cook ER, Palmer JG, D'Arrigo RD. 2002. Evidence for a 'Medieval Warm Period' in a 1,100 year tree-ring reconstruction of past austral summer temperatures in New Zealand: Medieval warm period in New Zealand. Geophysical Research Letters, 29(14): 12-1-12–4. https://doi.org/10.1029/2001GL014580.

Dhomse SS, Mann GW, Antuña Marrero JC, Shallcross SE, Chipperfield MP, Carslaw KS, Marshall L, Abraham NL, Johnson CE. 2020. Evaluating the simulated radiative forcings, aerosol properties, and stratospheric warmings from the 1963 Mt Agung, 1982 El Chichón, and 1991 Mt Pinatubo volcanic aerosol clouds. Atmospheric Chemistry and Physics. Copernicus GmbH, 20(21): 13627–13654. https://doi.org/10.5194/acp-20-13627-2020.

Dieng HB, Cazenave A, Meyssignac B, von Schuckmann K, Palanisamy H. 2017. Sea and land surface temperatures, ocean heat content, Earth’s energy imbalance and net radiative forcing over the recent years: sea and land surface temperature. International Journal of Climatology, 37: 218–229. https://doi.org/10.1002/joc.4996.

Dittus AJ, Karoly DJ, Donat MG, Lewis SC, Alexander LV. 2018. Understanding the role of sea surface temperature-forcing for variability in global temperature and precipitation extremes. Weather and Climate Extremes, 21: 1–9. https://doi.org/10.1016/j.wace.2018.06.002.

Dogar MM, Stenchikov G, Osipov S, Wyman B, Zhao M. 2017. Sensitivity of the regional climate in the Middle East and North Africa to volcanic perturbations: sensitivity of MENA region to volcanism. Journal of Geophysical Research: Atmospheres, 122(15): 7922–7948. https://doi.org/10.1002/2017JD026783.

Driscoll S, Bozzo A, Gray LJ, Robock A, Stenchikov G. 2012. Coupled Model Intercomparison Project 5 (CMIP5) simulations of climate following volcanic eruptions. Journal of Geophysical Research: Atmospheres, 117(D17): D17105. https://doi.org/10.1029/2012JD017607.

Dunwiddie PW, LaMarche VC. 1980. A climatically responsive tree-ring record from Widdringtonia cedarbergensis, Cape Province, South Africa. Nature, 286(5775): 796–797. https://doi.org/10.1038/286796a0.

Efron B. 1979. Bootstrap Methods: another look at the Jackknife. The Annals of Statistics, 7(1): 1–26. https://doi.org/10.1214/aos/1176344552.

Engelbrecht CJ, Engelbrecht FA. 2016. Shifts in Köppen-Geiger climate zones over southern Africa in relation to key global temperature goals. Theoretical and Applied Climatology, 123(1–2): 247–261. https://doi.org/10.1007/s00704-014-1354-1.

Engelbrecht FA, McGregor JL, Engelbrecht CJ. 2008. Dynamics of the Conformal-Cubic Atmospheric Model projected climate-change signal over southern Africa. International Journal of Climatology, 29(7): 1013–1033. https://doi.org/10.1002/joc.1742.

Esper J, Schneider L, Krusic PJ, Luterbacher J, Büntgen U, Timonen M, Sirocko F, Zorita E. 2013. European summer temperature response to annually dated volcanic eruptions over the past nine centuries. Bulletin of Volcanology, 75(7): 736. https://doi.org/10.1007/s00445-013-0736-z.

Gentilli J. 1948. Present-day volcanicity and climatic change. Geological Magazine, 85(3): 172–175.

Gergis JL, Fowler AM. 2009. A history of ENSO events since A.D. 1525: implications for future climate change. Climatic Change, 92(3–4): 343–387. https://doi.org/10.1007/s10584-008-9476-z.

Gilliland RL. 1982. Solar, volcanic, and CO2 forcing of recent climatic changes. Climatic Change, 4(2): 111–131. https://doi.org/10.1007/BF02423387.

Gleckler PJ, Wigley TML, Santer BD, Gregory JM, AchutaRao K, Taylor KE. 2006. Volcanoes and climate: Krakatoa's signature persists in the ocean. Nature, 439(7077): 675. https://doi.org/10.1038/439675a.

Grab SW, Nash DJ. 2010. Documentary evidence of climate variability during cold seasons in Lesotho, southern Africa, 1833-1900. Climate Dynamics, 34(4): 473–499.

Grab SW, Simpson AJ. 2000. Climatic and environmental impacts of cold fronts over KwaZulu-Natal and the adjacent interior of southern Africa. South African Journal of Science, 96: 602–608.

Gupta M, Marshall J. 2018. The climate response to multiple volcanic eruptions mediated by ocean heat uptake: damping processes and accumulation potential. Journal of Climate, 31(21): 8669–8687. https://doi.org/10.1175/JCLI-D-17-0703.1.

Harvey PJ, Grab SW, Malherbe J. 2020. Major volcanic eruptions and their impacts on southern hemisphere temperatures during the late 19th and 20th centuries, as simulated by CMIP5 models. Geophysical Research Letters, 47(14). https://doi.org/10.1029/2020GL087792.

Haurwitz MW, Brier GW. 1981. A critique of the Superposed Epoch Analysis Method: Its application to solar–weather relations. Monthly Weather Review, 109(10): 2074–2079. https://doi.org/10.1175/1520-0493(1981)109<2074:ACOTSE>2.0.CO;2.

Humphreys WJ. 1913. Volcanic dust and other factors in the production of climatic changes, and their possible relation to ice ages. Journal of the Franklin Institute, 176(2): 131–160. https://doi.org/10.1016/S0016-0032(13)91294-1.

Kandlbauer J, Hopcroft PO, Valdes PJ, Sparks RSJ. 2013. Climate and carbon cycle response to the 1815 Tambora volcanic eruption. Journal of Geophysical Research: Atmospheres, 118(22): 12,497-12,507. https://doi.org/10.1002/2013JD019767.

Klein F, Goosse H. 2018. Reconstructing East African rainfall and Indian Ocean sea surface temperatures over the last centuries using data assimilation. Climate Dynamics, 50(11–12): 3909–3929. https://doi.org/10.1007/s00382-017-3853-0.

Kondo J. 1988. Volcanic eruptions, cool summers, and famines in the northeastern part of Japan. Journal of Climate, 1(8): 775–788.

Köppen W. 1936. Das geographisca system der Klimate. In: Köppen W and Geiger G (eds) Handbuch der Klimatologie. Gebr, Borntraeger: Berlin, 44.

Kremser S, Thomason LW, von Hobe M, Hermann M, Deshler T, Timmreck C, Toohey M, Stenke A, Schwarz JP, Weigel R, Fueglistaler S, Prata FJ, Vernier J-P, Schlager H, Barnes JE, Antuña-Marrero J-C, Fairlie D, Palm M, Mahieu E, Notholt J, Rex M, Bingen C, Vanhellemont F, Bourassa A, Plane JMC, Klocke D, Carn SA, Clarisse L, Trickl T, Neely R, James AD, Rieger L, Wilson JC, Meland B. 2016. Stratospheric aerosol-Observations, processes, and impact on climate: Stratospheric Aerosol. Reviews of Geophysics, 54(2): 278–335. https://doi.org/10.1002/2015RG000511.

Krishnamohan K-PS-P, Bala G, Cao L, Duan L, Caldeira K. 2019. Climate system response to stratospheric sulfate aerosols: sensitivity to altitude of aerosol layer. Earth System Dynamics, 10(4): 885–900. https://doi.org/10.5194/esd-10-885-2019.

Kruger AC, Sekele SS. 2013. Trends in extreme temperature indices in South Africa: 1962-2009. International Journal of Climatology, 33(3): 661–676. https://doi.org/10.1002/joc.3455.

Lakhraj-Govender R, Grab SW. 2018. Assessing the impact of El Niño-Southern Oscillation on South African temperatures during austral summer. International Journal of Climatology, 39(1): 143–156. https://doi.org/10.1002/joc.5791.

LaMarche VC, Hirschboeck KK. 1984. Frost rings in trees as records of major volcanic eruptions. Nature, 307(5947): 121–126. https://doi.org/10.1038/307121a0.

Lamb HH. 1970. Volcanic dust in the atmosphere; with a chronology and assessment of its meteorological significance. Philosophical Transactions of the Royal Society of London. Series A, Mathematical and Physical Sciences, 266(1178): 425–533. https://doi.org/10.1098/rsta.1970.0010.

Landman WA, Malherbe J, Engelbrecht FA. 2017. Understanding the social and environmental implications of global change. In: Mambo J and Faccer K (eds) South Africa’s present-day climate. Africa Sun Media: Stellenbosch, 7–12.

Liu F, Zhao T, Wang B, Liu J, Luo W. 2018. Different global precipitation responses to solar, volcanic, and greenhouse gas forcings. Journal of Geophysical Research: Atmospheres, 123(8): 4060–4072. https://doi.org/10.1029/2017JD027391.

Lough JM, Fritts HC. 1987. An assessment of the possible effects of volcanic eruptions on North American climate using tree-ring data, 1602 to 1900 A.D. Climatic Change, 10(3): 219–239. https://doi.org/10.1007/BF00143903.

Lyu K, Zhang X, Church JA, Hu J. 2015. Quantifying internally generated and externally forced climate signals at regional scales in CMIP5 models: internal and forced climate signals. Geophysical Research Letters, 42(21): 9394–9403. https://doi.org/10.1002/2015GL065508.

Man W, Zhou T, Jungclaus JH. 2014. Effects of large volcanic eruptions on global summer climate and East Asian Monsoon changes during the Last Millennium: analysis of MPI-ESM simulations. Journal of Climate, 27(19): 7394–7409. https://doi.org/10.1175/JCLI-D-13-00739.1.

Mason SJ. 2001. El Niño, climate change, and Southern African climate: El Nino-Southern Oscillation phenomenon. Environmetrics, 12(4): 327–345. https://doi.org/10.1002/env.476.

Mass CF, Portman DA. 1989. Major volcanic eruptions and climate: a critical evaluation. Journal of Climate, 2(6): 566–593. https://doi.org/10.1175/1520-0442(1989)002<0566:MVEACA>2.0.CO;2.

McGraw MC, Barnes EA, Deser C. 2016. Reconciling the observed and modeled Southern Hemisphere circulation response to volcanic eruptions: Reconciling SH Response to Volcanoes. Geophysical Research Letters, 43(13): 7259–7266. https://doi.org/10.1002/2016GL069835.

McGregor HV, Evans MN, Goosse H, Leduc G, Martrat B, Addison JA, Mortyn PG, Oppo DW, Seidenkrantz M-S, Sicre M-A, Phipps SJ, Selvaraj K, Thirumalai K, Filipsson HL, Ersek V. 2015. Robust global ocean cooling trend for the pre-industrial Common Era. Nature Geoscience. Nature Publishing Group, 8(9): 671–677. https://doi.org/10.1038/ngeo2510.

Ménégoz M, Bilbao R, Bellprat O, Guemas V, Doblas-Reyes FJ. 2018. Forecasting the climate response to volcanic eruptions: prediction skill related to stratospheric aerosol forcing. Environmental Research Letters, 13(6): 064022. https://doi.org/10.1088/1748-9326/aac4db.

Monerie P-A, Moine M-P, Terray L, Valcke S. 2017. Quantifying the impact of early 21st century volcanic eruptions on global-mean surface temperature. Environmental Research Letters, 12(5): 054010. https://doi.org/10.1088/1748-9326/aa6cb5.

Neely III RR, Schmidt A. 2016. VolcanEESM: Global volcanic sulphur dioxide (SO_2) emissions database from 1850 to present. Centre for Environmental Data Analysis.

Neukom R, Gergis J, Karoly DJ, Wanner H, Curran M, Elbert J, González-Rouco F, Linsley BK, Moy AD, Mundo I, Raible CC, Steig EJ, van Ommen T, Vance T, Villalba R, Zinke J, Frank D. 2014. Inter-hemispheric temperature variability over the past millennium. Nature Climate Change, 4(5): 362–367. https://doi.org/10.1038/nclimate2174.

Nicholson SE, Kim J. 1997. The relationship of the El Niño–Southern Oscillation to African rainfall. International Journal of Climatology, 17(2): 117–135. https://doi.org/10.1002/(SICI)1097-0088(199702)17:2<117::AID-JOC84>3.0.CO;2-O.

Oman L, Robock A, Stenchikov G, Schmidt GA, Ruedy R. 2005. Climatic response to high-latitude volcanic eruptions. Journal of Geophysical Research: Atmospheres, 110(D13): D13103. https://doi.org/10.1029/2004JD005487.

Palmer JG, Xiong L. 2004. New Zealand climate over the last 500 years reconstructed from Libocedrus bidwillii Hook. f. tree-ring chronologies. The Holocene, 14(2): 282–289. https://doi.org/10.1191/0959683604hl679rr.

Pausata FSR, Karamperidou C, Caballero R, Battisti DS. 2016. ENSO response to high-latitude volcanic eruptions in the Northern Hemisphere: The role of the initial conditions: ENSO Response to High-Latitude Volcanic Eruptions. Geophysical Research Letters, 43(16): 8694–8702. https://doi.org/10.1002/2016GL069575.

Pepler AS, Fong J, Alexander LV. 2016. Australian east coast mid-latitude cyclones in the 20th Century Reanalysis ensemble. International Journal of Climatology, 37(4): 2187–2192. https://doi.org/10.1002/joc.4812.

Perlwitz J, Graf H-F. 1995. The statistical connection between tropospheric and stratospheric circulation of the northern hemisphere in winter. Journal of Climate, 8: 2281–2295.

Pezza AB, Simmonds I, Renwick JA. 2007. Southern hemisphere cyclones and anticyclones: recent trends and links with decadal variability in the Pacific Ocean. International Journal of Climatology, 27(11): 1403–1419. https://doi.org/10.1002/joc.1477.

Philippon N, Rouault M, Richard Y, Favre A. 2012. The influence of ENSO on winter rainfall in South Africa. International Journal of Climatology, 32(15): 2333–2347. https://doi.org/10.1002/joc.3403.

Picas J, Grab SW 2020. Potential impacts of major nineteenth century volcanic eruptions on temperature over Cape Town, South Africa: 1834–1899. Climatic Change, 159(4): 523-544. https://doi.org/10.1007/s10584-020-02678-6.

Pidwirny M. 2006. Climate Classification and Climatic Regions of the World. Fundamentals of Physical Geography.

Rao MP, Cook BI, Cook ER, D'Arrigo RD, Krusic PJ, Anchukaitis KJ, LeGrande AN, Buckley BM, Davi NK, Leland C, Griffin KL. 2017. European and Mediterranean hydroclimate responses to tropical volcanic forcing over the last millennium. Geophysical Research Letters, 44(10): 5104–5112. https://doi.org/10.1002/2017GL073057.

Robock A. 2000. Volcanic eruptions and climate. Reviews of Geophysics, 38(2): 191–219. https://doi.org/10.1029/1998RG000054.

Robock A, Mao J. 1995. The volcanic signal in surface temperature observations. Journal of Climate, 8(5): 1086–1103. https://doi.org/10.1175/1520-0442(1995)008<1086:TVSIST>2.0.CO;2.

Roffe SJ, Fitchett JM, Curtis CJ. 2020. Determining the utility of a percentile-based wet-season start- and end-date metrics across South Africa. Theoretical and Applied Climatology, 140(3–4): 1331–1347. https://doi.org/10.1007/s00704-020-03162-y.

Roig FA, Villalba R. 2008. Understanding climate from Patagonian tree rings. In: Rabassa J (ed) Developments in Quaternary Sciences. Elsevier, 411–435.

Salinger MJ. 1998. New Zealand climate: the impact of major volcanic eruptions. Weather and Climate, 18(1): 11–19.

Santer BD, Painter JF, Bonfils C, Mears CA, Solomon S, Wigley TML, Gleckler PJ, Schmidt GA, Doutriaux C, Gillett NP, Taylor KE, Thorne PW, Wentz FJ. 2013. Human and natural influences on the changing thermal structure of the atmosphere. Proceedings of the National Academy of Sciences, 110(43): 17235–17240. https://doi.org/10.1073/pnas.1305332110.

Sato M, Hansen JE, McCormick MP, Pollack JB. 1993. Stratospheric aerosol optical depths, 1850–1990. Journal of Geophysical Research, 98(D12): 22987. https://doi.org/10.1029/93JD02553.

Schneider DP, Ammann CM, Otto-Bliesner BL, Kaufman DS. 2009. Climate response to large, high-latitude and low-latitude volcanic eruptions in the Community Climate System Model. Journal of Geophysical Research: Atmospheres, 114(D15): D15101. https://doi.org/10.1029/2008JD011222.

Shindell DT. 2004. Dynamic winter climate response to large tropical volcanic eruptions since 1600. Journal of Geophysical Research, 109(D5): D05104. https://doi.org/10.1029/2003JD004151.

Stevenson S, Fasullo JT, Otto-Bliesner BL, Tomas RA, Gao C. 2017. Role of eruption season in reconciling model and proxy responses to tropical volcanism. Proceedings of the National Academy of Sciences, 114(8): 1822–1826. https://doi.org/10.1073/pnas.1612505114.

Sun W, Wang B, Liu J, Chen D, Gao C, Ning L, Chen L. 2019. How northern high-latitude volcanic eruptions in different seasons affect ENSO. Journal of Climate, 32(11): 3245–3262. https://doi.org/10.1175/JCLI-D-18-0290.1.

Taylor KE, Stouffer RJ, Meehl GA. 2012. An overview of CMIP5 and the experiment design. Bulletin of the American Meteorological Society, 93(4): 485–498. https://doi.org/10.1175/BAMS-D-11-00094.1.

Tett SFB. 2002. Estimation of natural and anthropogenic contributions to twentieth century temperature change. Journal of Geophysical Research, 107(D16): 4306. https://doi.org/10.1029/2000JD000028.

Textor C, Graf H-F, Timmreck C, Robock A. 2004. Emissions from volcanoes. In: Granier C, Artaxo P and Reeves CE (eds) Emissions of Atmospheric Trace Compounds. Springer Netherlands: Dordrecht, 269–303.

Thompson DWJ, Wallace JM, Jones PD, Kennedy JJ. 2009. Identifying signatures of natural climate variability in time series of global-mean surface temperature: methodology and insights. Journal of Climate, 22(22): 6120–6141. https://doi.org/10.1175/2009JCLI3089.1.

Timmreck C. 2012. Modeling the climatic effects of large explosive volcanic eruptions. WIREs: Climate Change, 3(6): 545–564. https://doi.org/10.1002/wcc.192.

Timmreck C. 2018. Climatic effects of large volcanic eruptions. Habilitation Thesis, Hamburg, Universität Hamburg.

Trigo RM, Vaquero JM, Stothers RB. 2010. Witnessing the impact of the 1783–1784 Laki eruption in the Southern Hemisphere. Climatic Change, 99: 535–546. https://doi.org/DOI 10.1007/s10584-009-9676-1.

Tyson PD, Tyson PD, Preston-Whyte RA. 2000. The Weather and Climate of Southern Africa. Oxford University Press.

Vincent L, Pierre G, Michel S, Robert N, Masson-Delmotte V. 2007. Tree-rings and the climate of New Caledonia (SW Pacific). Palaeogeography, Palaeoclimatology, Palaeoecology, 253(3–4): 477–489. https://doi.org/10.1016/j.palaeo.2007.06.019.

Visioni D, Pitari G, Tuccella P, Curci G. 2018. Sulfur deposition changes under sulfate geoengineering conditions: quasi-biennial oscillation effects on the transport and lifetime of stratospheric aerosols. Atmospheric Chemistry and Physics, 18(4): 2787–2808. https://doi.org/10.5194/acp-18-2787-2018.

Wexler H. 1951. On the Effects of Volcanic Dust on Insolation and Weather (I). Bulletin of the American Meteorological Society, 32(1): 10–15. https://doi.org/10.1175/1520-0477-32.1.10.

Wilmes SB, Raible CC, Stocker TF. 2012. Climate variability of the mid- and high-latitudes of the Southern Hemisphere in ensemble simulations from 1500 to 2000 AD. Climate of the Past, 8(1): 373–390. https://doi.org/10.5194/cp-8-373-2012.

Yang J, Xiao C. 2017. The evolution and volcanic forcing of the southern annular mode during the past 300 years. International Journal of Climatology, 38(4): 1706–1717. https://doi.org/10.1002/joc.5290.

Zambri B, LeGrande AN, Robock A, Slawinska J. 2017. Northern Hemisphere winter warming and summer monsoon reduction after volcanic eruptions over the last millennium. Journal of Geophysical Research: Atmospheres, 122(15): 7971–7989. https://doi.org/10.1002/2017JD026728.

Zambri B, Robock A. 2016. Winter warming and summer monsoon reduction after volcanic eruptions in Coupled Model Intercomparison Project 5 (CMIP5) simulations. Geophysical Research Letters, 43(20): 10,920-10,928. https://doi.org/10.1002/2016GL070460.

Zanchettin D, Bothe O, Timmreck C, Bader J, Beitsch A, Graf H-F, Notz D, Jungclaus JH. 2014. Inter-hemispheric asymmetry in the sea-ice response to volcanic forcing simulated by MPI-ESM (COSMOS-Mill). Earth System Dynamics, 5(1): 223–242. https://doi.org/10.5194/esd-5-223-2014.

Zanchettin D, Timmreck C, Toohey M, Jungclaus JH, Bittner M, Lorenz SJ, Rubino A. 2019. Clarifying the relative role of forcing uncertainties and initial-condition unknowns in spreading the climate response to volcanic eruptions. Geophysical Research Letters, 46(3): 1602–1611. https://doi.org/10.1029/2018GL081018.

Zhang D, Blender R, Fraedrich K. 2013. Volcanoes and ENSO in millennium simulations: global impacts and regional reconstructions in East Asia. Theoretical and Applied Climatology, 111(3–4): 437–454. https://doi.org/10.1007/s00704-012-0670-6.

Zuo M, Man W, Zhou T, Guo Z. 2018. Different impacts of Northern, Tropical, and Southern Volcanic Eruptions on the Tropical Pacific SST in the Last Millennium. Journal of Climate, 31(17): 6729–6744. https://doi.org/10.1175/JCLI-D-17-0571.1.

Chapter Five: Australian Sub-Regional Temperature Responses to Volcanic Forcing: A Critical Analysis using CMIP5 Models

(Intending to submit to International Journal of Climatology)

Abstract

It is now well established that global to local climate is impacted by volcanic forcing associated with major eruptions. Much attention has been given to the way in which climate is affected by such eruptions, particularly for the Northern Hemisphere, and to a considerably lesser extent for the Southern Hemisphere. Research knowledge gaps remain on such forcing impacts at finer sub-regional spatial scales. To this end, temperature responses are examined across eight sub-regions of Australia following four major volcanic eruptions (i.e. Krakatau, 1883; Santa Maria, 1902; Agung, 1963; Pinatubo, 1991) as simulated by CMIP5 models. Such responses are then compared with station and reanalysis datasets. Model outputs indicate strongest temperature responses over more northerly regions than southerly regions of Australia, with weakest responses over Tasmania. Eastern regions of Australia seem to have strongest seasonal cooling during austral autumn, while that for north-western coastal regions is during austral winter. In contrast, central regions of Australia cool most substantially during austral summer and/or winter, depending on the eruption. Despite such variability, initial temperature responses occur during the warmer austral months (September to February). It is found that uncertainties exist in the reliability of the CMIP5 data. For instance, temperature responses from later eruptions (Agung and Pinatubo) seem to be in stronger agreement with reanalysis data than earlier eruptions (Krakatau and Santa Maria), and while most seasonal temperature responses are stronger than those provided through reanalysis data, they are often weaker in austral spring.

1. Introduction

Climate change is a product of multiple forcing factors, including both internal circulation (e.g. the El Niño Southern Oscillation) and external forcing mechanisms (anthropogenic or natural) (Lyu *et al*., 2015; Dieng *et al*., 2017). Volcanic forcing has had significant impact on earth's climate through the course of history, albeit usually with short-term impact lasting 1-3 years after an eruption (Robock, 2000; Rao *et al.*, 2017). However, much longer-lasting impacts are likely, following Ultra-Plinian eruptions such as Toba (*ca*. 74000 years ago) when cooling lasted for centuries (Gathorne-Hardy and Harcourt-Smith, 2003). Alternatively, several major volcanic eruptions in short succession, as was the case between 1667 and 1694 (such as Long Island, Mt Usu, Mt Tarumae), likely contributed to the coldest period of the Little Ice Age (Crowley *et al.*, 2008). The dynamical and mechanistic role of volcanic forcing through its upper atmospheric chemical loading, radiative forcing and multi-faceted global to regional scale impacts on circulation systems has been detailed in numerous prominent papers (e.g. Robock, 2000; Timmreck, 2018), and is thus not repeated here.

Temperatures associated with volcanic forcing have been said to cool by as much as 15°C in high latitudes and by 3-5°C globally following the massive Toba eruption (73 -74K yrs BP; Gathorne-Hardy and Harcourt-Smith, 2003). Other large negative temperature departures have been proposed following major volcanic eruptions during the last 200 years, such as those for the 1815 Tambora eruption (-1.00°C; Kandlbauer *et al*., 2013), El Chichón event (-0.24°C; Wigley, 2000; Wigley *et al.*, 2005) and Pinatubo eruption (-0.61°C; Wigley, 2000; Wigley *et al.*, 2005). However, the response to volcanic forcing is not globally or even hemispherically uniform (Jones *et al.*, 2003; Cook *et al.*, 2012). The Northern Hemisphere (NH) typically experiences stronger cooling than the Southern Hemisphere (SH) (Man *et al.*, 2014; Neukom *et al.*, 2014; Monerie *et al.*, 2017; Harvey *et al*., 2020). For instance, mean cooling following eruptions during the period 2008-2012 is estimated at -0.035°C for the NH, but only half that (-0.016°C) for the SH (Haywood *et al.*, 2014). This is owing to the SH having a smaller landmass, much of which is located at relatively low latitudes, compared to that of the NH. Consequently, the SH has its temperatures regulated by large expanses of oceans (Raible *et al.*, 2016). These oceans also regulate the jet streams and general atmospheric circulation, resulting in additional climatic feedbacks (Robock *et al.*, 2007), many of which are still not fully understood in the context of their association with volcanic forcing.

Although few studies have quantified volcanic forcing effects on the climate of Australia, several palaeo-climate studies have identified notable (and sometimes abrupt) climatic (temperature, snowfall, precipitation) anomalies following major historical eruptions over the region. In Kosciuszko National Park (Australia), speleothems have been used to reconstruct temperature and snow cover over the period 188BCE to 2012CE (McGowan *et al.*, 2018). Findings show sudden decreases in temperature and increased snowfall following the major eruptions of Calbuco, Melimoyu and Taupo (~200-260 CE), Dakataua and Mt Taranaki (800-820 CE), Paektu (945-984 CE), Minchinmávida (1541-1550 CE), and Tambora (1815 CE) (McGowan *et al.*, 2018). In contrast, however, tree ring records from multiple tree species (*Lagarostrobos franklinii, Athrotaxis selaginoides, Athrotaxis cupressoides* and *Phyllocladus aspleniifolius)* in Tasmania show no clear connection to volcanic forcing between 900 AD and 2009 AD (Cook *et al.*, 1992; Allen *et al.*, 2018). Using 39 historical sources of instrumental records covering the period 1788-1859, Ashcroft *et al.* (2014) identified two prominent cool periods centred on 1836 and 1847-1849, which, as highlighted by the authors, coincidently follow major volcanic eruptions (Nicaraguan in 1835 and Amargura in 1846 respectively). Despite several Australasian climate reconstructions covering the last few centuries, such as rainfall reconstructions from coral in the Great Barrier Reef (e.g. Lough, 2007), temperature reconstructions from tree rings in Tasmania and New Zealand (e.g. Cook *et al.*, 2006), and documentary (e.g. ship log books) based weather reconstructions (e.g. Chappell and Lorrey, 2014), few have investigated the potential impacts of past major volcanic eruptions on regional weather and climates of the past.

Given the general absence of quantitative investigations and information concerning volcanic forcing impacts on sub-regional climates of Australia, the aim is to identify and compare Australian sub-regional temperature responses to four relatively recent and major volcanic eruptions (i.e. Krakatau, 1883; Santa Maria, 1902; Agung, 1963; Pinatubo, 1991) using historical simulations of the Coupled Model Intercomparison Project, Phase 5 (CMIP5). The model outputs are then compared (verified) against 20th Century Reanalysis V2 (20CRv2) data, some instrumental station data, and documentary records (newspapers) where these are available for the respective sub-regions.

2. Methodology

2.1 Study region

Australia lies between 10° and 44°S latitude, and 112° and 154°E longitude. It is bounded by the Indian, South Pacific and Southern Oceans. The strongest drivers of temperature variability over the continent include the El Niño Southern Oscillation (ENSO) (Trenberth, 1997; Power *et al.*, 1999), the Southern Annular Mode (SAM), atmospheric blocking, and the subtropical ridge (Fierro and Leslie, 2014; Crimp *et al.*, 2018). Southwestern and southern regions of Australia are impacted by mid-latitude cyclones (westerly waves; cold fronts), affecting southern parts of Australia year round. El Niño conditions can cause a reduction in sea surface temperatures (SSTs) over the lower west coast and warmer summer SSTs along the eastern and northern coasts of Australia, as well as reduced rainfall and tropical cyclone activity. La Niña conditions can cause increased SSTs along the west coast, bringing with it increased tropical cyclone activity. The SAM, which dominates SH circulation as a whole, plays a significant role in affecting Australian climate as the position of the westerlies changes (Rogers and van Loon, 1982; Marshall, 2003; Meneghini *et al.*, 2007). During a positive SAM, westerlies intensify and contract towards the poles, allowing easterly winds from the Tasman Sea to move over southern Australia (Hendon *et al.*, 2007; Crimp *et al.*, 2018). During a negative SAM, westerly winds tend to shift equatorward, and thus more strongly impact Australian weather and climate, resulting in stronger storms and frontal systems reaching further inland (Crimp *et al.*, 2018). A positive SAM causes significant cooling and wet conditions over most of Australia (Gillett *et al.*, 2006). Atmospheric blocking mostly occurs in the mid-latitudes over the Tasman Sea and the southwestern Pacific, and although it influences climate throughout the year, it is most dominant during austral winter (Coughlan, 1983; Pook and Gibson, 1999), however, the location and intensity of the blocking changes over time (Crimp *et al.*, 2018). Depending on the location of such blocking effects, it can force the movement of cold polar air towards either south-eastern Australia, or Western Australia, with consequential cooling effects (Fierro and Leslie, 2014; Crimp *et al.*, 2018). The subtropical ridge over eastern Australia can weaken such frontal systems, resulting in positive temperature anomalies, particularly during summer (Drosdowsky, 2005; Grose *et al.*, 2015). In winter, the high pressure system moves further north, bringing cold and dry air behind such systems (Fierro and Leslie, 2014; Crimp *et al.*, 2018).

Given the relatively strongly contrasting sub-regional climates and climate influencing mechanisms over Australia, the region was divided into sub-regions according to the popular Köppen-Geiger (Köppen, 1936; Zhou *et al.*, 2010) climate classifications (Figure 1). Due to the scope of this study, the entire continent of Australia is not covered, but instead eight sub-regions that have similar latitudes to sub-regions in southern Africa were chosen, which permits future inter-continental comparisons. This includes four temperate sub-regions; namely the South Western coast (SWE), Victoria, Tasmania, and the Eastern Coast (EAC). There are also four arid sub-regions which include the Central Western Coast (CWC), Central Eastern Coast (CEC), North Western Coast (NWC) and Eastern Subcontinent (EAS). The sub-regions, their locations and climate classifications are presented in Table 1.

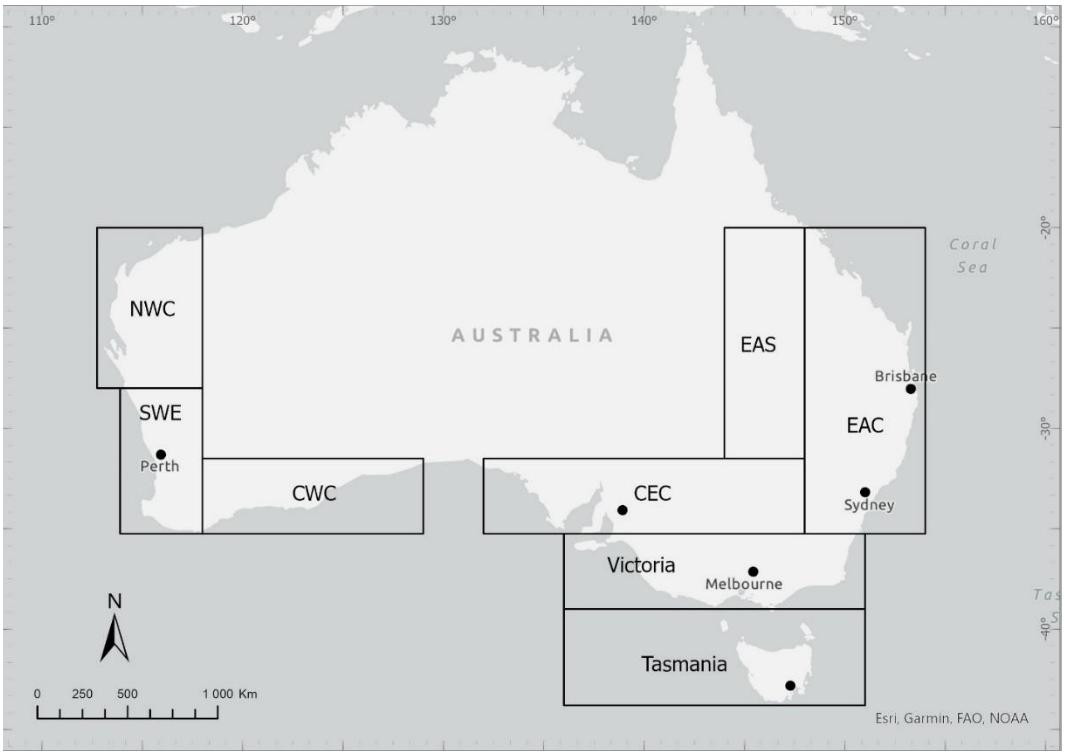

Figure 1. The eight Australian sub-regions used in this study. SWE = South Western coast; CWC = Central Western Coast ; CEC = Central Eastern Coast; Vic = Victoria; Tas = Tasmania; NWC = North Western Coast; EAS = Eastern Subcontinent; EAC = Eastern Coast. The circles represent the stations.

Table 1. Climatic sub-regions of Australia characterized according to their location and Köppen-Geiger Classification.

Sub-Regions	Abbreviation	Latitude	Longitude	Köppen-Geiger Classification (Majority)	Classification Meaning
South Western Coast	SWE	-29 to -35	112 to 118	Csa + Csb	Temperate, dry summer, hot summer
Central Western Coast	CWC	-31 to -35	118 to 130	BSk	Arid, steppe, cold
Central Eastern Coast	CEC	-31 to -35	132 to 148	BSk	Arid, steppe, cold
Victoria	Vic	-35 to -39	136 to 151	Cfb	Temperate, without dry season, warm summer
Tasmania	Tas	-39 to -43	136 to 151	Cfb	Temperate, without dry season, warm summer
North Western Coast	NWC	-20 to -29	112 to 118	BWh	Arid, desert, hot
Eastern Subcontinent	EAS	-20 to -31	144 to 148	BSh	Arid, Steppe, hot
Eastern Coast	EAC	-20 to -35	148 to 154	Cfa	Temperate, without dry season, hot summer

2.2 Models and data

Near-surface (2m) temperatures from CMIP5 historical experiments for the period 1850-2005 are analysed. Models were selected based on their ability to simulate a suitable lower-stratosphere response to volcanic forcing (see Barnes *et al.*, 2016 for more information). Eleven climate models were selected (Table 2), and, where available, used the first three realizations of each. The volcanic forcing dataset was not prescribed for the CMIP5 experiments, hence models have used datasets from either Sato *et al.* (1993) or Ammann *et al*. (2007). With the GISS-E2_R model, both the first (prescribed volcanic forcing) and third (internally calculated volcanic forcing) physics versions were incorporated, which equate to a total of 31 simulations used.

The 31 simulations were remapped to a 2° by 2° latitude/longitude grid, after which an ensemble was created. Annual, seasonal and monthly temperature anomalies were calculated using a 20-year running mean. Area averages of the anomalies from the sub-regions of Australia are used to analyse and compare the temperature responses. The statistical significance of anomalies was then tested using a bootstrap approach (Efron, 1979). The time-series of anomalies was resampled 5000 times, and significance calculated at the 5th and 95th percentiles of the bootstrapped dataset (Haurwitz and Brier, 1981; Rao *et al.*, 2017).

Table 2. The climate models and datasets used to determine volcanic forcing (after Driscoll *et al*., 2012; Taylor *et al*., 2012; Harvey and Grab, submitted).

Model Name	Institution	Volcanic Forcing
CanESM2	Canadian Centre for Climate Modelling and Analysis	Sato *et al*. (1993)
CCSM4	National Center for Atmospheric Research	Ammann *et al*. (2007)
CNRM-CM5	Centre National de Recherches Météorologiques & Centre Européen de Recherche et de Formation Avancée en Calcul Scientifique	Ammann *et al*. (2007)
CSIRO-Mk3-6-0	Commonwealth Scientific and Industrial Research Organisation	Sato *et al*. (1993)
GISS-E2-H	NASA Goddard Institute for Space Studies	Sato *et al*. (1993)
GISS-E2-R (P1)	NASA Goddard Institute for Space Studies	Sato *et al*. (1993)
GISS-E2-R (P3)	NASA Goddard Institute for Space Studies	Sato *et al*. (1993)
MIROC-ESM	Japan Agency for Marine-Earth Science and Technology, Atmosphere and Ocean Research Institute (The University of Tokyo), and National Institute for Environmental Studies	Sato *et al*. (1993)
MIROC-ESM-CHEM		Sato *et al*. (1993)
MRI-CGCM3	Meteorological Research Institute	Interactive
NorESM1-M	Norwegian Climate Centre	Ammann *et al*. (2007)

Four major volcanic eruptions are focused on in this study (Table 3). Each eruption had a VEI ≥ 4, occurred in the tropics, and are known to have impacted SH temperatures (Mass and Portman, 1989; Gleckler *et al.*, 2006; Zanchettin *et al.*, 2012; Khodri *et al.*, 2017; Ménégoz *et al.*, 2018; Harvey *et al.*, 2020). The first major eruption, Krakatau, occurred in August 1883 and emitted 22 Tg of SO_2 into the stratosphere. It occurred in Indonesia at 6°S and was classified as a VEI 6 event. The second eruption, Santa Maria (VEI 6), emitted 3.8 Tg of SO_2 when it erupted during October 1902 in Guatemala at 15°N. Mount Agung, also in Indonesia at 8°S, erupted in March 1963, emitting 7.5 Tg of SO_2. Of all eruptions investigated, the Agung event had the lowest VEI (4). The final eruption, Mount Pinatubo (15°N in the Philippines), erupted in June 1991, emitted 18 Tg of SO_2 and ranked with a VEI of 6.

Table 3. Summary information for the four major volcanic eruptions examined.

Eruption	Date	Latitude	VEI	DVI	Total Emission (Tg of SO_2)
Krakatau	27 August 1883	6S	6	1000	22
Santa Maria	24 October 1902	15N	6	600	3.8
Mt Agung	17 March 1963	8S	4	800	7.5
Mt Pinatubo	15 June 1991	15N	6	1000	18

CMIP5 outputs are thought to exaggerate the climatic response to volcanic forcing (Driscoll *et al.*, 2012). To test the general validity of CMIP5 modelled temperature outputs, these are compared with 20th Century Reanalysis V2 (20CRv2) data from NOAA/OAR/ESRL, some station data, and several quotes from documentary sources. The 20CRv2 data were processed in the same manner as CMIP5 data through the calculation of annual, seasonal and monthly anomalies (and their significance). Although station data provide only location specific temperature anomalies, as opposed to averaged conditions across an entire sub-region, these likely provide the most reliable reference to *true* near-surface temperature conditions/responses, as opposed to CMIP5 and reanalysis data outputs. Station data were obtained from the National Oceanic and Atmospheric Administration's (NOAA) National Centers for Environmental Information (NCEI). NCEI processes, validates and runs numerous quality control algorithms on the data they provide. Global summary of the month (GSOM) datasets of average monthly temperatures were obtained for six stations located within the investigated Australian sub-regions. Given the scarcity of station data, and general absence of recording stations during the 19th century, only two stations had reliable and complete temperature data during the time Krakatau erupted in 1883; namely Hobart (station location: Ellerslie Road; Tasmania) and Melbourne (station location:

Regional Office; Victoria). From the time of the Santa Maria eruption, other stations had started recording temperature; these include Perth (station location: Regional Office; SWE), Adelaide (station location: West Terrace; CEC), Brisbane (station location: Regional Office; EAC (central)) and Sydney (station location: Observatory Hill, EAC (south)). Stations at Brisbane and Adelaide have missing data around the Pinatubo eruption, and Perth station unfortunately has a data gap from 1993. Annual and seasonal anomalies were calculated with respect to a 20-year running climatology.

3. Results

3.1 Krakatau (1883)

Of the four eruptions investigated here, the Krakatau eruption emitted the largest amount of SO_2 into the lower stratosphere. Unsurprisingly, the average annual cooling following this eruption is strongest for most Australian sub-regions (Figure 2; regional average = -0.26°C for the first three post-eruption years [y1, y2, y3]), apart from Tasmania, where the strongest negative temperature departures follow the Pinatubo eruption (-0.12°C). For each year (y1-y3), mean annual temperatures are strongest over either EAS or CEC (y1= EAS, -0.44°C; y2= CEC, -0.29°C; y3= EAS, -0.36°C) and weakest over Tasmania (3-year average = -0.10°C). In y1, weak (between -0.25°C and -0.30°C) responses occur over SWE, CWC, CEC, and Victoria (southern parts of Australia), while strong (between -0.36°C and -0.44°C) responses occur over NWC, EAS and EAC (northern parts of Australia). Over CWC, NWC, EAS and EAC, the strongest negative annual anomaly occurs in y1, whereas over SWE, Victoria and Tasmania the strongest annual anomaly occurs in y2, and over CEC the strongest anomaly occurs in y3. The weakest annual responses occur in y3 for each region, except CEC, EAS and EAC where the weakest responses occur in y2. Negative temperature anomalies were significant (see Table 4 for values) in y1 after the eruption over all regions except Tasmania. In y2, anomalies were significantly below normal over most regions, except over EAS and EAC. In y3, negative anomalies are significantly below normal over most regions, except SWE, Tasmania and NWC. During June 1886, Tarawera (VEI 5) erupted in neighbouring New Zealand. Coincidently, the results show significantly below normal mean annual temperatures during 1887 over SWE (-0.22°C) and NWC (-0.34°C). It is possible that the Tarawera eruption extended the period of negative temperature anomalies associated with the Krakatau eruption (Harvey *et al.*, 2020), implying a potential volcanic 'double-forcing' effect (see also Toohey *et al.*, 2016).

Seasonal temperature responses are now considered for each sub-region. In y1, DJF (austral summer), MAM (austral autumn) and JJA (austral winter) seasonal anomalies are significantly below normal over SWE, CWC, CEC, Victoria, EAS and EAC (see Table 5 for values), but in Tasmania only MAM is significant. For NWC, the months of DJF, JJA and SON (austral spring) are significantly below normal. In y2, SWE has three seasonal averages that are significantly below normal (MAM, JJA, SON). CWC, Victoria and Tasmania have two significantly negative anomalies below normal (CWC: JJA and SON; Victoria DJF, JJA; Tasmania: DJF and MAM). Only one anomaly is significantly below normal over CEC (JJA) and NWC (SON), while no significant anomalies are modelled for EAS or EAC in y2 (Table 5). However, more seasons are significantly below normal in y3, with all four seasons significantly below normal over EAC and CEC, three seasons below normal over EAS (not SON), two seasons below normal over Victoria (MAM and SON), and one season below normal over SWE, CWC (both SON). The exceptions are Tasmania and NWC; neither sub-region recorded significant negative temperature anomalies in y3. The strongest average seasonal response over all regions occurs in MAM in y1 (-0.42°C), DJF in y2 (-0.25°C) and in SON in y3 (-0.28°C). Weakest overall responses occur during SON in y1 (-0.17°C) and in JJA in y2 (-0.19°C) and y3 (-0.20°C). However, the MAM seasonal response in y1 are only strongest over SWE, Victoria, Tasmania, EAS and EAC (Table 5), while NWC, CEC and CWC record strongest responses during DJF (Table 5).

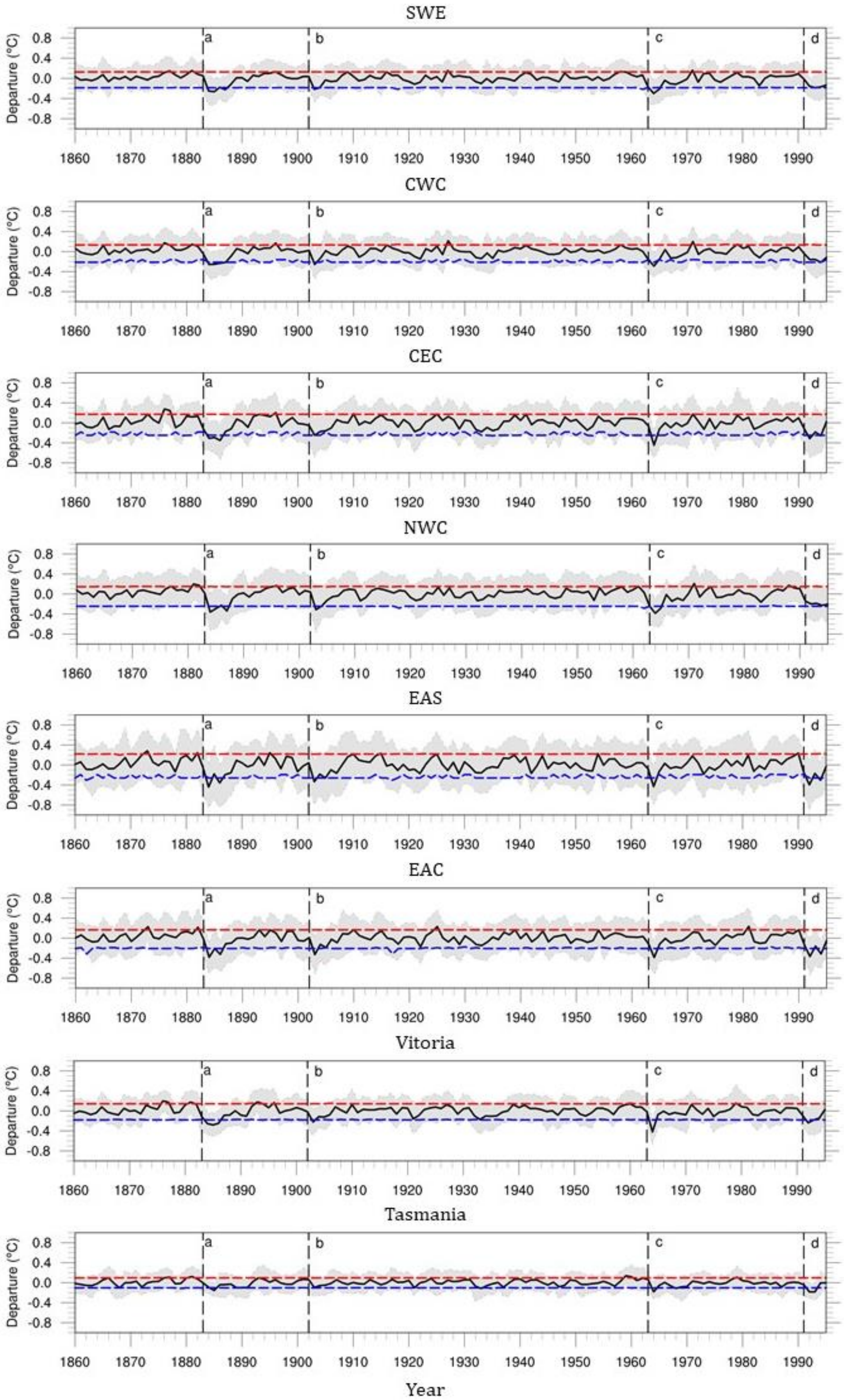

Figure 2. CMIP5-simulated annual temperature anomalies for the eight Australian sub-regions.

Table 4. Mean annual temperature anomalies for the eight sub-regions of Australia following the four eruptions for CMIP5, 20CRv2 and station data. Grey shading = year of eruption; blue shading = significant anomalies.

Eruption	Data	Year	SWE	CWC	CEC	Victoria	Tasmania	NWC	EAS	EAC
Krakatau	CMIP5	1883	0.05	-0.05	-0.12	-0.12	0.00	0.02	-0.05	-0.02
		1884	-0.25	-0.26	-0.31	-0.26	-0.09	-0.36	-0.44	-0.38
		1885	-0.26	-0.25	-0.29	-0.28	-0.16	-0.29	-0.18	-0.21
		1886	-0.18	-0.23	-0.35	-0.25	-0.04	-0.23	-0.36	-0.32
	20CRv2	1883	-0.13	-0.11	0.14	0.20	0.31	-0.07	0.05	-0.12
		1884	-0.28	-0.01	0.32	0.15	-0.01	-0.40	0.36	0.49
		1885	-0.05	0.14	0.77	0.47	0.03	0.03	0.57	0.49
		1886	-0.18	-0.18	-0.28	-0.17	0.21	-0.11	-0.21	-0.03
	Station Data					**Melbourne (Victoria)**	**Hobart (Tasmania)**			
		1883				0.43	0.57			
		1884				-0.22	-0.28			
		1885				-0.29	-0.42			
		1886				-0.45	-0.47			
			SWE	**CWC**	**CEC**	**Victoria**	**Tasmania**	**NWC**	**EAS**	**EAC**
Santa Maria	CMIP5	1902	0.04	0.02	-0.05	-0.02	0.06	0.04	0.04	0.01
		1903	-0.22	-0.26	-0.25	-0.22	-0.10	-0.31	-0.33	-0.33
		1904	-0.18	-0.14	-0.17	-0.12	-0.06	-0.24	-0.18	-0.13
		1905	-0.03	0.02	-0.16	-0.12	-0.05	-0.13	-0.26	-0.19
	20CRv2	1902	0.45	0.61	0.59	0.44	-0.07	0.09	0.78	0.79
		1903	-0.19	-0.10	0.06	0.24	0.00	-0.44	0.12	0.19
		1904	0.21	0.22	0.26	0.26	0.00	-0.32	-0.15	-0.12
		1905	-0.19	-0.16	-0.43	-0.45	-0.43	-0.58	-0.34	-0.43
	Station Data		**Perth (SWE)**		**Adelaide (CEC)**	**Melbourne (Victoria)**	**Hobart (Tasmania)**		**Sydney (EAC)**	**Brisbane (EAC)**
		1902	-0.37		0.69	-0.22	-0.55		0.46	0.60
		1903	-0.22		-0.02	-0.09	0.05		-2.72	0.04
		1904	0.14		0.02	-0.27	-0.29		0.36	-0.14
		1905	-0.26		-0.72	-0.50	-0.47		-2.90	-0.28
			SWE	**CWC**	**CEC**	**Victoria**	**Tasmania**	**NWC**	**EAS**	**EAC**
Agung	CMIP5	1963	-0.17	-0.16	-0.06	-0.02	0.07	-0.24	-0.08	-0.12
		1964	-0.30	-0.29	-0.45	-0.42	-0.18	-0.38	-0.43	-0.39
		1965	-0.22	-0.15	-0.12	-0.07	-0.05	-0.28	-0.13	-0.12
		1966	-0.04	0.04	0.00	-0.01	0.00	-0.01	0.03	-0.01
	20CRv2	1963	0.39	0.20	0.18	-0.03	-0.33	0.32	-0.01	-0.05
		1964	-0.72	-0.69	-0.53	-0.71	-0.63	-0.56	0.48	0.34
		1965	-0.21	0.25	0.56	0.00	-0.50	-0.27	0.80	0.57
		1966	-0.54	-0.31	-0.39	-0.34	-0.28	-0.84	-0.27	-0.32
	Station Data		**Perth (SWE)**		**Adelaide (CEC)**	**Melbourne (Victoria)**	**Hobart (Tasmania)**		**Sydney (EAC)**	**Brisbane (EAC)**
		1963	0.58		0.04	0.07	-0.33		-0.11	-0.12
		1964	-0.49		-0.65	-0.46	-0.53		0.18	0.21
		1965	0.08		0.35	-0.04	-0.25		-0.02	0.22
		1966	-0.63		-0.15	-0.26	-0.18		-0.42	-0.09
			SWE	**CWC**	**CEC**	**Victoria**	**Tasmania**	**NWC**	**EAS**	**EAC**
Pinatubo	CMIP5	1991	-0.01	-0.04	-0.12	-0.09	-0.04	-0.14	-0.15	-0.14
		1992	-0.15	-0.16	-0.31	-0.24	-0.18	-0.20	-0.40	-0.37
		1993	-0.19	-0.16	-0.18	-0.18	-0.18	-0.19	-0.17	-0.16
		1994	-0.17	-0.21	-0.26	-0.14	-0.01	-0.23	-0.31	-0.32
	20CRv2	1991	-0.06	0.25	-0.11	-0.32	-0.30	-0.02	-0.40	-0.11
		1992	-0.75	-0.65	-1.32	-1.08	-0.35	-1.00	-0.76	-0.93
		1993	-0.68	-0.41	-0.29	-0.27	0.03	-0.74	0.05	0.05
		1994	1.44	1.42	0.64	0.66	0.46	1.82	1.04	1.16
	Station Data		**Perth (SWE)**			**Melbourne (Victoria)**	**Hobart (Tasmania)**		**Sydney (EAC)**	
		1991	-0.04			-0.09	-0.09		0.54	
		1992	4.36			-0.45	-0.68		-0.53	
		1993				0.13	0.46		0.11	
		1994				-0.28	-0.03		0.01	

Table 5. Mean seasonal temperature departures following the Krakatau eruption, for CMIP5, 20CRv2 and station data. Grey shading = year of eruption; blue shading = significant anomalies.

			SWE				CWC				CEC				Victoria			
		Year	DJF	MAM	JJA	SON	DJF	MAM	JJA	SON	DJF	MAM	JJA	SON	DJF	MAM	JJA	SON
Krakatau	CMIP5	1883	0.03	0.07	0.10	0.05	0.05	-0.12	0.03	-0.08	0.06	-0.22	0.02	-0.25	-0.02	-0.22	0.07	-0.22
		1884	-0.29	-0.30	-0.18	-0.19	-0.38	-0.35	-0.25	-0.15	-0.56	-0.55	-0.32	0.00	-0.43	-0.49	-0.27	-0.03
		1885	-0.22	-0.26	-0.24	-0.34	-0.13	-0.16	-0.30	-0.33	-0.28	-0.12	-0.26	-0.26	-0.29	-0.22	-0.21	-0.15
		1886	-0.08	-0.13	-0.13	-0.29	-0.20	-0.21	-0.19	-0.30	-0.40	-0.41	-0.31	-0.40	-0.28	-0.25	-0.19	-0.32
	20CRv2	1883	0.08	0.19	0.15	-0.43	-0.30	0.49	0.23	-0.98	0.05	0.63	0.71	-0.61	0.22	0.62	0.44	-0.32
		1884	-0.58	0.37	0.14	-0.42	0.08	0.37	0.53	-0.05	-0.54	0.38	1.05	0.76	-0.83	0.23	1.01	0.33
		1885	-1.19	-0.02	0.52	-0.70	-1.03	-0.08	0.55	-0.56	0.20	-0.07	0.91	0.18	0.27	-0.02	0.55	0.01
		1886	0.23	0.32	0.44	-1.20	0.65	0.11	0.67	-0.91	0.30	-0.32	1.18	-0.97	0.15	-0.51	1.05	-0.47
	Station Data														Melbourne - Victoria			
		Year													DJF	MAM	JJA	SON
		1883													0.43	0.34	0.65	0.30
		1884													-1.19	0.02	0.36	-0.08
		1885													-0.20	-0.63	-0.49	0.16
		1886													-0.62	-0.91	-0.37	0.09
	3-season Averages	CMIP5	-0.19	-0.23	-0.18	-0.27	-0.24	-0.24	-0.25	-0.26	-0.41	-0.36	-0.30	-0.22	-0.33	-0.32	-0.22	-0.17
		20CRv2	-0.51	0.23	0.37	-0.77	-0.10	0.13	0.58	-0.51	-0.02	0.00	1.05	-0.01	-0.14	-0.10	0.87	-0.04
		Station													-0.67	-0.51	-0.17	0.06

			Tasmania				NWC				EAS				EAC			
			DJF	MAM	JJA	SON	DJF	MAM	JJA	SON	DJF	MAM	JJA	SON	DJF	MAM	JJA	SON
Krakatau	CMIP5	1883	0.08	-0.10	0.11	-0.06	0.31	0.02	0.08	-0.09	0.28	0.03	-0.08	-0.13	0.25	0.10	0.00	-0.16
		1884	-0.08	-0.26	-0.06	0.03	-0.52	-0.32	-0.30	-0.40	-0.41	-0.57	-0.47	-0.31	-0.43	-0.52	-0.35	-0.31
		1885	-0.27	-0.24	-0.12	0.00	-0.19	-0.26	-0.22	-0.48	-0.34	-0.17	-0.06	-0.17	-0.25	-0.28	-0.10	-0.15
		1886	0.08	-0.03	-0.08	-0.06	-0.14	-0.23	-0.18	-0.27	-0.48	-0.43	-0.30	-0.32	-0.44	-0.38	-0.25	-0.32
	20CRv2	1883	0.37	0.39	0.39	0.13	0.63	0.07	0.49	-0.76	-0.02	0.21	0.88	-0.98	-0.31	-0.06	0.50	-1.00
		1884	-0.41	0.12	0.52	-0.32	-0.60	0.20	-0.08	-0.65	0.10	-0.38	1.11	0.55	0.70	-0.41	0.97	0.46
		1885	0.01	-0.11	0.09	-0.07	-0.73	-0.03	0.89	-1.11	0.69	0.43	1.07	-0.11	1.12	0.48	0.80	-0.20
		1886	0.24	-0.21	0.74	0.31	-0.30	0.30	0.39	-0.56	-0.20	-0.54	1.69	-1.00	0.10	-0.36	1.67	-1.03
	Station Data		Hobart - Tasmania															
		Year	DJF	MAM	JJA	SON												
		1883	0.26	0.99	1.25	-0.16												
		1884	-1.20	0.19	0.40	-0.44												
		1885	-0.09	-0.64	-0.55	-0.34												
		1886	-0.63	-0.77	-0.44	0.03												
	3-season Averages	CMIP5	-0.09	-0.18	-0.09	-0.01	-0.28	-0.27	-0.24	-0.38	-0.41	-0.39	-0.28	-0.27	-0.37	-0.39	-0.23	-0.26
		20CRv2	-0.05	-0.07	0.45	-0.02	-0.54	0.16	0.40	-0.77	0.20	-0.16	1.29	-0.19	0.64	-0.10	1.15	-0.26
		Station	-0.64	-0.41	-0.20	-0.25												

Most monthly temperature departures are below normal following the Krakatau eruption, (Figure 3; 90-93% of months from the time of the eruption to the end of y3 for all regions except Tasmania which = 78%). The percentage of months that were significantly below normal was between 48-63% for CEC, Victoria, NWC, EAS, EAC, but considerably lower over SWE (34%), CWC (39%), and much lower over

Tasmania (9.7%). The first significant negative monthly anomaly occurs during the warmer SH months; in November 1883 over CEC, Victoria, EAS and EAC and in December 1883 over NWC. CWC had its first significant negative monthly anomaly in January 1884, and SWE in February 1884. Interestingly, the first significant negative anomaly in Tasmania occurred a year later (January 1885). The strongest monthly responses are recorded for EAS (-0.72°C, May 1884), CEC (-0.67°C, January 1884) and NWC (-0.66°C, November 1885).

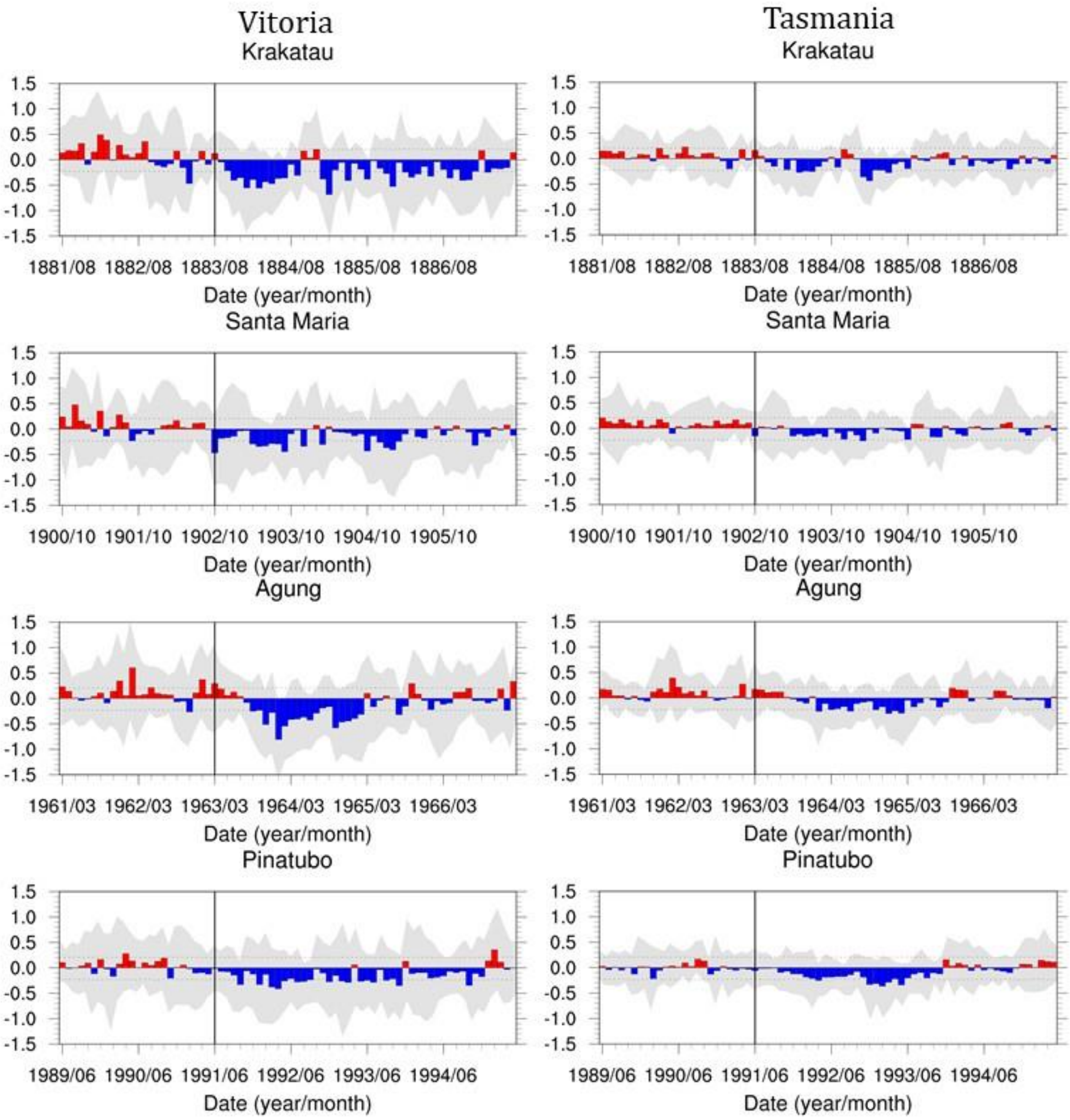

Figure 3. CMIP5-simulated monthly temperature anomalies for the eight Australian sub-regions.

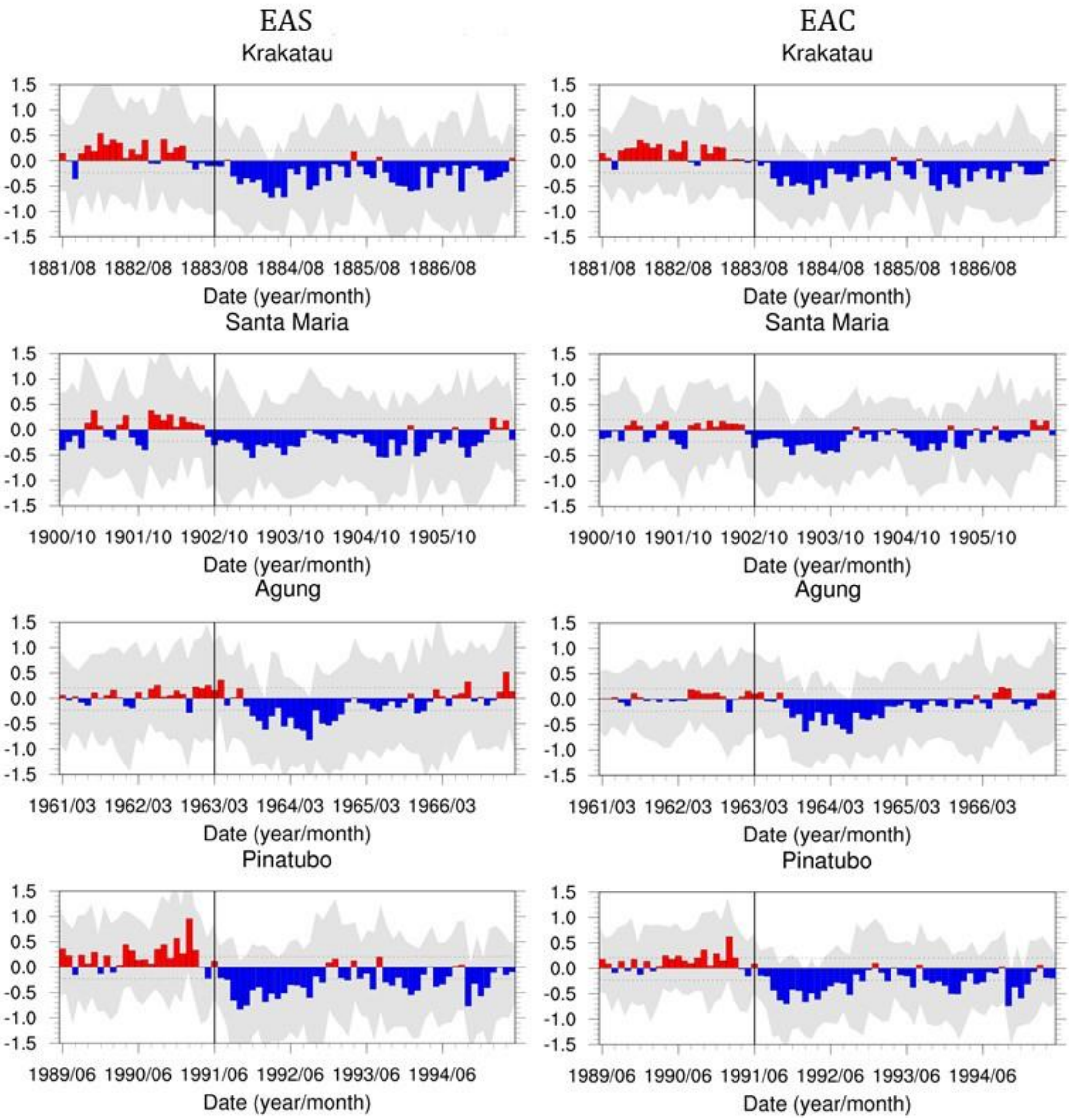

Figure 3 continued.

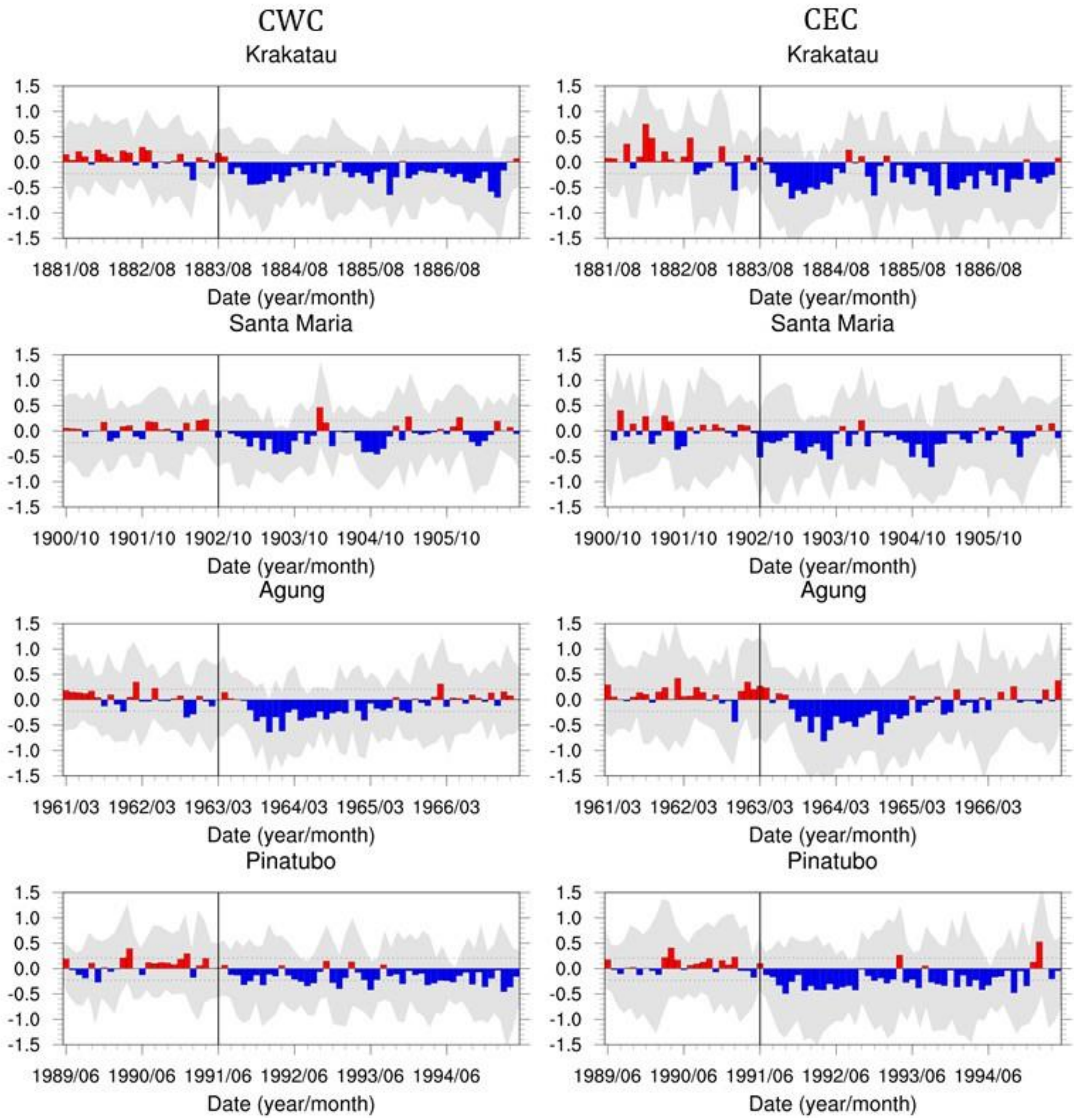

Figure 3 continued.

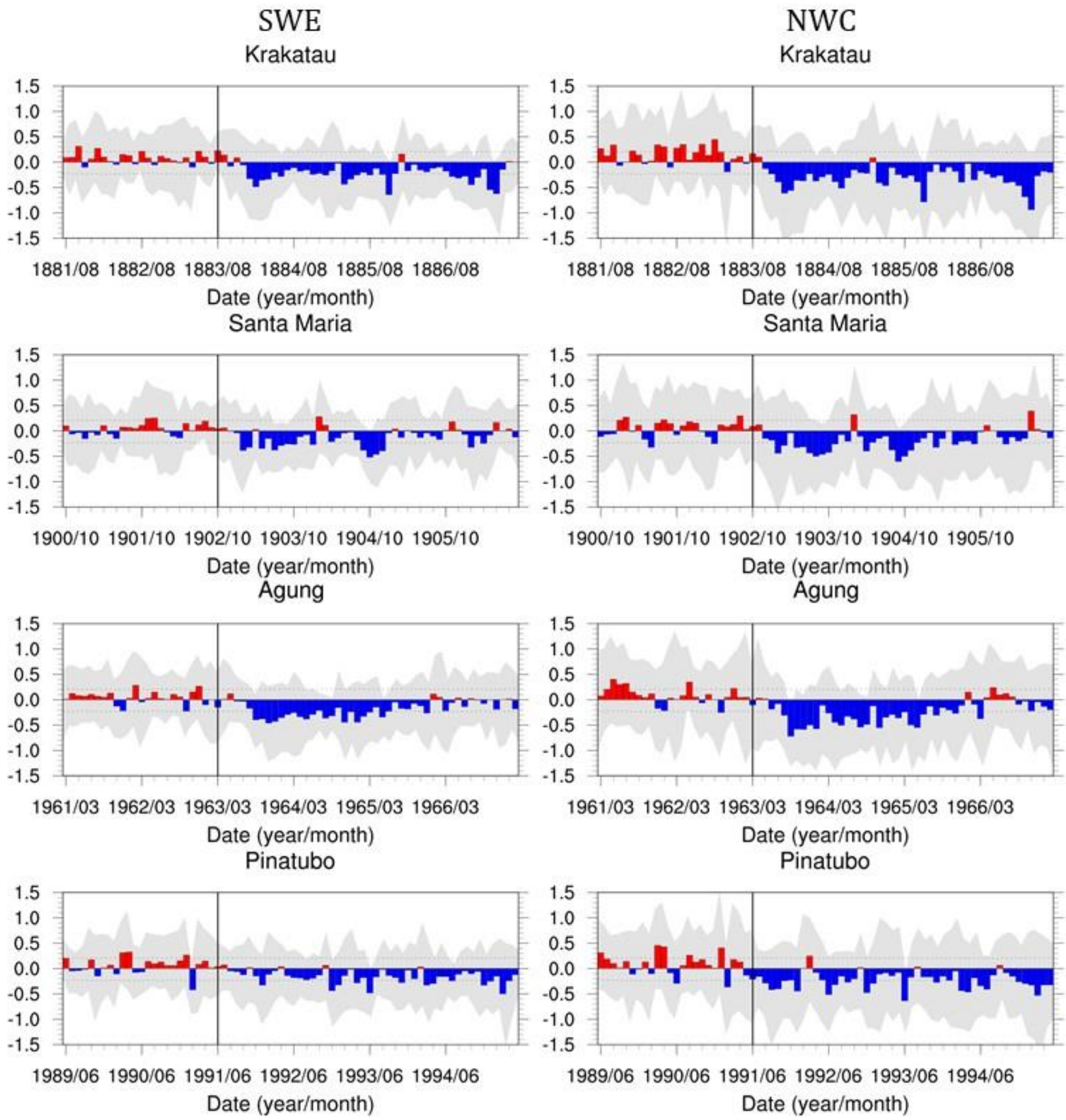

Figure 3 continued

Mean annual and seasonal temperature departures for the Hobart (in Tasmania) and Melbourne (in Victoria) stations are presented in Tables 4 and 5 respectively for years following Krakatau. For both stations, mean annual temperature departures are below normal for the three post-volcanic years, and in fact the strongest mean negative anomalies of all the eruptions investigated in this paper. Mean temperature departures are also stronger (3-year average: Hobart -0.39°C; Melbourne -0.32°C) than those modelled for the respective sub-regions from

CMIP5 (3-year average: Tasmania -0.10°C; Victoria -0.26°C. For both Hobart and Melbourne, strongest negative temperature departures are recorded in y3 (-0.47°C and -0.45°C respectively) and weakest in y1 (Hobart: -0.28°C, Melbourne: -0.22°C), which is in contradiction to the CMIP5 results (strongest: y2, weakest: y3). Strongest seasonal temperature departures in Hobart and Melbourne occur during DJF of y1 (-1.20°C and -1.19°C for both stations respectively) instead of during DJF of y2 over Tasmania and in MAM of y1 over Victoria, as provided by CMIP5 outputs (Table 5). As with the CMIP5 data, weakest responses occur during SON at both stations (3-year average: -0.25°C and -0.05°C for Hobart and Melbourne respectively; CMIP5 3-year average: Tasmania –0.01°C; Victoria -0.17°C). CMIP5 data indicate that in both regions, negative anomalies occur in each season for y1-y3, apart from SON (y1) and DJF (y3) over Tasmania. In contrast, both station records recorded above normal temperatures during MAM and JJA of y1, and during SON of y3. Melbourne experienced an additional positive anomaly during SON of y2 (Table 5).

Temperatures from the 20CRv2 reanalysis dataset are now analysed . While most of the CMIP5 annual departures were significantly below normal, none of the annual 20CRv2 anomalies are significant. For the CMIP5 ensemble, all annual anomalies were below normal in y1-y3, however, for 20CRv2, anomalies are only below normal (Table 4) in y1-y3 over SWE, in y1 and y3 over CWC and NWC, in y1 over Tasmania, and in y3 over CEC, Victoria, EAS and EAC. In fact, above normal (i.e. warm) anomalies (stronger than the negative anomalies) are measured for CEC (av= +0.54°C), EAC (av= +0.49°C), EAS (av= +0.47°C), Victoria (av= +0.31°C), and in y1-y2. Reanalysis anomalies are only fractionally cooler (by an average of 0.02°C) than CMIP5 anomalies in y1 and y2 over the SWE region and in y1 over the NWC region. Following the Krakatau eruption, reanalysis data show strongest cooling over the SWE (av= -0.17°C) and NWC (av= -0.16°C) regions. This is in disagreement with CMIP5 outputs, which model strongest cooling (for the three post-eruption years) over CEC (av= -0.32°C) and EAS (av= -0.33°C). However, it is in these regions and over EAC where strongest warming (av= CEC: +0.27°C, EAS:

+0.24°C, EAC: +0.32°C) is recorded in the reanalysis dataset. As with the CMIP5 data, the smallest variation (weakest response) occurs over Tasmania.

The CMIP5 ensemble shows half the seasonal departures from all regions being significantly below normal for y1-y3, however, only two of the seasonal departures using 20CRv2 are below normal after the Krakatau eruption (SWE y2: DJF -1.19°C; y3: SON -1.20°C). The general pattern for reanalysis anomalies following the Krakatau eruption is a usually positive anomaly in MAM and JJA, but negative in DJF and SON. Overall, strongest negative anomalies generally occur in SON (av= -0.32°C) in contrast to both CMIP5 and station data. Strongest positive anomalies generally occur in JJA (av= +0.77°C). Despite quantitative differences, the reanalysis data are in agreement with CMIP5 outputs for the depiction of strongest 3-year seasonal average temperature departures across most sub-regions (i.e. DJF: CEC, Victoria; MAM: Tasmania; SON: SWE, CWC, NWC; Table 5). The only exceptions are for EAS and EAC, where CMIP5 indicates strongest mean seasonal departures in DJF and MAM respectively, while the reanalysis data indicate maximum departures during SON for both these regions.

3.2 Santa Maria (1902)

Mean temperature responses following the Santa Maria eruption were ~0.10°C warmer than those following Krakatau (3-year average for all regions: -0.17°C). Three-year temperature anomalies were weakest after Santa Maria compared to the other three eruptions over SWE (-0.14°C), CWC (-0.13°C), Victoria (-0.15°C) and Tasmania (-0.07°C) (Figure 2). Annual departures are significantly below normal in y1 over SWE, CWC, Victoria, NWC, EAS, EAC (See Table 4 for values). No anomalies are significantly below normal in y2 and y3. The strongest annual response occurs during y1 over all regions and the weakest in y3 over most regions; the exceptions being Victoria, EAS and EAC (Table 4). As with the Krakatau eruption, the strongest regional response is observed over EAS in y1 and y3, but over NWC in y2 (Table 4), and is weakest over Tasmania (3-year annual average: -0.07°C). Strong responses are measured for more northerly regions (NWC, EAS and EAC: 3-year annual averages between –0.21°C and -0.23°C), while weaker responses are modelled for southern regions (29°S and southwards- SWE, CWC, CEC, Victoria and Tasmania) where 3-year annual averages are between -0.07°C and -0.19°C.

According to CMIP5 outputs, less significant seasonal anomalies follow the Santa Maria eruption than after Krakatau. In y1, EAS and EAC both record three seasons in which temperatures are significantly below normal (MAM, JJA, SON); over NWC two seasons are significantly below normal (JJA and SON); and over SWE, CWC, CEC, Victoria and Tasmania only JJA temperatures are significantly below normal (Table 6). In y2, more than half the regions have no significant seasonal anomalies (CEC, Victoria, Tasmania, EAS and EAC), while SWE, CWC and NWC have only one significant seasonal negative temperature anomaly (SON) (Table 6). The average seasonal response over all regions is strongest in JJA of y1 (-0.30°C), SON of y2 (-0.30°C) and DJF of y3 (-0.25°C), while the weakest response occurs in DJF of y1 (-0.15°C) and y2 (-0.05°C), and SON of y3 (-0.05°C). However, average seasonal values differ per region, with the strongest y1 response occurring in JJA over SWE, CWC, CEC, Victoria, Tasmania and NWC; in MAM over EAS; and in SON over EAC (Table 6). Weakest responses are measured in DJF over SWE, CWC, Victoria, Tasmania, EAS and EAC; MAM over NWC; and in SON over CEC.

Table 6. Mean seasonal temperature departures following the Santa Maria eruption, for CMIP5, 20CRv2 and station data. Grey shading = year of eruption; blue shading = significant anomalies.

			SWE				CWC				CEC				Victoria			
		Year	DJF	MAM	JJA	SON	DJF	MAM	JJA	SON	DJF	MAM	JJA	SON	DJF	MAM	JJA	SON
Santa Maria	CMIP5	1902	0.10	-0.03	0.11	0.06	0.08	-0.02	0.15	-0.04	0.03	0.05	0.04	-0.26	-0.01	0.10	0.08	-0.22
		1903	-0.14	-0.21	-0.27	-0.21	-0.10	-0.28	-0.34	-0.23	-0.19	-0.29	-0.32	-0.18	-0.12	-0.22	-0.30	-0.18
		1904	-0.02	-0.08	-0.08	-0.45	0.04	-0.05	-0.08	-0.43	-0.05	-0.12	-0.12	-0.33	-0.09	-0.10	-0.09	-0.22
		1905	-0.13	-0.05	-0.09	0.01	-0.12	0.02	-0.05	0.02	-0.50	-0.12	-0.15	-0.07	-0.34	-0.11	-0.11	-0.03
	20CRv2	1902	-0.88	0.95	0.74	0.75	-0.05	0.88	0.66	0.75	0.92	0.22	0.17	1.25	0.60	0.17	0.20	0.93
		1903	-0.43	-0.52	0.14	-0.11	0.26	-0.36	-0.03	-0.04	-0.28	0.54	-0.05	0.69	-0.25	0.63	-0.04	1.03
		1904	0.02	0.53	-0.09	0.59	-0.06	0.47	-0.28	0.41	-0.49	0.86	-0.45	0.01	-0.12	0.83	-0.19	-0.24
		1905	-0.61	-0.29	-0.33	0.27	0.00	-0.39	-0.50	0.26	0.56	-0.02	-0.78	-1.09	0.42	-0.01	-0.44	-1.28
	Station Data		Perth - SWE								Adelaide - CEC				Melbourne - Victoria			
			DJF	MAM	JJA	SON					DJF	MAM	JJA	SON	DJF	MAM	JJA	SON
		1902	-2.04	0.89	0.05	-0.43					-0.83	1.53	0.33	1.73	-0.74	-0.18	-0.50	0.52
		1903	0.46	-1.26	0.02	-0.13					-1.02	0.31	-0.26	0.90	-0.86	0.11	-0.47	0.87
		1904	0.14	0.32	0.07	-0.02					-0.91	1.59	-0.14	-0.46	-0.82	0.10	0.26	-0.62
		1905	-0.38	-0.03	-0.41	-0.28					-0.82	0.93	-0.32	-2.68	-0.58	0.47	0.28	-2.15
	3-season Averages	CMIP5	-0.10	-0.11	-0.15	-0.22	-0.06	-0.10	-0.16	-0.21	-0.25	-0.18	-0.20	-0.19	-0.18	-0.15	-0.17	-0.14
		20CRv2	-0.34	-0.09	-0.10	0.25	0.07	-0.09	-0.27	0.21	-0.07	0.46	-0.42	-0.13	0.01	0.48	-0.23	-0.16
		Station	0.08	-0.32	-0.11	-0.14					-0.92	0.94	-0.24	-0.75	-0.75	0.23	0.02	-0.63

			Tasmania				NWC				EAS				EAC			
			DJF	MAM	JJA	SON	DJF	MAM	JJA	SON	DJF	MAM	JJA	SON	DJF	MAM	JJA	SON
Santa Maria	CMIP5	1902	0.06	0.09	0.11	-0.01	0.11	-0.08	0.17	0.08	0.28	0.20	0.12	-0.22	0.08	0.14	0.12	-0.21
		1903	0.02	-0.09	-0.14	-0.09	-0.26	-0.22	-0.42	-0.38	-0.24	-0.42	-0.32	-0.38	-0.17	-0.37	-0.32	-0.43
		1904	-0.14	-0.12	-0.02	-0.06	0.01	-0.24	-0.21	-0.50	-0.09	-0.19	-0.12	-0.23	-0.08	-0.16	-0.03	-0.18
		1905	-0.03	-0.05	-0.08	0.00	-0.14	-0.16	-0.22	-0.06	-0.43	-0.24	-0.38	-0.18	-0.36	-0.19	-0.27	-0.10
	CR20v2	1902	-0.07	-0.12	0.00	-0.32	-0.79	0.27	0.55	0.29	2.13	-0.31	0.55	0.98	1.69	-0.40	0.68	1.08
		1903	-0.16	0.04	-0.26	0.45	-0.92	-0.14	0.19	-0.91	0.63	0.40	0.22	-0.11	0.98	0.64	0.18	-0.34
		1904	0.38	0.23	-0.23	-0.28	-0.56	0.03	-0.47	-0.32	-0.33	-0.59	-0.63	0.44	-0.05	-0.36	-0.53	0.22
		1905	-0.40	-0.27	-0.22	-0.74	-0.67	-0.59	-0.54	-0.48	0.54	0.81	-1.15	-1.22	0.26	0.57	-1.07	-1.14
	Station Data		Hobart - Tasmania								Sydney - EAC				Brisbane - EAC			
			DJF	MAM	JJA	SON					DJF	MAM	JJA	SON	DJF	MAM	JJA	SON
		1902	-0.84	-0.64	-0.69	0.17					0.24	-0.41	0.49	1.51	1.26	-0.06	0.76	0.44
		1903	0.09	0.04	-0.49	0.73					-0.02	0.62	0.22	-11.70	0.99	0.46	-0.02	-1.25
		1904	0.43	0.40	-0.10	-0.20					-0.21	-0.29	0.68	1.27	-0.02	-0.37	-0.59	0.43
		1905	-0.50	0.16	0.33	-1.66					-0.45	0.39	1.38	-12.91	-0.03	0.36	-0.55	-0.91
	3-season Averages	CMIP5	-0.05	-0.09	-0.08	-0.05	-0.13	-0.21	-0.28	-0.31	-0.25	-0.29	-0.27	-0.26	-0.20	-0.24	-0.21	-0.24
		20CRv2	-0.06	0.00	-0.24	-0.19	-0.72	-0.23	-0.27	-0.57	0.28	0.21	-0.52	-0.30	0.40	0.28	-0.47	-0.42
		Station	0.00	0.20	-0.09	-0.38					-0.23	0.24	0.76	-7.78	0.31	0.15	-0.38	-0.58

Following the Santa Maria eruption, the percentage of months with negative temperature anomalies from the time of the eruption to the end of y3 ranged between 95% (EAS) and 77% (SWE) (Figure 3). The percentage of months with significant negative temperature anomalies remains high for EAS (56%), but is considerably less for NWC and EAC (41% each), CEC (35%), Victoria (31%), CWC (26%), SWE (23%) and Tasmania (3%). Significant negative temperature departures first occurred over CEC, Victoria and EAS during October 1902, followed by SWE and NWC in February 1903, EAC in March 1903, and over CWC in May 1903. In contrast, Tasmania only records its first significant monthly temperature anomaly during March 1904. The strongest peak cooling (-0.65°C) is modelled over CEC in January 1905.

Station data reflect negative mean annual temperature anomalies for y1-3 in Victoria, and most years for the remaining regions (Table 6). However, positive mean annual anomalies are recorded for y1 in Hobart (Tasmania) and Brisbane (EAC), and for y2 in Perth (SWE), Adelaide (CEC) and Sydney (EAC)(Table 6). The strongest mean annual response is measured in Sydney (y1: -2.72°C; y3: -2.90°C), which coincides with strongest sub-regional departures modelled in CMIP5 (although of considerably lower amplitude, especially for y2: -0.33°C). Instrumental station data indicate weakest 3-year anomalies for Perth (SWE), whereas CMIP5 outputs suggest weakest responses for Tasmania. Strongest negative temperature departures for stations are recorded in y3 for all regions, which is in direct contrast to the CMIP5 outputs, which model weakest responses for y3. Strongest station-based seasonal anomalies occur during JJA of y1 (same as CMIP5), DJF of y2 (CMIP5 = SON), and SON of y3 (CMIP5 = DJF). The strongest 3-year mean seasonal negative temperature departures occurred during SON using both instrumental (-0.39°C) and CMIP5 (-0.17°C) data sources. The warmest 3-year mean seasonal temperature response occurred during MAM, likewise for both instrumental (+0.24°C) and CMIP5 (-0.15°C) data sources.

Comparing the CMIP5 results to reanalysis data again reveals no significant annual anomalies, and that while all but one (CWC y3: +0.02°C) annual anomaly are below normal when using CMIP5 data, this is reflected far less so in the 20CRv2 data (see Table 4). In y1 and y2, CMIP5 anomalies are cooler than reanalysis outputs for most regions; the exception being over NWC. However, this switches in y3 when reanalysis values reflect greater cooling than do CMIP5 outputs (difference of 0.26°C). Strongest 3-year mean cooling occurs over EAS using the CMIP5 ensemble (-0.26°C), and over NWC using the 20CRv2 data (-0.45°C). Both data sets indicate strongest y1-3 warming over Victoria and the smallest overall response over Tasmania (as was the case for Krakatau).

The 20CRv2 seasonal anomalies following Santa Maria are only significantly below normal in SON of y3 over Victoria and Tasmania (Table 6). Unlike the anomalies following Krakatau, there is no seasonal pattern of above or below normal temperature anomalies following Santa Maria. In addition, the season during which strongest departures occur do not correspond with the CMIP5 results (see Table 6). One possible explanation for this might be that the considerably weaker magnitude of Santa Maria, compared to Krakatau, may have led to the climate response being masked by internal climate variability, which CMIP5 cannot account for.

3.3 Agung (1963)

The 3-year annual average temperature departure across all Australian regions following the Agung eruption was slightly weaker (-0.166°C) than that following Santa Maria (-0.173°C) (Figure 2). However, this differs across sub-regions, which includes some stronger sub-regional responses than those modelled for post Santa Maria, including over SWE (-0.18°C), CWC (-0.13°C), Victoria (-0.17°C) and Tasmania (-0.07°C). In addition, y1 responses are stronger than those following Santa Maria across all sub-regions (Table 4). In fact, y1 responses following Agung are even stronger than those in y1 following Krakatau across most regions (except EAS). This highlights the importance of analysing responses at finer (i.e. regional to sub-regional) spatial scales. However, temperatures after Agung recover sooner than those after Krakatau (Table 4). Although anomalies in y1 are significant for all sub-regions, those in y2 are only significant over SWE and NWC (Table 4).

Temperature anomalies in y3 are negligible (between 0.00°C and -0.04°C), hence strongly influencing the relatively low amplitude three-year average temperature departure. As was the case for Krakatau and Santa Maria, the weakest response occurs over Tasmania, and strongest over CEC in y1 (-0.45°C), NWC in y2 (-0.28°C) and SWE in y3 (-0.04°C). Following Krakatau and Santa Maria, more southerly regions of Australia had weaker responses. In contrast, following Agung, southerly regions of SWE, CEC and Victoria yield comparatively stronger responses in some post eruption years (Table 4).

Most seasonal temperature anomalies in y1 are significantly below normal following the Agung eruption - only anomalies in DJF over EAS and Tasmania, and SON over CWC, are not significantly below normal (Table 7). In y2, however, the only significant anomalies modelled are for DJF and MAM over NWC, and DJF over SWE, CEC, Victoria and Tasmania. CMIP5 outputs show no significant seasonal temperature anomalies in y3. The strongest seasonal response over all regions is for DJF in y1 (-0.40°C) and y2 (-0.26°C), and for SON in y3 (-0.06°C). Weakest seasonal responses are for SON in y1 (-0.34°C) and y2 (-0.07°C), and JJA in y3 (+0.07°C). Regionally, strongest seasonal responses are for MAM (austral autumn) over Tasmania, EAS and EAC, for DJF (austral summer) over SWE, CWC and CEC and Victoria, and for JJA (austral winter) over NWC (Table 7).

The percentage of monthly temperature anomalies that fall below normal from the time of the eruption to the end of y3 are between 93% (SWE) and 63% (Tasmania)(Figure 3). However, significant negative monthly temperature anomalies are less frequent and vary from 52% (NWC) to only 7% (Tasmania) of months. The first significant anomalies are modelled for NWC in August of 1963, while most remaining regions experience their first significant anomaly in September 1963, apart from Victoria and Tasmania which have more delayed responses (November 1963 and January 1964 respectively). The strongest negative monthly anomalies are modelled for EAS (June 1964: -0.83°C) and CEC (Jan 1964: -0.79°C).

Most station data indicate negative average temperature anomalies for post-Agung eruption years 1-3. However, this is not the case for Sydney (y1), Brisbane (y1 and y2) and Perth/ Adelaide (y2; Table 6). The strongest negative anomalies are calculated for Adelaide (CEC) in y1 (-0.65°C) and in Perth (SWE) in y3 (-0.63°C), whilst the strongest 3-year average anomaly is also recorded for Perth (-0.35°C). This is agreeable with the CMIP5 outputs, which too demonstrate strongest annual responses over CEC and SWE. The weakest negative 3-year instrumental station-based response is for Sydney (EAC: -0.08°C), whereas that using CMIP5 is for Tasmania. A positive 3-year average response of 0.12°C occurs in Brisbane (central EAC). The strongest average (of all regions) seasonal anomalies occur in DJF, both for y1 (av = -0.84°C) and y1-3 (av = -0.41°C), which is in agreement with the CMIP5 outputs, despite these being more conservative (y1 av = -0.40°C; y1-3 av = -0.25°C). Although weakest station-based seasonal anomalies for post eruption years 1-3 are for SON (av = -0.06°C), that modelled by CMIP5 is for JJA (-0.12°C).

Unlike the earlier two eruptions, there are some significant negative annual temperature anomalies reflected in the reanalysis data, following Agung. The number of significant anomalies are still much less than those modelled by CMIP5 (3 vs 10); these occur in Tasmania in y1 and y2, and in NWC in y3 (Table 4). There are also fewer positive anomalies in the 20CRv2 dataset following Agung, than with the previous two eruptions. Positive anomalies occur in y1 and y2 over EAS and EAC, and in y2 over CWC and CEC. Interestingly, the reanalysis outputs are now more often cooler than those produced by CMIP5 (for most regions except over EAS and EAC in y1, Tasmania in y2, and all regions in y3). In fact, the 20CRv2 mean temperature departure for post eruption years 1-3 across all regions is cooler than that modelled by CMIP5 (-0.21°C and -0.17°C respectively). Despite CMIP5 again modelling the weakest sub-regional response over Tasmania, the 20CRv2 data indicate relatively strong cooling (-0.47°C). Both data sets indicate strongest cooling over NWC during y3 (CMIP5: av= -0.23°C; 20CRv2: av= -0.56°C).

Significantly negative seasonal temperature departures following Agung occur over SWE during SON of y1, over Victoria during DJF of y2, over NWC during SON of y1 and DJF of y3, and Tasmania (y1: DJF and JJA, y2: DJF and MAM; Table 7). Some strong positive anomalies are recorded during JJA of y1 (over SWE, CWC, CEC), MAM of y2 (over SWE, CWC, CEC, NWC), and during SON of y2 (over CEC and Victoria; Table 7). EAS and EAC record positive temperature anomalies during most seasons of y1 and y2 (av= +0.66°C; the exception being for SON of y1). Tasmania is the only region in which only negative temperature anomalies occur during the three post eruption years. As was the case with Santa Maria, strongest mean seasonal negative temperature departures may differ for some sub-regions and reflect similar outcomes for other sub-regions, when comparing CMIP5 and 20CRv2 data outputs (Table 7).

3.4 Pinatubo (1991)

The 3-year annual average temperature departure across all Australian regions following the Pinatubo eruption is -0.21°C (according to CMIP5 outputs); thus, weaker than that following Krakatau but stronger than the post Santa Maria and Agung events (Figure 2). Of all four eruptions investigated, Tasmania records the strongest average 3-year post-eruption temperature response following Pinatubo (-0.12°C); in contrast, NWC records the weakest 3-year post-eruption temperature response after Pinatubo (-0.20°C). The only annual temperature anomalies significantly below normal in y1 are for CEC, Victoria, Tasmania, EAS and EAC (Table 4). In y2, only SWE and Tasmania record significant negative annual temperature departures, while in y3 this expands geographically to CWC, CEC, EAS and EAC. The strongest annual responses occur in y1 for all regions except SWE (y2), CWC (y3) and NWC (y3). Strongest temperature responses following Pinatubo occur over EAS in y1 (-0.40°C), NWC in y2 (-0.19°C) and EAC in y3 (-0.32°C).

Table 7. Mean seasonal temperature departures following the Agung eruption, for CMIP5, 20CRv2 and station data. Grey shading = year of eruption; blue shading = significant anomalies.

		Year	SWE DJF	SWE MAM	SWE JJA	SWE SON	CWC DJF	CWC MAM	CWC JJA	CWC SON	CEC DJF	CEC MAM	CEC JJA	CEC SON	Victoria DJF	Victoria MAM	Victoria JJA	Victoria SON
Agung	CMIP5	1963	0.06	-0.01	-0.08	-0.41	-0.03	0.06	-0.07	-0.47	0.24	0.15	0.01	-0.47	0.19	0.18	0.03	-0.33
		1964	-0.36	-0.32	-0.29	-0.31	-0.40	-0.32	-0.32	-0.25	-0.59	-0.41	-0.39	-0.45	-0.54	-0.40	-0.30	-0.40
		1965	-0.34	-0.25	-0.15	-0.13	-0.21	-0.15	-0.11	-0.10	-0.32	-0.09	-0.10	-0.05	-0.38	-0.03	-0.09	0.08
		1966	-0.03	-0.08	-0.04	-0.09	0.08	-0.02	0.02	-0.01	-0.09	-0.02	0.07	-0.04	-0.10	-0.03	0.09	-0.06
	20CRv2	1963	0.22	0.83	0.10	0.94	-0.38	0.20	0.05	1.05	-0.90	0.32	-0.16	0.86	-0.90	-0.15	-0.26	0.82
		1964	-0.64	-0.32	0.27	-1.77	-0.99	-0.54	0.33	-1.07	-0.82	0.02	0.47	-0.50	-1.07	-0.29	0.02	-0.42
		1965	-0.34	0.09	-0.06	-1.00	0.15	0.07	0.02	-0.11	-1.03	0.28	-0.02	1.23	-1.61	-0.33	-0.04	0.59
		1966	-0.76	-0.64	-0.30	-0.60	-0.05	-0.16	-0.31	-0.39	0.33	-0.28	-0.51	-0.27	-0.20	-0.12	-0.50	-0.12
	Station Data		Perth - SWE								Adelaide - CEC				Melbourne - Victoria			
			DJF	MAM	JJA	SON					DJF	MAM	JJA	SON	DJF	MAM	JJA	SON
		1963	0.29	0.93	0.02	1.07					-0.06	-0.50	-0.21	0.93	-0.05	-0.42	-0.21	0.96
		1964	-1.01	-0.40	0.89	-1.43					-2.04	-0.33	0.03	-0.25	-1.70	-0.41	0.51	-0.23
		1965	0.29	0.32	-0.06	-0.24					0.85	-0.54	0.02	1.06	-0.23	-0.69	0.00	0.77
		1966	-0.86	-0.47	-0.69	-0.52					-0.11	-0.31	-0.31	0.12	-0.55	-0.10	-0.61	0.23
	3-season Averages	CMIP5	-0.24	-0.22	-0.16	-0.17	-0.18	-0.16	-0.14	-0.12	-0.33	-0.17	-0.14	-0.18	-0.34	-0.15	-0.10	-0.13
		20CRv2	-0.58	-0.29	-0.03	-1.12	-0.30	-0.21	0.01	-0.52	-0.51	0.00	-0.02	0.16	-0.96	-0.25	-0.17	0.02
		Station	-0.53	-0.18	0.05	-0.73					-0.43	-0.39	-0.09	0.31	-0.83	-0.40	-0.03	0.26

		Year	Tasmania DJF	Tasmania MAM	Tasmania JJA	Tasmania SON	NWC DJF	NWC MAM	NWC JJA	NWC SON	EAS DJF	EAS MAM	EAS JJA	EAS SON	EAC DJF	EAC MAM	EAC JJA	EAC SON
Agung	CMIP5	1963	0.10	0.15	0.09	-0.06	0.11	-0.02	-0.19	-0.63	0.23	0.13	0.02	-0.47	0.07	0.07	-0.03	-0.43
		1964	-0.12	-0.20	-0.15	-0.16	-0.39	-0.40	-0.42	-0.39	-0.36	-0.53	-0.52	-0.43	-0.40	-0.46	-0.44	-0.36
		1965	-0.28	-0.11	-0.07	0.09	-0.33	-0.43	-0.24	-0.21	-0.05	-0.19	-0.13	-0.09	-0.13	-0.16	-0.09	-0.10
		1966	0.03	0.04	0.05	-0.03	-0.02	-0.03	0.09	-0.11	-0.05	-0.01	0.12	-0.05	-0.03	-0.05	0.12	-0.13
	20CRv2	1963	-0.22	-0.70	-0.36	0.18	0.02	0.66	0.11	0.92	-1.02	0.64	-0.01	-0.16	-0.52	0.45	0.05	-0.38
		1964	-0.97	-0.62	-0.67	-0.14	-0.37	-0.07	-0.06	-1.44	0.46	1.16	0.79	-0.05	0.45	0.71	0.34	-0.21
		1965	-0.97	-0.63	-0.40	-0.30	-0.18	0.28	-0.09	-1.20	0.34	0.67	0.35	1.56	-0.01	0.63	0.26	1.54
		1966	-0.26	-0.29	-0.43	-0.10	-1.38	-0.58	-0.69	-1.04	-0.26	-0.24	-0.04	-0.42	-0.35	-0.22	-0.30	-0.49
	Station Data		Hobart - Tasmania								Sydney - EAC				Brisbane - EAC			
			DJF	MAM	JJA	SON					DJF	MAM	JJA	SON	DJF	MAM	JJA	SON
		1963	-0.11	-1.13	-0.79	0.70					0.32	0.10	-0.36	-0.51	0.31	0.20	-0.04	-0.96
		1964	-1.62	-0.46	-0.22	0.18					0.32	-0.23	0.42	0.22	1.03	-0.07	-0.01	-0.10
		1965	-0.63	-0.85	0.24	0.26					-0.87	-0.11	0.09	0.83	0.30	0.39	-0.23	0.44
		1966	-0.61	-0.05	-0.56	0.49					-0.48	-0.46	-0.51	-0.23	0.56	-0.14	-0.26	-0.50
	3-season Averages	CMIP5	-0.12	-0.09	-0.06	-0.03	-0.25	-0.29	-0.19	-0.24	-0.15	-0.25	-0.17	-0.19	-0.19	-0.22	-0.14	-0.20
		20CRv2	-0.73	-0.51	-0.50	-0.18	-0.64	-0.12	-0.28	-1.23	0.18	0.53	0.37	0.36	0.03	0.37	0.10	0.28
		Station	-0.95	-0.45	-0.18	0.31					-0.34	-0.27	0.00	0.28	0.63	0.06	-0.17	-0.06

The only region in which seasonal temperature anomalies are significantly below normal in all seasons following the Pinatubo eruption in y1 is over EAS. Three seasons are significantly below normal over Tasmania (MAM, JJA, SON) and EAC (DJF, MAM, JJA), two are significantly below normal over CEC (MAM and JJA) and Victoria (MAM and JJA), and one over SWE, CWC and NWC (JJA). In y2, temperatures are significantly below normal in every season over Tasmania, in DJF and JJA over SWE, in DJF over CWC and NWC, and in SON over Victoria. No seasons record significantly below normal temperatures over CEC, EAS and EAC in y2. In y3, however, there are again stronger (significant) negative temperature departures over CWC, SWE and NWC (all in MAM and JJA) and over EAS and EAC (both in DJF and SON). No significant anomalies are recorded for CEC, Tasmania and Victoria in y3. The regional-averaged seasonal response is strongest in JJA (-0.28°C) of y1, SON (-0.23°C) of y2 and MAM (-0.22°C) of y3, while the weakest response occurs in SON (-0.17°C) of y1, MAM (-0.13°C) of y2 and DJF (-0.16°C) in y3 (Table 8). However, this pattern is not uniform across regions; for instance, strongest y1 responses during JJA only apply to SWE, CWC and NWC, as other regions (CEC, Victoria, Tasmania, EAS and EAC) have their strongest response in MAM of y1. (Table 8).

The percentage of monthly temperature anomalies that fall below normal from the eruption date to the end of y3 are between 95% (Victoria) and 81% (EAS) (Figure 3). However, significant monthly negative temperature anomalies vary from 65% (over EAS) to only 14% (over Tasmania) of months. The first significant response is modelled for EAS in August 1991, followed by CEC, NWC and EAC in September 1991, and CWC and Victoria in October 1991. More delayed initial negative temperature anomalies occur over SWE (January 1992) and Tasmania (April 1992). The strongest monthly temperature departures are modelled for EAS (Oct 1991: -0.83°C) and EAC (Nov 1991: -0.64°C).

Table 8. Mean seasonal temperature departures following the Pinatubo eruption, for CMIP5, 20CRv2 and station data. Grey shading = year of eruption; blue shading = significant anomalies.

		Year	SWE				CWC				CEC				Victoria			
			DJF	MAM	JJA	SON	DJF	MAM	JJA	SON	DJF	MAM	JJA	SON	DJF	MAM	JJA	SON
Pinatubo	CMIP5	1991	0.00	0.08	0.02	-0.06	0.10	0.09	-0.01	-0.23	0.15	-0.09	-0.06	-0.36	0.02	-0.11	-0.05	-0.18
		1992	-0.20	-0.05	-0.20	-0.09	-0.19	-0.07	-0.27	-0.07	-0.30	-0.38	-0.37	-0.19	-0.19	-0.35	-0.25	-0.12
		1993	-0.30	-0.16	-0.22	-0.20	-0.29	-0.06	-0.19	-0.19	-0.24	-0.07	-0.18	-0.30	-0.23	-0.16	-0.19	-0.27
		1994	-0.07	-0.26	-0.17	-0.07	-0.09	-0.28	-0.22	-0.15	-0.18	-0.33	-0.22	-0.19	-0.03	-0.16	-0.11	-0.17
	20CRv2	1991	-0.31	0.07	0.22	-0.40	-0.23	0.09	0.36	0.49	1.02	-0.31	0.10	-0.07	0.64	-0.30	-0.14	-0.42
		1992	-0.24	-0.91	0.10	-1.63	0.22	-0.47	-0.05	-1.81	-1.70	-0.25	-0.46	-2.58	-1.71	-0.23	-0.55	-1.96
		1993	-0.77	-0.93	-0.66	-0.79	-0.25	-0.39	-0.74	-0.55	-0.76	0.43	0.18	-0.77	-0.22	-0.05	0.27	-0.68
		1994	-0.08	2.34	1.42	1.53	-0.03	2.57	1.45	1.12	-0.76	0.48	0.95	0.44	-0.11	0.48	0.99	0.16
	Station Data		Perth - SWE												Melbourne - Victoria			
			DJF	MAM	JJA	SON									DJF	MAM	JJA	SON
		1991	0.11	0.36	0.56	-0.43									-0.46	-0.61	0.54	0.19
		1992	1.34	1.53											-0.97	0.39	-0.31	-0.93
		1993													0.10	0.36	0.50	-0.43
		1994													0.24	-0.47	-0.16	-0.73
	3-season Averages	CMIP5	-0.19	-0.16	-0.20	-0.12	-0.19	-0.14	-0.22	-0.14	-0.24	-0.26	-0.26	-0.23	-0.15	-0.22	-0.18	-0.19
		20CRv2	-0.36	0.16	0.29	-0.30	-0.02	0.57	0.22	-0.41	-1.07	0.22	0.22	-0.97	-0.68	0.06	0.24	-0.83
		Station	1.34	1.53											-0.21	0.09	0.01	-0.70

			Tasmania				NWC				EAS				EAC			
			DJF	MAM	JJA	SON	DJF	MAM	JJA	SON	DJF	MAM	JJA	SON	DJF	MAM	JJA	SON
Pinatubo	CMIP5	1991	-0.02	-0.03	-0.03	-0.06	0.02	0.06	-0.22	-0.35	0.60	0.04	-0.11	-0.75	0.36	0.01	-0.07	-0.58
		1992	-0.14	-0.22	-0.18	-0.13	-0.22	-0.02	-0.33	-0.15	-0.51	-0.55	-0.37	-0.36	-0.50	-0.51	-0.31	-0.30
		1993	-0.34	-0.28	-0.14	-0.14	-0.29	-0.10	-0.26	-0.20	0.02	-0.12	-0.12	-0.29	-0.01	-0.12	-0.15	-0.26
		1994	0.09	0.02	-0.04	-0.06	-0.15	-0.36	-0.29	-0.06	-0.47	-0.17	-0.17	-0.35	-0.45	-0.22	-0.15	-0.36
	20CRv2	1991	-0.23	-0.42	-0.30	-0.23	0.58	0.32	0.21	-0.87	-0.42	-0.45	-0.23	0.11	0.92	0.17	-0.36	-0.27
		1992	-0.45	-0.04	-0.62	-0.48	-1.08	-0.85	-0.12	-1.78	-0.66	0.11	-0.73	-1.72	-0.67	-0.55	-0.71	-1.61
		1993	0.46	0.19	-0.07	-0.22	-1.07	-0.50	-0.84	-1.31	0.04	0.59	0.54	-0.46	0.01	0.29	0.54	-0.51
		1994	0.40	0.42	0.52	0.27	1.24	2.10	1.77	1.81	1.23	0.62	0.72	0.64	1.71	0.47	0.83	1.16
	Station Data		Hobart - Tasmania								Sydney - EAC							
			DJF	MAM	JJA	SON					DJF	MAM	JJA	SON				
		1991	-0.23	-0.54	0.43	-0.02					0.83	-0.08	0.53	0.89				
		1992	-1.02	0.16	-1.06	-0.81					-1.02	-0.13	-0.34	-0.64				
		1993	0.58	0.31	0.82	0.15					0.37	-0.16	0.16	0.07				
		1994	0.52	0.05	-0.14	-0.53					0.27	-0.59	-0.11	0.46				
	3-season Averages	CMIP5	-0.13	-0.16	-0.12	-0.11	-0.22	-0.16	-0.29	-0.14	-0.32	-0.28	-0.22	-0.33	-0.32	-0.29	-0.20	-0.30
		20CRv2	0.14	0.19	-0.06	-0.15	-0.30	0.25	0.27	-0.42	0.20	0.44	0.18	-0.51	0.35	0.07	0.22	-0.32
		Station	0.03	0.17	-0.13	-0.40					-0.13	-0.29	-0.10	-0.04				

Post Pinatubo station data were only available to us for Hobart (Tasmania), Melbourne (Victoria) and Sydney (EAC). Mean annual negative temperature departures in y1 are recorded for Hobart (-0.68°C), Melbourne (-0.45°C) and Sydney (-0.53°C), and in y3 for Hobart (-0.03°C) and Melbourne (-0.28°C)(Table 6). The remaining anomalies are positive (Hobart y2: +0.46°C; Melbourne y2 +0.13°C; Sydney y2: +0.11°C, y3: +0.01°C). In contradiction to CMIP5 data, station data indicate that Hobart (Tasmania) had the strongest annual anomaly (y1) of all Australian sub-regions (-0.68°C). However, there is also some agreement between station and CMIP5 datasets, which both show strongest negative temperature anomalies for y1 across all Australian regions investigated (Table 6). Both station data and CMIP5 data indicate a return to 'near normal' temperatures in y2. However, strongest y1-3 seasonal instrumental-based temperature departures are recorded for SON (-0.38°C), and weakest for MAM (0.14°C), yet the CMIP5 model outputs show just the opposite with MAM recording strongest response (-0.22°C) and SON the weakest (-0.19°C).

A higher occurrence of significantly negative departures are recorded after Pinatubo than after the other eruptions when using reanalysis data. These occur in y1 in CEC, Victoria, NWC and EAC (Table 4). The reanalysis data show below normal annual anomalies for all sub-regions in y1, and for most sub-regions in y2 (except over Tasmania, EAS and EAC). However, anomalies are significantly above normal in every region in y3 (av= +1.08°C). The reanalysis anomalies are cooler than the CMIP5 anomalies in every region in y1, and in all regions except Tasmania, EAS and EAC in y2, but warmer in all regions in y3. As is the case with the CMIP5 outputs, the reanalysis data also show weakest overall temperature variability for the three post eruption years over Tasmania. Strongest cooling (y1-y2) portrayed in the reanalysis data is over NWC (-0.87°C), while that using CMIP5 outputs is for EAS (-0.28°C). This implies that CMIP5 has under-estimated negative temperature anomalies over at least some sub-regions of Australia.

Although 20CRv2 data indicate more significant negative temperature anomalies following Pinatubo, than after the other eruptions, these are, however, weaker than CMIP5 outputs (see Table 8). 20CRv2 data show negative seasonal anomalies throughout most of y1 (av= -0.82°C), and through the first half of y2 (av= -0.28°C), but positive anomalies dominate in y3 (av= +0.90°C). The strongest mean seasonal cooling anomaly for all sub-regions is during SON (-0.49°C), while strongest warming occurs during MAM (av= +0.25°C) for post eruption years 1-3. However, such anomalies differ across sub-regions. Strongest cooling occurs during SON of y1 over most regions (av= -1.87°C); the exception being Tasmania where strongest cooling occurs during JJA. In contrast, CMIP5 results demonstrate strongest y1 cooling during MAM or JJA.

4. Discussion

To date, little is known about SH regional to sub-regional climatic responses following major volcanic eruptions, hence the initiative to explore and compare potential temperature responses across various regions of Australia using an ensemble of CMIP5 models. In addition, the opportunity to test the CMIP5 outputs against station data and reanalysis data is taken. For the purposes of this study, regions of Australia were identified based on their Köppen Geiger climate classification. Here post-volcanic temperature responses are compared between sub-regions of the same classification, namely over CWC and CEC (arid) and over Victoria and Tasmania (temperate). Despite occurring within the same climate type, post-volcanic responses differ in magnitude between CEC (av for all eruptions y1-3 = -0.24°C) and CWC (av for all eruptions y1-3 = -0.17°C). Yet, seasonal patterns of response are agreeable between sub-regions, with both sub-regions generally recording strongest negative temperature responses during DJF, followed by JJA, and weakest responses in SON. Responses over Victoria and Tasmania also differ in magnitude (av for all eruptions y1-3: Victoria -0.19°C; Tasmania -0.09°C) and timing (first significant monthly response occurs around 3.75 months after an eruption in Victoria but 13.5 months after an eruption in Tasmania). However, yet again strongest and weakest seasonal responses are agreeable between sub-regions, with DJF most often recording strongest responses, followed by JJA, and weakest responses in SON.

According to CMIP5 outputs, temperature responses to volcanic forcing vary spatially, with more northerly regions of Australia (i.e. NWC, EAS, EAC) typically recording stronger responses (regional av = -0.25°C for all eruptions, y1-3) than more southerly regions (i.e. SWE, CWC, CEC: av = -0.20°C for all eruptions, y1-3). Tasmania, which is not part of continental Australia, repeatedly records weakest responses (av = -0.09°C for all eruptions, y1-3). Similarly, sub-regional responses to the same volcanic eruptions over southern Africa record stronger negative anomalies over more northerly than southerly regions (Harvey and Grab, conditionally accepted). This is likely owing to the more northerly/continental regions having larger diurnal temperature ranges (Jakob and Walland, 2016; Harvey *et al.*, 2020). It is likewise not surprising that Tasmania records weakest responses for the Australia region given its maritime climate moderated by the South Pacific Ocean, which accounts for low amplitude temperature variations (Briffa, 2000). However, station data (Hobart) indicate third strongest cooling (of six Australian stations) over Tasmania after the four eruptions, both annually and seasonally, except during SON, which is weakest for Hobart. In addition, post-eruption temperature departures after Santa Maria and Agung generally reflect ~50% opposing responses between CMIP5 outputs and station data (i.e. where one is stronger, the other is weaker, or vice versa). This may, in part, be a product of CMIP5 representing an averaged response over large regions. For instance, EAC covers an area of 1,001,971km^2 and extends over -20°S to -35°S latitude. In this region, Brisbane records weakest post-eruption negative annual and summer temperature departures, but strongest negative winter departures. In contrast, Sydney, which is also located in EAC but 6.39° south of Brisbane, records strongest annual negative temperature departures of all six Australian stations used in this study. This highlights strongly contrasting temperature responses even within given (climatic) regions of Australia, which emphasizes the necessity of greater caution when using CMIP5 or other downscaled climate model outputs for establishing post-eruption temperature responses. Overall, there is no consistency in how the CMIP5 and station data compare, as after some eruptions they have similar responses, such as the same strongest (e.g. following Agung) or weakest (e.g. after Santa Maria and Krakatau) seasonal response, but at other times they may have directly opposing seasonal responses (e.g. following Pinatubo).

Overall, the 20CRv2 data indicate less significant post-eruption temperature departures (av for y1-3 = -0.06°C) than those modelled through CMIP5 (av for y1-3 = -0.20°C). An inherent limitation with CMIP5 is, at times, incorrect simulation of climate modes, such as the Southern Annular Mode (SAM). For instance, CMIP5 simulates a positive SAM following the Pinatubo eruption, when in fact observational data recorded a negative SAM (Barnes *et al.*, 2016). This is possibly owing to internal variability masking true responses to volcanic forcing in observations (Barnes *et al.*, 2016; McGraw *et al.*, 2016). In addition, several authors have argued that CMIP5 overestimates the volcanic temperature response, which may be a product of the radiative forcing being too strong in CMIP5 models (e.g. Driscoll *et al.*, 2012; Marotzke and Forster, 2015; Chylek *et al.*, 2020). The extent of CMIP5 overestimation is apparently greatest during winter, due to the way the CMIP5 models parameterize how aerosols interact with mixed phase and ice clouds (Chylek *et al*., 2020). However, for Australia, such overestimation is found to only be the case after the two earlier eruptions (Krakatau and Santa Maria), and not so after Agung and Pinatubo. In fact, the 20CRv2 data for the SON and DJF seasons regularly indicate stronger (cooler) anomalies than the CMIP5 outputs for specific regions. This implies that CMIP5 likely underestimates (or provides conservative responses to) volcanic forcing in at least some spatio-temporal contexts (see also Harvey and Grab, conditionally accepted). The next phase of CMIP (phase 6) has had improvements made to the volcanic forcing dataset used, which hopes to combat the issues the CMIP5 models presented, and aid in giving a more accurate understanding to the climatic responses to volcanic eruptions (Dhomse *et al.*, 2020).

Maximum cooling of global temperatures typically occurs within 7-18 months after an eruption (Wigley *et al*., 2005), although in the case of European temperatures this may be delayed to 2 years after an eruption, before temperatures start to recover (Esper *et al.,* 2013). A noteworthy finding from CMIP5 data for the Australian sub-regions of EAS and EAC, is that their post-eruption temperature anomalies were strong in y1 (mean: -0.38°C), weak in y2 (mean: -0.16°C) and then stronger again in y3 (mean: -0.22°C). This is further supported by the 20CRv2 data after Krakatau and Agung. This pattern has similarly been reported for the South Western Cape and Eastern Cape Coastal regions of South Africa, following the Krakatau and Pinatubo eruptions (Harvey and Grab, conditionally accepted), and particularly in autumn following major eruptions between 1834–1899 in Cape Town, South Africa (Picas and Grab, 2020). Australian station data likewise support these CMIP5 outputs, with negative temperature departures in y3 often stronger than y2, and in fact even stronger than in y1 for Hobart, Melbourne and Adelaide following Santa Maria, and in Perth, Sydney, and Brisbane following both Santa Maria and Agung. This is likewise the case after the Krakatau eruption in Hobart and Melbourne (data not available for other stations post Krakatau). Coincidently, in Victoria and Queensland, record lowest temperatures were measured on 15 June 1965 (-11.7°C) and 12 July 1965 (-10.6°C) respectively, which was y3 post Agung (Australian Government, Bureau of Meteorology, 2019). In New South Wales, the lowest temperature ever recorded (-23°C) was on 29 June 1994, which was y3 post Pinatubo (Australian Government, Bureau of Meteorology, 2019). In fact, this is the record lowest temperature ever measured for Australia. In Melbourne and Adelaide following Agung, and in Hobart, Melbourne and Sydney following Pinatubo, although y3 negative temperature departures were weaker than in y1, they were all stronger than in y2. The 20CRv2 reanalysis data similarly support strongest cooling in y3 for all regions (in at least one season) except Tasmania after the Agung eruption. Such findings imply a 3-year delayed (lagged) negative temperature response. The El Niño Southern Oscillation (ENSO) has a strong climatic (rainfall and temperature) influence over Australia (Power *et al.*, 1999; Cai *et al.*, 2012), and may itself be affected by volcanic forcing (Wang *et al.*, 2018; Sun *et al.*, 2019; Pausata *et al.*, 2020). To this end, the ensemble indicates a La Niña event following each of the four major eruptions, when in fact an El Niño event was active at the time of each of the four eruptions (Gergis and Fowler, 2009). However, studies have shown that La Niña-like conditions typically occur three to five years after an eruption (Wahl *et al.*, 2014; Maher *et al.*, 2015), which might be the key factor contributing to cooling in post eruption y3. Weaker anomalies in y2 are likely associated with this being a more neutral ENSO year.

Of the four eruptions studied here, the strongest volcanically-induced negative temperature departures followed the 1883 Krakatau eruption over both the NH and SH as a whole (Harvey *et al.*, 2020). However, in the case of Australian sub-regions, CMIP5 post-eruption y1 negative temperature departures following the 1963 Agung eruption were stronger (combined av= -0.36°C) than y1 responses following the Krakatau eruption (combined av= -0.31°C) over all regions except Tasmania and EAS, despite the Krakatau response lasting longer (negative anomalies continuing even until 1888 in some regions. The extended cooling period following Krakatau is most likely aided by the major (VEI 5) 1886 Tarawera erupted in neighbouring New Zealand. Although there are only two station records (Hobart and Melbourne) at the time Krakatau erupted, both support stronger cooling post Agung (av= -0.49°C) than following Krakatau (-0.25°C). Notwithstanding CMIP5 model outputs indicating strongest negative temperature departures following the Krakatau eruption over the African subcontinent, some regions (i.e. Western Cape, western subcontinent and central subcontinent) also record strongest cooling following the Agung eruption (Harvey and Grab, provisionally accepted). Such findings are despite Krakatau having emitted substantially more SO_2 into the lower stratosphere (22 Tg) than did Agung (7.5 Tg). Both eruptions occurred in tropical Indonesia, just several 100km north of the Australian continent. This would suggest that both eruption locality and magnitude were not the primary factors responsible for a stronger negative temperature response over Australia following Agung. This may imply that pre-existing climate modes and their strengths (e.g. ENSO, SAM), and the ways in which they might have been (differently) affected at the times of these eruptions, significantly contributed to post-eruption climatic outcomes. Krakatau erupted in late austral winter while Agung erupted in late austral autumn. It is thus also possible that the time of year played an important role through its influence on ocean circulation (e.g. Brewer-Dobson circulation) and subsequent feedback mechanism over post volcanic years 1-3 (see also Perlwitz and Graf, 1995; Birner and Bönisch, 2010; Young *et al.*, 2011; Harvey *et al.*, 2020).

The general seasonal pattern of post-volcanic cooling over Australia suggests this is strongest during the cooler months/seasons. Over eastern regions (EAS, EAC, Victoria and Tasmania), strongest cooling responses usually occur during austral autumn (MAM), while the north-western region of NWC experiences strongest cooling during austral winter (JJA). For remaining regions at similar latitudes (SWE, CWC and CEC), there is no clear seasonal pattern of response, as the strongest seasonal departures usually occurred in either DJF (following Krakatau and Agung) or JJA (following Santa Maria and Pinatubo). Weakest seasonal responses generally occurred during austral spring or summer (SON/DJF) in all regions except for those along the west coast (NWC and SWE). Although strongest seasonal cooling typically occurs during the cooler seasons, initial significant negative monthly departures tend to occur during warmer austral months (between September and February), but may begin as early as August over NWC in the case of Agung, or as late as May over CWC following Santa Maria. CMIP5 models tend to simulate a positive SAM following volcanic eruptions (Barnes *et al.*, 2016; McGraw *et al.*, 2016) and remain in a positive mode for three years after such eruptions (Yang and Xiao, 2017). However, internal variability often masks the SAM, which is why the modelled SAM and observations do not always agree (Barnes *et al.*, 2016; McGraw *et al.*, 2016; Yang and Xiao, 2017). A positive SAM may reduce maximum temperatures over south central and eastern Australia during spring and summer, and over western parts of Australia during autumn (Hendon *et al.*, 2007). During winter, minimum temperatures are reduced over south-eastern and southwestern regions (Hendon *et al.*, 2007). Yet, this does not coincide with strongest post-volcanic seasonal cooling over Australia, as indicated through CMIP5 model outputs. A positive SAM usually yields intensified cyclogenesis with strong cold frontal systems impacting southern regions of Australia, which may contribute to relatively strong post-volcanic negative temperature departures during cooler seasons. Documentary evidence also supports this. For instance, *The Herald* reports on 25 September 1905 (pg. 1) that 'extraordinary [extremely cold] weather for September…[was] caused by a cyclonic depression' (Table 9). This would also be in agreement with similar observations and suggestions made by Picas and Grab (2020) for southern Africa.

Table 9. Quotes of 'unusual' or 'extreme' weather in years following the four major eruptions.

Date (of article)	Source	Page	Sub-Region	Location	Quote
13 Sep 1904	Glen Innes Examiner and General Advertiser	4	Central EAC	New England (NSW)	'The total absence of snow in this part of New England during the present year is a climatic peculiarity often commented upon. During 60 years no white man can remember a winter passing without snow failing, and its non-appearance this year, to say the least, is remarkable. Probably the extraordinary frequency of frosts, in number quite beyond the memory of the oldest inhabitant in any single season previously, may have had something to do with the change.'
25 Sep 1905	The Herald	1	Victoria	Melbourne (Vic)	'"Isn't this extraordinary weather for September?" Mr Baracchi was asked by a Herald representative this morning. "It is most extraordinary", was the reply, "It is caused by a cyclonic depression" … The extremely cold weather commenced on Saturday afternoon, and has continued ever since. It made its appearance so suddenly. … Mr Baracchi was asked if he could say when we had snow in Melbourne before, but he was unable to do so. "Certainly not within my recollection." he said. … The thermometer went down to 35.5F '
05 Jun 1964	The Beverly Times	1	SWE	Beverly District (Western Australia)	'Monday last saw the end of one of the coldest snaps ever experienced in the State. It was considered by many of the older generation of the Beverley district as the coldest eight day period they could remember. It gave the seasonal outlook a setback, as rain has been urgently needed for some time past. The successive frosts dried out what moisture was in the ground'
21 Jun 1964	Victor Harbour Times	2	CEC	South Coast districts (SA)	'In common with other parts of the State, South Coast districts this week have been experiencing an unusually cold spell with heavy frosts… Victor Harbour's minimum temperatures since Monday have been 34 degrees for four consecutive mornings This is several degrees below the minimum for Adelaide'

Atmospheric blocking can be one of the leading drivers of temperature variability over Australia, which, in this instance, entails a stationary strong high pressure cell to the south of Australia forcing cold polar air northwards, towards Australia, and which is a stimulus for extreme weather (Fierro and Leslie, 2014; Crimp *et al.*, 2018; Patterson *et al.*, 2019). Atmospheric blocking may occur at any time of year but is strongest during austral winter (Patterson *et al.*, 2019). If the atmospheric blocking occurs around 115°E longitude, it can enhance cold polar air movement over Western Australia (Crimp *et al.*, 2018). A consequence of such blocking is widespread, unusual, and severe frosts due to the exceptionally cold air that is advected into southern Australia (Risbey *et al.*, 2019). It is noted that newspapers report of exceptional cold and severe frosts in New South Wales in September 1904 as well as Western Australia and South Australia, in June 1964 (Table 9). Accurately simulating atmospheric blocking in climate models (including CMIP5) is difficult and thus inconclusive (Cowan *et al.*, 2013; Patterson *et al.*, 2019). However, atmospheric blocking is mentioned here as this is a likely mechanism for the unusual and severe frosts reported over EAC, SWE and CEC after both the Santa Maria and Agung eruptions. It is thus proposed that volcanic forcing might favour the development of atmospheric blocking events during post-eruption years, but this would require further investigation for verification.

5. Conclusion

Despite much global interest on the impacts of volcanic forcing on climate, the focus has primarily been at the macro-spatial and temporal scale. Hence the efforts here to explore and compare temperature responses at sub-regional and seasonal to monthly scales for central and southern parts of Australia. The importance of such a finer-scaled investigative approach is evident from rather contrasting spatial and temporal anomalies (responses). In particular, the work demonstrates that relatively weak annual temperature responses may be a consequence of relatively strong but opposing seasonal anomalies masking each other out to provide for a 'dampened' annual response, or alternatively, that such masking effects may be owing to dissimilar sub-regional responses. Generally, strongest temperature responses (i.e. negative anomalies) are recorded for more northerly/interior regions, and weaker responses for more southerly (coastal) and oceanic (Tasmania) regions. Seasonal responses also differ across sub-regions, with eastern regions experiencing strongest cooling during austral autumn and weakest response during austral spring, while western regions do not record a clear seasonal pattern of response.

Numerous studies have reported that CMIP5 overestimates the climatic response to volcanic forcing (e.g. Driscoll *et al.*, 2012; Barnes *et al.*, 2016; McGraw *et al.*, 2016). To this end, the CMIP5 ensemble is compared to both station and reanalysis datasets. The comparison between CMIP5 and station records show some general agreement, such as a) negative anomalies occurring after each of the four eruptions, b) strongest negative temperature departures following Krakatau, c) weakest anomalies occurring during SON following Krakatau and Santa Maria, d) strongest responses occurring in the same regions following both Santa Maria and Agung, e) temperatures start to recover (return to normal) in y2 after Pinatubo, sooner than the other eruptions. More significant temperature responses occur in the CMIP5 ensemble than in the reanalysis. CMIP5 temperature responses seem to differ more strongly from the reanalysis data following the earlier two eruptions (Krakatau and Santa Maria), but then are in broad agreement for the latter two eruptions (Agung and Pinatubo). Possible better agreement during more recent times may be due to the reanalysis data being more accurate in later years given the greater availability of reliable instrumental data, compared to the earlier years (Ke and Hui, 2013; Zhang *et al.*, 2013). CMIP5 models tend to simulate stronger autumn and winter (austral) responses, and weaker spring and occasional summer responses than 20CRv2. Although CMIP5 has proven a useful tool for the detection and attribution of climate responses stemming from volcanic eruptions, uncertainties remain, as they also do when using reanalysis and observational data (Compo *et al.*, 2011; Dhomse *et al.*, 2020). With the improvements to models and quality of forcing datasets used in CMIP6, it is likely that more accurate simulations will be forthcoming in years ahead. However, to establish the level of confidence one might place in any given modelling output, it will remain an important task to cross-validate model outputs with quality palaeo-climate and instrumental data sets.

6. References

Allen KJ, Cook ER, Evans R, Francey R, Buckley BM, Palmer JG, Peterson MJ, Baker PJ. 2018. Lack of cool, not warm, extremes distinguishes late 20th Century climate in 979-year Tasmanian summer temperature reconstruction. Environmental Research Letters, 13(3): 034041. https://doi.org/10.1088/1748-9326/aaafd7.

Ammann CM, Joos F, Schimel DS, Otto-Bliesner BL, Tomas RA. 2007. Solar influence on climate during the past millennium: Results from transient simulations with the NCAR Climate System Model. Proceedings of the National Academy of Sciences, 104(10): 3713–3718. https://doi.org/10.1073/pnas.0605064103.

Ashcroft L, Gergis J, Karoly DJ. 2014. A historical climate dataset for southeastern Australia, 1788–1859. Geoscience Data Journal, 1(2): 158–178. https://doi.org/10.1002/gdj3.19.

Australian Government, Bureau of Meteorology. 2019. Rainfall and Temperature Extremes. Bureau of Meteorology. Accessed 03/04/2021. <http://www.bom.gov.au/climate/extreme/records.shtml>

Barnes EA, Solomon S, Polvani LM. 2016. Robust wind and precipitation responses to the Mount Pinatubo eruption, as simulated in the CMIP5 models. Journal of Climate, 29(13): 4763–4778. https://doi.org/10.1175/JCLI-D-15-0658.1.

Birner T, Bönisch H. 2010. Residual circulation trajectories and transit times into the extratropical lowermost stratosphere. Atmospheric Chemistry and Physics Discussions, 10(7): 16837–16860. https://doi.org/10.5194/acpd-10-16837-2010.

Briffa KR. 2000. Annual climate variability in the Holocene: interpreting the message of ancient trees. Quaternary Science Reviews, 19: 87–105.

Cai W, Rensch P van, Cowan T, Hendon HH. 2012. An Asymmetry in the IOD and ENSO Teleconnection Pathway and Its Impact on Australian Climate.

Journal of Climate. American Meteorological Society, 25(18): 6318–6329. https://doi.org/10.1175/JCLI-D-11-00501.1.

Chappell PR, Lorrey AM. 2014. Identifying New Zealand, Southeast Australia, and Southwest Pacific historical weather data sources using Ian Nicholson's Log of Logs. Geoscience Data Journal, 1(1): 49–60. https://doi.org/10.1002/gdj3.1.

Chylek P, Folland C, Klett JD, Dubey MK. 2020. CMIP5 climate models overestimate cooling by volcanic aerosols. Geophysical Research Letters, 47(3). https://doi.org/10.1029/2020GL087047.

Compo GP, Whitaker JS, Sardeshmukh PD, Matsui N, Allan RJ, Yin X, Gleason BE, Vose RS, Rutledge G, Bessemoulin P, Brönnimann S, Brunet M, Crouthamel RI, Grant AN, Groisman PY, Jones PD, Kruk MC, Kruger AC, Marshall GJ, Maugeri M, Mok HY, Nordli Ø, Ross TF, Trigo RM, Wang XL, Woodruff SD, Worley SJ. 2011. The Twentieth Century Reanalysis Project. Quarterly Journal of the Royal Meteorological Society. John Wiley & Sons, Ltd, 137(654): 1–28. https://doi.org/10.1002/qj.776.

Cook E, Bird T, Peterson M, Buckleyn B, D'Arrigo R, Barbetti M, Francey R. 1992. Climatic change over the last millennium in Tasmania reconstructed from tree-rings., 13.

Cook ER, Buckley BM, Palmer JG, Fenwick P, Peterson MJ, Boswijk G, Fowler A. 2006. Millennia-long tree-ring records from Tasmania and New Zealand: a basis for modelling climate variability and forcing, past, present and future. Journal of Quaternary Science, 21(7): 689–699. https://doi.org/10.1002/jqs.1071.

Cook ER, Krusic PJ, Anchukaitis KJ, Buckley BM, Nakatsuka T, Sano M, PAGES Asia2k Members. 2012. Tree-ring reconstructed summer temperature anomalies for temperate East Asia since 800 C.E. Climate Dynamics, 41(11–12): 2957–2972. https://doi.org/10.1007/s00382-012-1611-x.

Coughlan MJ. 1983. A comparative climatology of blocking action in the two hemispheres. Australian meteorological magazine Melbourne, 31(1): 3–13.

Cowan T, van Rensch P, Purich A, Cai W. 2013. The Association of Tropical and Extratropical Climate Modes to Atmospheric Blocking across Southeastern Australia. Journal of Climate, 26: 7555–7569.

Crimp S, Nicholls N, Kokic P, Risbey JS, Gobbett D, Howden M. 2018. Synoptic to large-scale drivers of minimum temperature variability in Australia - long-term changes: DRIVERS OF AUSTRALIAN MINIMUM TEMPERATURE VARIABILITY. International Journal of Climatology, 38: e237–e254. https://doi.org/10.1002/joc.5365.

Crowley T, Zielinsk G, Vinther BM, Udisti R, Kreutz K, Cole-Dai J, Castellano E. 2008. Volcanism and the Little Ice Age. PAGES News, 16(2): 22–23.

Dhomse SS, Mann GW, Antuña Marrero JC, Shallcross SE, Chipperfield MP, Carslaw KS, Marshall L, Abraham NL, Johnson CE. 2020. Evaluating the simulated radiative forcings, aerosol properties, and stratospheric warmings from the 1963 Mt Agung, 1982 El Chichón, and 1991 Mt Pinatubo volcanic aerosol clouds. Atmospheric Chemistry and Physics. Copernicus GmbH, 20(21): 13627–13654. https://doi.org/10.5194/acp-20-13627-2020.

Dieng HB, Cazenave A, Meyssignac B, von Schuckmann K, Palanisamy H. 2017. Sea and land surface temperatures, ocean heat content, Earth’s energy imbalance and net radiative forcing over the recent years: sea and land surface temperature. International Journal of Climatology, 37: 218–229. https://doi.org/10.1002/joc.4996.

Driscoll S, Bozzo A, Gray LJ, Robock A, Stenchikov G. 2012. Coupled Model Intercomparison Project 5 (CMIP5) simulations of climate following volcanic eruptions. Journal of Geophysical Research: Atmospheres, 117(D17): D17105. https://doi.org/10.1029/2012JD017607.

Drosdowsky W. 2005. The latitude of the subtropical ridge over Eastern Australia: TheL index revisited. International Journal of Climatology, 25(10): 1291–1299. https://doi.org/10.1002/joc.1196.

Efron B. 1979. Bootstrap Methods: another look at the Jackknife. The Annals of Statistics, 7(1): 1–26. https://doi.org/10.1214/aos/1176344552.

Esper J, Schneider L, Krusic PJ, Luterbacher J, Büntgen U, Timonen M, Sirocko F, Zorita E. 2013. European summer temperature response to annually dated volcanic eruptions over the past nine centuries. Bulletin of Volcanology, 75(7): 736. https://doi.org/10.1007/s00445-013-0736-z.

Fierro AO, Leslie LM. 2014. Relationships between Southeast Australian Temperature Anomalies and Large-Scale Climate Drivers. Journal of Climate, 27(4): 1395–1412. https://doi.org/10.1175/JCLI-D-13-00229.1.

Gathorne-Hardy FJ, Harcourt-Smith WEH. 2003. The super-eruption of Toba, did it cause a human bottleneck? Journal of Human Evolution, 45(3): 227–230. https://doi.org/10.1016/S0047-2484(03)00105-2.

Gergis JL, Fowler AM. 2009. A history of ENSO events since A.D. 1525: implications for future climate change. Climatic Change, 92(3–4): 343–387. https://doi.org/10.1007/s10584-008-9476-z.

Gillett NP, Kell TD, Jones PD. 2006. Regional climate impacts of the Southern Annular Mode. Geophysical Research Letters, 33(23): L23704. https://doi.org/10.1029/2006GL027721.

Gleckler PJ, Wigley TML, Santer BD, Gregory JM, AchutaRao K, Taylor KE. 2006. Volcanoes and climate: Krakatoa's signature persists in the ocean. Nature, 439(7077): 675. https://doi.org/10.1038/439675a.

Grose M, Timbal B, Wilson L, Bathols J, Kent D. 2015. The subtropical ridge in CMIP5 models, and implications for projections of rainfall in southeast Australia. Australian Meteorological and Oceanographic Journal, 65(1): 90–106. https://doi.org/10.22499/2.6501.007.

Harvey PJ, Grab SW, Malherbe J. 2020. Major volcanic eruptions and their impacts on southern hemisphere temperatures during the late 19th and 20th centuries, as simulated by CMIP5 models. Geophysical Research Letters, 47(14). https://doi.org/10.1029/2020GL087792.

Haurwitz MW, Brier GW. 1981. A critique of the Superposed Epoch Analysis Method: Its application to solar–weather relations. Monthly Weather

Review, 109(10): 2074–2079. https://doi.org/10.1175/1520-0493(1981)109<2074:ACOTSE>2.0.CO;2.

Haywood JM, Jones A, Jones GS. 2014. The impact of volcanic eruptions in the period 2000-2013 on global mean temperature trends evaluated in the HadGEM2-ES climate model: Impact of modest volcanic eruptions on the global warming trends. Atmospheric Science Letters, 15(2): 92–96. https://doi.org/10.1002/asl2.471.

Hendon HH, Thompson DWJ, Wheeler MC. 2007. Australian Rainfall and Surface Temperature Variations Associated with the Southern Hemisphere Annular Mode. Journal of Climate, 20(11): 2452–2467. https://doi.org/10.1175/JCLI4134.1.

Jakob D, Walland D. 2016. Variability and long-term change in Australian temperature and precipitation extremes. Weather and Climate Extremes. Elsevier, 14: 36–55. https://doi.org/10.1016/j.wace.2016.11.001.

Jones PD, Moberg A, Osborn TJ, Briffa KR. 2003. Surface climate responses to explosive volcanic eruptions seen in long European temperature records and mid-to-high latitude tree-ring density around the Northern Hemisphere. Washington DC American Geophysical Union Geophysical Monograph Series, 139: 239–254. https://doi.org/10.1029/139GM15.

Kandlbauer J, Hopcroft PO, Valdes PJ, Sparks RSJ. 2013. Climate and carbon cycle response to the 1815 Tambora volcanic eruption. Journal of Geophysical Research: Atmospheres, 118(22): 12,497-12,507. https://doi.org/10.1002/2013JD019767.

Ke F, Hui L. 2013. Evaluation of Atmospheric Circulation in the Southern Hemisphere in 20CRv2. Atmospheric and Oceanic Science Letters, 6(5): 337–342. https://doi.org/10.1080/16742834.2013.11447104.

Khodri M, Izumo T, Vialard J, Janicot S, Cassou C, Lengaigne M, Mignot J, Gastineau G, Guilyardi E, Lebas N, Robock A, McPhaden MJ. 2017. Tropical explosive volcanic eruptions can trigger El Niño by cooling tropical Africa. Nature Communications, 8(1). https://doi.org/10.1038/s41467-017-00755-6.

Köppen W. 1936. Das geographisca system der Klimate. In: Köppen W and Geiger G (eds) Handbuch der Klimatologie. Gebr, Borntraeger: Berlin, 44.

Lough JM. 2007. Tropical river flow and rainfall econstructions from coral luminescence: Great Barrier Reef, Australia. Paleoceanography, 22. https://doi.org/doi:10.1029/2006PA001377.

Lyu K, Zhang X, Church JA, Hu J. 2015. Quantifying internally generated and externally forced climate signals at regional scales in CMIP5 models: internal and forced climate signals. Geophysical Research Letters, 42(21): 9394–9403. https://doi.org/10.1002/2015GL065508.

Maher N, McGregor S, England MH, Gupta AS. 2015. Effects of volcanism on tropical variability: EFFECTS OF VOLCANISM. Geophysical Research Letters, 42(14): 6024–6033. https://doi.org/10.1002/2015GL064751.

Man W, Zhou T, Jungclaus JH. 2014. Effects of large volcanic eruptions on global summer climate and East Asian Monsoon changes during the Last Millennium: analysis of MPI-ESM simulations. Journal of Climate, 27(19): 7394–7409. https://doi.org/10.1175/JCLI-D-13-00739.1.

Marotzke J, Forster PM. 2015. Forcing, feedback and internal variability in global temperature trends. Nature, 517(7536): 565–570. https://doi.org/10.1038/nature14117.

Marshall GJ. 2003. Trends in the Southern Annular Mode from Observations and Reanalyses. Journal of Climate, 16(24): 4134–4143. https://doi.org/10.1175/1520-0442(2003)016<4134:TITSAM>2.0.CO;2.

Mass CF, Portman DA. 1989. Major volcanic eruptions and climate: a critical evaluation. Journal of Climate, 2(6): 566–593. https://doi.org/10.1175/1520-0442(1989)002<0566:MVEACA>2.0.CO;2.

McGowan H, Callow JN, Soderholm J, McGrath G, Campbell M, Zhao J. 2018. Global warming in the context of 2000 years of Australian alpine temperature and snow cover. Scientific Reports, 8(1). https://doi.org/10.1038/s41598-018-22766-z.

McGraw MC, Barnes EA, Deser C. 2016. Reconciling the observed and modeled Southern Hemisphere circulation response to volcanic eruptions: Reconciling SH Response to Volcanoes. Geophysical Research Letters, 43(13): 7259–7266. https://doi.org/10.1002/2016GL069835.

Meneghini B, Simmonds I, Smith IN. 2007. Association between Australian rainfall and the Southern Annular Mode. International Journal of Climatology, 27(1): 109–121. https://doi.org/10.1002/joc.1370.

Ménégoz M, Bilbao R, Bellprat O, Guemas V, Doblas-Reyes FJ. 2018. Forecasting the climate response to volcanic eruptions: prediction skill related to stratospheric aerosol forcing. Environmental Research Letters, 13(6): 064022. https://doi.org/10.1088/1748-9326/aac4db.

Monerie P-A, Moine M-P, Terray L, Valcke S. 2017. Quantifying the impact of early 21st century volcanic eruptions on global-mean surface temperature. Environmental Research Letters, 12(5): 054010. https://doi.org/10.1088/1748-9326/aa6cb5.

Neukom R, Gergis J, Karoly DJ, Wanner H, Curran M, Elbert J, González-Rouco F, Linsley BK, Moy AD, Mundo I, Raible CC, Steig EJ, van Ommen T, Vance T, Villalba R, Zinke J, Frank D. 2014. Inter-hemispheric temperature variability over the past millennium. Nature Climate Change, 4(5): 362–367. https://doi.org/10.1038/nclimate2174.

Patterson M, Bracegirdle T, Woollings T. 2019. Southern Hemisphere Atmospheric Blocking in CMIP5 and Future Changes in the Australia-New Zealand Sector. Geophysical Research Letters. John Wiley & Sons, Ltd, 46(15): 9281–9290. https://doi.org/10.1029/2019GL083264.

Pausata FSR, Zanchettin D, Karamperidou C, Caballero R, Battisti DS. 2020. ITCZ shift and extratropical teleconnections drive ENSO response to volcanic eruptions. Science Advances, 6.

Perlwitz J, Graf H-F. 1995. The statistical connection between tropospheric and stratospheric circulation of the northern hemisphere in winter. Journal of Climate, 8: 2281–2295.

Picas J, Grab S. 2020. Potential impacts of major nineteenth century volcanic eruptions on temperature over Cape Town, South Africa: 1834–1899. Climatic Change. https://doi.org/10.1007/s10584-020-02678-6.

Pook MJ, Gibson T. 1999. Atmospheric blocking and storm tracks during SOP-1 of the FROST Project. Australian Meteorological Magazine, (June Special Edition): 51–60.

Power S, Casey T, Folland C, Colman A, Mehta V. 1999. Inter-decadal modulation of the impact of ENSO on Australia. Climate Dynamics, 15(5): 319–324. https://doi.org/10.1007/s003820050284.

Raible CC, Brönnimann S, Auchmann R, Brohan P, Frölicher TL, Graf H-F, Jones P, Luterbacher J, Muthers S, Neukom R, Robock A, Self S, Sudrajat A, Timmreck C, Wegmann M. 2016. Tambora 1815 as a test case for high impact volcanic eruptions: Earth system effects. Wiley Interdisciplinary Reviews: Climate Change, 7(4): 569–589. https://doi.org/10.1002/wcc.407.

Rao MP, Cook BI, Cook ER, D'Arrigo RD, Krusic PJ, Anchukaitis KJ, LeGrande AN, Buckley BM, Davi NK, Leland C, Griffin KL. 2017. European and Mediterranean hydroclimate responses to tropical volcanic forcing over the last millennium. Geophysical Research Letters, 44(10): 5104–5112. https://doi.org/10.1002/2017GL073057.

Risbey JS, Monselesan DP, O'Kane TJ, Tozer CR, Pook MJ, Hayman PT. 2019. Synoptic and Large-Scale Determinants of Extreme Austral Frost Events. Journal of Applied Meteorology and Climatology. American Meteorological Society, 58(5): 1103–1124. https://doi.org/10.1175/JAMC-D-18-0141.1.

Robock A. 2000. Volcanic eruptions and climate. Reviews of Geophysics, 38(2): 191–219. https://doi.org/10.1029/1998RG000054.

Robock A, Adams T, Moore M, Oman L, Stenchikov G. 2007. Southern Hemisphere atmospheric circulation effects of the 1991 Mount Pinatubo eruption. Geophysical Research Letters, 34(23): L23710. https://doi.org/10.1029/2007GL031403.

Rogers JC, van Loon H. 1982. Spatial Variability of Sea Level Pressure and 500 mb Height Anomalies over the Southern Hemisphere. Monthly Weather Review, 110(10): 1375–1392. https://doi.org/10.1175/1520-0493(1982)110<1375:SVOSLP>2.0.CO;2.

Sato M, Hansen JE, McCormick MP, Pollack JB. 1993. Stratospheric aerosol optical depths, 1850–1990. Journal of Geophysical Research, 98(D12): 22987. https://doi.org/10.1029/93JD02553.

Sun W, Wang B, Liu J, Chen D, Gao C, Ning L, Chen L. 2019. How northern high-latitude volcanic eruptions in different seasons affect ENSO. Journal of Climate, 32(11): 3245–3262. https://doi.org/10.1175/JCLI-D-18-0290.1.

Timmreck C. 2018. Climatic effects of large volcanic eruptions. Habilitation Thesis, Hamburg, Universität Hamburg.

Toohey M, Krüger K, Sigl M, Stordal F, Svensen H. 2016. Climatic and societal impacts of a volcanic double event at the dawn of the Middle Ages. Climatic Change, 136(3–4): 401–412. https://doi.org/10.1007/s10584-016-1648-7.

Trenberth KE. 1997. The Definition of El Nino. Bulletin of the American Meteorological Society, 78(12).

Wahl ER, Diaz HF, Smerdon JE, Ammann CM. 2014. Late winter temperature response to large tropical volcanic eruptions in temperate western North America: Relationship to ENSO phases. Global and Planetary Change, 122: 238–250. https://doi.org/10.1016/j.gloplacha.2014.08.005.

Wang T, Guo D, Gao Y, Wang H, Zheng F, Zhu Y, Miao J, Hu Y. 2018. Modulation of ENSO evolution by strong tropical volcanic eruptions. Climate Dynamics, 51(7–8): 2433–2453. https://doi.org/10.1007/s00382-017-4021-2.

Wigley TML. 2000. ENSO, volcanoes and record-breaking temperatures. Geophysical Research Letters, 27(24): 4101–4104.

Wigley TML, Ammann CM, Santer BD, Raper SCB. 2005. Effect of climate sensitivity on the response to volcanic forcing. Journal of Geophysical Research: Atmospheres. John Wiley & Sons, Ltd, 110(D9). https://doi.org/10.1029/2004JD005557.

Yang J, Xiao C. 2017. The evolution and volcanic forcing of the southern annular mode during the past 300 years. International Journal of Climatology, 38(4): 1706–1717. https://doi.org/10.1002/joc.5290.

Young PJ, Thompson DWJ, Rosenlof KH, Solomon S, Lamarque J-F. 2011. The Seasonal Cycle and Interannual Variability in Stratospheric Temperatures and Links to the Brewer–Dobson Circulation: An Analysis of MSU and SSU Data. Journal of Climate, 24(23): 6243–6258. https://doi.org/10.1175/JCLI-D-10-05028.1.

Zanchettin D, Timmreck C, Graf H-F, Rubino A, Lorenz S, Lohmann K, Krüger K, Jungclaus JH. 2012. Bi-decadal variability excited in the coupled ocean–atmosphere system by strong tropical volcanic eruptions. Climate Dynamics, 39(1–2): 419–444. https://doi.org/10.1007/s00382-011-1167-1.

Zhang D, Blender R, Fraedrich K. 2013. Volcanoes and ENSO in millennium simulations: global impacts and regional reconstructions in East Asia. Theoretical and Applied Climatology, 111(3–4): 437–454. https://doi.org/10.1007/s00704-012-0670-6.

Zhou L, Dickinson RE, Dai A, Dirmeyer P. 2010. Detection and attribution of anthropogenic forcing to diurnal temperature range changes from 1950 to 1999: comparing multi-model simulations with observations. Climate Dynamics, 35(7–8): 1289–1307. https://doi.org/10.1007/s00382-009-0644-2.

Chapter Six: Conclusions

1. Introduction

While extensive research attention has focussed on how volcanic forcing has affected climates of the Northern Hemisphere (NH), far fewer publications dealing with such impacts have been forthcoming for the Southern Hemisphere (SH). Given that climate change has been a major theme of global interest, concern and discussion in recent times, understanding remaining research gaps in climate driving mechanisms, has become a priority for many regions of the world. To address knowledge gaps concerning volcanic forcing impacts on climates of the SH, this PhD study set out to examine the impacts of relatively recent (since the mid 19th century) major volcanic eruptions affecting temperatures across much of the terrestrial hemisphere at various spatial (hemispheric, continental, and sub-regional) and temporal (annual, seasonal, and monthly) scales.

Due to the scarcity of instrumental records and climate proxies, climate models from the Coupled Model Intercomparison Project, Phase 5 (CMIP5; Taylor *et al.*, 2012), are used as the main data source for this PhD. However, in order to test the robustness of the data, both reanalysis and instrumental data were used for comparison with CMIP5 model outputs. The reanalysis dataset used (i.e. 20th Century Reanalysis v2 [20CRv2] dataset) was obtained from the NOAA/OAR/ESRL PSL. Instrumental data from the Australian region were acquired from the NOAA National Centers for Environmental Information. Additional instrumental data were used to identify potential volcanic forcing effects on temperature over the south western Cape sub-region (Picas and Grab, 2020) of southern Africa; in particular to compare the findings of the CMIP5 outputs with station data for the historic Krakatau eruption. This chapter summarizes and synthesises findings from the four primary research chapters, and in addition, offers some general conclusions of the study. The final thoughts go to suggested areas for future expansion of such research.

2. Key Outcomes

2.1 Eruptions from 1850-2005 that significantly impacted SH temperatures

The main aim of this PhD was to identify possible SH temperature responses following major volcanic eruptions since 1850, at various spatial and temporal scales. The first stage of the PhD was to establish volcanically-induced temperature responses at a hemispheric scale. To achieve this, the first key objective was to detect and attribute whether in fact a measurable response is observed using the CMIP5 models, following eight major identified volcanic eruptions since 1850. In this case, a volcanic eruption is classified as 'major' on the basis of it being classified with a magnitude of VEI ≥ 5, or having emitted more than 5 Tg of SO_2 into the lower stratosphere. A decrease in temperatures (although not [always] necessarily significant) was observed after each of the eight eruptions. Various forcing experiments (natural, volcanic, solar, historical, anthropogenic) of the CMIP5 models were used to determine whether simulated temperatures are indeed a response to volcanic forcing (please see supplementary material of Chapter 2: Figure S1). The study demonstrates that temperature decreases following the eight eruptions are only observed when experiments included volcanic forcing. In other words, cooling does not occur in experiments where volcanic forcing was absent, thus providing confidence that the observed reduction in temperatures is indeed a response to the eruptions.

Although it is well-established and expected that temperatures cool after major volcanic eruptions, this is not always the case. NH winter warming is a well-acknowledged response to large eruptions, such as after Krakatau and Pinatubo (e.g. Marshall *et al.*, 2009; Zanchettin *et al.*, 2013; Zambri *et al.*, 2017). Such warming is a result of the polar vortex strengthening in response to volcanic forcing (Perlwitz and Graf, 1995). Observations have shown that warming occurs between the mid- to high latitudes, specifically over northern Europe/Asia, and occasionally some regions of North America (Robock, 2000; Timmreck, 2012; Zambri *et al.*, 2017). There are disagreements as to how well climate models can simulate winter warming; for instance, some report that climate models (including CMIP5 models) are unable to accurately simulate winter warming as they simulate a weaker and less significant warming (Timmreck, 2012; Driscoll *et al.*, 2012; Zambri *et al.*, 2017). However, others suggest that CMIP5 models do accurately simulate NH winter warming (Zambri and Robock, 2016), and that they also accurately simulate the strengthening of the polar vortex (Barnes *et al.*, 2016). For the SH, winter warming has not been widely researched, and was suggested that it does not occur due to the absence of land in the mid- to high latitudes (Robock and Mao, 1992). As such, this PhD confirms (based on model outputs) that no significant positive temperature anomalies occur over continental SH regions following several relatively recent major volcanic eruptions. However, models suggest that there may have been warming over SH oceans at high latitudes, but this was not explored in the PhD, as only terrestrial temperatures were considered. Warming in the NH mostly occurs during boreal winters, yet in the SH, austral winter is when CMIP5 models show strongest seasonal cooling. Given that the regions studied in this PhD are located at low to mid- latitudes, and the fact that CMIP5 models have likely overestimated cooling of surface temperatures, it is unsurprising to find an absence of warming in CMIP5 model outputs. Despite CMIP5 not showing significant warm anomalies, reanalysis data show some (to a small extent) significant positive temperature departures. Significantly positive seasonal anomalies occur at a continental scale over southern South America during JJA (+0.78°C) and SON (+0.82°C) of 1905 (y3 post Santa Maria) and during MAM (+0.98°C) of 1994 (y3 post Pinatubo). While no significant positive anomalies are recorded over Australia at the continental investigative scale, reanalysis data show that at a smaller sub-regional scale, significant positive anomalies occur during 1994 over three regions: south western coast (annual av= 1.44°C), central western coast (annual av= 1.42°C) and the north western coast (1.81°C). Positive anomalies also occur over the eastern subcontinent during SON of 1965 (1.56°C), and along the east coast during JJA of 1886 (1.67°C; y3 post Krakatau) and during SON of 1965 (1.54°C; y2 post Agung). There are not sufficient positive anomalies to conclude a confirmed pattern of positive temperature responses following such major volcanic eruptions over the SH. However, given occasional strong positive responses at downscales levels of investigation, this warrants more detailed future work.

Of the eight eruptions analysed in Chapter 2, four are found to have produced significant negative temperature departures. These four eruptions (Krakatau, 1883; Santa Maria, 1902; Agung, 1963; Pinatubo, 1991) became the central focus for the remainder of the PhD. Of these four eruptions, Krakatau produces the strongest and longest lasting response at each location, while the strength and length of responses following the other eruptions would change by region. Interestingly, while a significant NH response (−0.27°C) to the El Chichón (1982) eruption is simulated, a negligible response is simulated for the SH (-0.08°C). In general, responses were found to be stronger between 10°S and 30°S, and weaker at higher latitudes, potentially due to the absence of large land masses at high latitudes. SH temperature responses were compared to NH responses, and it was found that SH responses were weaker than NH responses (av difference= 0.07°C), which is in agreement with earlier scientific findings (e.g. Neukom *et al.*, 2014; Monerie *et al.*, 2017). The greatest difference between temperature responses was following the Krakatau eruption (av difference= 0.14°C). The PhD also found that SH temperatures begin to cool (1-2 months) before those in the NH, although negative departures only become significantly cooler ~1-2 months after those in the NH temperatures. Negative SH temperature departures also reach their peak (4–6 months) before NH departures, with peak cooling occurring between 6-15 months in the SH and between 12 to 21 months in the NH. This is in agreement with previous findings, as global temperatures are said to generally reach their peak cooling within 7-18 months after an eruption (Wigley *et al.*, 2005), with European temperatures taking up to 2 years to reach their peak (Esper *et al.*, 2013). The huge expanse of SH oceans causes the regulation of temperatures in this hemisphere, which likely results in weaker, and shorter-lived responses (Joseph and Zeng, 2011; Raible *et al.*, 2016). Eruptions that impacted SH temperatures significantly had occurred in the tropics and had emitted more than

3 Tg of SO_2. While weakest SH cooling was found to occur during austral spring, strongest SH cooling is typically observed during austral autumn or winter, which coincides with summer cooling over the NH (Schneider *et al.*, 2009; Timmreck, 2018).

2.2 Intercontinental comparison

A second objective was "to study and compare SH continental temperature responses" for the four eruptions identified as making an impact on SH temperatures in Chapter 2 (Krakatau-1883, Santa Maria-1902, Agung-1963 and Pinatubo-1991). In order to do this, temperature responses were studied at a continental scale, and the responses for southern South America (SSA), southern Africa (SAF) and Australia compared to each other (Chapter 3). It is found that responses occur earliest (5-month average) and seasonal maximums are strongest over Australia, while responses are most delayed (9-month average) and seasonal maximums weakest over SSA. There are also a greater number of significant monthly anomalies over Australia, and least so over SSA. It is proposed that Australia's temperatures may respond earlier and be stronger (i.e. cooler) due to the continent being relatively flat compared to that of SSA. The continent is thus more susceptible to circulation changes that result from volcanic forcing, such as the impacts on the Southern Annular Mode (SAM) and frontal systems (Power *et al.*, 1999; Meneghini *et al.*, 2007; Crimp *et al.*, 2018). In contrast weather conditions over the SSA continent are modulated to a considerable extent by topography, in particular, a large portion of the continent is to some extent shielded from atmospheric circulation by the Andes mountain range (Insel *et al.*, 2010). Volcanic forcing can affect the SAM (Roscoe and Haigh, 2007; Barnes *et al.*, 2016) as well as cyclogenesis (Picas and Grab, 2020), which to an extent, is likely impacted (spatially) due to such atmospheric blocking by the Andes.

A further notable finding from the PhD is that even though the three continents occupy similar latitudes, the responses vary considerably at comparable latitudes. While no strong latitudinal pattern is observed over Australia, responses were strongest between 20-30°S over SAF, possibly due to cold fronts reaching further into the continent (Tyson *et al.*, 2000). Responses were strongest between 0- 25°S over SSA, possibly given that more southern regions are shielded by the Andes, and/or perhaps by an increased occurrence or intensity of cold surges reaching these latitudes. Cold surges are a result of anticyclones over southern Argentina intensifying and the cold mid-latitude air being forced equatorward, sometimes reaching as far as the tropics (Vera and Vigliarolo, 2000; Garreaud, 2001; Espinoza *et al.*, 2013). Cold surges over SSA can cause frost and freezing temperatures in Brazil, with consequent damage to crops (Vera and Vigliarolo, 2000; Espinoza *et al.*, 2013). The cold surges also bring dryer air (Garreaud, 2001), which could explain why there was an unusual drought in Brazil in 1817, soon after the Tambora (1815) eruption.

2.3 Sub-regional responses

A third and fourth objective was "to observe and compare sub-regional southern African [and Australian] temperature responses following the eruptions of Krakatau (1883), Santa Maria (1902), Agung (1963) and Pinatubo (1991)". The southern African and Australian continents were sub-divided into sub-regions, to investigate how responses might vary at smaller spatial scales (Chapter 4). To this end, greater variance in the strength and timing of the responses is found. For instance, when investigating seasonal responses at a larger hemispheric or continental scale, stronger responses usually occur during austral autumn and winter, and weakest responses during austral spring. However, this is not the case for all sub-regions. For instance, in southern African sub-regions, while all regions demonstrate strongest responses during either austral autumn or winter, the weakest response is measured in austral spring in only three out of the six regions. The western and central subcontinental regions experience weakest responses during DJF and the Eastern Cape coast during MAM. Over the Australian sub-continent, eastern regions record the strongest responses during austral autumn and the weakest responses during spring. However, less of a pattern is observed for western regions. The strongest cooling in either austral autumn or winter coincides with the summer cooling experienced over the NH (e.g. Esper *et al.*, 2013). One should thus plan for much colder than normal autumn/winter seasons in the SH following major tropical eruptions, particularly for the agricultural sector.

The strength (i.e. extent of temperature departure) of volcanic responses also vary between sub-regions of Africa and Australia. Over both African and Australian sub-regions, stronger responses are measured over more northern than southern sub-regions. While no given region always experiences the strongest response after every eruption, when examining the weakest responses, there is indeed a sub-region that typically (always) records weakest responses. For southern African sub-regions, weakest responses occur over the Eastern Cape coast, and for Australian sub-regions, Tasmania records weakest responses, possibly due to both regions being flanked by their respective oceans, and their climate being regulated more so than other regions which have a stronger continental climatic component (Joseph and Zeng, 2011). The timing of responses also changes between sub-regions. For instance, over African sub-regions, the central subcontinental region reaches maximum response soonest (12 month average) after a major eruption, while the Eastern Cape coast records the most delayed response (21 month average), while other sub-regions reach their peak response ~17 months post eruption date. The central subcontinent is the only southern African sub-region not bordered by an ocean, whereas most of the Eastern Cape coast sub-region is oceanic in character. Continentality of the CSub region may explain why it experiences a faster post-volcanic climate response compared to other sub-regions which are bordered by an ocean, and hence which experience a more delayed response time (Joseph and Zeng, 2011; Kruger and Sekele, 2013).

A 3-year global cooling of -0.05°C followed the eruption of Mount Agung (Ménégoz *et al.*, 2018). However, most of the cooling occurred in the SH, as the aerosol cloud mostly remained in the SH (Sato *et al.*, 1993; Ménégoz *et al.*, 2018). Despite the eruption being smaller than the other three main eruptions studied in this PhD (VEI 4), the CMIP5 ensemble used in this PhD indicates that it caused significant temperature cooling over the SH (3-year av= -0.15°C). When considering temperature responses at hemispheric scale, departures following Agung are weakest (-0.15°C) out of all the eruptions, and at a continental scale the responses are also weakest following Agung over SSA (-0.12°C) and SAF (-0.19°C), and second weakest over Australia (-0.20°C; with the weakest response following Santa Maria in Australia). Despite this weak response observed at a continental scale over Australia, some Australian sub-regions (SWE, CWC, CEC, Victoria, NWC and EAC) had their strongest annual response for those respective regions follow y1 (i.e. 1964) after Agung, despite the Krakatau eruption emitting considerably more SO_2, and both eruptions occurring in close proximity to each other (Indonesia). However, the Agung eruption occurred before winter (March) and Krakatau at the end of winter (August), so perhaps the more favourable transportation of aerosols aided the stronger response over the nearby continent of Australia (Perlwitz and Graf, 1995; Birner and Bönisch, 2010; Young *et al.*, 2011).

Also of notable interest is that over the Australian sub-regions of EAS and EAC, temperature departures in the third post-eruption year are stronger than responses in the second post-eruption year for all eruptions except Agung. This is also noted for the southern African sub-regions of the South Western Cape and Eastern Cape Coast, after Krakatau and Pinatubo. This y3 cooling may be a result of a La Niña event, which might follow an eruption 3-5 years later, as proposed by Wahl *et al.,* (2014) and Maher *et al.* (2015). However, when examining responses at a continental scale, responses become masked and such a finding not recorded. The fact that responses vary at continental scales and even more so at sub-regional scales, highlights the importance of studying the responses at various spatial and temporal scales, and particularly at downscaled levels. This PhD also accentuates the importance of investigating responses to volcanic eruptions individually, and not only as an ensemble of many eruptions, given that responses differ between eruptions. This is best demonstrated in the super-posed epoch analysis (SEA) images in Chapter 2 (Figure S3) where the SEA is undertaken in two ways: – firstly with all eight eruptions originally studied, and secondly using only the four main eruptions (Krakatau, Santa Maria, Agung and Pinatubo). The response is much greater where only the four main eruptions are used, as opposed to eight eruptions. The risk of using an ensemble of the responses is that unique or unusual responses could be missed, and the enormity of a response may be dampened by smaller (less or insignificant) responses.

2.4 Expectations from future eruptions

Understanding how SH climate is affected by volcanic forcing can contribute towards mitigating risk such as damage to crops, livelihoods and even human life. For instance, it is estimated that over 71 000 people lost their lives following the mega-colossal Toba eruption (VEI 8; ca. 74000 years ago; Oppenheimer, 2003). The PhD results can help predict how SH temperatures may react, following future eruptions of similar kind to the eruptions studied here (tropical, emitting more than 3.8 Tg SO_2). For instance, the CMIP5 ensemble in this PhD indicates which seasons are likely to respond with stronger cooling (either MAM or JJA in most regions of the SH), which continent is expected to have an earlier and stronger response (Australia), or a later and weaker response (southern South America). However, the strength and timing of the responses unquestionably depends on many factors such as the location and magnitude of the eruption, and time of year during which the eruption occurred (e.g. Oman *et al.*, 2005; Colose *et al.*, 2015; Predybaylo *et al.*, 2017; Stevenson *et al.*, 2017; Zuo *et al.*, 2018; Krishnamohan *et al.*, 2019; Sun *et al.*, 2019). Based on the eruptions studied in this PhD, if a major tropical eruption emits at least 3.8 Tg of SO_2 into the lower stratosphere, a temperature response can be expected to occur over the SH, however, if the eruption occurs during the SH autumn or winter (MAM or JJA), it is likely to cause a stronger SH temperature response. This is due to more favourable atmospheric circulation for the transportation of volcanic aerosols in the SH, in association with the Brewer-Dobson circulation (Perlwitz and Graf, 1995; Birner and Bönisch, 2010).

2.5 Reliability of CMIP5 models

The main focus of this PhD was to use CMIP5 models to explore SH temperature responses, but a secondary aim was to “establish the relative reliability of CMIP5 model data outputs in depicting temperature responses to volcanic eruptions through a comparison with instrumental temperature records and reanalysis data". CMIP5 models and reanalysis data do not always agree. In some cases, it seems that CMIP5 models over-exaggerated the temperature response to volcanic forcing (as discussed in Chapter 5, e.g. Driscoll et al., 2012; Barnes et al., 2016; McGraw et al., 2016), which seems to be particularly true for the continental (or macro-scale) temperature responses (Table 1), where majority of the CMIP5 temperature anomalies are cooler than the reanalysis anomalies. On average, CMIP5 anomalies are 0.30°C cooler than the reanalysis anomalies. There is a greater difference in the SSA region (CMIP5 0.39°C cooler on average), followed by the SAF region (CMIP5 0.27°C cooler on average) and then Australia (CMIP5 0.24°C cooler on average). The greatest differences between CMIP5 and 20CRv2 follows the Krakatau and Pinatubo eruptions (CMIP5 0.37°C cooler on average for both eruptions), then the Santa Maria eruption (CMIP5 0.30°C cooler on average), and lastly the Agung eruption (CMIP5 0.15°C cooler on average). The differences between 3-year (y1-y3 after an eruption) averages per region and per eruption is greatest following the Santa Maria eruption in the SSA region (CMIP5 0.68°C cooler), and weakest after the Agung eruption in the SAF region (0.00°C). Comparing seasonal averages shows that the greatest differences between CMIP5 and 20CRv2 occurs during austral autumn (CMIP5 0.39°C cooler on average), which is when the CMIP5 results show the strongest responses occur in the SH. The smallest difference occurs during austral spring (CMIP5 0.14°C cooler on average) with average SON CMIP5 anomalies actually being warmer (by 0.09°C) than the reanalysis data following the Agung eruption.

However, when examining responses at a downscaled (i.e. sub-regional) level, reanalysis data more frequently show stronger negative temperature anomalies when compared with CMIP5 outputs. For instance, for Australian sub-regions (Table 2), CMIP5 anomalies seem to be mostly cooler than the reanalysis anomalies for the earlier two eruptions, especially over regions of CEC, Vic, EAS and EAC, but not for the latter two eruptions when the 20CRv2 temperature anomalies are generally lower than CMIP5 values, especially over regions of SWE, CWC, Tas and NWC. However, it needs to be acknowledged that comparing the CMIP5 responses to station/observation data is complicated due to the station data being point data (i.e. for a specific locality), while CMIP5 data represent average conditions over large areas (several 1000s km^2). However, record low temperatures from observational data suggest that extreme cooling events did indeed followed such major eruptions. For example, record lows for Victoria on 15 June 1965 (−11.7°C), Queensland on 12 July 1965 (−10.6 °C), and New South Wales on 29 June 1994 (−23.0 °C) (Australian Government, Bureau of Meteorology, 2019). In summary, while the CMIP5 model outputs seems to broadly provide an accurate temperature pattern, I would caution that numeric values need to be held lightly. However, comparing the CMIP5 responses to both reanalysis data and station/observational data has proven valuable, particularly in identifying where they are in agreement, but also where they differ most strongly. Such similarities and differences can thus assist in establishing confidence levels.

The over-estimation seen in the CMIP5 models is likely due to the climate models not simulating the internal variability accurately (Barnes *et al.*, 2016; McGraw *et al.*, 2016). Neither do these models accurately simulate the removal or redistribution process of the aerosols (Dhomse *et al.*, 2020), and may be further limited given their inaccurate parameterization of the relationship between aerosols and ice, and mixed phase clouds (Chylek *et al.*, 2020). To aid solving these issues, recent modifications to the models have yielded the release of CMIP6 (not used in this thesis given it recent release). One such initiative was to have a common volcanic forcing dataset that all models use, with the hope to help decrease uncertainty between models. The volcanic forcing dataset combines two datasets, one pre satellite era (1850-1979: a 2-D interactive stratospheric aerosol model; Arfeuille *et al.*, 2014) and one post satellite era (1979-onwards: the Global Space-based Stratospheric Aerosol Climatology; Thomason et al., 2018). It is currently the best volcanic forcing dataset available, so CMIP6 may be the best set of climate models to use for future studies, until again further improvements are made (Dhomse *et al.*, 2020).

Table 1. Difference between 20CRv2 and CMIP5 temperature anomalies, for the continents of Australia, southern Africa and southern South America. Blue colours indicate where the 20CRv2 anomalies are cooler than the CMIP5 temperature anomalies, and red colours indicate where the 20CRv2 anomalies are warmer than the CMIP5 anomalies. The darker the colour, the greater the difference.

		AUS- Australia					SAF- Southern Africa					SSA- Southern South America				
	Year	Annual	DJF	MAM	JJA	SON	Annual	DJF	MAM	JJA	SON	Annual	DJF	MAM	JJA	SON
Krakatau	1884	0.51	0.35	0.54	1.06	0.44	0.32	0.70	0.55	-0.04	0.26	0.33	0.26	0.14	0.73	0.18
	1885	0.65	0.38	0.26	1.04	0.04	0.33	0.32	0.34	0.34	0.30	0.26	0.19	0.08	0.05	0.60
	1886	0.14	0.39	0.03	1.05	-0.21	0.49	0.60	0.84	0.13	0.44	0.22	0.53	0.31	0.13	0.10
Santa Maria	1903	0.24	0.16	0.38	0.48	0.32	0.23	0.38	0.69	0.06	-0.11	0.67	0.79	0.62	0.75	0.69
	1904	-0.03	-0.53	0.00	-0.32	0.25	0.07	-0.11	-0.22	0.26	0.31	0.56	0.23	0.33	0.57	0.96
	1905	-0.17	0.32	0.16	-0.48	-0.50	0.33	0.28	0.18	0.58	0.24	0.79	0.71	0.62	0.95	0.91
Agung	1964	0.40	0.36	0.85	0.94	-0.13	-0.07	0.74	0.32	-0.33	-0.82	0.16	0.76	0.58	-0.29	-0.20
	1965	0.57	0.51	0.43	0.24	0.78	-0.24	-0.11	-0.40	-0.17	-0.32	0.18	0.06	-0.17	0.27	0.33
	1966	-0.29	-0.22	0.03	-0.16	-0.46	0.28	0.29	0.23	0.62	-0.06	0.22	0.50	0.27	0.28	0.03
Pinatubo	1992	-0.18	-0.09	0.64	0.28	-1.20	0.32	0.78	0.69	-0.01	0.01	0.14	0.29	0.30	-0.03	-0.04
	1993	-0.07	-0.49	0.51	0.22	-0.44	0.27	0.13	0.49	0.09	0.27	0.46	0.56	0.54	0.27	0.43
	1994	1.00	0.99	0.80	0.63	0.81	0.80	0.85	0.88	0.73	0.71	0.74	0.86	1.19	0.44	0.22

Table 2. Difference between 20CRv2 and CMIP5 temperature anomalies, for the subregions of Australia. Blue colours indicate where the 20CRv2 anomalies are cooler than the CMIP5 temperature anomalies, and red colours indicate where the 20CRv2 anomalies are warmer than the CMIP5 anomalies. The darker the colour, the greater the difference.

		SWE					CWC					CEC					Victoria				
		Annual	DJF	MAM	JJA	SON	Annual	DJF	MAM	JJA	SON	Annual	DJF	MAM	JJA	SON	Annual	DJF	MAM	JJA	SON
Krakatau	1884	-0.03	-0.29	0.67	0.32	-0.22	0.25	0.45	0.72	0.79	0.10	0.62	0.02	0.94	1.37	0.76	0.40	-0.39	0.72	1.29	0.37
	1885	0.22	-0.97	0.24	0.76	-0.36	0.40	-0.90	0.07	0.84	-0.23	1.06	0.47	0.05	1.17	0.44	0.75	0.56	0.20	0.76	0.17
	1886	0.00	0.30	0.46	0.58	-0.91	0.05	0.85	0.31	0.86	-0.61	0.08	0.70	0.09	1.49	-0.57	0.08	0.43	-0.26	1.24	-0.15
Santa Maria	1903	0.03	-0.29	-0.30	0.41	0.10	0.16	0.36	-0.08	0.31	0.19	0.31	-0.09	0.83	0.27	0.87	0.46	-0.14	0.85	0.26	1.22
	1904	0.40	0.04	0.61	-0.01	1.04	0.36	-0.09	0.52	-0.20	0.84	0.44	-0.44	0.98	-0.32	0.35	0.38	-0.04	0.94	-0.10	-0.02
	1905	-0.15	-0.48	-0.24	-0.24	0.26	-0.18	0.12	-0.41	-0.45	0.24	-0.27	1.06	0.10	-0.63	-1.02	-0.32	0.76	0.10	-0.33	-1.25
Agung	1964	-0.42	-0.28	0.01	0.56	-1.46	-0.40	-0.59	-0.22	0.65	-0.82	-0.08	-0.24	0.42	0.86	-0.05	-0.29	-0.52	0.10	0.32	-0.02
	1965	0.00	0.00	0.33	0.09	-0.87	0.40	0.35	0.23	0.13	-0.01	0.68	-0.71	0.37	0.07	1.29	0.07	-1.22	-0.30	0.05	0.51
	1966	-0.50	-0.73	-0.56	-0.26	-0.51	-0.35	-0.13	-0.13	-0.33	-0.38	-0.39	0.42	-0.26	-0.58	-0.23	-0.34	-0.10	-0.09	-0.60	-0.06
Pinatubo	1992	-0.59	-0.05	-0.86	0.30	-1.55	-0.49	0.41	-0.39	0.22	-1.74	-1.00	-1.41	0.13	-0.09	-2.39	-0.84	-1.51	0.12	-0.30	-1.84
	1993	-0.49	-0.48	-0.77	-0.44	-0.59	-0.25	0.04	-0.33	-0.55	-0.36	-0.11	-0.52	0.50	0.36	-0.47	-0.09	0.01	0.11	0.46	-0.41
	1994	1.61	-0.01	2.60	1.59	1.60	1.63	0.06	2.86	1.66	1.27	0.90	-0.58	0.81	1.17	0.63	0.81	-0.09	0.64	1.10	0.33

		Tasmania					NWC					EAS					EAC				
		Annual	DJF	MAM	JJA	SON	Annual	DJF	MAM	JJA	SON	Annual	DJF	MAM	JJA	SON	Annual	DJF	MAM	JJA	SON
Krakatau	1884	0.08	-0.32	0.38	0.58	-0.35	-0.04	-0.08	0.52	0.22	-0.24	0.80	0.51	0.20	1.58	0.86	0.88	1.13	0.11	1.32	0.76
	1885	0.18	0.28	0.13	0.21	-0.06	0.32	-0.54	0.23	1.11	-0.63	0.75	1.03	0.59	1.14	0.06	0.70	1.37	0.76	0.90	-0.05
	1886	0.25	0.17	-0.18	0.82	0.37	0.11	-0.15	0.53	0.58	-0.29	0.15	0.28	-0.11	1.98	-0.68	0.29	0.54	0.01	1.92	-0.72
Santa Maria	1903	0.09	-0.18	0.13	-0.12	0.54	-0.12	-0.67	0.08	0.61	-0.52	0.46	0.87	0.82	0.54	0.27	0.52	1.14	1.01	0.50	0.09
	1904	0.05	0.51	0.35	-0.21	-0.21	-0.08	-0.58	0.27	-0.27	0.17	0.03	-0.24	-0.39	-0.51	0.67	0.00	0.04	-0.21	-0.49	0.39
	1905	-0.38	-0.37	-0.22	-0.14	-0.74	-0.46	-0.54	-0.43	-0.32	-0.42	-0.07	0.97	1.06	-0.77	-1.04	-0.24	0.62	0.76	-0.79	-1.04
Agung	1964	-0.44	-0.85	-0.41	-0.52	0.02	-0.18	0.02	0.34	0.36	-1.05	0.92	0.82	1.70	1.31	0.38	0.73	0.84	1.17	0.78	0.15
	1965	-0.45	-0.69	-0.52	-0.33	-0.39	0.01	0.15	0.71	0.15	-0.99	0.93	0.40	0.86	0.47	1.65	0.68	0.12	0.79	0.35	1.65
	1966	-0.29	-0.29	-0.33	-0.48	-0.06	-0.83	-1.37	-0.55	-0.79	-0.93	-0.30	-0.22	-0.23	-0.16	-0.37	-0.31	-0.32	-0.18	-0.42	-0.36
Pinatubo	1992	-0.17	-0.31	0.18	-0.45	-0.35	-0.80	-0.86	-0.83	0.21	-1.62	-0.37	-0.15	0.66	-0.37	-1.36	-0.56	-0.17	-0.04	-0.40	-1.31
	1993	0.22	0.80	0.47	0.07	-0.08	-0.56	-0.78	-0.40	-0.58	-1.11	0.22	0.03	0.70	0.66	-0.17	0.21	0.01	0.41	0.69	-0.25
	1994	0.46	0.31	0.40	0.56	0.33	2.04	1.39	2.46	2.06	1.87	1.35	1.70	0.80	0.89	0.99	1.47	2.15	0.69	0.98	1.51

While CMIP5 models have received much criticism (e.g. Driscoll *et al.*, 2012; Gillett *et al.*, 2013; Jones *et al.*, 2013), there is also much uncertainty associated with the use of reanalysis data (e.g. Borsche *et al.*, 2015; Dhomse *et al.*, 2020). Reanalysis datasets are a combination of several different datasets. The datasets include an assimilation of observational data (e.g. weather stations, satellites, radiosondes etc.) and data from climate models which then provide an estimate of climatic conditions (Compo *et al.*, 2011). The various reanalysis datasets are left with errors themselves, depending on the dataset, such as incorrect representation of variability over Antarctica and the tropics, or of storm tracks (Newman *et al.*, 2000; Hodges *et al.*, 2003; Bromwich and Fogt, 2004; Compo *et al.*, 2011). The 20CRv2 dataset used, seems to acceptably represent SH circulation between 1979 and 2010, during which time numerous observational data also become available. However, prior to this, climate models are more heavily relied upon and the dataset is thus less accurate (Ke and Hui, 2013; Zhang *et al.*, 2013).

Uncertainties also exist with station based instrumental data. For example, while satellite data are able to capture the dispersion of the aerosols following an eruption, they are unable to capture the extent of the stratospheric aerosol cloud following an eruption, which is true even for the most recent eruption of Pinatubo, and for which there was much available observational and satellite data. The actual cooling from the Pinatubo eruption, even with all the available data, is still unclear (Dhomse *et al.*, 2020). Studying climate before 1979 proves to be even more complicated as fewer instrumental data are available, especially for the SH where such records are generally scarce over large areas (Brönnimann *et al.*, 2019; Dätwyler *et al.*, 2020). Climate proxies are continuously being used to reconstruct SH climate (e.g. Patrut *et al.*, 2015; Jara *et al.*, 2017; Lavergne *et al.*, 2017; Allen *et al.*, 2018), such that ever more climate reconstructions are becoming available. This will become immensely valuable to further identify potential climatic effects from volcanic eruptions. Thus, there is still much scope for refined/improved investigations into understanding, detecting and attributing volcanic forcing effects on climates of the SH. To have a perfect climate modelling system is currently an unrealistic expectation. Notwithstanding the criticism of the CMIP5 models, the fact remains that climate models are the best tools for detection and attribution of studies such as this PhD, where historical climate can be studied and variations between experiments and responses attributed to different climate forcers (Hegerl and Zwiers, 2011; Dhomse *et al.*, 2020).

3. Future Work

Exploring atmospheric dynamics associated with volcanic forcing was not the aim of this PhD study, but rather the focus was to fill a research gap of knowledge concerning the quantification of temperature responses to such forcing. To this end, much work lies ahead to establish such dynamics and climate feedbacks affecting SH climates during post eruption years. A better understanding of the dynamics involved would serve an important role to future model developers so that models incorporate the correct and necessary mechanisms they should.

This PhD study focussed specifically on temperature responses to volcanic forcing, due to the importance of understanding how temperatures respond to volcanic forcing in order to better prepare socio-economic situations for future eruptions. However, other very important climate variables such as wind and precipitation urgently need research attention too. Again, wide attention has been given to global scale and NH response to various climate variables, such as sea surface temperatures, wind, sea level pressure and precipitation, with many studies combining all or some of these variables (e.g. Schneider *et al.*, 2009; Zanchettin *et al.*, 2012; Barnes *et al.*, 2016; McGraw *et al.*, 2016; Khodri *et al.*, 2017). However, little is known is such regard concerning the SH. For instance, several studies have examined the effect of volcanic forcing on precipitation at the global (e.g. Iles and Hegerl, 2014; Liu *et al.*, 2018) and NH (e.g. Rao *et al.*, 2017) scale. In addition, there have been more focussed investigations on the impacts such eruptions have on the Asian and African monsoons (e.g. Oman *et al.*, 2006; Man *et al.*, 2014) and over parts of South America (Colose *et al.*, 2015, 2016). Given the paucity of information on how volcanic forcing affects precipitation over much of the SH, this is something that needs priority attention. Climate has a strong impact on socio-economic sectors, especially in Africa where, in particular, rural subsistence economies are very dependent on the weather. Hence, understanding the magnitude and timing of extreme hydrological responses to volcanic forcing is of particular importance and should be a future research priority for the SH and continental sub-regions of the South.

When the current PhD was initiated, CMIP5 was the latest group of climate models available, but that has now been superseded by version 6 (CMIP6; Eyring *et al.*, 2016). CMIP5 has left uncertainties of how well it models the climatic effects of volcanic forcing, and hence attempts have been made to improve the capabilities of CMIP6 to address some of these shortcomings (Dhomse *et al.*, 2020; Rieger *et al.*, 2020). It would be valuable and necessary to critically establish the potential accuracy of CMIP6, and quantify its improved performance over that of CMIP5, especially if CMIP6 is to be used for the immediate future. For instance, it would be beneficial to test if the CMIP6 models no longer overestimate the temperature response, and if the recommendation to use the same volcanic forcing dataset has improved output accuracy. Should CMIP6 models prove to accurately simulate the response to volcanic forcing, then such models could be used to re-evaluate some of the downscaled initiatives undertaken for this PhD for a more improved output.

Chapter 4 focussed on southern African sub-regions, but did not compare the data with station or reanalysis data across all sub-regions or following each eruption. Clearly, this is a necessary next-step for the region in order to better understand the impacts on the region and to test the reliability of the results shown by the CMIP5 ensemble. In addition, while Colose *et al.* (2015, 2016) investigated climatic responses in South America, a sub-regional analysis for this region is also still required in a similar manner, as has been undertaken for the southern African and Australian regions. In particular, a comparison between the climatic response at different latitudes would be most interesting as the continent covers such a vast latitudinal area, and is impacted by different internal climate variables such as the SAM, westerlies and easterlies etc. The Antarctic and southern Ocean regions are worthy almost of another PhD level analysis, given their considerable impact on climate dynamics of the SH. The CMIP5 ensemble used in this study indicated a cooling over the Antarctic continent, perhaps even stronger than that observed over southern Africa, southern South America and Australia (See Figure 4 from Chapter 3 and Figure S1, S2 and S3 in Chapter 3's Supplementary Document). Given the great expanse of SH oceans, and their influence on regulating SH climate, a particular focus of future research should entail the impact of volcanic eruptions on SH SSTs and consequential feedback mechanisms. This is particularly important in the context of oceans maintaining a cooling signal for many more years than is reflected in terrestrial air temperature records (Gleckler *et al.*, 2006b, 2006a), with oceans then regulating terrestrial temperatures and also providing for potentially multi-decadal climate impacts (Raible *et al*., 2016).

The PhD used historical documents to identify any unusual or extreme weather events. Several interesting quotes were found, such as for example following the Krakatau eruption of a snow storm in March 1886 over Moss Vale New South Wales, Australia, during March 1886 - termed “quite a phenomenon at the present time of year” (Newcastle Morning Herald and Miners’ Advocate, 15 March 1886, Pg. 5). Another “unusual sight of snow in October” (Goulburn Evening Penny Post, 26 October 2886, Pg. 2) occurred in Goulburn, NSW, Australia in 1886. Following the Santa Maria eruption, temperatures in July 1903 for Adelaide, Australia were “the lowest since observations were first taken in 1856” (The Brisbane Courier, 14 Jul 1903, Pg. 5). “Extreme cold and rain” also fell in North Western Tasmania a year later, and the depth of snow was said to be “to a greater depth than had occurred before in the memory of old inhabitants” (The North Western Advocate and the Emu Bay Times, 18 July 1904, Pg. 3). Records such as these from historical documents may complement instrumental and model data, and prove to be invaluable to help verify the impacts of volcanic eruptions on climates of the SH, but in addition can also reveal the impact such events had on the livelihoods of people, particularly in the periods before instrumental records were available. Thus, a potential avenue to explore would be to thoroughly use historical documents (among other climate proxies) to further identify climatic responses, and possibly also socio-economic consequences, following major eruptions.

Eruptions of greater magnitude than those studied in this PhD have occurred in the past, for example Tambora (VEI 7; 1815) and Toba (VEI 8; ca. 74000 years ago). Both these eruptions are thought to have greatly impacted global climate and society (e.g. Ambrose, 2003; Gathorne-Hardy and Harcourt-Smith, 2003). For instance, it has been proposed that the Toba event may have caused a volcanic winter that destroyed human populations over large parts of the world (Ambrose, 2003; Gathorne-Hardy and Harcourt-Smith, 2003). In the case of Tambora, the year 1816 became known as 'the year without a summer' due to an exceptionally cool summer over much of western Europe (Kandlbauer *et al.*, 2013), but also impacted Asian monsoon strength, the Atlantic hurricane season, and increased temperatures over the Atlantic (Chenoweth, 1996). Tambora also (indirectly) affected human livelihoods through ensuing droughts (e.g. Brazil: Chenoweth, 1996) and caused food shortages, malnutrition and loss of human lives due to decreased harvests in Europe (Oppenheimer, 2003; Luterbacher and Pfister, 2015). The impact of such eruptions on the SH, perhaps also from a socio-economic perspective, deserves (more) attention, particularly as there are already suggestions that the human population in South Africa thrived during the time of the Toba eruption, while other human populations perished (Smith *et al.*, 2018). Future studies could involve modelling the climatic effects of these eruptions, but also explore historical documents where these are available for given time-periods, which can help improve our understanding on how past major eruptions impacted human life in the SH.

4. References

Allen KJ, Cook ER, Evans R, Francey R, Buckley BM, Palmer JG, Peterson MJ, Baker PJ. 2018. Lack of cool, not warm, extremes distinguishes late 20th Century climate in 979-year Tasmanian summer temperature reconstruction. Environmental Research Letters, 13(3): 034041. https://doi.org/10.1088/1748-9326/aaafd7.

Ambrose SH. 2003. Did the super-eruption of Toba cause a human population bottleneck? Reply to Gathorne-Hardy and Harcourt-Smith. Journal of Human Evolution, 45(3): 231–237. https://doi.org/10.1016/j.jhevol.2003.08.001.

Australian Government, Bureau of Meteorology. 2019. Rainfall and Temperature Extremes. Bureau of Meteorology. Accessed 03/04/2021. <http://www.bom.gov.au/climate/extreme/records.shtml>

Barnes EA, Solomon S, Polvani LM. 2016. Robust wind and precipitation responses to the Mount Pinatubo eruption, as simulated in the CMIP5 models. Journal of Climate, 29(13): 4763–4778. https://doi.org/10.1175/JCLI-D-15-0658.1.

Birner T, Bönisch H. 2010. Residual circulation trajectories and transit times into the extratropical lowermost stratosphere. Atmospheric Chemistry and Physics Discussions, 10(7): 16837–16860. https://doi.org/10.5194/acpd-10-16837-2010.

Borsche M, Kaiser-Weiss AK, Undén P, Kaspar F. 2015. Methodologies to characterize uncertainties in regional reanalyses. , 12.

Bromwich DH, Fogt RL. 2004. Strong Trends in the Skill of the ERA-40 and NCEP–NCAR Reanalyses in the High and Midlatitudes of the Southern Hemisphere, 1958–2001. Journal of Climate. American Meteorological Society, 17(23): 4603–4619. https://doi.org/10.1175/3241.1.

Brönnimann S, Allan R, Ashcroft L, Baer S, Barriendos M, Brázdil R, Brugnara Y, Brunet M, Brunetti M, Chimani B, Cornes R, Domínguez-Castro F, Filipiak J, Founda D, Herrera RG, Gergis J, Grab S, Hannak L, Huhtamaa H, Jacobsen KS, Jones P, Jourdain S, Kiss A, Lin KE, Lorrey A, Lundstad E, Luterbacher J, Mauelshagen F, Maugeri M, Maughan N, Moberg A, Neukom R, Nicholson S, Noone S, Nordli Ø, Ólafsdóttir KB, Pearce PR, Pfister L, Pribyl K, Przybylak R, Pudmenzky C, Rasol D, Reichenbach D, Řezníčková L, Rodrigo FS, Rohr C, Skrynyk O, Slonosky V, Thorne P, Valente MA, Vaquero JM, Westcottt NE, Williamson F, Wyszyński P. 2019. Unlocking Pre-1850 Instrumental Meteorological Records: A Global Inventory. Bulletin of the American Meteorological Society, 100(12): ES389–ES413. https://doi.org/10.1175/BAMS-D-19-0040.1.

Chenoweth M. 1996. Ships' Logbooks and "The Year Without a Summer." Bulletin of the American Meteorological Society, 77(9): 2077–2094. https://doi.org/10.1175/1520-0477(1996)077<2077:SLAYWA>2.0.CO;2.

Chylek P, Folland C, Klett JD, Dubey MK. 2020. CMIP5 climate models overestimate cooling by volcanic aerosols. Geophysical Research Letters, 47(3). https://doi.org/10.1029/2020GL087047.

Colose CM, LeGrande AN, Vuille M. 2015. The influence of tropical volcanic eruptions on the climate of South America during the last millennium. Climate of the Past, 11: 3375–3424. https://doi.org/10.5194/cpd-11-3375-2015.

Colose CM, LeGrande AN, Vuille M. 2016. Hemispherically asymmetric volcanic forcing of tropical hydroclimate during the last millennium. Earth System Dynamics, 7(3): 681–696. https://doi.org/10.5194/esd-7-681-2016.

Compo GP, Whitaker JS, Sardeshmukh PD, Matsui N, Allan RJ, Yin X, Gleason BE, Vose RS, Rutledge G, Bessemoulin P, Brönnimann S, Brunet M, Crouthamel RI, Grant AN, Groisman PY, Jones PD, Kruk MC, Kruger AC, Marshall GJ, Maugeri M, Mok HY, Nordli Ø, Ross TF, Trigo RM, Wang XL, Woodruff SD, Worley SJ. 2011. The Twentieth Century Reanalysis Project. Quarterly Journal of the Royal Meteorological Society. John Wiley & Sons, Ltd, 137(654): 1–28. https://doi.org/10.1002/qj.776.

Crimp S, Nicholls N, Kokic P, Risbey JS, Gobbett D, Howden M. 2018. Synoptic to large-scale drivers of minimum temperature variability in Australia - long-term changes: DRIVERS OF AUSTRALIAN MINIMUM TEMPERATURE VARIABILITY. International Journal of Climatology, 38: e237–e254. https://doi.org/10.1002/joc.5365.

Dätwyler C, Grosjean M, Steiger NJ, Neukom R. 2020. Teleconnections and relationship between the El Niño–Southern Oscillation (ENSO) and the Southern Annular Mode (SAM) in reconstructions and models over the past millennium. Climate of the Past, 16(2): 743–756. https://doi.org/10.5194/cp-16-743-2020.

Dhomse SS, Mann GW, Antuña Marrero JC, Shallcross SE, Chipperfield MP, Carslaw KS, Marshall L, Abraham NL, Johnson CE. 2020. Evaluating the simulated radiative forcings, aerosol properties, and stratospheric warmings from the 1963 Mt Agung, 1982 El Chichón, and 1991 Mt Pinatubo volcanic aerosol clouds. Atmospheric Chemistry and Physics. Copernicus GmbH, 20(21): 13627–13654. https://doi.org/10.5194/acp-20-13627-2020.

Driscoll S, Bozzo A, Gray LJ, Robock A, Stenchikov G. 2012. Coupled Model Intercomparison Project 5 (CMIP5) simulations of climate following volcanic eruptions. Journal of Geophysical Research: Atmospheres, 117(D17): D17105. https://doi.org/10.1029/2012JD017607.

Esper J, Schneider L, Krusic PJ, Luterbacher J, Büntgen U, Timonen M, Sirocko F, Zorita E. 2013. European summer temperature response to annually dated volcanic eruptions over the past nine centuries. Bulletin of Volcanology, 75(7): 736. https://doi.org/10.1007/s00445-013-0736-z.

Espinoza JC, Ronchail J, Lengaigne M, Quispe N, Silva Y, Bettolli ML, Avalos G, Llacza A. 2013. Revisiting wintertime cold air intrusions at the east of the Andes: propagating features from subtropical Argentina to Peruvian Amazon and relationship with large-scale circulation patterns. Climate Dynamics, 41(7–8): 1983–2002. https://doi.org/10.1007/s00382-012-1639-y.

Eyring V, Bony S, Meehl GA, Senior CA, Stevens B, Stouffer RJ, Taylor KE. 2016. Overview of the Coupled Model Intercomparison Project Phase 6 (CMIP6) experimental design and organization. Geoscientific Model Development, 9(5): 1937–1958. https://doi.org/10.5194/gmd-9-1937-2016.

Garreaud RD. 2001. Subtropical cold surges: regional aspects and global distribution. International Journal of Climatology, 21(10): 1181–1197. https://doi.org/10.1002/joc.687.

Gathorne-Hardy FJ, Harcourt-Smith WEH. 2003. The super-eruption of Toba, did it cause a human bottleneck? Journal of Human Evolution, 45(3): 227–230. https://doi.org/10.1016/S0047-2484(03)00105-2.

Gillett NP, Arora VK, Matthews D, Allen MR. 2013. Constraining the Ratio of Global Warming to Cumulative CO2 Emissions Using CMIP5 Simulations. Journal of Climate. American Meteorological Society, 26(18): 6844–6858. https://doi.org/10.1175/JCLI-D-12-00476.1.

Gleckler PJ, AchutaRao K, Gregory JM, Santer BD, Taylor KE, Wigley TML. 2006a. Krakatoa lives: The effect of volcanic eruptions on ocean heat content and thermal expansion. Geophysical Research Letters. John Wiley & Sons, Ltd, 33(17). https://doi.org/10.1029/2006GL026771.

Gleckler PJ, Wigley TML, Santer BD, Gregory JM, AchutaRao K, Taylor KE. 2006b. Volcanoes and climate: Krakatoa's signature persists in the ocean. Nature, 439(7077): 675. https://doi.org/10.1038/439675a.

Hegerl G, Zwiers F. 2011. Use of models in detection and attribution of climate change: Models in detection and attribution of climate change. Wiley Interdisciplinary Reviews: Climate Change, 2(4): 570–591. https://doi.org/10.1002/wcc.121.

Hodges KI, Hoskins BJ, Boyle J, Thorncroft C. 2003. A Comparison of Recent Reanalysis Datasets Using Objective Feature Tracking: Storm Tracks and Tropical Easterly Waves. Monthly Weather Review. American Meteorological Society, 131(9): 2012–2037. https://doi.org/10.1175/1520-0493(2003)131<2012:ACORRD>2.0.CO;2.

Iles CE, Hegerl GC. 2014. The global precipitation response to volcanic eruptions in the CMIP5 models. Environmental Research Letters, 9(10): 104012. https://doi.org/10.1088/1748-9326/9/10/104012.

Insel N, Poulsen CJ, Ehlers TA. 2010. Influence of the Andes Mountains on South American moisture transport, convection, and precipitation. Climate Dynamics, 35(7–8): 1477–1492. https://doi.org/10.1007/s00382-009-0637-1.

Jara IA, Newnham RM, Alloway BV, Wilmshurst JM, Rees AB. 2017. Pollen-based temperature and precipitation records of the past 14,600 years in northern New Zealand (37°S) and their linkages with the Southern Hemisphere atmospheric circulation. The Holocene, 1–13. https://doi.org/DOI: 10.1177/0959683617708444.

Jones GS, Stott PA, Christidis N. 2013. Attribution of observed historical near-surface temperature variations to anthropogenic and natural causes using CMIP5 simulations: ATTRIBUTION OF TEMPERATURES WITH CMIP5. Journal of Geophysical Research: Atmospheres, 118(10): 4001–4024. https://doi.org/10.1002/jgrd.50239.

Joseph R, Zeng N. 2011. Seasonally Modulated Tropical Drought Induced by Volcanic Aerosol. Journal of Climate, 24(8): 2045–2060. https://doi.org/DOI: 10.1175/2009JCLI3170.1.

Kandlbauer J, Hopcroft PO, Valdes PJ, Sparks RSJ. 2013. Climate and carbon cycle response to the 1815 Tambora volcanic eruption. Journal of Geophysical Research: Atmospheres, 118(22): 12,497-12,507. https://doi.org/10.1002/2013JD019767.

Ke F, Hui L. 2013. Evaluation of Atmospheric Circulation in the Southern Hemisphere in 20CRv2. Atmospheric and Oceanic Science Letters, 6(5): 337–342. https://doi.org/10.1080/16742834.2013.11447104.

Khodri M, Izumo T, Vialard J, Janicot S, Cassou C, Lengaigne M, Mignot J, Gastineau G, Guilyardi E, Lebas N, Robock A, McPhaden MJ. 2017. Tropical explosive volcanic eruptions can trigger El Niño by cooling tropical Africa. Nature Communications, 8(1). https://doi.org/10.1038/s41467-017-00755-6.

Krishnamohan K-PS-P, Bala G, Cao L, Duan L, Caldeira K. 2019. Climate system response to stratospheric sulfate aerosols: sensitivity to altitude of aerosol layer. Earth System Dynamics, 10(4): 885–900. https://doi.org/10.5194/esd-10-885-2019.

Kruger AC, Sekele SS. 2013. Trends in extreme temperature indices in South Africa: 1962-2009. International Journal of Climatology, 33(3): 661–676. https://doi.org/10.1002/joc.3455.

Lavergne A, Daux V, Villalba R, Pierre M, Stievenard M, Srur AM. 2017. Improvement of isotope-based climate reconstructions in Patagonia through a better understanding of climate influences on isotopic fractionation in tree rings. Earth and Planetary Science Letters. Elsevier, 459: 372–380. https://doi.org/10.1016/j.epsl.2016.11.045.

Liu F, Zhao T, Wang B, Liu J, Luo W. 2018. Different global precipitation responses to solar, volcanic, and greenhouse gas forcings. Journal of Geophysical Research: Atmospheres, 123(8): 4060–4072. https://doi.org/10.1029/2017JD027391.

Luterbacher J, Pfister C. 2015. The year without a summer. Nature Geoscience, 8(4): 246–248. https://doi.org/10.1038/ngeo2404.

Maher N, McGregor S, England MH, Gupta AS. 2015. Effects of volcanism on tropical variability: EFFECTS OF VOLCANISM. Geophysical Research Letters, 42(14): 6024–6033. https://doi.org/10.1002/2015GL064751.

Man W, Zhou T, Jungclaus JH. 2014. Effects of large volcanic eruptions on global summer climate and East Asian Monsoon changes during the Last Millennium: analysis of MPI-ESM simulations. Journal of Climate, 27(19): 7394–7409. https://doi.org/10.1175/JCLI-D-13-00739.1.

Marshall AG, Scaife AA, Ineson S. 2009. Enhanced Seasonal Prediction of European Winter Warming following Volcanic Eruptions. Journal of Climate. American Meteorological Society, 22(23): 6168–6180. https://doi.org/10.1175/2009JCLI3145.1.

McGraw MC, Barnes EA, Deser C. 2016. Reconciling the observed and modeled Southern Hemisphere circulation response to volcanic eruptions: Reconciling SH Response to Volcanoes. Geophysical Research Letters, 43(13): 7259–7266. https://doi.org/10.1002/2016GL069835.

Meneghini B, Simmonds I, Smith IN. 2007. Association between Australian rainfall and the Southern Annular Mode. International Journal of Climatology, 27(1): 109–121. https://doi.org/10.1002/joc.1370.

Ménégoz M, Bilbao R, Bellprat O, Guemas V, Doblas-Reyes FJ. 2018. Forecasting the climate response to volcanic eruptions: prediction skill related to stratospheric aerosol forcing. Environmental Research Letters, 13(6): 064022. https://doi.org/10.1088/1748-9326/aac4db.

Monerie P-A, Moine M-P, Terray L, Valcke S. 2017. Quantifying the impact of early 21st century volcanic eruptions on global-mean surface temperature. Environmental Research Letters, 12(5): 054010. https://doi.org/10.1088/1748-9326/aa6cb5.

Neukom R, Gergis J, Karoly DJ, Wanner H, Curran M, Elbert J, González-Rouco F, Linsley BK, Moy AD, Mundo I, Raible CC, Steig EJ, van Ommen T, Vance T, Villalba R, Zinke J, Frank D. 2014. Inter-hemispheric temperature variability over the past millennium. Nature Climate Change, 4(5): 362–367. https://doi.org/10.1038/nclimate2174.

Newman M, Sardeshmukh PD, Bergman JW. 2000. An Assessment of the NCEP, NASA, and ECMWF Reanalyses over the Tropical West Pacific Warm Pool. Bulletin of the American Meteorological Society. American Meteorological Society, 81(1): 41–48. https://doi.org/10.1175/1520-0477(2000)081<0041:AAOTNN>2.3.CO;2.

Oman L, Robock A, Stenchikov G, Schmidt GA, Ruedy R. 2005. Climatic response to high-latitude volcanic eruptions. Journal of Geophysical Research: Atmospheres, 110(D13): D13103. https://doi.org/10.1029/2004JD005487.

Oman L, Robock A, Stenchikov GL, Thordarson T. 2006. High-latitude eruptions cast shadow over the African monsoon and the flow of the Nile. Geophysical Research Letters, 33(18): L18711. https://doi.org/10.1029/2006GL027665.

Oppenheimer C. 2003. Climatic, environmental and human consequences of the largest known historic eruption: Tambora volcano (Indonesia) 1815. Progress in Physical Geography, 27(2): 230–259. https://doi.org/10.1191/0309133303pp379ra.

Patrut A, Woodborne S, von Reden KF, Hall G, Hofmeyr M, Lowy DA, Patrut RT. 2015. African Baobabs with False Inner Cavities: The Radiocarbon

Investigation of the Lebombo Eco Trail Baobab. PLOS ONE, 10(1): e0117193. https://doi.org/10.1371/journal.pone.0117193.

Perlwitz J, Graf H-F. 1995. The statistical connection between tropospheric and stratospheric circulation of the northern hemisphere in winter. Journal of Climate, 8: 2281–2295.

Picas J, Grab S. 2020. Potential impacts of major nineteenth century volcanic eruptions on temperature over Cape Town, South Africa: 1834–1899. Climatic Change. https://doi.org/10.1007/s10584-020-02678-6.

Power S, Casey T, Folland C, Colman A, Mehta V. 1999. Inter-decadal modulation of the impact of ENSO on Australia. Climate Dynamics, 15(5): 319–324. https://doi.org/10.1007/s003820050284.

Predybaylo E, Stenchikov GL, Wittenberg AT, Zeng F. 2017. Impacts of a Pinatubo-size volcanic eruption on ENSO. Journal of Geophysical Research: Atmospheres, 122(2): 925–947. https://doi.org/10.1002/2016JD025796.

Raible CC, Brönnimann S, Auchmann R, Brohan P, Frölicher TL, Graf H-F, Jones P, Luterbacher J, Muthers S, Neukom R, Robock A, Self S, Sudrajat A, Timmreck C, Wegmann M. 2016. Tambora 1815 as a test case for high impact volcanic eruptions: Earth system effects. Wiley Interdisciplinary Reviews: Climate Change, 7(4): 569–589. https://doi.org/10.1002/wcc.407.

Rao MP, Cook BI, Cook ER, D'Arrigo RD, Krusic PJ, Anchukaitis KJ, LeGrande AN, Buckley BM, Davi NK, Leland C, Griffin KL. 2017. European and Mediterranean hydroclimate responses to tropical volcanic forcing over the last millennium. Geophysical Research Letters, 44(10): 5104–5112. https://doi.org/10.1002/2017GL073057.

Rieger LA, Cole JNS, Fyfe JC, Po-Chedley S, Cameron-Smith PJ, Durack PJ, Gillett NP, Tang Q. 2020. Quantifying CanESM5 and EAMv1 sensitivities to Mt. Pinatubo volcanic forcing for the CMIP6 historical experiment. Geoscientific Model Development. Copernicus GmbH, 13(10): 4831–4843. https://doi.org/10.5194/gmd-13-4831-2020.

Robock A. 2000. Volcanic eruptions and climate. Reviews of Geophysics, 38(2): 191–219. https://doi.org/10.1029/1998RG000054.

Robock A, Mao J. 1992. Winter warming from large volcanic eruptions. Geophysical Research Letters, 19(24): 2405–2408. https://doi.org/10.1029/92GL02627.

Roscoe HK, Haigh JD. 2007. Influences of ozone depletion, the solar cycle and the QBO on the Southern Annular Mode. Quarterly Journal of the Royal Meteorological Society, 133(628): 1855–1864. https://doi.org/10.1002/qj.153.

Sato M, Hansen JE, McCormick MP, Pollack JB. 1993. Stratospheric aerosol optical depths, 1850–1990. Journal of Geophysical Research, 98(D12): 22987. https://doi.org/10.1029/93JD02553.

Schneider DP, Ammann CM, Otto-Bliesner BL, Kaufman DS. 2009. Climate response to large, high-latitude and low-latitude volcanic eruptions in the Community Climate System Model. Journal of Geophysical Research: Atmospheres, 114(D15): D15101. https://doi.org/10.1029/2008JD011222.

Smith EI, Jacobs Z, Johnsen R, Ren M, Fisher EC, Oestmo S, Wilkins J, Harris JA, Karkanas P, Fitch S, Ciravolo A, Keenan D, Cleghorn N, Lane CS, Matthews T, Marean CW. 2018. Humans thrived in South Africa through the Toba eruption about 74,000 years ago. Nature, 555(7697): 511–515. https://doi.org/10.1038/nature25967.

Stevenson S, Fasullo JT, Otto-Bliesner BL, Tomas RA, Gao C. 2017. Role of eruption season in reconciling model and proxy responses to tropical volcanism. Proceedings of the National Academy of Sciences, 114(8): 1822–1826. https://doi.org/10.1073/pnas.1612505114.

Sun W, Wang B, Liu J, Chen D, Gao C, Ning L, Chen L. 2019. How northern high-latitude volcanic eruptions in different seasons affect ENSO. Journal of Climate, 32(11): 3245–3262. https://doi.org/10.1175/JCLI-D-18-0290.1.

Taylor KE, Stouffer RJ, Meehl GA. 2012. An overview of CMIP5 and the experiment design. Bulletin of the American Meteorological Society, 93(4): 485–498. https://doi.org/10.1175/BAMS-D-11-00094.1.

Thomason LW, Ernest N, Millán L, Rieger L, Bourassa A, Vernier J-P, Manney G, Luo B, Arfeuille F, Peter T. 2018. A global space-based stratospheric aerosol climatology: 1979–2016. Earth System Science Data. Copernicus GmbH, 10(1): 469–492. https://doi.org/10.5194/essd-10-469-2018.

Timmreck C. 2012. Modeling the climatic effects of large explosive volcanic eruptions. WIREs: Climate Change, 3(6): 545–564. https://doi.org/10.1002/wcc.192.

Timmreck C. 2018. Climatic effects of large volcanic eruptions. Habilitation Thesis, Hamburg, Universität Hamburg.

Tyson PD, Tyson PD, Preston-Whyte RA. 2000. The Weather and Climate of Southern Africa. Oxford University Press.

Vera CS, Vigliarolo PK. 2000. A Diagnostic Study of Cold-Air Outbreaks over South America. Monthly Weather Review, 128(1): 3–24. https://doi.org/10.1175/1520-0493(2000)128<0003:ADSOCA>2.0.CO;2.

Wahl ER, Diaz HF, Smerdon JE, Ammann CM. 2014. Late winter temperature response to large tropical volcanic eruptions in temperate western North America: Relationship to ENSO phases. Global and Planetary Change, 122: 238–250. https://doi.org/10.1016/j.gloplacha.2014.08.005.

Wigley TML, Ammann CM, Santer BD, Raper SCB. 2005. Effect of climate sensitivity on the response to volcanic forcing. Journal of Geophysical Research: Atmospheres. John Wiley & Sons, Ltd, 110(D9). https://doi.org/10.1029/2004JD005557.

Young PJ, Thompson DWJ, Rosenlof KH, Solomon S, Lamarque J-F. 2011. The Seasonal Cycle and Interannual Variability in Stratospheric Temperatures and Links to the Brewer–Dobson Circulation: An Analysis of MSU and SSU Data. Journal of Climate, 24(23): 6243–6258. https://doi.org/10.1175/JCLI-D-10-05028.1.

Zambri B, LeGrande AN, Robock A, Slawinska J. 2017. Northern Hemisphere winter warming and summer monsoon reduction after volcanic eruptions over the last millennium. Journal of Geophysical Research: Atmospheres, 122(15): 7971–7989. https://doi.org/10.1002/2017JD026728.

Zambri B, Robock A. 2016. Winter warming and summer monsoon reduction after volcanic eruptions in Coupled Model Intercomparison Project 5 (CMIP5) simulations. Geophysical Research Letters, 43(20): 10,920-10,928. https://doi.org/10.1002/2016GL070460.

Zanchettin D, Timmreck C, Bothe O, Lorenz SJ, Hegerl G, Graf H-F, Luterbacher J, Jungclaus JH. 2013. Delayed winter warming: A robust decadal response to strong tropical volcanic eruptions? Geophysical Research Letters. John Wiley & Sons, Ltd, 40(1): 204–209. https://doi.org/10.1029/2012GL054403.

Zanchettin D, Timmreck C, Graf H-F, Rubino A, Lorenz S, Lohmann K, Krüger K, Jungclaus JH. 2012. Bi-decadal variability excited in the coupled ocean–atmosphere system by strong tropical volcanic eruptions. Climate Dynamics, 39(1–2): 419–444. https://doi.org/10.1007/s00382-011-1167-1.

Zhang Q, Körnich H, Holmgren K. 2013. How well do reanalyses represent the southern African precipitation? Climate Dynamics, 40(3–4): 951–962. https://doi.org/10.1007/s00382-012-1423-z.

Zuo M, Man W, Zhou T, Guo Z. 2018. Different impacts of Northern, Tropical, and Southern Volcanic Eruptions on the Tropical Pacific SST in the Last Millennium. Journal of Climate, 31(17): 6729–6744. https://doi.org/10.1175/JCLI-D-17-0571.1.

Appendix A: Published Versions of Chapter 2 and Chapter 4

Geophysical Research Letters

RESEARCH LETTER
10.1029/2020GL087792

Key Points:
- Tropical eruptions emitting 20 Tg SO_2 or more cause significant reductions in Southern Hemispheric temperatures
- Southern Hemisphere temperatures typically respond (significantly) 1–2 months after Northern Hemisphere temperature responses
- Maximum Southern Hemisphere cooling occurs in austral autumn/winter, alongside boreal summer cooling

Supporting Information:
- Supporting Information S1

Correspondence to:
P. J. Harvey,
pamjharvey14@gmail.com

Citation:
Harvey, P. J., Grab, S. W., & Malherbe, J. (2020). Major volcanic eruptions and their impacts on Southern Hemisphere temperatures during the late 19th and 20th centuries, as simulated by CMIP5 models. *Geophysical Research Letters*, *47*, e2020GL087792. https://doi.org/10.1029/2020GL087792

Received 6 MAR 2020
Accepted 19 JUN 2020
Accepted article online 8 JUL 2020

Major Volcanic Eruptions and Their Impacts on Southern Hemisphere Temperatures During the Late 19th and 20th Centuries, as Simulated by CMIP5 Models

P. J. Harvey[1], S. W. Grab[1], and J. Malherbe[2,3]

[1]School of Geography, Archaeology and Environmental Studies, University of the Witwatersrand, Johannesburg, South Africa, [2]CSIR Natural Resources and the Environment: Climate Studies, Modelling and Environmental Health, Pretoria, South Africa, [3]Agriculture Research Council—Institute for Soil, Climate and Water, Pretoria, South Africa

Abstract While much is known about the impacts of volcanic forcing on Northern Hemisphere (NH) climates, knowledge about Southern Hemisphere (SH) responses is still in its infancy. We examine volcanic impacts on SH temperatures following eight major late 19th and 20th century eruptions (Agung, 1963; Colima, 1913; El Chichón, 1982; Pinatubo, 1991; Krakatau, 1883; Quizapu, 1932; Santa Maria, 1902; Tarawera, 1886). Coupled Model Intercomparison Project, Phase 5 (CMIP5) historical simulations are used to analyze near-surface land temperatures. We demonstrate that four of the eight major eruptions (Krakatau, Santa Maria, Agung, and Pinatubo) significantly lowered mean SH temperatures; these tropical eruptions emitted at least 20 Tg of SO_2 into the stratosphere. SH responses typically lagged NH temperature cooling responses by 1–2 months, excluding Pinatubo. Responses differ spatially and temporally with each eruption, highlighting the importance of investigating events individually. Overall, we observe relatively strong (between −0.19°C and −0.36°C) austral autumn/winter SH cooling.

Plain Language Summary Climate is affected by major volcanic eruptions if the eruption emits large amounts of SO_2 into the stratosphere. Volcanic forcing generally causes temperatures to cool, but in some instances, temperatures rise. Many studies have identified Northern Hemisphere (NH) climatic responses to volcanic forcing, but the Southern Hemisphere (SH) has received less attention in this regard, hence our investigation on SH climatic responses to volcanic forcing. Temperature responses to eight eruptions that occurred during the late 19th and 20th centuries are established. SH and NH responses to these eruptions are compared. Using climate models from Coupled Model Intercomparison Project, Phase 5 (CMIP5) experiments, we find that four of the eight major eruptions significantly cooled SH temperatures. These four eruptions emitted 20 Tg or more of SO_2 into the stratosphere and occurred in the tropics. We find that responses were not uniform but differed according to location and time. A generally strong austral autumn/winter cooling response occurs over SH continental regions. Following the four major eruptions of Krakatau, Santa Maria, Agung, and Pinatubo, SH temperatures typically responded later than temperatures in the NH. Understanding the impact that major volcanic eruptions have on regional climates is important for establishing early warning systems, particularly where climate-sensitive biosystems and agriculture are influenced by such events.

1. Introduction

Major volcanic eruptions can significantly influence climate (Man et al., 2014; Neukom et al., 2014; Sigl et al., 2015) if a substantial quantity of SO_2 (sulfur dioxide) is emitted into the lower stratosphere. The SO_2 converts to sulfuric acid or sulfate aerosols which can be globally dispersed within a few weeks (Cole-Dai, 2010; Robock, 2000) altering radiation budgets through increasing the scattering and absorption of incoming solar radiation (Kremser et al., 2016; Liu et al., 2018; Textor et al., 2004). Major tropical eruptions can impact climates globally (e.g., Krakatau, 1883; Pinatubo, 1991; Tambora, 1815) through the effective upwelling of the Brewer-Dobson circulation which facilitates poleward transportation of stratospheric aerosols in both hemispheres more efficiently than eruptions occurring at high latitudes (e.g., Laki, 1783; Katmai, 1912) (Young et al., 2011). Middle- to high-latitude eruptions have less-severe, shorter-term impacts that are restricted to the hemisphere in which the eruption occurred (Oman et al., 2005; Schneider et al., 2009; Timmreck, 2012, 2018).

10.1029/2020GL087792

Findings typically indicate that mean annual global temperatures may decrease for 2–3 years after a major eruption, from as little as a fraction of a degree (Kremser et al., 2016) to as much as 0.4°C after the Pinatubo eruption (Kremser et al., 2016; Thompson et al., 2009). Northern Hemisphere (NH) temperature responses to volcanic forcing has received substantial research attention (e.g., Esper et al., 2013; Oman et al., 2005; Toohey et al., 2019; Zambri et al., 2017). Establishing temperature responses across various subregions of the NH has received much focus, such as over North America (Lough & Fritts, 1987), Europe (e.g., Esper et al., 2013; Rao et al., 2017), and Asia (e.g., Zhang et al., 2013). Although general trends indicate cooling throughout the NH, middle to high latitudes often experience winter warming (Robock, 2000; Timmreck, 2012; Zambri et al., 2017). However, winter warming is not coincident after every major eruption (Schneider et al., 2009), and in some cases summer warming occurs (Stothers, 1999), suggesting that temperature responses are spatially diverse and disparate following such eruptions (Zanchettin et al., 2019).

In contrast, knowledge on volcanic forcing impacts on Southern Hemisphere (SH) climates is in its infancy. Nonetheless, it is understood that asymmetric results are expected between hemispheres (Zanchettin et al., 2014); for instance, studies show that volcanic forcing impacts have a generally weaker impact on SH than NH climate (especially temperature) (Man et al., 2014; Monerie et al., 2017; Neukom et al., 2014). SH climate is potentially influenced more by internal than external variability (Neukom et al., 2014; Wilmes et al., 2012). Mean SH temperature departures are only 0.10–0.37°C below normal for 1–2 years after major eruptions (Mass & Portman, 1989; Neukom et al., 2014; Robock & Mao, 1995). However, temperatures at individual locations in the SH can reduce by as much as 2–3°C (Wilmes et al., 2012). At regional scales, widespread cooling is identified for South America (Colose et al., 2015; Graf et al., 1993), significant cooling occurs over southern Africa (Man et al., 2014), and rapid negative temperature departures (−0.3°C to −0.4°C) prevail over New Zealand (Salinger, 1998). However, climatic responses over the SH (as is the case for the NH) are strongly dependent on the volcanic event itself (e.g., season, location, magnitude, and aerosol altitude) (e.g., Colose et al., 2015; Krishnamohan et al., 2019; Oman et al., 2005; Stevenson et al., 2017; Sun et al., 2019; Zanchettin et al., 2014; Zuo et al., 2018).

Climate models are now widely used to provide expansive good resolution depictions of climatic responses to major volcanic eruptions and can adequately simulate associated SH circulation (Hopcroft et al., 2018; Hua et al., 2019; McGraw et al., 2016; Raible et al., 2016; Toohey et al., 2019). Therefore, given the largely NH focus thus far, our aim is to use the Coupled Model Intercomparison Project, Phase 5 (CMIP5) (Taylor et al., 2012), to better quantify temperature responses across the SH following the major eruptions of Krakatau (1883), Tarawera (1886), Santa Maria (1902), Colima (1913), Quizapu (1932), Agung (1963), El Chichón (1982), and Pinatubo (1991). More specifically, we investigate SH temperature response times and the magnitude of temperature departures in comparison to those for the NH. While we consider latitudinal variability of such responses, longitudinal (i.e., intercontinental) differences will be discussed in a subsequent paper.

2. Models and Data

Historical experiments from CMIP5 (Taylor et al., 2012) are used in this study and selected based on how well they simulated a lower-stratosphere temperature response to volcanic forcing (after Barnes et al., 2016). The first three realizations (r1, r2, and r3; which represent different initial conditions) are used for each model; apart from the MIROC-ESM-CHEM model, for which only r1 is available. The first physics version is used for each model. Given differences in the ways in which aerosols are calculated in the GISS-E2_R model, both Physics-Versions 1 (p1) and 3 (p3) are used. While aerosols in p1 are prescribed, those in p3 are calculated in the model simulation. We analyzed an ensemble of 31 simulations (Table S1 in the supporting information). Different variations of the historical experiments (covering the period 1850–2005) are explored to establish any "unusual" anomalies (see Text S1).

Given that volcanic forcing was not uniquely prescribed for CMIP5, the schemes used are according to either Ammann et al. (2007) or Sato et al. (1993), except for the MRI_CGCM3 model which computed stratospheric aerosols interactively (comparison in Text S2). While all models used had performed the historical experiments, not all had contributed to the Historical Nat or Historical Misc experiments. Table S1 indicates (a) which models had executed these experiments and (b) the volcanic forcing data set incorporated for each model.

Table 1
Volcanic Eruptions Analyzed in This Study (Driscoll et al., 2012

Label	Eruption	Date	Latitude	VEI[a]	DVI[b]	Lower stratosphere SO_2, mass (Tg)
a	Krakatau	27 August 1883	6°S	6	1,000	44
b	Tarawera	10 June 1886	38°S	5	800	4–5
c	Santa Maria	24 October 1902	15°N	6	600	30
d	Colima	1913	19°N	5	?	?
e	Quizapu	10 April 1932	36°S	5	70	3
f	Agung	17 March 1963	8°S	4	800	20
g	El Chichón	4 April 1982	17°N	5	800	7
h	Mount Pinatubo	15 June 1991	15°N	6	1,000	20

Note. Labels given to these eruptions are used in all figures.
[a]VEI, Volcanic explosivity index (Newhall & Self, 1982). [b]DVI, Dust veil index (Lamb, 1970): A measure of the impact (e.g., on climate) of dust and aerosols released from an eruption.

Near-surface (2m) land temperatures are considered for this study. Models are linearly regridded to a 2° by 2° latitude-longitude grid. Multimodel means are used for all analyses, and anomalies are calculated with respect to a 20-year running mean. Only land temperatures are considered to avoid oceanic masking effects on land temperature responses, given that ocean temperatures have a delayed response to radiative forcing (Joseph & Zeng, 2011).

The quantity of SO_2 emitted into the lower stratosphere greatly influences potential climatic responses (Oman et al., 2005), with 5 Tg or more required to impact climate (Timmreck, 2012). In this study, we test climate responses following eight major tropical and SH eruptions with a VEI $>$ 5 (volcanic explosivity index; measuring the explosiveness of an eruption (Newhall & Self, 1982). These include Krakatau (1883), Tarawera (1886), Santa Maria (1902), Colima (1913), Quizapu (1932), El Chichón (1982), and Pinatubo (1991). We also consider the 1963 Agung eruption which had a VEI value of 4, but a lower stratosphere SO_2 mass of 20 Tg (see Table 1).

To test multimodel mean robustness, the 25th and 75th percentiles of individual model responses to historical forcing experiments are considered. Statistical significance was calculated by resampling 5,000 time series using the bootstrap approach (Efron, 1979) whereby the 5th and 95th percentiles were used to distinguish between likely random occurrences and significant climatic responses (Haurwitz & Brier, 1981; Rao et al., 2017).

3. Results and Discussion

3.1. SH Near-Surface Land (Terrestrial) Temperatures Following Major Eruptions

CMIP5 historical experiment outputs indicate reductions in mean annual near-surface temperatures after each of the eight eruptions (Table 1) for the NH, and seven of the eight for the SH (Figure 1). However, only four of the temperature reductions are statistically significant for the SH; namely after the Krakatau (1883), Santa Maria (1902), Agung (1963), and Pinatubo (1991) eruptions. For the purpose of this paper, these four eruptions are referred to as the "primary eruptions." The NH-averaged annual temperatures are significantly cooler after only three of the primary eruptions, as cooling after the Agung eruption is not significant (−0.21°C). Of these primary eruptions, three had a VEI of 6, and Agung a VEI of 4. However, all four of these eruptions had emitted 20 Tg or more of SO_2 and originated between 8°S and 15°N latitude. This would have facilitated effective distribution of SO_2 around both hemispheres by the Brewer-Dobson circulation (Butchart, 2014; Robock, 2000; Trepte et al., 1993; Young et al., 2011). The remaining four eruptions (Colima, 1913; El Chichón, 1982; Quizapu, 1932; Tarawera, 1886) occurred either in SH midlatitude or NH tropical regions, but had emitted less than 8 Tg of SO_2 into the lower stratosphere. Coincidently, apart from Tarawera, none of these are associated with a significant surface temperature response in the SH. Following Tarawera, significant anomalies occur in SH summer and autumn and NH winter; however, this response is a likely enhancement (extension) of the Krakatau response. NH temperatures are significantly reduced following the El Chichón eruption. The above suggests that for a significant response to occur in the SH, an eruption would ideally be in the tropics and emit 20 Tg or more of SO_2 into the lower stratosphere.

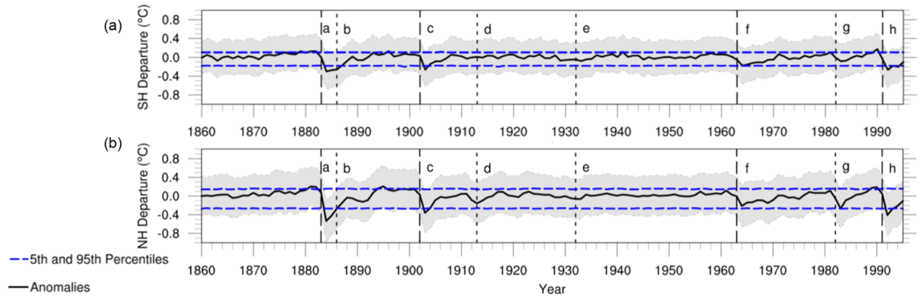

Figure 1. Annual SH (a) and NH (b) land-only near-surface temperatures anomalies. Vertical lines represent eruptions. Long dashed lines signify the primary eruptions and short dashed lines the remaining eruptions. The ensemble spread (25th to 75th percentiles) of the 12-month moving average is depicted by gray shading, and statistical significance at the 90% confidence interval by the blue lines. See Table 1 for eruption names.

Both magnitude and duration of significant temperature responses vary between major eruptions (Table 2). The longest response follows Krakatau, lasting 4 years. Negative temperature departures were significant for only 1 year following Santa Maria, for both SH and NH annual anomalies. Response following Agung was weakest of the primary eruptions, with negative anomalies only significant in austral winter (June-July-August, JJA). Anomalies after Pinatubo were significant for two consecutive years in both hemispheres. Temperature responses to these eruptions do not correspond directly with the quantity of SO_2 emitted by each eruption (Figure S2). For instance, Santa Maria placed 30 Tg of SO_2 into the stratosphere but produced weaker temperature responses than Pinatubo, which emitted only 20 Tg and was associated with a considerably stronger temperature response. Hence, while large amounts of SO_2 are required to cause a temperature response, other factors can affect posteruption responses. Such factors include season and location of eruption, aerosol layer height, and state of the atmosphere and ocean at the time of eruption; all of which likely contribute to observed differences in responses (Krishnamohan et al., 2019; Stevenson et al., 2017; Sun et al., 2019; Zuo et al., 2018). For instance, Pinatubo erupted during the SH winter but Santa Maria during spring. Atmospheric circulation is most favorable to distributing aerosols during SH winter when coupling between the troposphere and stratosphere is strongest and the Brewer-Dobson circulation most pronounced (Birner & Bönisch, 2010; Perlwitz & Graf, 1995; Young et al., 2011), which might explain the stronger response after Pinatubo.

Internal variability is considered, as past ensemble simulations have shown that these obscure volcanic forcing impacts (e.g., Frölicher et al., 2013; Lehner et al., 2016). In addition, eruptions themselves can affect internal variability, indirectly influencing temperatures. Studies using CMIP5 models suggest a positive Southern Annular Mode (SAM) after major eruptions (Barnes et al., 2016; McGraw et al., 2016). This implies that westerlies intensify and contract poleward resulting in significantly cooler temperatures over Antarctica and most of Australia, but warming over regions between 40°S and 60°S (Gillett et al., 2006). Volcanic eruptions can strengthen the polar vortex, resulting in cooling over the poles (Barnes et al., 2016; Karpechko et al., 2010; Perlwitz & Graf, 1995; Zambri & Robock, 2016) and influence El Niño–Southern Oscillation (ENSO) (Pausata et al., 2015). Varied ENSO responses are likely associated with different volcanic forcing stages (Wang et al., 2018). To this end, our model-generated SSTs indicate a tendency to be depressed in the Nino3.4 area, implying La Niña-like conditions following the four major eruptions, as found by Maher et al. (2015). La Niña-like conditions usually imply overall cooler SH temperatures (Kuleshov et al., 2008), which may have contributed to the observed cooling after eruptions.

Tarawera (1886) erupted 3 years after Krakatau and marks the strongest known midlatitude SH (38°S) eruption during the last couple of centuries. Although it emitted only 4–5 Tg of SO_2 into the lower stratosphere, this occurred during an already volcanically induced cool period, and thus offers a unique opportunity to consider the so-called "volcanic-double" forcing effect as discussed by Toohey et al. (2016). Both NH and SH mean temperatures remain below normal for an extended period (significant anomalies remained until 1887, 4 years after Krakatau). This temporally extended negative temperature anomaly is in strong contrast to all other major eruptions, particularly so when compared with Pinatubo (see Figure 2); thus demonstrating the likely combined influence of Krakatau and Tarawera, supporting the case for a "volcanic-double"

10.1029/2020GL087792

Table 2
Annual SH and NH Near-Surface Temperature Anomalies Following the Four Primary Eruptions

		SH anomaly					NH anomaly				
Eruption	Year	ANN	DJF	MAM	JJA	SON	ANN	DJF	MAM	JJA	SON
Krakatau	1883	0.00	0.17	0.05	0.07	−0.15	0.08	0.13	0.16	0.11	0.00
	1884	−0.30	−0.21	−0.36	−0.36	−0.24	−0.54	−0.23	−0.40	−0.65	−0.68
	1885	−0.27	−0.31	−0.24	−0.27	−0.26	−0.42	−0.47	−0.41	−0.44	−0.43
Tarawera	1886	−0.26	−0.31	−0.25	−0.26	−0.23	−0.28	−0.35	−0.34	−0.23	−0.27
	1887	−0.17	−0.21	−0.26	−0.15	−0.07	−0.15	−0.27	−0.16	−0.12	−0.11
Santa Maria	1902	0.03	0.10	0.07	0.04	−0.04	0.03	0.03	0.03	0.09	0.02
	1903	−0.26	−0.15	−0.31	−0.32	−0.24	−0.36	−0.22	−0.29	−0.43	−0.44
	1904	−0.14	−0.16	−0.15	−0.10	−0.17	−0.26	−0.28	−0.23	−0.26	−0.25
	1905	−0.08	−0.15	−0.13	−0.12	0.02	−0.09	−0.19	−0.06	−0.11	−0.10
Agung	1963	−0.05	0.03	0.00	−0.07	−0.13	−0.01	−0.01	0.00	−0.02	−0.05
	1964	−0.17	−0.19	−0.19	−0.20	−0.15	−0.21	−0.12	−0.19	−0.22	−0.16
	1965	−0.15	−0.13	−0.16	−0.12	−0.16	−0.14	−0.23	−0.14	−0.16	−0.17
	1966	−0.12	−0.12	−0.10	−0.15	−0.10	−0.13	−0.13	−0.09	−0.16	−0.10
Pinatubo	1991	−0.04	0.20	0.12	0.00	−0.30	0.05	0.20	0.14	0.07	−0.10
	1992	−0.26	−0.28	−0.30	−0.27	−0.23	−0.41	−0.26	−0.34	−0.51	−0.47
	1993	−0.18	−0.22	−0.21	−0.14	−0.21	−0.27	−0.20	−0.29	−0.30	−0.30
	1994	−0.20	−0.15	−0.18	−0.18	−0.24	−0.21	−0.29	−0.21	−0.17	−0.19

Note. Blue shading indicates significant anomalies and gray shading the year of the eruption.

forcing effect. Although Toohey et al. (2016) provide an example of a strong "volcanic-double" forced cooling effect for the Middle Ages, our example above is the first (and possibly only) such example of a "volcanic-double" climate forcing effect since the late modern period. Notably, mean negative temperature departures were marginally stronger in the SH than NH in 1887 (SH: −0.17°C; NH: −0.15°C) following Tarawera, thus indicating a slightly stronger initial (and volcanic cumulative) impact on the SH than NH. The three remaining major eruptions (Colima, 1913; Quizapu, 1932; El Chichón, 1982; Table 1) investigated here do not indicate statistically significant temperature responses in the SH; however, weak responses are noticeable. Weak responses are most likely due to insufficient SO_2 emitted into the stratosphere. It is suggested that >5 Tg of SO_2 needs to reach the stratosphere for any notable temperature effect (Timmreck, 2018). In the NH, the strength of temperature responses after these smaller eruptions coincides with the amount of SO_2 that each eruption emitted into the stratosphere, but not so in the SH. The strongest of these eruptions (El Chichón) emitted 7 Tg of SO_2 into the lower stratosphere and coincides with a statistically insignificant negative annual NH temperature anomaly in 1983 (−0.27°C). In contrast, the SH response is negligible (1983: −0.08°C). The stronger NH response is to be expected given weaker SH Brewer-Dobson circulation than that in the NH (Rosenlof, 1995; Young et al., 2011).

We now consider monthly surface temperature response times for both hemispheres, following the four primary eruptions (Figure 2). With the exception of anomalies following Pinatubo, SH anomalies develop before (1–2 months), peak earlier (4–6 months), and terminate before NH anomalies. However, given that SH anomalies are weaker (peak anomalies in SH: −0.27°C to −0.42°C; NH: −0.38°C to −0.72°C for all eruptions), they only become significant 1–2 months after those in the NH. In addition, the NH had a higher percentage of significantly cooler than normal months during the first 36 months following each primary eruption (NH: 55–83%; SH: 22–72%), apart from Agung when both hemispheres had only 3 months of significantly depressed temperatures. These outcomes are in agreement with previous work which has emphasized stronger NH than SH temperature responses (e.g., Man et al., 2014; Monerie et al., 2017; Neukom et al., 2014). The delayed significant response in the SH is likely associated with the vast expanse of oceans which help regulate surface temperatures (Joseph & Zeng, 2011) and the weaker SH Brewer-Dobson circulation (Young et al., 2011). The first significant responses in the NH are typically observed between December and February and in the SH between February and September (i.e., cooler seasons of each

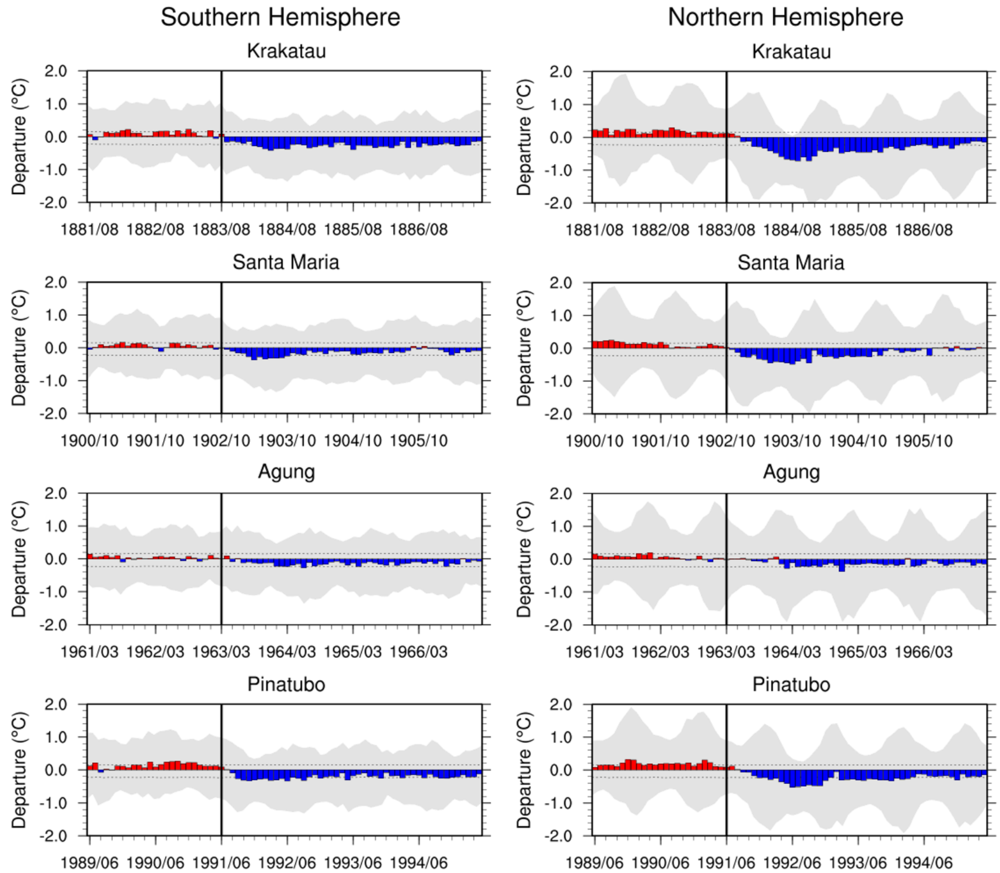

Figure 2. Monthly near-surface temperature responses for the four primary eruptions for the (left column) SH and (right column) NH. Vertical lines indicate the eruption month. Gray shading depicts the ensemble spread between the 25th and 75th percentiles of the monthly moving averages. Statistical significance at the 90% confidence interval is represented by the horizontal dotted lines.

hemisphere), but maximum anomalies generally occur during SH winter and coincide with maximum cooling during NH summer/autumn (Zanchettin et al., 2019).

As alluded to earlier, temperature departures in response to volcanic forcing may be spatially highly variable at the hemispheric scale. While strong negative temperature anomalies may be detected across most NH latitudes after the four primary eruptions, the same is not observed in the SH (Figure 3). Following each eruption, stronger cooling occurs in the NH than SH in the first (y1) and second (y2) years after eruptions, and in the third year (y3) after Krakatau and Pinatubo. Negative temperature departures after Agung are strongest between 20°S and 40°S (−0.20°C) in y1 but uniform over all latitudes in y2 and y3 (−0.11°C and −0.18°C, respectively). Following Santa Maria, negative departures in y3 are strongest over the tropics of both hemispheres (−0.18°C). For all eruptions, strongest negative SH anomalies occur between 10°S and 30°S for y1 to y3 (y1: −0.34°C; y2:−0.23°C; y3: −0.21°C). Weakest anomalies are observed at high latitudes (y1: −0.11°C, y2: −0.13°C, y3: −0.08°C).

3.2. Statistics

The 25th and 75th percentiles of the models indicate that temperature responses are similar to mean values obtained from the four primary eruptions, suggesting that responses shown by the multimodel mean are robust. A superposed epoch analysis (Figure S3) suggests that significantly cooler mean NH and SH land temperatures may occur after major eruptions, with 20 Tg or greater SO_2 loading in the lower stratosphere, for up to 3–4 years. The superposed epoch analysis (SEA) and bootstrap methods (Efron, 1979; Haurwitz & Brier, 1981; Rao et al., 2017) further indicate that responses are statistically significant, as these occur below the 5th percentile. Although studies have used composites of multiple eruptions to study the spatial effects of

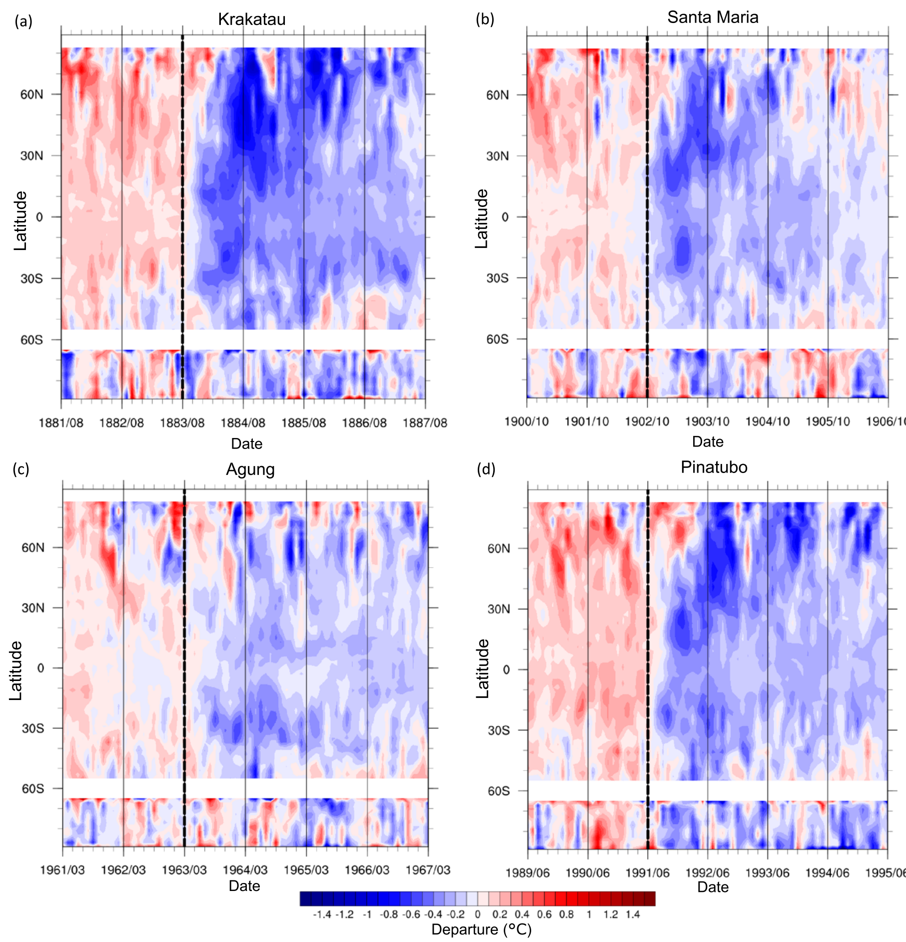

Figure 3. Zonal averages of the land-only near-surface temperature anomalies over time for the (a) Krakatau, (b) Santa Maria, (c) Agung, and (d) Pinatubo eruptions. Thick dashed vertical lines represent eruptions. The gaps around 90°N and 60°S are a result of the absence of land at those latitudes.

volcanic forcing (e.g., Alfaro-Sánchez et al., 2018; Zambri et al., 2017), it must be acknowledged that the timing, location, strength, and chemistry of the eruption, in combination with other forcing mechanisms, will result in different temperature response outcomes. It should also be cautioned that if larger-magnitude eruptions are composited with weaker ones, it might mask out the full response exhibited by larger eruptions (Figures S2c and S2d).

4. Conclusion

Past work comparing Northern and Southern Hemispheric temperature responses to volcanic forcing has generally focused on mean annual or seasonal trends during posteruption years and has broadly shown weaker responses in the SH. While our findings are largely in agreement with this, they also indicate some exceptions to this "rule," and particularly so when examining responses at a finer temporal scale (i.e., months rather than years). For instance, significant SH temperature responses lag by 1–2 months compared to those in the NH following major eruptions. However, initial cooling (although insignificant) starts earlier (by 1 to 2 months) in the SH. Our findings suggest that common factors resulting in an eruption causing a significant SH temperature response include the eruption occurring in the tropics and emitting 20Tg or more of SO_2 into the lower stratosphere. However, eruptions with a SO_2 mass between 10 and 20 Tg still need further consideration for the SH. Eruptions occurring during SH autumn or winter induce a greater temperature response due to more favorable circulation conditions in winter. The SH response is strongest during autumn/winter, which coincides with strongest NH cooling in summer/autumn. While subtropical and mid-latitude SH eruptions do not force a significant temperature response, in the case of Tarawera, it prolonged negative temperature anomalies (initially in response to Krakatau) in both hemispheres, demonstrating a relatively recent so-called "volcanic double" forcing effect. We thus caution analyses considering only mean annual temperature responses. Immediate and relatively strong monthly negative temperature anomalies in the SH, following major eruptions, have important implications for climate-sensitive biosystems and the agricultural sector in particular.

Data Availability Statement

Data are available at this site (https://esgf-data.dkrz.de).

Acknowledgments
We thank the CMIP5 initiative and all climate modeling groups for contributing to CMIP5 and making their model outputs available. We thank Jacobus van der Merwe and the National Research Foundation (NRF) for helping obtain the CMIP5 data. We much appreciate the valuable constructive inputs provided by anonymous referees.

References

Alfaro-Sánchez, R., Nguyen, H., Klesse, S., Hudson, A., Belmecheri, S., Köse, N., et al. (2018). Climatic and volcanic forcing of tropical belt northern boundary over the past 800 years. *Nature Geoscience*, *11*(12), 933–938. https://doi.org/10.1038/s41561-018-0242-1

Ammann, C. M., Joos, F., Schimel, D. S., Otto-Bliesner, B. L., & Tomas, R. A. (2007). Solar influence on climate during the past millennium: Results from transient simulations with the NCAR climate system model. *Proceedings of the National Academy of Sciences*, *104*(10), 3713–3718. https://doi.org/10.1073/pnas.0605064103

Barnes, E. A., Solomon, S., & Polvani, L. M. (2016). Robust wind and precipitation responses to the Mount Pinatubo eruption, as simulated in the CMIP5 models. *Journal of Climate*, *29*(13), 4763–4778. https://doi.org/10.1175/JCLI-D-15-0658.1

Birner, T., & Bönisch, H. (2010). Residual circulation trajectories and transit times into the extratropical lowermost stratosphere. *Atmospheric Chemistry and Physics Discussions*, *10*(7), 16,837–16,860. https://doi.org/10.5194/acpd-10-16837-2010

Butchart, N. (2014). The Brewer-Dobson circulation. *Reviews of Geophysics*, *52*, 157–184. https://doi.org/10.1002/2013RG000448

Cole-Dai, J. (2010). Volcanoes and climate. *Wiley Interdisciplinary Reviews: Climate Change*, *1*(6), 824–839. https://doi.org/10.1002/wcc.76

Colose, C. M., LeGrande, A. N., & Vuille, M. (2015). The influence of tropical volcanic eruptions on the climate of South America during the last millennium. *Climate of the Past*, *11*(4), 3375–3424. https://doi.org/10.5194/cpd-11-3375-2015

Driscoll, S., Bozzo, A., Gray, L. J., Robock, A., & Stenchikov, G. (2012). Coupled Model Intercomparison Project 5 (CMIP5) simulations of climate following volcanic eruptions. *Journal of Geophysical Research*, *117*, D17105. https://doi.org/10.1029/2012JD017607

Efron, B. (1979). Bootstrap methods: Another look at the Jackknife. *The Annals of Statistics*, *7*(1), 1–26. https://doi.org/10.1214/aos/1176344552

Esper, J., Schneider, L., Krusic, P. J., Luterbacher, J., Büntgen, U., Timonen, M., et al. (2013). European summer temperature response to annually dated volcanic eruptions over the past nine centuries. *Bulletin of Volcanology*, *75*(7), 736. https://doi.org/10.1007/s00445-013-0736-z

Frölicher, T. L., Joos, F., Raible, C. C., & Sarmiento, J. L. (2013). Atmospheric CO_2 response to volcanic eruptions: The role of ENSO, season, and variability. *Global Biogeochemical Cycles*, *27*, 239–251. https://doi.org/10.1002/gbc.20028

Gillett, N. P., Kell, T. D., & Jones, P. D. (2006). Regional climate impacts of the Southern Annular Mode. *Geophysical Research Letters*, *33*, L23704. https://doi.org/10.1029/2006GL027721

Graf, H.-F., Kirchner, I., Robock, A., & Schult, I. (1993). Pinatubo eruption winter climate effects: Model versus observations. *Climate Dynamics*, *9*(2), 81–93. https://doi.org/10.1007/BF00210011

Haurwitz, M. W., & Brier, G. W. (1981). A critique of the superposed epoch analysis method: Its application to solar–weather relations. *Monthly Weather Review*, *109*(10), 2074–2079. https://doi.org/10.1175/1520-0493(1981)109%3C2074:ACOTSE%3E2.0.CO;2

Hopcroft, P. O., Kandlbauer, J., Valdes, P. J., & Sparks, R. S. J. (2018). Reduced cooling following future volcanic eruptions. *Climate Dynamics*, *51*(4), 1449–1463. https://doi.org/10.1007/s00382-017-3964-7

Hua, W., Dai, A., Zhou, L., Qin, M., & Chen, H. (2019). An externally forced decadal rainfall seesaw pattern over the Sahel and Southeast Amazon. *Geophysical Research Letters*, *46*, 923–932. https://doi.org/10.1029/2018GL081406

Joseph, R., & Zeng, N. (2011). Seasonally modulated tropical drought induced by volcanic aerosol. *Journal of Climate*, *24*(8), 2045–2060. https://doi.org/10.1175/2009JCLI3170.1

Karpechko, A. Y., Gillett, N. P., Dall'Amico, M., & Gray, L. J. (2010). Southern Hemisphere atmospheric circulation response to the El Chichón and Pinatubo eruptions in coupled climate models. *Quarterly Journal of the Royal Meteorological Society*, *136*(652), 1813–1822. https://doi.org/10.1002/qj.683

Kremser, S., Thomason, L. W., von Hobe, M., Hermann, M., Deshler, T., Timmreck, C., et al. (2016). Stratospheric aerosol-observations, processes, and impact on climate: Stratospheric aerosol. *Reviews of Geophysics*, *54*, 278–335. https://doi.org/10.1002/2015RG000511

Krishnamohan, K.-P. S.-P., Bala, G., Cao, L., Duan, L., & Caldeira, K. (2019). Climate system response to stratospheric sulfate aerosols: Sensitivity to altitude of aerosol layer. *Earth System Dynamics*, *10*(4), 885–900. https://doi.org/10.5194/esd-10-885-2019

Kuleshov, Y., Qi, L., Fawcett, R., & Jones, D. (2008). On tropical cyclone activity in the Southern Hemisphere: Trends and the ENSO connection. *Geophysical Research Letters*, *35*, L14S08. https://doi.org/10.1029/2007GL032983

Lamb, H. H. (1970). Volcanic dust in the atmosphere; with a chronology and assessment of its meteorological significance. *Philosophical Transactions of the Royal Society A: Mathematical, Physical and Engineering Sciences*, *266*(1178), 425–533. https://doi.org/10.1098/rsta.1970.0010

Lehner, F., Schurer, A. P., Hegerl, G. C., Deser, C., & Frölicher, T. L. (2016). The importance of ENSO phase during volcanic eruptions for detection and attribution. *Geophysical Research Letters*, *43*, 2851–2858. https://doi.org/10.1002/2016GL067935

Liu, F., Zhao, T., Wang, B., Liu, J., & Luo, W. (2018). Different global precipitation responses to solar, volcanic, and greenhouse gas forcings. *Journal of Geophysical Research: Atmospheres*, *123*, 4060–4072. https://doi.org/10.1029/2017JD027391

Lough, J. M., & Fritts, H. C. (1987). An assessment of the possible effects of volcanic eruptions on north American climate using tree-ring data, 1602 to 1900 a.D. *Climatic Change*, *10*(3), 219–239. https://doi.org/10.1007/BF00143903

Maher, N., McGregor, S., England, M. H., & Gupta, A. S. (2015). Effects of volcanism on tropical variability: Effects of volcanism. *Geophysical Research Letters*, *42*, 6024–6033. https://doi.org/10.1002/2015GL064751

Man, W., Zhou, T., & Jungclaus, J. H. (2014). Effects of large volcanic eruptions on global summer climate and East Asian monsoon changes during the last millennium: Analysis of MPI-ESM simulations. *Journal of Climate*, *27*(19), 7394–7409. https://doi.org/10.1175/JCLI-D-13-00739.1

Mass, C. F., & Portman, D. A. (1989). Major volcanic eruptions and climate: A critical evaluation. *Journal of Climate*, *2*(6), 566–593. https://doi.org/10.1175/1520-0442(1989)002%3C0566:MVEACA%3E2.0.CO;2

McGraw, M. C., Barnes, E. A., & Deser, C. (2016). Reconciling the observed and modeled Southern Hemisphere circulation response to volcanic eruptions: Reconciling SH response to volcanoes. *Geophysical Research Letters*, *43*, 7259–7266. https://doi.org/10.1002/2016GL069835

Monerie, P.-A., Moine, M.-P., Terray, L., & Valcke, S. (2017). Quantifying the impact of early 21st century volcanic eruptions on global-mean surface temperature. *Environmental Research Letters*, *12*(5), 054010. https://doi.org/10.1088/1748-9326/aa6cb5

Neukom, R., Gergis, J., Karoly, D. J., Wanner, H., Curran, M., Elbert, J., et al. (2014). Inter-hemispheric temperature variability over the past millennium. *Nature Climate Change*, *4*(5), 362–367. https://doi.org/10.1038/nclimate2174

Newhall, C. G., & Self, S. (1982). The volcanic explosivity index (VEI) an estimate of explosive magnitude for historical volcanism. *Journal of Geophysical Research*, *87*(C2), 1231–1238. https://doi.org/10.1029/JC087iC02p01231

Oman, L., Robock, A., Stenchikov, G., Schmidt, G. A., & Ruedy, R. (2005). Climatic response to high-latitude volcanic eruptions. *Journal of Geophysical Research*, *110*, D13103. https://doi.org/10.1029/2004JD005487

Pausata, F. S. R., Chafik, L., Caballero, R., & Battisti, D. S. (2015). Impacts of high-latitude volcanic eruptions on ENSO and AMOC. *Proceedings of the National Academy of Sciences*, *112*(45), 13,784–13,788. https://doi.org/10.1073/pnas.1509153112

Perlwitz, J., & Graf, H.-F. (1995). The statistical connection between tropospheric and stratospheric circulation of the Northern Hemisphere in winter. *Journal of Climate*, *8*(10), 2281–2295. https://doi.org/10.1175/1520-0442(1995)008%3C2281:TSCBTA%3E2.0.CO;2

Raible, C. C., Brönnimann, S., Auchmann, R., Brohan, P., Frölicher, T. L., Graf, H.-F., et al. (2016). Tambora 1815 as a test case for high impact volcanic eruptions: Earth system effects. *Wiley Interdisciplinary Reviews: Climate Change*, *7*(4), 569–589. https://doi.org/10.1002/wcc.407

Rao, M. P., Cook, B. I., Cook, E. R., D'Arrigo, R. D., Krusic, P. J., Anchukaitis, K. J., et al. (2017). European and Mediterranean hydroclimate responses to tropical volcanic forcing over the last millennium. *Geophysical Research Letters*, *44*, 5104–5112. https://doi.org/10.1002/2017GL073057

Robock, A. (2000). Volcanic eruptions and climate. *Reviews of Geophysics*, *38*(2), 191–219. https://doi.org/10.1029/1998RG000054

Robock, A., & Mao, J. (1995). The volcanic signal in surface temperature observations. *Journal of Climate*, *8*(5), 1086–1103. https://doi.org/10.1175/1520-0442(1995)008%3C1086:TVSIST%3E2.0.CO;2

Rosenlof, K. H. (1995). Seasonal cycle of the residual mean meridional circulation in the stratosphere. *Journal of Geophysical Research*, *100*(D3), 5173. https://doi.org/10.1029/94JD03122

Salinger, M. J. (1998). New Zealand climate: The impact of major volcanic eruptions. *Weather and Climate*, *18*(1), 11–19. https://doi.org/10.2307/44280024

Sato, M., Hansen, J. E., McCormick, M. P., & Pollack, J. B. (1993). Stratospheric aerosol optical depths, 1850–1990. *Journal of Geophysical Research*, *98*(D12), 22987. https://doi.org/10.1029/93JD02553

Schneider, D. P., Ammann, C. M., Otto-Bliesner, B. L., & Kaufman, D. S. (2009). Climate response to large, high-latitude and low-latitude volcanic eruptions in the community climate system model. *Journal of Geophysical Research*, *114*, D15101. https://doi.org/10.1029/2008JD011222

Sigl, M., Winstrup, M., McConnell, J. R., Welten, K. C., Plunkett, G., Ludlow, F., et al. (2015). Timing and climate forcing of volcanic eruptions for the past 2,500 years. *Nature*, *523*(7562), 543–549. https://doi.org/10.1038/nature14565

Stevenson, S., Fasullo, J. T., Otto-Bliesner, B. L., Tomas, R. A., & Gao, C. (2017). Role of eruption season in reconciling model and proxy responses to tropical volcanism. *Proceedings of the National Academy of Sciences*, *114*(8), 1822–1826. https://doi.org/10.1073/pnas.1612505114

Stothers, R. B. (1999). Volcanic dry fogs, climate cooling, and plague pandemics in Europe and the Middle East. *Climatic Change*, *42*, 713–723. https://doi.org/10.1023/A:1005480105370

Sun, W., Wang, B., Liu, J., Chen, D., Gao, C., Ning, L., & Chen, L. (2019). How northern high-latitude volcanic eruptions in different seasons affect ENSO. *Journal of Climate*, *32*(11), 3245–3262. https://doi.org/10.1175/JCLI-D-18-0290.1

Taylor, K. E., Stouffer, R. J., & Meehl, G. A. (2012). An overview of CMIP5 and the experiment design. *Bulletin of the American Meteorological Society*, *93*(4), 485–498. https://doi.org/10.1175/BAMS-D-11-00094.1

Textor, C., Graf, H.-F., Timmreck, C., & Robock, A. (2004). Emissions from volcanoes. In C. Granier, P. Artaxo, & C. E. Reeves (Eds.), *Emissions of atmospheric trace compounds* (Vol. 18, pp. 269–303). Netherlands: Springer. https://doi.org/10.1007/978-1-4020-2167-1_7

Thompson, D. W. J., Wallace, J. M., Jones, P. D., & Kennedy, J. J. (2009). Identifying signatures of natural climate variability in time series of global-mean surface temperature: Methodology and insights. *Journal of Climate*, *22*(22), 6120–6141. https://doi.org/10.1175/2009JCLI3089.1

Timmreck, C. (2012). Modeling the climatic effects of large explosive volcanic eruptions. *WIREs Climate Change*, *3*(6), 545–564. https://doi.org/10.1002/wcc.192

Timmreck, C. (2018). Climatic effects of large volcanic eruptions. *Habilitation Thesis*. Hamburg: Universität Hamburg. https://doi.org/10.17617/2.2566000

Toohey, M., Krüger, K., Schmidt, H., Timmreck, C., Sigl, M., Stoffel, M., & Wilson, R. (2019). Disproportionately strong climate forcing from extratropical explosive volcanic eruptions. *Nature Geoscience*, *12*(2), 100–107. https://doi.org/10.1038/s41561-018-0286-2

Toohey, M., Krüger, K., Sigl, M., Stordal, F., & Svensen, H. (2016). Climatic and societal impacts of a volcanic double event at the dawn of the middle ages. *Climatic Change*, *136*(3–4), 401–412. https://doi.org/10.1007/s10584-016-1648-7

Trepte, C. R., Veiga, R. E., & McCormick, M. P. (1993). The poleward dispersal of Mount Pinatubo volcanic aerosol. *Journal of Geophysical Research*, *98*(D10), 18,563–18,573. https://doi.org/10.1029/93JD01362

Wang, T., Guo, D., Gao, Y., Wang, H., Zheng, F., Zhu, Y., et al. (2018). Modulation of ENSO evolution by strong tropical volcanic eruptions. *Climate Dynamics*, *51*(7–8), 2433–2453. https://doi.org/10.1007/s00382-017-4021-2

Wilmes, S. B., Raible, C. C., & Stocker, T. F. (2012). Climate variability of the mid- and high-latitudes of the Southern Hemisphere in ensemble simulations from 1500 to 2000 AD. *Climate of the Past*, *8*(1), 373–390. https://doi.org/10.5194/cp-8-373-2012

Young, P. J., Thompson, D. W. J., Rosenlof, K. H., Solomon, S., & Lamarque, J.-F. (2011). The seasonal cycle and interannual variability in stratospheric temperatures and links to the Brewer–Dobson circulation: An analysis of MSU and SSU data. *Journal of Climate*, *24*(23), 6243–6258. https://doi.org/10.1175/JCLI-D-10-05028.1

Zambri, B., LeGrande, A. N., Robock, A., & Slawinska, J. (2017). Northern Hemisphere winter warming and summer monsoon reduction after volcanic eruptions over the last millennium. *Journal of Geophysical Research: Atmospheres*, *122*, 7971–7989. https://doi.org/10.1002/2017JD026728

Zambri, B., & Robock, A. (2016). Winter warming and summer monsoon reduction after volcanic eruptions in Coupled Model Intercomparison Project 5 (CMIP5) simulations. *Geophysical Research Letters*, *43*, 10,920–10,928. https://doi.org/10.1002/2016GL070460

Zanchettin, D., Bothe, O., Timmreck, C., Bader, J., Beitsch, A., Graf, H.-F., et al. (2014). Inter-hemispheric asymmetry in the sea-ice response to volcanic forcing simulated by MPI-ESM (COSMOS-mill). *Earth System Dynamics*, *5*(1), 223–242. https://doi.org/10.5194/esd-5-223-2014

Zanchettin, D., Timmreck, C., Toohey, M., Jungclaus, J. H., Bittner, M., Lorenz, S. J., & Rubino, A. (2019). Clarifying the relative role of forcing uncertainties and initial-condition unknowns in spreading the climate response to volcanic eruptions. *Geophysical Research Letters*, *46*, 1602–1611. https://doi.org/10.1029/2018GL081018

Zhang, D., Blender, R., & Fraedrich, K. (2013). Volcanoes and ENSO in millennium simulations: Global impacts and regional reconstructions in East Asia. *Theoretical and Applied Climatology*, *111*(3–4), 437–454. https://doi.org/10.1007/s00704-012-0670-6

Zuo, M., Man, W., Zhou, T., & Guo, Z. (2018). Different impacts of northern, tropical, and southern volcanic eruptions on the tropical Pacific SST in the last millennium. *Journal of Climate*, *31*(17), 6729–6744. https://doi.org/10.1175/JCLI-D-17-0571.1

Received: 7 November 2020 | Revised: 30 March 2021 | Accepted: 7 April 2021

DOI: 10.1002/joc.7135

RESEARCH ARTICLE

International Journal of Climatology RMetS

Southern African temperature responses to major volcanic eruptions since 1883: Simulated by CMIP5 models

Pamela J. Harvey | **Stefan W. Grab**

School of Geography, Archaeology and Environmental Studies, University of the Witwatersrand, Johannesburg, South Africa

Correspondence
Pamela J. Harvey, School of Geography, Archaeology and Environmental Studies, University of the Witwatersrand, Johannesburg, South Africa.
Email: pamjharvey14@gmail.com

Funding information
National Research Foundation, Grant/Award Numbers: 102161, 111491

Abstract

Although volcanic forcing impacts on climate have gained much international attention during recent years, focus has largely been at hemispheric scale, and most particularly on the Northern Hemisphere (NH). Here we investigate the impact of major volcanic eruptions since 1883 on southern African climate, with a view to establishing potential sub-regional differences across a variety of temporal scales. To this end, we use historical simulations from the Coupled Model Intercomparison Project, Phase 5 (CMIP5) to study near-surface temperature responses to four major eruptions (Krakatau, 1883; Santa Maria, 1902; Agung, 1963; Pinatubo, 1991) over six sub-regions of southern Africa. Results show significant cooling across all sub-regions after each eruption. However, we detect considerable sub-regional differences in the amplitude, timing and duration of responses. For instance, stronger temperature departures occur in northern rather than southern sub-regions where diurnal and annual temperature ranges are normally greater. While significant responses occur within the first year after each eruption, there is a more delayed response in three of the sub-regions (southwestern coast and central southern Africa) following the Santa Maria eruption. Strongest responses follow the Krakatau eruption in all sub-regions, while the weakest response follows the Santa Maria eruption in western sub-regions and the Agung eruption in eastern sub-regions. Most regions experience the strongest temperature departures during austral autumn and winter (MAM and JJA), and weakest during spring (SON).

KEYWORDS

climate modelling, CMIP5, southern Africa, sub-regional scale, temperature response, volcanic forcing

1 | INTRODUCTION

Global to regional climates are affected by both internal variability (e.g., El Niño–Southern Oscillation, Southern Annular Mode etc.) and external forcing mechanisms (e.g., solar, volcanic, anthropogenic CO_2 etc.) (Lyu *et al*., 2015; Dieng *et al*., 2017). Although the role of volcanic forcing on earth's climate has captured scientific interest for over a century (e.g., Humphreys, 1913; Gentilli, 1948; Wexler, 1951; Lamb, 1970; Gilliland, 1982), such inquiry has grown substantially over the last ~30 years (Robock, 2000; Timmreck, 2012). Major volcanic eruptions releasing more than five Teragrams (Tg) of emitted sulfur dioxide (SO_2) into the lower stratosphere can affect global, hemispheric and regional climates (Timmreck, 2018). SO_2 from extratropical volcanic eruptions are predominantly transported within the hemisphere in which the eruption occurred, while those from tropical eruptions are typically transported throughout both hemispheres (Oman *et al*., 2005), depending on the quasi-biennial oscillation phase (a westerly phase will cause aerosols to be transported towards the winter hemisphere faster than during the easterly phase, during which the aerosols would then be transferred to both hemispheres (Dhomse *et al*., 2020). The aerosol lifetime is also longer if the eruption occurs during a westerly phase (Visioni *et al*., 2018). Volcanic aerosols increase the scattering and absorption of incoming solar radiation, thereby altering the earth's energy budget (Textor *et al*., 2004; Kremser *et al*., 2016; Liu *et al*., 2018). A further consequence of this is the strengthening of zonal winds and increase in temperature and density differences between the equator and poles, thus also affecting atmospheric circulation (Perlwitz and Graf, 1995; Zambri and Robock, 2016).

Volcanic impact on hemispheric- to regional-scale climates is complex and seems highly variable given multiple influencing factors. These include eruption size, duration, location and timing, and contemporaneous internal climate variability (e.g., ENSO and Northern or Southern Annular Modes) (Zanchettin *et al*., 2014; Colose *et al*., 2015; Stevenson *et al*., 2017; Sun *et al*., 2019). Negative global temperature departures of as much as 1.00°C have been proposed following the Tambora (1815) eruption (Kandlbauer *et al*., 2013); but even for somewhat lower magnitude eruptions such as Pinatubo (1991), global temperatures may be reduced by as much as 0.40°C (Thompson *et al*., 2009; Kremser *et al*., 2016). Summer cooling and winter warming is a common climatic response to major eruptions over North America, large parts of Europe and northern Eurasia (Robock, 2000; Timmreck, 2012; Zambri *et al*., 2017). However, the response is not uniform throughout the Northern Hemisphere (NH) and is not the same after each eruption; for instance, the strength and timing of the response can vary by location as well as by eruption. For example, a study using models, observations and reanalysis data (Dogar *et al*., 2017) found that the Middle East and northern Africa experienced both summer and winter cooling after the El Chichón (1982) and Pinatubo eruptions, with winter cooling being stronger than that in summer (between −0.50 and − 2.00°C). In Asia, a modelling study which uses a composite of 21 eruptions (AD 800 to 2005) occurring during neutral ENSO phases, found particularly strong cooling over western China (−2.00°C) in the first year after eruptions (Zhang *et al*., 2013), while instrumental data show that Japanese summer temperatures dropped by ∼1.3°C following major eruptions between 1835 and 1955 (Kondo, 1988). Temperature responses over Europe, identified from both tree ring and instrumental data, are also somewhat variable. Central Europe typically records cooling of ∼ − 0.18°C one year after major eruptions (i.e., those with a Volcanic Explosivity Index [VEI] value of ≥4), while northern Europe usually records stronger (−0.52°C) cooling responses, but with a two-year lag between the eruption and maximum cooling (Esper *et al*., 2013). North American responses are typified by cooling over northernmost regions but may include warming scenarios over parts of the USA, depending on eruption location (Lough and Fritts, 1987—tree ring data; Shindell, 2004—climate modelling).

Given that Southern Hemisphere (SH) climate is affected to a greater extent by internal variability than external forcing, temperature responses following major eruptions tend to be weaker than in the NH (Wilmes *et al*., 2012; Neukom *et al*., 2014; Monerie *et al*., 2017). Several authors (e.g., Mass and Portman, 1989; Robock and Mao, 1995; Harvey *et al*., 2020) have established mean negative SH temperature departures of between 0.10 and 0.36°C following major eruptions. Cooling is possible over South America, southern Africa and Australasia from as early as 1 month after a major eruption (Salinger, 1998; Man *et al*., 2014; Colose *et al*., 2016). Recently, Harvey *et al*. (2020) used historical simulations from the Coupled Model Intercomparison Project, Phase 5 (CMIP5), to establish finer temporal-scale (monthly/seasonal) SH continental temperature departures following the eruptions of Krakatau (1883), Santa Maria (1902), Agung (1963) and Pinatubo (1991). Their findings indicate significant cooling over continents in response to these eruptions, and that anomalies are generally strongest during austral autumn and winter seasons.

Given the relative scarcity of long and reliable instrumental weather records for much of the SH, a variety of other climate proxies have been used to reconstruct climates of the SH. Several tree ring based climate reconstructions for the Australasia and Patagonia regions have revealed strong negative temperature anomalies occurring around the time of major volcanic eruptions, such as after the Tambora, Krakatau and Santa Maria events (Cook *et al*., 2002; Palmer and Xiong, 2004; Vincent *et al*., 2007; Roig and Villalba, 2008). In the southwestern Cape region of South Africa, a *Widdringtonia cedarbergensis* tree ring record confirms unusual frost rings in 1787 and 1816 following the Laki (1783/4) and Tambora (1815) eruptions (Dunwiddie and LaMarche, 1980; LaMarche and Hirschboeck, 1984). In addition, evidence for unusual dry fog occurrences in Rio de Janeiro (Brazil, South America) between 1784 and

1786 coincidently occurred after the Laki eruption (Trigo *et al*., 2010). In central southern Africa, 19th century documentary accounts (e.g., diaries, newspapers, missionary reports) of severe cold and snow are regularly recorded in years after major eruptions (Grab and Nash, 2010). Most recently, Picas and Grab (2020) use a long station-based temperature series from the Royal Astronomical Observatory in Cape Town to demonstrate significant negative temperature departures following 19th century eruptions. Collectively, these studies indicate considerable climatic responses to volcanic forcing in the SH. Notwithstanding the value of these and previous modelling studies, a major knowledge gap remains with identifying finer spatiotemporal scale volcanic-forcing impacts across selected SH continental regions. Such an investigation is particularly important given that the impact of volcanic forcing on temperature is not necessarily spatially consistent across continents (Schneider *et al*., 2009). In fact, adjoining regions may sometimes experience contrasting temperature responses to volcanic forcing, which cannot be captured in globally or hemispherically averaged outputs (Lyu *et al*., 2015). To this end, we aim to establish the characteristics of near-surface temperature responses to four major volcanic eruptions (Krakatau, 1883; Santa Maria, 1902; Agung, 1963; Pinatubo, 1991) across sub-regions of southern Africa using simulations from CMIP5 (Taylor *et al*., 2012). This is achieved through a multi-temporal investigative approach (annual to monthly).

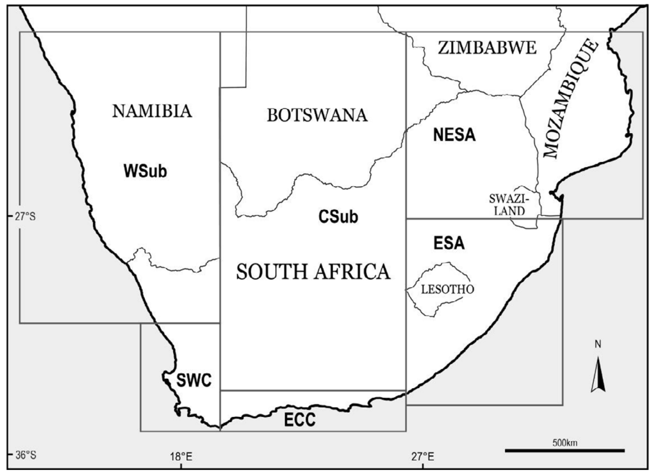

FIGURE 1 Various sub-regions of southern Africa used in this study (after Engelbrecht *et al*., 2008): SWC = South Western Cape; ECC = Eastern Cape Coast; ESA = Eastern South Africa; WSub = Western subcontinent; CSub = central subcontinent; NESA = North-Eastern South Africa, southern Zimbabwe and southern Mozambique

2 | METHODOLOGY

2.1 | Study region and climatic setting

The southern African region represented in this paper is located between 20 and 35°S latitude and 12.5 and 36°E longitude (Figure 1). This covers the southern parts of Namibia, Botswana, Zimbabwe and Mozambique, as well as the countries of South Africa, Eswatini and Lesotho. The region is flanked by the Indian Ocean along the east coast where the sub-continent is impacted by the warm southerly flowing Mozambique and Agulhas currents; while the Atlantic Ocean along the west coast experiences upwelling due to the cool northerly flowing Benguela current. Coupling between atmosphere and oceans greatly influences the climate of southern Africa (Tyson *et al*., 2000). In particular, ocean currents regulate temperatures along coastal sub-regions, with the Benguela current contributing to an arid climate, and the Mozambique and Agulhas currents resulting in warm and humid climates (Landman *et al*., 2017; Roffe *et al*., 2020).

Southern Africa's climate is strongly influenced by atmospheric circulation in tropical and temperate latitudes. High pressure systems resulting from anticyclonic circulation are dominant climatic influencers in the region, in particular the Subtropical South Atlantic and Subtropical South Indian Anticyclones, and the continental high (Tyson *et al*., 2000; Landman *et al*., 2017). However, the region is also affected by westerly waves and troughs, often resulting in cold fronts reaching into the southern sub-regions and interior of southern Africa. Although high-pressure systems dominate year round, both anticyclonic systems and westerlies strengthen and move equatorward during austral winter, which at times permits the passage of cold fronts over southern and central parts of the sub-continent (Grab and Simpson, 2000).

For the purpose of our study, we divide the southern African region into six climatically defined sub-regions according to Engelbrecht *et al*. (2008) (Figure 1). These include the South Western Cape (SWC), the Eastern Cape Coast (ECC), Eastern South Africa (ESA), the Western Subcontinent (WSub), the Central Subcontinent (CSub) and North-Eastern South Africa, southern Zimbabwe and southern Mozambique (NESA) (see Table 1 for exact latitude and longitude positions). Climates of these sub-regions are classified according to the Köppen-Geiger (Köppen, 1936) classification. The three southernmost sub-regions (SWC, ECC and ESA) have temperate climate types with warm humid summers and mild winters. The SWC has a Mediterranean climate with cool/wet winters and warm/dry summers, while the ECC has both Mediterranean and subtropical climate characteristics, with year-round rainfall. Both the SWC and ECC regions are affected by frontal weather associated with mid-

TABLE 1 Southern African sub-regions used in this study (adapted from Engelbrecht *et al*., 2008)

Region	Abbreviation	Latitude	Longitude
South-Western cape	SWC	−35° to −31°	17° to 20°
Eastern Cape Coast	ECC	−35° to −33.5°	20° to 27°
Eastern South Africa	ESA	−34° to −27°	27° to 33°
Western subcontinent	WSub	−31° to −20°	12.5° to 20°
Central subcontinent	CSub	−33.5° to −20°	20° to 27°
North-Eastern South Africa, southern Zimbabwe and southern Mozambique	NESA	−27° to −20°	27° to 36°

TABLE 2 Models used in this study, and the volcanic forcing data set used by each (after Driscoll *et al*., 2012; Taylor *et al*., 2012; Harvey and Grab, submitted)

Model name	Institution	Volcanic forcing
CanESM2	Canadian Centre for Climate Modelling and Analysis	Sato *et al*. (1993)
CCSM4	National Center for Atmospheric Research	Ammann *et al*. (2007)
CNRM-CM5	Centre National de Recherches Météorologiques & Centre Européen de Recherche et de Formation Avancée en Calcul Scientifique	Ammann *et al*. (2007)
CSIRO-Mk3-6-0	Commonwealth Scientific and Industrial Research Organization	Sato *et al*. (1993)
GISS-E2-H	NASA Goddard Institute for Space Studies	Sato *et al*. (1993)
GISS-E2-R (P1)	NASA Goddard Institute for Space Studies	Sato *et al*. (1993)
GISS-E2-R (P3)	NASA Goddard Institute for Space Studies	Sato *et al*. (1993)
MIROC-ESM MIROC-ESM-CHEM	Japan Agency for Marine-Earth Science and Technology, Atmosphere and Ocean Research Institute (the University of Tokyo), and National Institute for Environmental Studies	Sato *et al*. (1993) Sato *et al*. (1993)
MRI-CGCM3	Meteorological Research Institute	Interactive
NorESM1-M	Norwegian Climate Centre	Ammann *et al*. (2007)

latitude cyclones, particularly during late autumn, winter and early spring. The occurrence and passage of cold fronts are primary factors influencing winter severity over ESA and southern parts of WSub, CSub and NESA (Grab and Simpson, 2000), but their influence dissipates northwards, where they have increasingly rare/minimal impacts. ESA has a large annual temperature range but relatively small diurnal range (Pidwirny, 2006; Kruger and Sekele, 2013; Engelbrecht and Engelbrecht, 2016). The CSub and NESA regions are mostly semi-arid (steppe) and the WSub region is mostly dry arid (desert). The WSub and NESA regions have high annual and monthly mean temperatures with high diurnal temperature ranges (Pidwirny, 2006). In particular, the diurnal range for the WSub region is considerably higher than that for the other six regions (Kruger and Sekele, 2013). Continentality of the CSub region accounts for moderate-high annual and monthly mean temperatures and relatively cool winters (Pidwirny, 2006; Kruger and Sekele, 2013; Engelbrecht and Engelbrecht, 2016).

2.2 | Models and data

An assortment of CMIP5 (Taylor *et al*., 2012) models were used, of which 11 were selected (Table 2) based on their ability to simulate a reasonable lower stratospheric temperature response to volcanic forcing (see Santer *et al*., 2013; Figure S1). Historical experiments, incorporating both natural and anthropogenic forcing, were applied. Three ensemble members were used from each model (realizations 1–3), except for the MIROC-ESM-CHEM model, for which only one realization was available. Two different physics versions were used for the GISS-E2_R model: p1, which uses prescribed aerosols, and p3, in which aerosols are calculated within the model. This equates to 33 simulations for our study. All models used are either after Sato *et al*. (1993) or Ammann *et al*. (2007) for volcanic forcing, given that it was not prescribed for CMIP5, apart from MRI_CGCM3 which computed aerosols within the model itself.

Data were regridded linearly to a 2° by 2° latitude-longitude grid before having established a multi-model ensemble. Annual, seasonal and monthly near-surface (2 m) temperature anomalies (departures from mean) were calculated with respect to 20-year running means. Statistical significance of the anomalies is calculated through resampling the original time series of anomalies 5,000 times using the bootstrap approach (Efron, 1979). Thereafter, the 5th and 95th percentiles of this resampled time series were used to compare against the original time series in order to establish the likelihood of post-eruption responses occurring randomly, and from this, significant anomalies may be identified (Haurwitz and Brier, 1981; Rao *et al.*, 2017). The ensemble mean robustness is tested by comparing the 25th and 75th percentiles of individual simulations to the ensemble mean. In order to test for the reliability of the CMIP5 models in generating responses for southern African regions, monthly temperature responses for the SWC region for the Krakatau eruption were compared with the findings of Picas and Grab (2020), who used instrumental data to identify temperature response to eruptions between 1834 and 1899 in Cape Town, South Africa. Given that Picas and Grab (2020) use a climatological reference period of 1834–1899 to calculate temperature departures, it must be acknowledged that the differences in reference periods for anomaly calculations in our respective studies will account for some differences in the comparison.

We investigate four major volcanic eruptions: Krakatau (1883), Santa Maria (1902), Agung (1963) and Pinatubo (1991). Each of these eruptions significantly impacted mean SH and southern African temperatures (Harvey *et al.*, 2020). This paper presents considerably finer spatial-scale area-averaged temperature responses to these eruptions, than those of previous investigations for the SH. To this end, the timing, duration, seasonality and magnitude of temperature responses for each of the six sub-regions (i.e., climate types) of southern Africa, are established.

3 | RESULTS

3.1 | Krakatau

The SH (6°S—Indonesia) Krakatau eruption occurred in August 1883, with a VEI of 6 and emission of 22Tg of SO_2 into the stratosphere (Neely III and Schmidt, 2016). Negative mean annual temperature anomalies are simulated for all regions in southern Africa in the first 3 years after the eruption (Table 3). However, negative anomalies were only significant for all 3 years in the ESA, WSub and CSub regions; significant in the first (y1) and second (y2) post-eruption years in the NESA region; and in y1 and year y3 in the SWC and ECC regions. For each year, the weakest mean annual anomaly (−0.13 to −0.19°C) was observed in the ECC region, followed closely by the SWC region (−0.18 to −0.33°C). The strongest negative anomaly was depicted in the WSub region in y1 (−0.49°C), in NESA in y2 (−0.44°C) and in CSub in y3 (−0.40°C).

We now compare seasonal responses for each region following the Krakatau eruption (Figure 2). Anomalies

TABLE 3 Mean annual temperatures for each sub-region following the four eruptions

		SWC	ECC	ESA	WSub	CSub	NESA
Krakatau	1883	0.07	0.05	0.10	0.14	0.18	0.09
	1884	-0.33	-0.19	-0.44	-0.49	-0.47	-0.38
	1885	-0.18	-0.13	-0.41	-0.35	-0.39	-0.44
	1886	-0.21	-0.16	-0.33	-0.34	-0.40	-0.30
Santa Maria	1902	0.12	0.05	0.07	0.11	0.09	0.07
	1903	-0.11	-0.03	-0.31	-0.30	-0.34	-0.37
	1904	-0.22	-0.13	-0.28	-0.27	-0.36	-0.32
	1905	-0.12	-0.10	-0.13	-0.16	-0.20	-0.21
Agung	1963	-0.05	0.01	-0.08	-0.10	-0.11	-0.08
	1964	-0.35	-0.17	-0.37	-0.50	-0.50	-0.31
	1965	-0.19	-0.14	-0.14	-0.10	-0.12	-0.15
	1966	-0.14	-0.08	-0.05	-0.17	-0.09	-0.11
Pinatubo	1991	0.06	0.04	0.01	0.06	0.06	0.04
	1992	-0.29	-0.18	-0.34	-0.36	-0.37	-0.35
	1993	-0.17	-0.13	-0.22	-0.22	-0.23	-0.13
	1994	-0.20	-0.16	-0.18	-0.25	-0.24	-0.25

Note: Grey shading = year of eruption; blue shading = significant anomalies.

are negative for each season in each region for y1 to y3, albeit not always significant. Seasonal anomalies are most frequently significant in the ESA, WSub, CSub and NESA regions, and less so over the SWC and ECC regions. In the SWC, negative anomalies are significant in all seasons during y1 (Figure 3), in austral autumn (MAM) of y2 and in austral winter (JJA) and spring (SON) of y3 (Table 4). Although anomalies are not significant during austral summer (DJF) in the ECC, they are so for JJA in y1-y3, MAM in y2 and SON in y1 and y3 (Table 4). ESA has significant negative temperature anomalies in DJF for y1-3, and in MAM and JJA for y1-2, but only in SON for y3. The WSub has significant negative anomalies in each season in y1, in DJF and MAM of y2, and in DJF, JJA and SON of y3 (Table 4). The CSub is the only other region during which the DJF anomaly of y1 is not significant, however, anomalies for MAM and JJA are significant. In y2, the DJF anomaly becomes significant, and the MAM and JJA anomalies remain significant. In y3, significant anomalies occur during DJF, JJA and SON. Over NESA, significant negative anomalies occur in DJF for y1-y3, in MAM for y1-y2, in JJA for y1-y2 and SON for y2-y3 (Table 4). Notably, while anomalies in SON are not always significant in y1 or y2 for each region, they are always significant in y3.

Strongest y1 anomalies occur during austral autumn (MAM) in the WSub (−0.60°C), CSub (−0.58°C) and over NESA (−0.50°C), and during austral winter (JJA) over

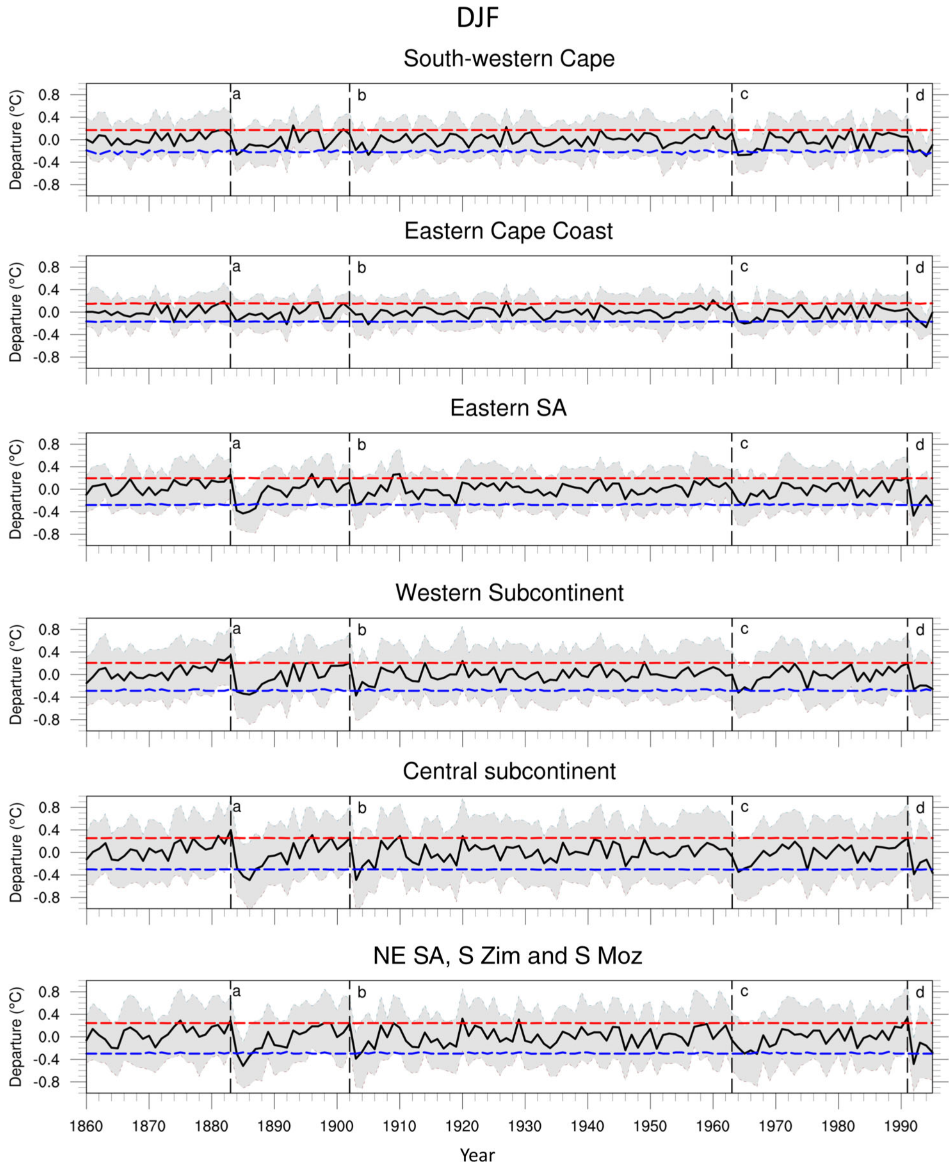

FIGURE 2 Seasonal temperature anomalies for each southern African sub-region (1860–1996). Vertical lines represent the eruptions: a = Krakatau, b = Santa Maria, c = Agung, d = Pinatubo. Grey shading represents the ensemble mean, and the blue and red lines the 5th and 95th percentile [Colour figure can be viewed at wileyonlinelibrary.com]

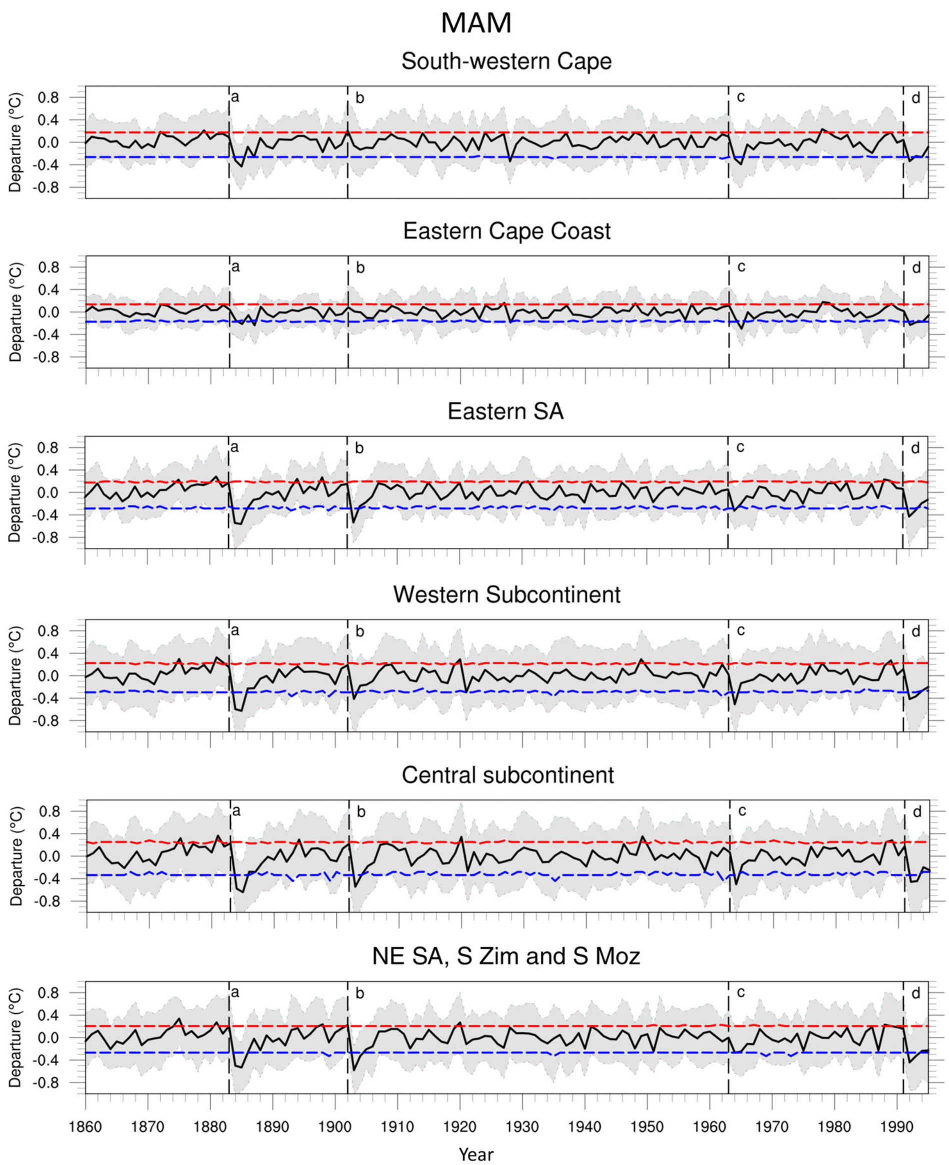

FIGURE 2 (Continued)

the ECC (−0.24°C), SWC (−0.39°C) and ESA (−0.56°C) regions. The weakest response occurs in DJF in the SWC (−0.27°C), CSub (−0.28°C) and WSub (−0.30°C) regions, in SON over NESA (−0.19°C) and ESA (−0.21°C) and in MAM over the ECC (−0.15°C) region. The strongest temperature response during the initial 3 years following Krakatau (Table 4) occurs during MAM of y2 for all regions (mean = −0.56°C) except the ECC, where the strongest response (−0.29°C) occurs during JJA of y3.

The strongest post-Krakatau monthly temperature departure occurs almost 2 years after the eruption (21 months), namely in May 1885 for all regions (mean = −0.76°C) except over NESA where the maximum monthly response occurs 4 months earlier (January 1885; −0.62°C; Figure 4). The strongest maximum monthly departure is recorded for the CSub region (−0.98°C—May 1885), followed by the WSub region (−0.85°C—May 1885), while the weakest peak response occurs in the ECC region (−0.53°C – May 1885). For the first 3 years post Krakatau, most mean monthly temperatures are below normal for all regions, ranging from 95% (NESA) to 83% (SWC) of months, however, significantly below normal mean values range from only 17% (ECC) to 68% (CSub) of months (Table 5).

To test the reliability of CMIP5 model results used in this study, we compare temperature responses following the Krakatau eruption for the SWC region to instrumental data provided by Picas and Grab (2020). Picas and Grab (2020) identify cooling within the first 24 months after the eruption, but then some recovery between months 25 and 32, only to be followed by another cooling phase between months 33 and 43. Our CMIP5 model outputs demonstrate a similar pattern, which provides for at

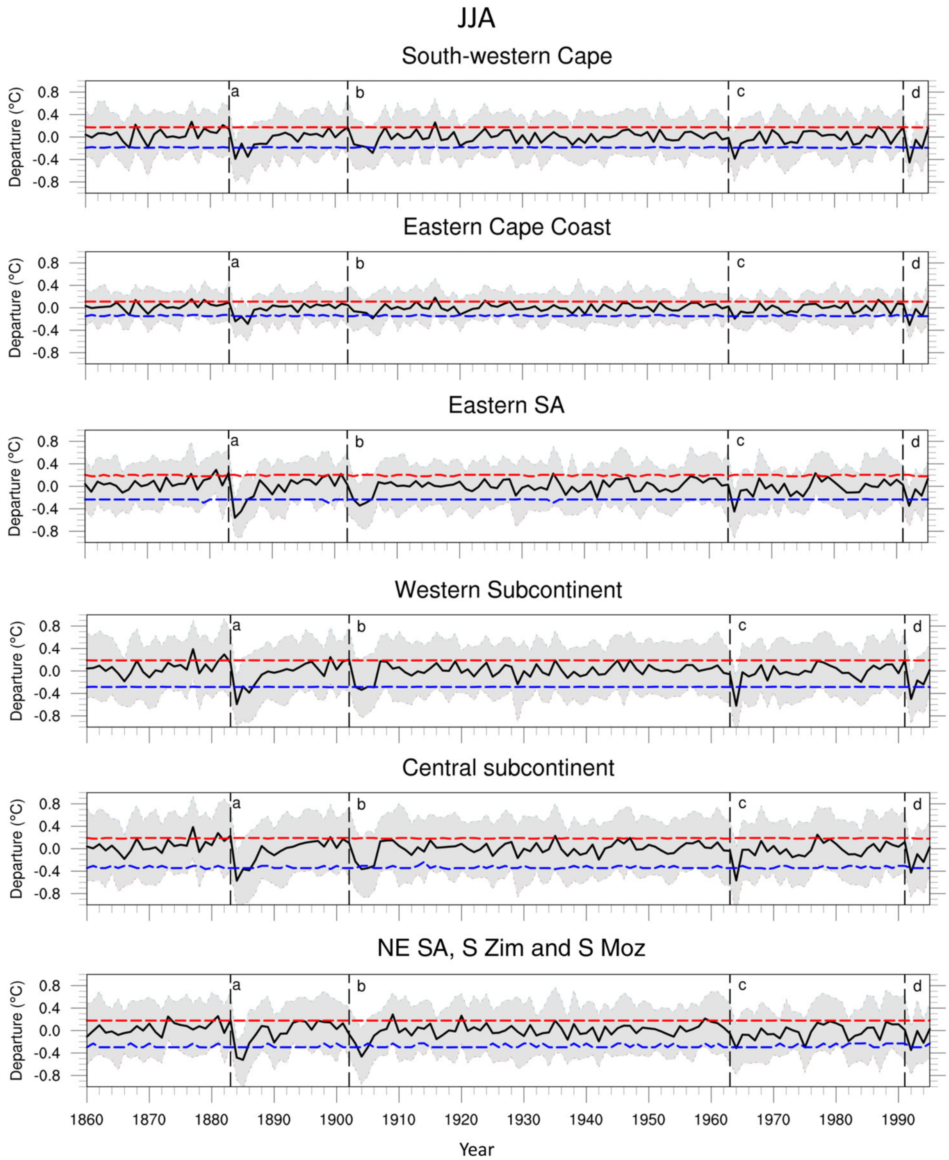

FIGURE 2 (Continued)

least a reasonable measure of confidence in our results. Instrumental records indicate that of the first 24 months following Krakatau, 15 of these had negative temperature departures, of which 12 were significantly below 'normal' (Picas and Grab, 2020). In comparison, although we find that 20 of these months are below 'normal', only nine are significantly below 'normal'. For seasonal averages, negative instrumental temperature departures are stronger than those of model departures during MAM of y2 and SON of both y1 and y3. In addition, maximum monthly cooling occurs in different months of y1, but during the same months of y2 and y3, when comparing model and instrumental data (Table 6). For months 1–13 following the Krakatau eruption, the mean instrumental temperature departure is −0.30°C, while that for CMIP5 model outputs is −0.22°C. According to Picas and Grab (2020), the strongest negative temperature departures are recorded during May 1885 (−1.75°C), which is also the case for our model outputs despite a considerably lower magnitude of departure (i.e., May 1885: −0.77°C). In summary, while values of temperature departure are not the same for the two data sets (Table 6), their temporal patterns of departure are very similar. Notably, while most modelling studies suggest that CMIP5 models overestimate cooling following volcanic eruptions (Chylek *et al*., 2020), we find the opposite to be true in the case of our comparative analysis for the SWC. Nonetheless, CMIP6 models are now required to use a common volcanic forcing data set (Space-based Stratospheric Aerosol Climatology) to improve reliability. This data set uses an improved and adjusted stratospheric aerosol optical depth, which should be more reliable than the forcing

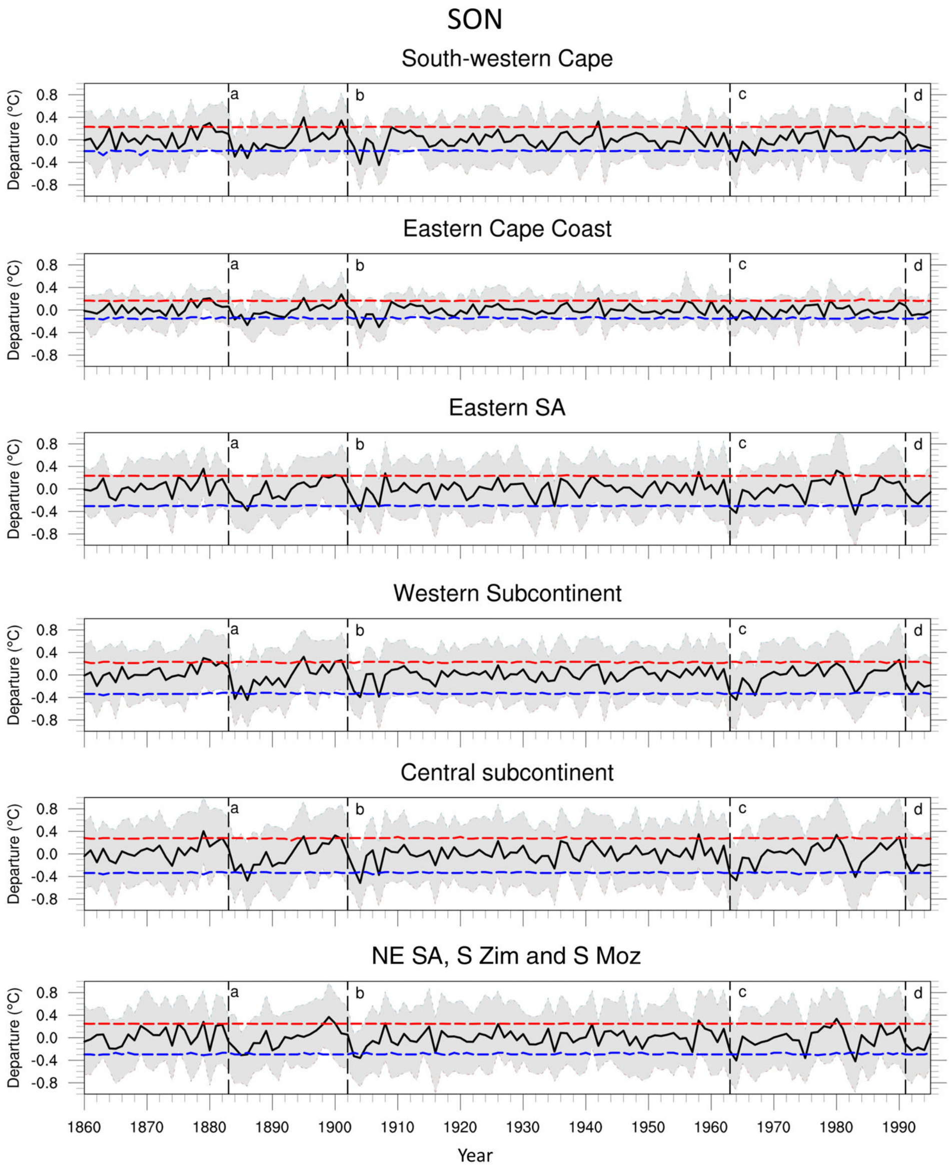

FIGURE 2 (Continued)

files available in CMIP5 models (Dhomse *et al*., 2020). CMIP6 should thus help to resolve some of the over/under-estimation issues encountered in CMIP5.

3.2 | Santa Maria

The eruption of Santa Maria (VEI 6) occurred in the NH tropics (15°N - Guatemala) during October 1902, emitting 3.8 Tg of SO_2 into the lower stratosphere (Neely III and Schmidt, 2016). Mean annual temperatures following the eruption were below normal during y1–y3 for all regions (Table 3). However, they were only significantly below normal for 2 years in NESA (y1 = −0.37°C and y2 = −0.32°C), and for 1 year (y1) in ESA (0.31°C) and the WSub (−0.30°C). While temperature anomalies were not significantly below normal during y1 in the SWC, ECC and CSub regions, significant negative temperature departures are recorded for y2 (−0.22, −0.13 and – 0.36°C, respectively). However, by y3, anomalies were weaker and not significant in any region. The strongest responses occurred in NESA during y1 (−0.37°C) and y3 (−0.21°C), and in the CSub (−0.36°C) during y2, while the weakest negative anomalies again occurred in the ECC each year (−0.03 to −0.13°C).

Significant seasonal anomalies following the Santa Maria eruption are less pronounced than after the Krakatau eruption. In fact, in the SWC and ECC regions, significant responses do not occur at all during y1 (Figure 3). However, they occur during SON (y2) and DJF (y3) for

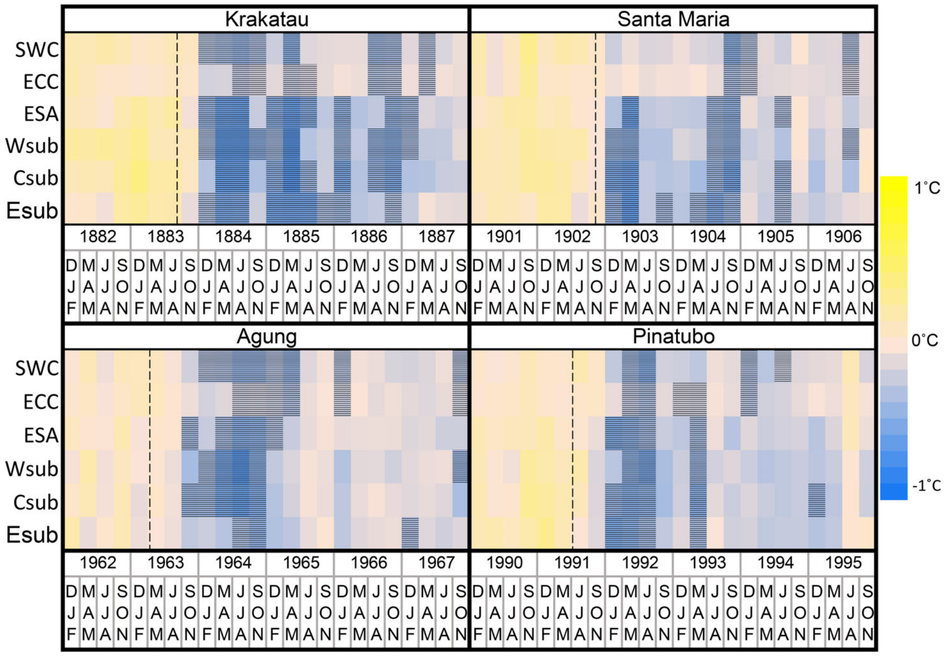

FIGURE 3 Seasonal temperature anomalies for each southern African sub-region for the eruptions of Krakatau, Santa Maria, Agung and Pinatubo. Eruption events are depicted by dashed vertical lines and significant anomalies are depicted by horizontal hashed lines [Colour figure can be viewed at wileyonlinelibrary.com]

both these regions (Table 4). In ESA, a negative anomaly occurs in MAM of y1, in JJA and SON of y2 and JJA of y3. Significant negative anomalies occur in DJF and MAM of y1 as well as JJA and SON of y2 in both the WSub and CSub, as well as JJA of y3 in the CSub (Table 4). In NESA, significant negative anomalies occur in DJF, MAM and SON of y1, MAM, JJA and SON of y2 and JJA of y3.

The strongest seasonal responses in y1 occur during MAM over the WSub (−0.41°C), ESA (−0.53°C), CSub (−0.55°C) and NESA (−0.58°C), and during JJA over the ECC (−0.06°C; not significant) (Figure 2). The SWC anomaly is the strongest during DJF (−0.19; not significant), which contrasts with the Krakatau response which recorded weakest anomalies during these months (Table 4). The weakest negative temperature departures occurred during MAM in the ECC (0.01°C) and SWC (−0.06°C), during SON in ESA (−0.21°C), during both SON and JJA over the WSub (both −0.29°C), and in JJA for both the CSub (−0.23°C) and NESA (−0.23°C). In most regions, the strongest overall negative temperature departures occur in y1, except for the SWC and ECC regions where the strongest responses are recorded during SON of y2 (−0.43, −0.32°C, respectively).

As was the case for Krakatau, the strongest negative monthly temperature departures occurred over the CSub region (−0.66°C in February 1903), followed by the SWC and NESA regions (both −0.62°C in September 1904 and May 1903, respectively), but was weakest over the ECC region in September 1904 (−0.40°C). Maximum response occurred 23–24 months (i.e., September and October 1904) after the Santa Maria eruption in the SWC, ECC, ESA and WSub regions, but as early as four (February 1903) to seven (May 1903) months post-eruption in the CSub and NESA regions respectively. For the first 3 years post Santa Maria, most mean monthly temperatures are below normal, ranging from 92% (NESA) to 77% (ECC) of months, however, significantly below normal mean values range from only 5% (ECC) to 54% (CSub) of months (Table 5).

3.3 | Agung

Mount Agung (8°S—Indonesia) erupted during March 1963 and emitted 7.5Tg of SO_2 into the stratosphere (Neely III and Schmidt, 2016). Unlike the other eruptions discussed in this paper, it had a VEI of only four. During y1, all regions record a significant negative mean annual temperature anomaly, varying from as much as −0.50°C (WSub and CSub) to as little as −0.17°C (ECC)(Table 3). During y2, however, only the SWC (−0.19°C) and ECC (−0.13°C) regions record significant mean annual temperature departures. The weakest responses occurred over the ECC during y1 (0.17°C), over the WSub during y2 (−0.10°C) and over ESA during y3 (−0.05°C). In strong contrast to the Krakatau and Santa Maria eruptions, the SWC records the strongest response of all subregions in y2 (−0.19°C) and second the strongest response in y3 (−0.14°C).

Seasonal temperature anomalies in response to the Agung eruption are below normal during y1–y3 (Figure 2), but overall less significant than following the Krakatau eruption. Again, in contrast with Krakatau,

TABLE 4 Seasonal temperatures for each sub-region following the four eruptions

Season	SWC				ECC				ESA			
	DJF	MAM	JJA	SON	DJF	MAM	JJA	SON	DJF	MAM	JJA	SON
1883	0.07	0.09	0.14	0.10	0.02	0.04	0.10	0.06	0.26	0.17	0.24	-0.03
1884	**-0.27**	**-0.32**	**-0.39**	**-0.30**	-0.16	-0.15	**-0.24**	**-0.17**	**-0.38**	**-0.54**	**-0.56**	-0.21
1885	-0.19	**-0.43**	-0.12	-0.09	-0.10	**-0.21**	**-0.16**	-0.08	**-0.43**	**-0.56**	**-0.44**	-0.24
1886	-0.08	-0.08	**-0.35**	**-0.33**	-0.03	-0.06	**-0.29**	**-0.27**	**-0.40**	-0.29	-0.24	**-0.39**
1902	0.10	0.21	0.17	0.07	0.06	0.08	0.05	0.06	0.12	0.15	0.03	0.01
1903	-0.19	-0.06	-0.13	-0.12	-0.05	0.01	-0.06	-0.03	-0.28	**-0.53**	-0.23	-0.21
1904	-0.05	-0.13	-0.16	**-0.43**	-0.04	-0.01	-0.08	**-0.32**	-0.22	-0.25	**-0.34**	**-0.40**
1905	**-0.27**	-0.09	-0.18	0.02	**-0.22**	-0.11	-0.09	-0.07	-0.06	-0.17	**-0.29**	0.02
1963	0.12	0.10	-0.01	-0.17	0.13	0.11	0.02	-0.06	-0.01	0.05	0.03	**-0.33**
1964	**-0.28**	**-0.29**	**-0.39**	**-0.39**	-0.16	-0.11	**-0.19**	**-0.18**	-0.21	**-0.33**	**-0.45**	**-0.43**
1965	**-0.27**	**-0.39**	-0.12	-0.03	**-0.20**	**-0.30**	-0.07	0.00	**-0.29**	-0.21	-0.08	-0.02
1966	**-0.26**	-0.04	-0.07	-0.14	**-0.19**	0.00	-0.09	-0.05	-0.08	-0.07	-0.06	-0.06
1991	0.05	0.04	0.17	0.07	0.06	0.01	0.07	0.08	0.21	0.06	0.03	-0.06
1992	-0.22	**-0.34**	**-0.45**	-0.17	-0.08	**-0.23**	**-0.31**	-0.10	**-0.47**	**-0.43**	**-0.35**	-0.20
1993	-0.19	-0.25	-0.05	-0.09	**-0.17**	**-0.18**	-0.02	-0.07	-0.25	**-0.32**	-0.05	-0.27
1994	**-0.29**	-0.26	**-0.20**	-0.12	**-0.27**	-0.17	-0.15	-0.08	-0.11	-0.19	-0.17	-0.15
	WSub				CSub				NESA			
Season	DJF	MAM	JJA	SON	DJF	MAM	JJA	SON	DJF	MAM	JJA	SON
1883	0.34	0.15	0.14	0.12	0.40	0.23	0.23	0.09	0.29	0.21	0.18	-0.07
1884	**-0.30**	**-0.60**	**-0.59**	**-0.42**	-0.28	**-0.58**	**-0.57**	-0.31	**-0.30**	**-0.50**	**-0.48**	-0.19
1885	**-0.34**	**-0.63**	-0.27	-0.20	**-0.43**	**-0.64**	**-0.37**	-0.19	**-0.52**	**-0.53**	**-0.52**	**-0.31**
1886	**-0.36**	-0.23	**-0.39**	**-0.44**	**-0.49**	-0.28	**-0.39**	**-0.47**	**-0.35**	-0.27	-0.23	**-0.30**
1902	0.21	0.19	0.20	0.00	0.26	0.22	0.10	-0.01	0.23	0.23	-0.06	0.05
1903	**-0.37**	**-0.41**	-0.29	-0.29	**-0.49**	**-0.55**	-0.23	-0.27	**-0.39**	**-0.58**	-0.23	**-0.33**
1904	-0.13	-0.18	**-0.34**	**-0.39**	-0.25	-0.34	**-0.36**	**-0.52**	-0.27	**-0.33**	**-0.46**	**-0.36**
1905	-0.21	-0.16	-0.28	0.01	-0.14	-0.18	**-0.35**	-0.03	-0.08	-0.21	**-0.30**	-0.15
1963	0.00	0.02	-0.06	-0.34	-0.08	0.07	-0.04	**-0.36**	-0.06	0.00	-0.05	-0.24
1964	**-0.32**	**-0.51**	**-0.62**	**-0.44**	**-0.35**	**-0.50**	**-0.57**	**-0.47**	-0.19	-0.27	**-0.31**	**-0.40**
1965	-0.23	-0.13	-0.02	-0.06	-0.28	-0.16	-0.02	-0.07	-0.30	-0.25	-0.07	0.02
1966	-0.29	-0.10	-0.10	-0.17	-0.24	-0.07	-0.02	-0.08	-0.24	-0.11	-0.08	-0.06
1991	0.20	0.12	0.19	-0.13	0.25	0.18	0.12	-0.12	0.33	0.15	0.01	-0.11
1992	-0.26	**-0.42**	**-0.50**	-0.32	**-0.39**	**-0.46**	**-0.43**	-0.34	**-0.48**	**-0.44**	**-0.35**	-0.23
1993	-0.19	**-0.37**	-0.17	-0.12	-0.18	**-0.44**	-0.10	-0.20	-0.10	**-0.33**	-0.01	-0.17
1994	-0.20	-0.27	-0.24	-0.21	-0.13	-0.20	-0.24	-0.21	-0.16	-0.24	-0.22	-0.22

Note: Grey shading = year of eruption; bold values = significant anomalies. The values have been ranked from the weakest to strongest seasonal response for each year in each region: Blue = strongest, green = second strongest, yellow = third strongest, red = weakest.

negative anomalies after the Agung eruption are most significant over the SWC and ECC regions. Negative anomalies in the SWC are significant during DJF for y1–y3, during MAM for y1 and y2, and during JJA and SON for y1 (Table 4). In the ECC region, negative temperature departures are significant during JJA and SON of y1 only. Anomalies are significant during DJF and MAM of y2, and during DJF of y3. In the ESA region, anomalies are significantly below normal in SON of y0, about 5 months after the eruption (Table 4). They are then not significant during DJF but are again significant during MAM, JJA and SON of y1. Both the WSub and CSub regions have significant negative temperature anomalies for each season in y1 only, except that the anomaly during SON of y0 in the CSub region is significantly below normal as well. Over NESA, negative temperature departures are only significant during JJA and SON of y1 (Table 4).

The strongest seasonal response of y1 occurred during JJA over all regions (mean: −0.44°C; Table 4) except NESA, where the strongest response occurred during SON (−0.40°C) (Figure 3). The weakest anomalies occur in DJF over all regions (mean: −0.27°C) except the ECC, where the weakest response is again recorded for MAM (−0.11°C). As was the case with Santa Maria, negative mean seasonal temperature anomalies are most pronounced in y1 over most sub-regions, apart from the SWC and ECC regions where the strongest response was in MAM of y2 (−0.39; −0.30, respectively).

The strongest monthly temperature response is again recorded in the CSub region (−0.70°C in February 1903), as was also the case for Krakatau and Santa Maria (Figure 4). In the ECC region, the strongest response is in May 1965 (−0.35°C), but this is the weakest maximum response for any of the regions following all four eruptions. The strongest monthly anomalies lack temporal uniformity between sub-regions, occurring earlier (13–17 months post-eruption) in the CSub, WSub and ESA regions, and later (20–26 months post-eruption) in the NESA, SWC and ECC regions. For the first 3 years post Agung, most mean monthly temperatures are below normal, ranging from 85% (SWC and WSub) to 70% (ESA) of months, however, significantly below normal mean values range from only 4% (ECC) to 37% (CSub) of months (Table 5). Although the SWC region had a comparably low percentage of significantly cooler than normal months after the Krakatau and Santa Maria eruptions, compared with most other sub-regions, the situation is somewhat different after the Agung eruption. In the latest case, the SWC region records 28% of months as significantly cooler than normal for y1–y3, while that for ESA and NESA is considerably less (17 and 16%, respectively).

3.4 | Pinatubo

Mount Pinatubo (15°N—Philippines) erupted in June 1991, emitting 18Tg of SO_2 into the stratosphere (Neely III and Schmidt, 2016) with a VEI = 6. Although mean annual temperature departures are again negative for y1–y3 (Table 3), significant departures for all regions are only recorded in y1 (mean: −0.32°C). No southern African region records a significant temperature anomaly in y2, however, in y3, significant departures are observed for the SWC and ECC regions (−0.20 and − 0.16°C, respectively). The weakest mean annual temperature response is once again recorded over the ECC region for

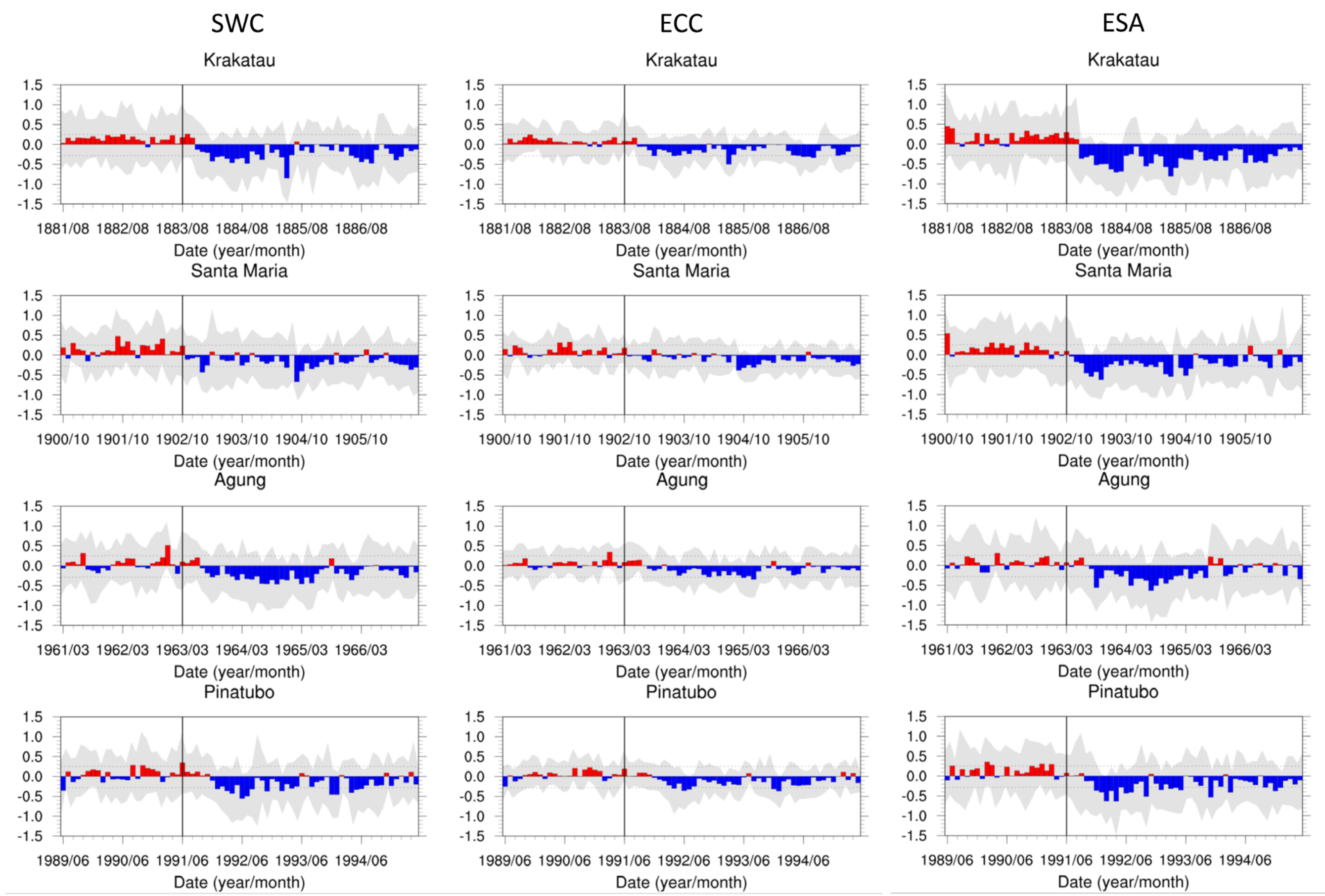

FIGURE 4 Sub-regional monthly temperature anomalies after the eruptions of Krakatau, Santa Maria, Agung and Pinatubo. Grey shading represents the ensemble mean [Colour figure can be viewed at wileyonlinelibrary.com]

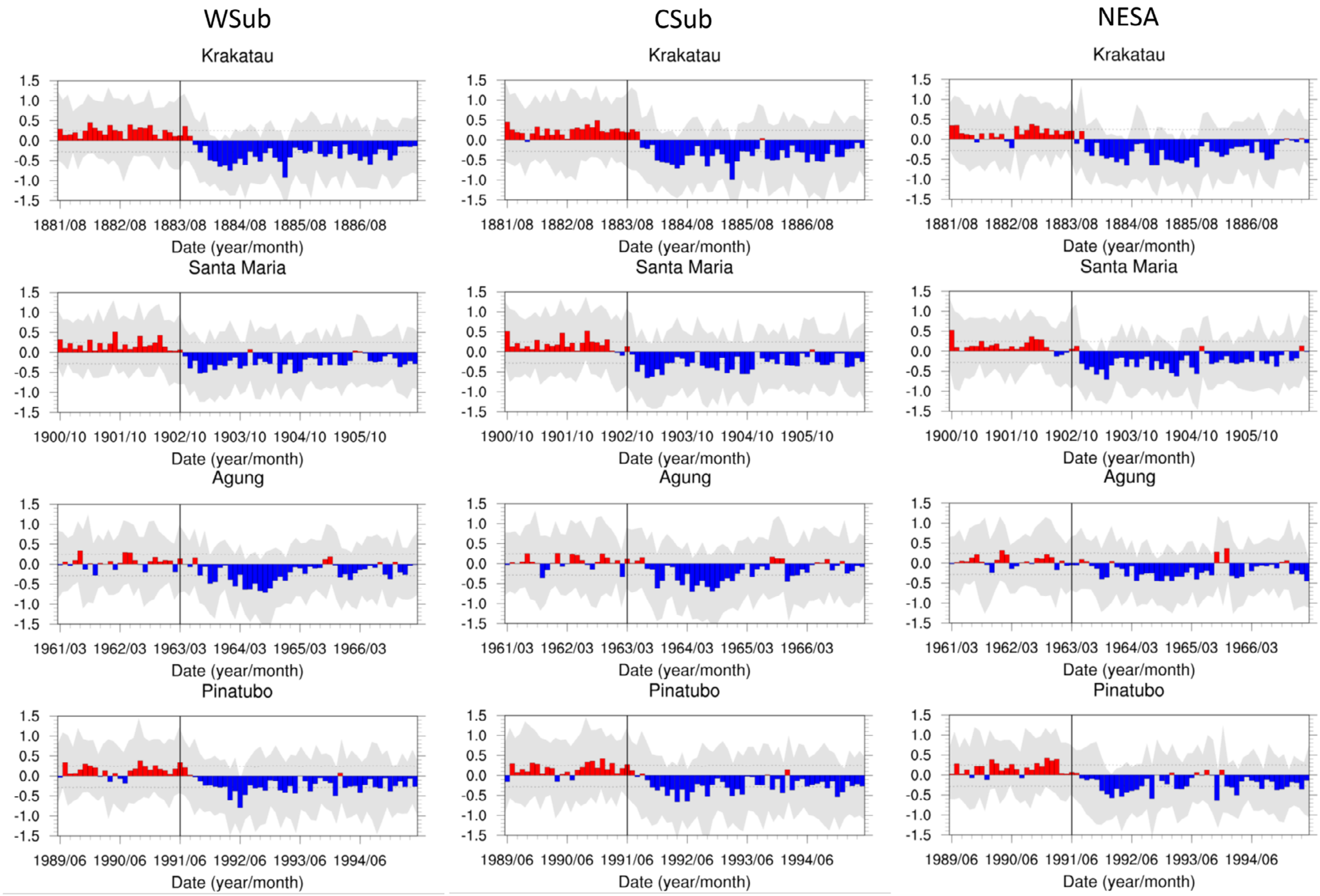

FIGURE 4 (Continued)

TABLE 5 Peak monthly temperature anomalies and the percentage of monthly anomalies below normal and significantly below normal [from the time of each eruption (y0) until the end of post-eruption year 3 (y3)]

Eruption	Region	SWC	ECC	ESA	Wsub	Csub	NESA	Mean
Krakatau	Peak monthly value (°C)	−0.77	−0.53	−0.69	−0.85	−0.98	−0.62	−0.74
	Percentage of negative monthly anomalies	83	88	93	93	90	95	90
	Percentage of significant negative monthly anomalies	32	17	54	54	68	61	48
Santa Maria	Peak monthly value (°C)	−0.62	−0.40	−0.48	−0.47	−0.66	−0.62	−0.54
	Percentage of negative monthly anomalies	82	77	92	90	90	92	87
	Percentage of significant negative monthly anomalies	13	5	23	23	54	38	26
Agung	Peak monthly value (°C)	−0.43	−0.35	−0.54	−0.62	−0.70	−0.42	−0.51
	Percentage of negative monthly anomalies	85	78	70	85	74	83	79
	Percentage of significant negative monthly anomalies	28	4	17	33	37	26	24
Pinatubo	Peak monthly value (°C)	−0.52	−0.35	−0.56	−0.72	−0.66	−0.58	−0.57
	Percentage of negative monthly anomalies	77	88	86	88	88	86	86
	Percentage of significant negative monthly anomalies	28	12	30	28	42	35	29
Mean	Peak monthly value (°C)	−0.58	−0.41	−0.57	−0.66	−0.75	−0.56	−0.59
	Percentage of negative monthly anomalies	82	83	85	89	86	89	86
	Percentage of significant negative monthly anomalies	25	10	31	34	50	40	32

TABLE 6 Comparison of instrumental (after Picas and Grab, 2020) and CMIP5 (current study) temperature departures for the SWC, following the Krakatau eruption

		This study			Picas and Grab (2020)		
		1884	**1885**	**1886**	**1884**	**1885**	**1886**
3-year departure (1884–1886)		−0.24			−0.06		
Annual departures		−0.33	−0.18	−0.21	−0.22	0.10	−0.06
Seasonal averages	**DJF**	−0.27	−0.19	−0.08	−0.16	0.56	0.07
	MAM	−0.32	−0.43	−0.08	−0.13	−0.73	0.35
	JJA	−0.39	−0.12	−0.35	−0.32	0.13	0.05
	SON	−0.30	−0.09	−0.33	−0.84	0.81	−0.56
Month of maximum monthly departure		June/September	May	October	November	May	October
Percentage of negative monthly anomalies from time of eruption to end y		383%			56%		

y1–y3 (mean: −0.16°C). The strongest annual response occurs over the CSub region during y1 (−0.37°C) and y2 (−0.23°C), and in the WSub region in y3 (−0.25°C). Notably, the SWC and ECC regions record significant cooling during both y1 and y3 but not y2, as was the case for Krakatau.

Although not always significant, seasonal temperature anomalies are below normal during all seasons for y1 to y3 (Figure 3). Over the SWC, significant negative anomalies are recorded during MAM and JJA in y1, and DJF and JJA in y3 (Table 4). Significant negative temperature departures over the ECC are observed during MAM and JJA in y1, DJF and MAM in y2, and DJF in y3. The SWC and ECC regions are the only sub-regions recording significant departures in y3. Over ESA, the CSub and NESA regions, significant negative temperature departures occur during DJF, MAM and JJA in y1, and MAM in y2. The WSub region follows the same pattern, apart from DJF of y1 not being significant (Table 4).

The strongest seasonal response during y1 is in JJA over the SWC, ECC and WSub regions (mean = −0.42°C, Table 4), in DJF over ESA and NESA (mean = −0.48°C), and in MAM over the CSub region (−0.44°C). The weakest responses occur in SON over the SWC, ESA, CSub and NESA regions (mean = −0.23°C), and in DJF in the ECC and WSub regions (mean = −0.17°C). Unlike the three earlier eruptions, the strongest overall seasonal responses after Pinatubo occur during y1.

The strongest monthly temperature responses following the Pinatubo eruption occur much earlier (within 10–12 months) across most southern African regions than was the case for the other eruptions, apart from NESA where the strongest response seems very delayed (29th month) (Figure 4). The strongest negative temperature departure occurs in the WSub region (−0.72°C in June 1992). Again, the strongest negative monthly anomaly in the ECC region (−0.35°C in June 1992) is the weakest of all regional maximum responses. For the first 3 years post Pinatubo, most mean monthly temperatures are below normal, ranging from 88% (ECC, WSub, and CSub) to 77% (SWC) of months, however, significantly below normal mean values range from only 12% (ECC) to 42% (CSub) of months (Table 5).

4 | DISCUSSION

Although countless studies have examined the impacts of major volcanic eruptions on global-, continental- and regional-scale temperatures, investigations at the sub-regional scale are limited for the NH (Kondo, 1988; Shindell, 2004; Esper *et al.*, 2013; Zhang *et al.*, 2013; Dogar *et al.*, 2017) and have been absent until now for the SH. To this end, our CMIP5 model outputs demonstrate significant temperature responses to major volcanic eruptions across the southern African region, yet also portray strong sub-regional contrasts in such responses over relatively small spatial scales. In particular, findings indicate that the magnitude and timing of the response, and also the season of maximum response varies considerably by region and by eruption location/timing/magnitude. In addition, underlying climatic conditions will vary with each eruption event and thus also impact on such forcing outcomes (Zanchettin *et al.*, 2014; Stevenson *et al.*, 2017; Krishnamohan *et al.*, 2019; Sun *et al.*, 2019).

Model outputs show mean annual negative temperature departures are strongest over the northern, arid regions (WSub, CSub and NESA) after all major eruptions investigated in this paper (mean of all eruptions = y1: −0.40°C; −y2: −0.26°C; y3: −0.23°C). In particular, the CSub region has the strongest anomalies following the Krakatau and Pinatubo eruptions, the

NESA region following the Santa Maria eruption, and in WSub following the Agung eruption. The weakest responses are consistently modelled for the ECC after each of the four eruptions investigated (mean of all eruptions = y1: −0.14°C; y2: −0.13°C; y3: −0.12°C). The SWC region with its Mediterranean climate, records second weakest responses after all eruptions (mean of all eruptions = y1: −0.27°C; y2: −0.19°C; y3: −0.17°C).

Post-eruption temperature responses vary in strength according to season. Overall, the weakest seasonal anomalies occur particularly during SON in the SWC, ESA and NESA regions and in DJF in the WSub and CSub regions. The exception to this being for the ECC region where the weakest negative temperature departures occur more often during MAM, while the strongest departures occur in JJA, and hence is in strong contrast to other subregions. The strongest cooling occurs most notably in MAM over the WSub, CSub, ESA and NESA regions and in JJA in the SWC and ECC regions, coinciding with strongest cooling in summer/autumn over the NH (Zanchettin *et al.*, 2019). However, the ESA and SWC regions also record strong cooling during austral summer (DJF). Strong autumn and winter cooling over the SWC region is most likely associated with more intense and frequent cold front overpasses during such seasons (Picas and Grab, 2020), and the result of more favourable circulation during winter when the Brewer-Dobson circulation is intensified (Harvey *et al.*, 2020). This response is seen most prominently following Krakatau and Pinatubo which erupted during August and June respectively (austral winter), thus transporting aerosols most effectively and contributing to the stronger observed responses (Perlwitz and Graf, 1995; Birner and Bönisch, 2010; Harvey *et al.*, 2020).

The CSub region usually experiences maximum monthly temperature departures at an earlier date (mean = 12 months after eruption date) than all other regions (mean = 17 months after eruption date), while that for the ECC is most delayed (mean = 21 months after eruption date). Maximum departures generally occur during the cooler austral months (March–August) after each eruption, except for the NESA (January following Krakatau, November following Pinatubo) and CSub (November following Agung) regions. The CSub region also records more significant negative monthly temperature departures (mean = 50%) than any other region (mean = 30%), while those for the ECC are lowest (mean = 10%). Our findings thus demonstrate strongly contrasting temperature responses to volcanic forcing between the more continental climatic/summer rainfall regions (CSub, NESA), and the Mediterranean/subtropical climates of the winter/all year rainfall regions (i.e., SWC/ECC respectively). Strong El Niño Southern Oscillation (ENSO) phases tend to have more significant temperature effects over the interior than coastal regions of southern Africa, with the CSub and NESA regions most strongly impacted by the El Niño anomaly, and result in positive temperature departures (Lakhraj-Govender and Grab, 2018). The somewhat weaker responses along coastal regions (ECC and SWC) may also be due to oceanic temperature-regulating effects, particularly the cool Benguela current that borders the SWC (Philippon *et al.*, 2012). Although SSTs are also affected by volcanic eruptions (Gleckler *et al.*, 2006; McGregor *et al.*, 2015; Klein and Goosse, 2018), these are not as extreme in amplitude (Gupta and Marshall, 2018) as those for terrestrial air temperatures. In addition, SSTs continue to dampen the impacts of climate change/variability along coastal regions (Dittus *et al.*, 2018). In contrast, the more continental southern African regions (i.e., CSub, WSub and NESA) typically experience stronger temperature extremes than coastal regions (Kruger and Sekele, 2013). Collectively, these are likely important factors regulating temperature responses, and account for sub-regional differences following major volcanic eruptions over the African sub-continent.

The southern African climate is strongly controlled by ENSO (Pezza *et al.*, 2007; Philippon *et al.*, 2012), which is known to have variable sub-regional climatic impacts across the sub-continent (Nicholson and Kim, 1997; Mason, 2001; Lakhraj-Govender and Grab, 2018). The central interior (coinciding with our CSub region) experiences the strongest ENSO-related temperature response, followed by the northern interior (coinciding with our NESA region); in contrast, the northeastern interior (coinciding with our ESA region) records the strongest temperature responses during La Niña events (Lakhraj-Govender and Grab, 2018). It has also been identified that responses to ENSO events are usually most pronounced during austral summer (Nicholson and Kim, 1997; Mason, 2001; Lakhraj-Govender and Grab, 2018). The SSTs generated in our study suggest a likeness to La Niña conditions following each of the four eruptions, which could contribute to the cooler temperatures over southern Africa. However, volcanic eruptions can themselves affect ENSO, with NH and tropical eruptions leading to a tendency towards El Niño-like anomalies (Pausata *et al.*, 2016; Ménégoz *et al.*, 2018; Zuo *et al.*, 2018). While La Niña conditions arise in the model simulations, in reality, El Niño events occurred during years after all the eruptions we investigate in this paper (for ENSO anomalies see Gergis and Fowler, 2009). Volcanic forcing possibly has a dual temperature impact over regions of the SH, not only through its cooling effects associated with an altered global energy budget, but indirectly through its influence on ENSO phases and strengths, which then either moderates (limits) or further enhances the extent of such cooling. Given El Niño generally has a warming effect over much of southern Africa, it is possible that this is the reason for somewhat weaker negative observed temperature departures following major eruptions, compared with the modelled response (Barnes *et al.*, 2016).

CMIP5 models tend to show a positive Southern Annular Mode (SAM) following major volcanic eruptions (Barnes *et al.*, 2016; McGraw *et al.*, 2016), as was also the case after the Agung and Pinatubo eruptions. A positive SAM generally means strengthened westerlies, which contract towards the poles and result in intensified cyclogenesis (Yang and Xiao, 2017). Mid-latitude cyclones cause most of the extreme weather encountered over mid-latitudes of the SH, or southernmost terrestrial regions of South America, southern Africa and Australasia (Pepler *et al.*, 2016). Picas and Grab (2020) suggested that an increase in strength or frequency of mid-latitude cyclones following volcanic eruptions could contribute to cooling observed over the SWC. Given that volcanic forcing has an impact on the Southern Annular Mode and Polar Vortex, it thus also (indirectly) influences the position and strength of mid-latitude cyclones. Given that the SWC and ECC sub-regions are regularly affected by cold fronts during the cooler seasons, any increase (equatorward extension) in frontal activity might only have a marginal impact on temperature reductions here. In contrast, the CSub, WSub and NESA regions, being further north, are less affected by frontal systems than the SWC and ECC. However, strong and further northward penetrating frontal systems, as is advocated during post-volcanic years, would have considerable cooling effects over the interior and northern regions of the sub-continent, hence accounting for stronger cooling than in southernmost regions.

Finally, we consider the changing nature of temperature responses for the earlier two eruptions (Krakatau and Santa Maria) with that for the latter two (Agung and Pinatubo). Significant seasonal cooling over the more northern and interior regions (WSub, CSub, NESA and ESA) seems reduced when comparing the earlier two eruptions (mean:−0.34°C) with the more recent two (mean: −0.24°C). Mean anomalies for the four regions combined show that the greatest difference between the earlier and more recent eruptions occurs in JJA (mean for earlier two: −0.36°C; latter two: −0.22°C), while the smallest difference occurs during SON (mean for earlier two: −0.27°C; latter two: −0.20°C). The weakened volcanic signature may, in part, be due to the variable strengths of these eruptions, but might also be influenced by an increased moderating effect of anthropogenic (CO_2) forcing during more recent times, as has similarly been suggested by Tett (2002) and Gleckler *et al.* (2006). However, in contrast to these southern African sub-regions, the same is not found for the more southerly SWC and ECC regions, where mean seasonal forcing after the earlier two eruptions is only marginally stronger than the more recent eruptions in JJA (mean for earlier two = −0.19°C; latter two = −0.18°C), while in DJF and MAM the seasonal response has actually strengthened over more recent times (DJF mean for earlier two = −0.14°C; latter two = −0.22°C. MAM mean for earlier two = −0.14°C; latter two = −0.21°C).

5 | CONCLUSION

Despite considerable recent advances in knowledge pertaining to volcanic forcing impacts on global to hemispheric scale climates, our understanding of such impacts at finer spatial scales, and particularly so in the southern hemisphere, has remained in its infancy. To this end, our paper demonstrates considerable variability (timing, duration and amplitude) of CMIP5 modelled temperature responses between climatic sub-regions of southernmost Africa. Importantly, this suggests that global- or hemispheric-scale modelled forcing-responses need to be considered with utmost caution for regional to sub-regional scale climate modelling, or when ascertaining likely volcanic impacts at such finer spatial scales. This is particularly critical to climate-sensitive agricultural regions such as southern Africa where down-scaled climatic responses need to be well understood for appropriate preparedness initiatives.

The strongest negative temperature departures following major volcanic eruptions are recorded for the northern semi-arid sub-regions of southern Africa, which coincides with regions that are climatically most responsive to ENSO. This reinforces the already established volcanic forcing impact on generating El Niño-like conditions. In this context, one would expect that regions most strongly impacted by El Niño, would thus also (indirectly) be strongly affected by such eruptions. However, CMIP5 models also simulate a positive phase of the Southern Annular Mode after such eruptions, which strengthens the westerlies, and hence cyclogenesis. This likely accounts for the strongest negative temperature departures during austral autumn (MAM) and winter (JJA) over most of the African sub-continent. It is possible, however, that the influence of El Niño conditions dampens the extent of seasonal/annual cooling, despite strengthened cyclogenesis. We acknowledge that such an inference requires further verification and detailed investigation, but might imply that volcanically induced climatic trigger events may not always reinforce a common climatic outcome (such as cooling) and thus possibly account for varied amplitudes of cooling (or in some cases possible seasonal warming) responses between sub-regions, regions and even hemispheres.

ACKNOWLEDGEMENTS

The authors wish to thank all those involved in the CMIP5 project, and Jacobus van der Merwe for helping obtain the data. Many thanks to Dr Picas for sharing her instrumental weather data for comparative analysis. We appreciate valuable inputs from anonymous referees who helped improve an earlier version of this manuscript.

ORCID

Pamela J. Harvey https://orcid.org/0000-0002-9559-7561

Stefan W. Grab https://orcid.org/0000-0001-7678-1526

REFERENCES

Ammann, C.M., Joos, F., Schimel, D.S., Otto-Bliesner, B.L. and Tomas, R.A. (2007) Solar influence on climate during the past millennium: results from transient simulations with the NCAR climate system model. *Proceedings of the National Academy of Sciences*, 104 (10), 3713–3718. https://doi.org/10.1073/pnas.0605064103.

Barnes, E.A., Solomon, S. and Polvani, L.M. (2016) Robust wind and precipitation responses to the mount Pinatubo eruption, as simulated in the CMIP5 models. *Journal of Climate*, 29(13), 4763–4778. https://doi.org/10.1175/JCLI-D-15-0658.1.

Birner, T. and Bönisch, H. (2010) Residual circulation trajectories and transit times into the extratropical lowermost stratosphere. *Atmospheric Chemistry and Physics Discussions*, 10(7), 16837–16860. https://doi.org/10.5194/acpd-10-16837-2010.

Chylek, P., Folland, C., Klett, J.D. and Dubey, M.K. (2020) CMIP5 climate models overestimate cooling by volcanic aerosols. *Geophysical Research Letters*, 47(3), e2020GL087047. https://doi.org/10.1029/2020GL087047.

Colose, C.M., LeGrande, A.N. and Vuille, M. (2015) The influence of tropical volcanic eruptions on the climate of South America during the last millennium. *Climate of the Past*, 11, 3375–3424. https://doi.org/10.5194/cpd-11-3375-2015.

Colose, C.M., LeGrande, A.N. and Vuille, M. (2016) The influence of volcanic eruptions on the climate of tropical South America during the last millennium in an isotope-enabled general circulation model. *Climate of the Past*, 12(4), 961–979. https://doi.org/10.5194/cp-12-961-2016.

Cook, E.R., Palmer, J.G. and D'Arrigo, R.D. (2002) Evidence for a 'medieval warm period' in a 1,100 year tree-ring reconstruction of past austral summer temperatures in New Zealand: medieval warm period in New Zealand. *Geophysical Research Letters*, 29 (14), 12-1–12-4. https://doi.org/10.1029/2001GL014580.

Dhomse, S.S., Mann, G.W., Antuña Marrero, J.C., Shallcross, S.E., Chipperfield, M.P., Carslaw, K.S., Marshall, L., Abraham, N.L. and Johnson, C.E. (2020) Evaluating the simulated radiative forcings, aerosol properties, and stratospheric warmings from the 1963 Mt Agung, 1982 El Chichón, and 1991 Mt Pinatubo volcanic aerosol clouds. *Atmospheric Chemistry and Physics. Copernicus GmbH*, 20(21), 13627–13654. https://doi.org/10.5194/acp-20-13627-2020.

Dieng, H.B., Cazenave, A., Meyssignac, B., von Schuckmann, K. and Palanisamy, H. (2017) Sea and land surface temperatures, ocean heat content, Earth's energy imbalance and net radiative forcing over the recent years: sea and land surface temperature. *International Journal of Climatology*, 37, 218–229. https://doi.org/10.1002/joc.4996.

Dittus, A.J., Karoly, D.J., Donat, M.G., Lewis, S.C. and Alexander, L.V. (2018) Understanding the role of sea surface temperature-forcing for variability in global temperature and precipitation extremes. *Weather and Climate Extremes*, 21, 1–9. https://doi.org/10.1016/j.wace.2018.06.002.

Dogar, M.M., Stenchikov, G., Osipov, S., Wyman, B. and Zhao, M. (2017) Sensitivity of the regional climate in the middle east and North Africa to volcanic perturbations: sensitivity of MENA region to volcanism. *Journal of Geophysical Research-Atmospheres*, 122(15), 7922–7948. https://doi.org/10.1002/2017JD026783.

Driscoll, S., Bozzo, A., Gray, L.J., Robock, A. and Stenchikov, G. (2012) Coupled model Intercomparison project 5 (CMIP5) simulations of climate following volcanic eruptions. *Journal of Geophysical Research-Atmospheres*, 117(D17), D17105. https://doi.org/10.1029/2012JD017607.

Dunwiddie, P.W. and LaMarche, V.C. (1980) A climatically responsive tree-ring record from Widdringtonia cedarbergensis, Cape Province, South Africa. *Nature*, 286(5775), 796–797. https://doi.org/10.1038/286796a0.

Efron, B. (1979) Bootstrap methods: another look at the jackknife. *The Annals of Statistics*, 7(1), 1–26. https://doi.org/10.1214/aos/1176344552.

Engelbrecht, C.J. and Engelbrecht, F.A. (2016) Shifts in Köppen-Geiger climate zones over southern Africa in relation to key global temperature goals. *Theoretical and Applied Climatology*, 123(1–2), 247–261. https://doi.org/10.1007/s00704-014-1354-1.

Engelbrecht, F.A., McGregor, J.L. and Engelbrecht, C.J. (2008) Dynamics of the conformal-cubic atmospheric model projected climate-change signal over southern Africa. *International Journal of Climatology*, 29(7), 1013–1033. https://doi.org/10.1002/joc.1742.

Esper, J., Schneider, L., Krusic, P.J., Luterbacher, J., Büntgen, U., Timonen, M., Sirocko, F. and Zorita, E. (2013) European summer temperature response to annually dated volcanic eruptions over the past nine centuries. *Bulletin of Volcanology*, 75(7), 736. https://doi.org/10.1007/s00445-013-0736-z.

Gentilli, J. (1948) Present-day volcanicity and climatic change. *Geological Magazine*, 85(3), 172–175.

Gergis, J.L. and Fowler, A.M. (2009) A history of ENSO events since A.D. 1525: implications for future climate change. *Climatic Change*, 92(3–4), 343–387. https://doi.org/10.1007/s10584-008-9476-z.

Gilliland, R.L. (1982) Solar, volcanic, and CO2 forcing of recent climatic changes. *Climatic Change*, 4(2), 111–131. https://doi.org/10.1007/BF02423387.

Gleckler, P.J., Wigley, T.M.L., Santer, B.D., Gregory, J.M., AchutaRao, K. and Taylor, K.E. (2006) Volcanoes and climate: Krakatoa's signature persists in the ocean. *Nature*, 439(7077), 675. https://doi.org/10.1038/439675a.

Grab, S.W. and Nash, D.J. (2010) Documentary evidence of climate variability during cold seasons in Lesotho, southern Africa, 1833-1900. *Climate Dynamics*, 34(4), 473–499.

Grab, S.W. and Simpson, A.J. (2000) Climatic and environmental impacts of cold fronts over KwaZulu-Natal and the adjacent interior of southern Africa. *South African Journal of Science*, 96, 602–608.

Gupta, M. and Marshall, J. (2018) The climate response to multiple volcanic eruptions mediated by ocean heat uptake: damping processes and accumulation potential. *Journal of Climate*, 31 (21), 8669–8687. https://doi.org/10.1175/JCLI-D-17-0703.1.

Harvey, P.J., Grab, S.W. and Malherbe, J. (2020) Major volcanic eruptions and their impacts on southern hemisphere temperatures during the late 19th and 20th centuries, as simulated by CMIP5 models. *Geophysical Research Letters*, 47(14), e2020GL087792. https://doi.org/10.1029/2020GL087792.

Haurwitz, M.W. and Brier, G.W. (1981) A critique of the superposed epoch analysis method: its application to solar–weather relations. *Monthly Weather Review*, 109(10), 2074–2079. https://doi.org/10.1175/1520-0493.

Humphreys, W.J. (1913) Volcanic dust and other factors in the production of climatic changes, and their possible relation to ice ages. *Journal of the Franklin Institute*, 176(2), 131–160. https://doi.org/10.1016/S0016-0032.

Kandlbauer, J., Hopcroft, P.O., Valdes, P.J. and Sparks, R.S.J. (2013) Climate and carbon cycle response to the 1815 Tambora volcanic eruption. *Journal of Geophysical Research-Atmospheres*, 118 (22), 12,497–12,507. https://doi.org/10.1002/2013JD019767.

Klein, F. and Goosse, H. (2018) Reconstructing east African rainfall and Indian Ocean sea surface temperatures over the last centuries using data assimilation. *Climate Dynamics*, 50(11–12), 3909–3929. https://doi.org/10.1007/s00382-017-3853-0.

Kondo, J. (1988) Volcanic eruptions, cool summers, and famines in the northeastern part of Japan. *Journal of Climate*, 1(8), 775–788.

Köppen, W. (1936) Das geographisca system der Klimate. In: Köppen, W. and Geiger, G. (Eds.) *Handbuch der Klimatologie*. Berlin: Gebr, Borntraeger, p. 44.

Kremser, S., Thomason, L.W., von Hobe, M., Hermann, M., Deshler, T., Timmreck, C., Toohey, M., Stenke, A., Schwarz, J. P., Weigel, R., Fueglistaler, S., Prata, F.J., Vernier, J.-P., Schlager, H., Barnes, J.E., Antuña-Marrero, J.-C., Fairlie, D., Palm, M., Mahieu, E., Notholt, J., Rex, M., Bingen, C., Vanhellemont, F., Bourassa, A., Plane, J.M.C., Klocke, D., Carn, S.A., Clarisse, L., Trickl, T., Neely, R., James, A.D., Rieger, L., Wilson, J.C. and Meland, B. (2016) Stratospheric aerosol-observations, processes, and impact on climate: stratospheric aerosol. *Reviews of Geophysics*, 54(2), 278–335. https://doi.org/10.1002/2015RG000511.

Krishnamohan, K.-P.S.-P., Bala, G., Cao, L., Duan, L. and Caldeira, K. (2019) Climate system response to stratospheric sulfate aerosols: sensitivity to altitude of aerosol layer. *Earth System Dynamics*, 10 (4), 885–900. https://doi.org/10.5194/esd-10-885-2019.

Kruger, A.C. and Sekele, S.S. (2013) Trends in extreme temperature indices in South Africa: 1962-2009. *International Journal of Climatology*, 33(3), 661–676. https://doi.org/10.1002/joc.3455.

Lakhraj-Govender, R. and Grab, S.W. (2018) Assessing the impact of El Niño-southern oscillation on south African temperatures during austral summer. *International Journal of Climatology*, 39 (1), 143–156. https://doi.org/10.1002/joc.5791.

LaMarche, V.C. and Hirschboeck, K.K. (1984) Frost rings in trees as records of major volcanic eruptions. *Nature*, 307(5947), 121–126. https://doi.org/10.1038/307121a0.

Lamb, H.H. (1970) Volcanic dust in the atmosphere; with a chronology and assessment of its meteorological significance. *Philosophical Transactions of the Royal Society of London. Series A, Mathematical and Physical Sciences*, 266(1178), 425–533. https://doi.org/10.1098/rsta.1970.0010.

Landman, W.A., Malherbe, J. and Engelbrecht, F.A. (2017) Understanding the social and environmental implications of global change. In: Mambo, J. and Faccer, K. (Eds.) *South Africa's Present-Day Climate*. Stellenbosch: Africa Sun Media, pp. 7–12.

Liu, F., Zhao, T., Wang, B., Liu, J. and Luo, W. (2018) Different global precipitation responses to solar, volcanic, and greenhouse gas forcings. *Journal of Geophysical Research-Atmospheres*, 123(8), 4060–4072. https://doi.org/10.1029/2017JD027391.

Lough, J.M. and Fritts, H.C. (1987) An assessment of the possible effects of volcanic eruptions on north American climate using tree-ring data, 1602 to 1900 A.D. *Climatic Change*, 10(3), 219–239. https://doi.org/10.1007/BF00143903.

Lyu, K., Zhang, X., Church, J.A. and Hu, J. (2015) Quantifying internally generated and externally forced climate signals at regional scales in CMIP5 models: internal and forced climate signals. *Geophysical Research Letters*, 42(21), 9394–9403. https://doi.org/10.1002/2015GL065508.

Man, W., Zhou, T. and Jungclaus, J.H. (2014) Effects of large volcanic eruptions on global summer climate and east Asian monsoon changes during the last millennium: analysis of MPI-ESM simulations. *Journal of Climate*, 27(19), 7394–7409. https://doi.org/10.1175/JCLI-D-13-00739.1.

Mason, S.J. (2001) El Niño, climate change, and southern African climate: El Nino-southern oscillation phenomenon. *Environmetrics*, 12(4), 327–345. https://doi.org/10.1002/env.476.

Mass, C.F. and Portman, D.A. (1989) Major volcanic eruptions and climate: a critical evaluation. *Journal of Climate*, 2(6), 566–593. https://doi.org/10.1175/1520-0442.

McGraw, M.C., Barnes, E.A. and Deser, C. (2016) Reconciling the observed and modeled southern hemisphere circulation response to volcanic eruptions: reconciling SH response to volcanoes. *Geophysical Research Letters*, 43(13), 7259–7266. https://doi.org/10.1002/2016GL069835.

McGregor, H.V., Evans, M.N., Goosse, H., Leduc, G., Martrat, B., Addison, J.A., Mortyn, P.G., Oppo, D.W., Seidenkrantz, M.-S., Sicre, M.-A., Phipps, S.J., Selvaraj, K., Thirumalai, K., Filipsson, H.L. and Ersek, V. (2015) Robust global ocean cooling trend for the pre-industrial common era. *Nature Geoscience. Nature Publishing Group*, 8(9), 671–677. https://doi.org/10.1038/ngeo2510.

Ménégoz, M., Bilbao, R., Bellprat, O., Guemas, V. and Doblas-Reyes, F.J. (2018) Forecasting the climate response to volcanic eruptions: prediction skill related to stratospheric aerosol forcing. *Environmental Research Letters*, 13(6), 064022. https://doi.org/10.1088/1748-9326/aac4db.

Monerie, P.-A., Moine, M.-P., Terray, L. and Valcke, S. (2017) Quantifying the impact of early 21st century volcanic eruptions on global-mean surface temperature. *Environmental Research Letters*, 12(5), 054010. https://doi.org/10.1088/1748-9326/aa6cb5.

Neely III, Ryan R. and Schmidt, A. (2016) *VolcanEESM: Global Volcanic Sulphur Dioxide (SO2) Emissions Database from 1850 to Present*. Centre for Environmental Data Analysis. [Dataset] https://doi.org/10.5285/76ebdc0b-0eed-4f70-b89e-55e606bcd568.

Neukom, R., Gergis, J., Karoly, D.J., Wanner, H., Curran, M., Elbert, J., González-Rouco, F., Linsley, B.K., Moy, A.D., Mundo, I., Raible, C.C., Steig, E.J., van Ommen, T., Vance, T., Villalba, R., Zinke, J. and Frank, D. (2014) Inter-hemispheric temperature variability over the past millennium. *Nature Climate Change*, 4(5), 362–367. https://doi.org/10.1038/nclimate2174.

Nicholson, S.E. and Kim, J. (1997) The relationship of the El Niño–southern oscillation to African rainfall. *International Journal of Climatology*, 17(2), 117–135. https://doi.org/10.1002/(SICI)1097-0088(199702)17:2<117::AID-JOC84>3.0.CO;2-O.

Oman, L., Robock, A., Stenchikov, G., Schmidt, G.A. and Ruedy, R. (2005) Climatic response to high-latitude volcanic eruptions. *Journal of Geophysical Research-Atmospheres*, 110(D13), D13103. https://doi.org/10.1029/2004JD005487.

Palmer, J.G. and Xiong, L. (2004) New Zealand climate over the last 500 years reconstructed from Libocedrus bidwillii Hook. f. tree-ring chronologies. *The Holocene*, 14(2), 282–289. https://doi.org/10.1191/0959683604hl679rr.

Pausata, F.S.R., Karamperidou, C., Caballero, R. and Battisti, D.S. (2016) ENSO response to high-latitude volcanic eruptions in the northern hemisphere: the role of the initial conditions: ENSO response to high-latitude volcanic eruptions. *Geophysical Research Letters*, 43(16), 8694–8702. https://doi.org/10.1002/2016GL069575.

Pepler, A.S., Fong, J. and Alexander, L.V. (2016) Australian east coast mid-latitude cyclones in the 20th century reanalysis ensemble. *International Journal of Climatology*, 37(4), 2187–2192. https://doi.org/10.1002/joc.4812.

Perlwitz, J. and Graf, H.-F. (1995) The statistical connection between tropospheric and stratospheric circulation of the northern hemisphere in winter. *Journal of Climate*, 8, 2281–2295.

Pezza, A.B., Simmonds, I. and Renwick, J.A. (2007) Southern hemisphere cyclones and anticyclones: recent trends and links with decadal variability in the Pacific Ocean. *International Journal of Climatology*, 27(11), 1403–1419. https://doi.org/10.1002/joc.1477.

Philippon, N., Rouault, M., Richard, Y. and Favre, A. (2012) The influence of ENSO on winter rainfall in South Africa. *International Journal of Climatology*, 32(15), 2333–2347. https://doi.org/10.1002/joc.3403.

Picas, J. and Grab, S.W. (2020) Potential impacts of major nineteenth century volcanic eruptions on temperature over Cape Town, South Africa: 1834–1899. *Climatic Change*, 159(4), 523–544. https://doi.org/10.1007/s10584-020-02678-6.

Pidwirny, M. (2006) Climate classification and climatic regions of the world. *Fundamentals of Physical Geography*, 2nd Edition. http://www.physicalgeography.net/fundamentals/7v.html.

Rao, M.P., Cook, B.I., Cook, E.R., D'Arrigo, R.D., Krusic, P.J., Anchukaitis, K.J., LeGrande, A.N., Buckley, B.M., Davi, N.K., Leland, C. and Griffin, K.L. (2017) European and Mediterranean hydroclimate responses to tropical volcanic forcing over the last millennium. *Geophysical Research Letters*, 44(10), 5104–5112. https://doi.org/10.1002/2017GL073057.

Robock, A. (2000) Volcanic eruptions and climate. *Reviews of Geophysics*, 38(2), 191–219. https://doi.org/10.1029/1998RG000054.

Robock, A. and Mao, J. (1995) The volcanic signal in surface temperature observations. *Journal of Climate*, 8(5), 1086–1103. https://doi.org/10.1175/1520-0442(1995)008<1086:TVSIST>2.0.CO;2.

Roffe, S.J., Fitchett, J.M. and Curtis, C.J. (2020) Determining the utility of a percentile-based wet-season start- and end-date metrics across South Africa. *Theoretical and Applied Climatology*, 140(3–4), 1331–1347. https://doi.org/10.1007/s00704-020-03162-y.

Roig, F. A. & Villalba, R.(2008) Understanding Climate from Patagonian Tree Rings. *Developments in Quaternary Sciences*, pp. 411–435. Netherlands: Elsevier. https://doi.org/10.1016/S1571-0866(07)10021-X.

Salinger, M.J. (1998) New Zealand climate: the impact of major volcanic eruptions. *Weather and Climate*, 18(1), 11–19.

Santer, B.D., Painter, J.F., Bonfils, C., Mears, C.A., Solomon, S., Wigley, T.M.L., Gleckler, P.J., Schmidt, G.A., Doutriaux, C., Gillett, N.P., Taylor, K.E., Thorne, P.W. and Wentz, F.J. (2013) Human and natural influences on the changing thermal structure of the atmosphere. *Proceedings of the National Academy of Sciences*, 110(43), 17235–17240. https://doi.org/10.1073/pnas.1305332110.

Sato, M., Hansen, J.E., McCormick, M.P. and Pollack, J.B. (1993) Stratospheric aerosol optical depths, 1850–1990. *Journal of Geophysical Research*, 98(D12), 22987. https://doi.org/10.1029/93JD02553.

Schneider, D.P., Ammann, C.M., Otto-Bliesner, B.L. and Kaufman, D.S. (2009) Climate response to large, high-latitude and low-latitude volcanic eruptions in the community climate system model. *Journal of Geophysical Research-Atmospheres*, 114(D15), D15101. https://doi.org/10.1029/2008JD011222.

Shindell, D.T. (2004) Dynamic winter climate response to large tropical volcanic eruptions since 1600. *Journal of Geophysical Research*, 109(D5), D05104. https://doi.org/10.1029/2003JD004151.

Stevenson, S., Fasullo, J.T., Otto-Bliesner, B.L., Tomas, R.A. and Gao, C. (2017) Role of eruption season in reconciling model and proxy responses to tropical volcanism. *Proceedings of the National Academy of Sciences*, 114(8), 1822–1826. https://doi.org/10.1073/pnas.1612505114.

Sun, W., Wang, B., Liu, J., Chen, D., Gao, C., Ning, L. and Chen, L. (2019) How northern high-latitude volcanic eruptions in different seasons affect ENSO. *Journal of Climate*, 32(11), 3245–3262. https://doi.org/10.1175/JCLI-D-18-0290.1.

Taylor, K.E., Stouffer, R.J. and Meehl, G.A. (2012) An overview of CMIP5 and the experiment design. *Bulletin of the American Meteorological Society*, 93(4), 485–498. https://doi.org/10.1175/BAMS-D-11-00094.1.

Tett, S.F.B. (2002) Estimation of natural and anthropogenic contributions to twentieth century temperature change. *Journal of Geophysical Research*, 107(D16), 4306. https://doi.org/10.1029/2000JD000028.

Textor, C., Graf, H.-F., Timmreck, C. and Robock, A. (2004) Emissions from volcanoes. In: Granier, C., Artaxo, P. and Reeves, C. E. (Eds.) *Emissions of Atmospheric Trace Compounds*. Dordrecht: Springer Netherlands, pp. 269–303.

Thompson, D.W.J., Wallace, J.M., Jones, P.D. and Kennedy, J.J. (2009) Identifying signatures of natural climate variability in time series of global-mean surface temperature: methodology and insights. *Journal of Climate*, 22(22), 6120–6141. https://doi.org/10.1175/2009JCLI3089.1.

Timmreck, C. (2012) Modeling the climatic effects of large explosive volcanic eruptions. *WIREs Climate Change*, 3(6), 545–564. https://doi.org/10.1002/wcc.192.

Timmreck, C. (2018) *Climatic Effects of Large Volcanic Eruptions*. Habilitation Thesis: Hamburg, Universität Hamburg.

Trigo, R.M., Vaquero, J.M. and Stothers, R.B. (2010) Witnessing the impact of the 1783–1784 Laki eruption in the southern hemisphere. *Climatic Change*, 99, 535–546. https://doi.org/10.1007/s10584-009-9676-1.

Tyson, P.D. and Preston-Whyte, R.A. (2000) *The Weather and Climate of Southern Africa*. Cape Town, South Africa: Oxford University Press Southern Africa.

Vincent, L., Pierre, G., Michel, S., Robert, N. and Masson-Delmotte, V. (2007) Tree-rings and the climate of New Caledonia (SW Pacific). *Palaeogeography, Palaeoclimatology, Palaeoecology*, 253(3–4), 477–489. https://doi.org/10.1016/j.palaeo.2007.06.019.

Visioni, D., Pitari, G., Tuccella, P. and Curci, G. (2018) Sulfur deposition changes under sulfate geoengineering conditions: quasi-biennial oscillation effects on the transport and lifetime of stratospheric aerosols. *Atmospheric Chemistry and Physics*, 18(4), 2787–2808. https://doi.org/10.5194/acp-18-2787-2018.

Wexler, H. (1951) On the effects of volcanic dust on insolation and weather (I). *Bulletin of the American Meteorological Society*, 32 (1), 10–15. https://doi.org/10.1175/1520-0477-32.1.10.

Wilmes, S.B., Raible, C.C. and Stocker, T.F. (2012) Climate variability of the mid- and high-latitudes of the southern hemisphere in ensemble simulations from 1500 to 2000 AD. *Climate of the Past*, 8(1), 373–390. https://doi.org/10.5194/cp-8-373-2012.

Yang, J. and Xiao, C. (2017) The evolution and volcanic forcing of the southern annular mode during the past 300 years. *International Journal of Climatology*, 38(4), 1706–1717. https://doi.org/10.1002/joc.5290.

Zambri, B., LeGrande, A.N., Robock, A. and Slawinska, J. (2017) Northern hemisphere winter warming and summer monsoon reduction after volcanic eruptions over the last millennium. *Journal of Geophysical Research-Atmospheres*, 122(15), 7971–7989. https://doi.org/10.1002/2017JD026728.

Zambri, B. and Robock, A. (2016) Winter warming and summer monsoon reduction after volcanic eruptions in coupled model Intercomparison project 5 (CMIP5) simulations. *Geophysical Research Letters*, 43(20), 10,920–10,928. https://doi.org/10.1002/2016GL070460.

Zanchettin, D., Bothe, O., Timmreck, C., Bader, J., Beitsch, A., Graf, H.-F., Notz, D. and Jungclaus, J.H. (2014) Inter-hemispheric asymmetry in the sea-ice response to volcanic forcing simulated by MPI-ESM (COSMOS-mill). *Earth System Dynamics*, 5(1), 223–242. https://doi.org/10.5194/esd-5-223-2014.

Zanchettin, D., Timmreck, C., Toohey, M., Jungclaus, J.H., Bittner, M., Lorenz, S.J. and Rubino, A. (2019) Clarifying the relative role of forcing uncertainties and initial-condition unknowns in spreading the climate response to volcanic eruptions. *Geophysical Research Letters*, 46(3), 1602–1611. https://doi.org/10.1029/2018GL081018.

Zhang, D., Blender, R. and Fraedrich, K. (2013) Volcanoes and ENSO in millennium simulations: global impacts and regional reconstructions in East Asia. *Theoretical and Applied Climatology*, 111 (3–4), 437–454. https://doi.org/10.1007/s00704-012-0670-6.

Zuo, M., Man, W., Zhou, T. and Guo, Z. (2018) Different impacts of northern, tropical, and southern volcanic eruptions on the tropical Pacific SST in the last millennium. *Journal of Climate*, 31 (17), 6729–6744. https://doi.org/10.1175/JCLI-D-17-0571.1.

How to cite this article: Harvey PJ, Grab SW. Southern African temperature responses to major volcanic eruptions since 1883: Simulated by CMIP5 models. *Int J Climatol*. 2021;1–20. https://doi.org/10.1002/joc.7135